19.

Wind Resource Assessment in the Vicinity of a Small, Low Relief Coastal Island for the Rhode Island Ocean Special Area Management Plan 2010

by

Malcolm L. Spaulding[1], Marty Bell[2], Jay Titlow[3], Ravi Sharma[1], Annette Grilli[1], Alexander Crosby[1], Lauren Decker[4] and Daniel Mendelsohn[4]

[1] Ocean Engineering, University of Rhode Island, Narragansett, RI

[2]Metlogic, 212 West Mountain Avenue, Fort Collins, CO 80521

[3]WeatherFlow, 790 Poquoson Ave, Poquoson, VA 23662

[4]Applied Science Associates, 55 Village Square, South County Commons, South Kingstown, RI 02879

June 9, 2010

Executive Summary

The focus of the paper is to assess the wind resources for the area in state waters (4.5 km from land) immediately south of Block Island, a small, 9 km by 6 km, low relief (35 m elevation) pear shaped island located 15 km off the coast of RI, for the siting of a small (5 to 8 turbine) wind farm. The area is being considered for designation as the potential site for offshore wind development. A review of existing wind observations was performed and showed that the wind speed and power density roses were dominated by westerly winds with NW dominant in the winter and SW in the summer. Wind shear measurements from meteorological tower observations on the island showed low shears in the winter during unstable atmospheric conditions and higher values during the stable summer winds. The shears were also strongly impacted by the Block Island land cover and the positioning of the observation tower relative to these features.

A template based scaling method was used to estimate the annual mean wind speed and power density distribution in the vicinity of the southern end of the island. Hindcast simulations were performed using a four level nested version of RAMS for eight points of the compass for selected time periods over the last two years. These model predictions were compared to observations at two locations on the island and showed good agreement for direction and temporal trends of the speed but consistently under predicted the speed. The results of the simulations were used in conjunction with a wind speed frequency rose in the study area and, assuming linear speed scaling, estimates were made for the annual mean values. The large scale patterns showed wind speeds and power increasing with distance offshore. This pattern was modified in the vicinity of the island by lee effects from the predominant and strong NW winds. The impacted area extended at least 8 km to the SE of the island. Areas to the W-WSW of the island were impacted by lee effects from NE winds and roughness effects from Long Island, immediately to the west. Predictions showed the highest annual mean wind speeds and power densities to the S of the island with sites to the SW and SE having lower values. Power production potential was estimated for three sites: SE, S and SW of island. Wind power at the S site was 4.9 % and 6.9 % greater than the SW and SE sites, respectively.

Three separate wake models were applied to the SE and S sites to assess the impact of turbine layout. The SW site was not viable for a farm because of seabed geology making installation of pile foundations challenging. The turbines were nominally spaced 1 km apart. Simulations were

performed for each wind direction and showed wake losses as high as 14 %, when the wind was in alignment with the field. When weighted by data from a nearby wind rose, the annual losses were shown to be several percent at the SE site and about half of that at the S site. The difference is due to the fact that SW winds are dominant in the summer while W winds are less frequent.

Considering both lee effects from the island and wake effects, the S site is the preferred location for a small wind farm.

Table of Contents

List of Figures

Figure 25 Wind direction as a function of time for the eight directional cases at Block Island, Jetty, upper panel includes all data and the lower panel only data that were within 15 degrees of the desired direction.

List of Tables

List of Attachments and Appendices

Appendix A: Wind frequency and power density roses (seasonal and annual) and Weibull fits to all observations or hindcasts in the study area.

Appendix B: Titlow, J. and D. Morris, 2010. Block Island modeling analysis, WeatherFlow Inc., Poquoson, VA, with model simulations by MetLogics, Fort Collins, CO.

Appendix C: Step by step protocol for the template based prediction method, prepared by L. Decker and D. Mendelsohn, Applied Science Associates, South Kingstown, RI.

Appendix D: Evaluation of the linear scaling analysis used in the template based method.

Abstract

The focus of the paper is to assess the wind resources for the area in state waters (4.5 km from land) immediately south of Block Island, a small, 9 km by 6 km, low relief (35 m elevation) pear shaped island located 15 km off the coast of RI, for the siting of a small (5 to 8 turbine) wind farm. The area is being considered for designation as the potential site for offshore wind development. A review of existing wind observations was performed and showed that the wind speed and power density roses were dominated by westerly winds with NW dominant in the winter and SW in the summer. Wind shear measurements from meteorological tower observations on the island showed low shears in the winter during unstable atmospheric conditions and higher values during the stable summer winds. The shears were also strongly impacted by the Block Island land cover and the positioning of the observation tower relative to these features.

A template based scaling method was used to estimate the annual mean wind speed and power density distribution in the vicinity of the southern end of the island. Hindcast simulations were performed using a four level nested version of RAMS for eight points of the compass for selected time periods over the last two years. These model predictions were compared to observations at two locations on the island and showed good agreement for direction and temporal trends of the speed but consistently under predicted the speed. The results of the simulations were used in conjunction with a wind speed frequency rose in the study area and, assuming linear speed scaling, estimates were made for the annual mean values. The large scale patterns showed wind speeds and power increasing with distance offshore. This pattern was modified in the vicinity of the island by lee effects from the predominant and strong NW winds. The impacted area extended at least 8 km to the SE of the island. Areas to the W-WSW of the island were impacted by lee effects from NE winds and roughness effects from Long Island, immediately to the west. Predictions showed the highest annual mean wind speeds and power densities to the S of the island with sites to the SW and SE having lower values. Power production potential was estimated for three sites: SE, S and SW of island. Wind power at the S site was 4.9 % and 6.9 % greater than the SW and SE sites, respectively.

Three separate wake models were applied to the SE and S sites to assess the impact of turbine layout. The SW site was not viable for a farm because of seabed geology making installation of pile foundations challenging. The turbines were nominally spaced 1 km apart. Simulations were performed for each wind direction and showed wake losses as high as 14 %, when the wind was

in alignment with the field. When weighted by data from a nearby wind rose, the annual losses were shown to be several percent at the SE site and about half of that at the S site. The difference is due to the fact that SW winds are dominant in the summer while W winds are less frequent.

Considering both lee effects from the island and wake effects, the S site is the preferred location for a small wind farm.

1 Introduction

Spaulding et al (2010a) have recently performed an application of a Technology Development Index to the RI coastal waters to assist in siting of wind farms in the Ocean Special Area Management Plan (SAMP) study area (Figure 1). The TDI estimates the technical challenge (technology type plus cable distance) in extracting offshore wind energy to the wind energy (power) available at a given location. The analysis was performed on a grid of approximately 200 m. Optimum sites have low TDI (low technical challenge and high power production potential). To remove the dependence on units, the TDI is non-dimensionalized by the optimum value in the study area. Optimum sites have a TDI of one and less desirable sites have values increasingly larger than one. This analysis, assuming a lattice jacket support structure (Hensel, 2009; Roarke, 2008) as the technology type, turbine hub height at 80 m, and considering the difficulty of installing foundation piles in glacial, end moraine sediments showed that the optimum site in state waters (3 miles (4.8 km) from land) was immediately south of Block Island. Even though the water depths in the area range from 20 to 40 m, the wind resources are significantly higher than near the mainland shoreline, shallow water areas. Grilli et al (2010) subsequently performed a high resolution TDI (Figure 2) for this area and identified a band from east to the southwest approximately 2 km wide, bounded on the outer edge by the state water boundary as optimum for wind farm siting. This analysis used NOAA ENC bathymetry, results of high resolution side scan and sub-bottom imagery, supplemented by boring logs to determine the effort to install the pile foundation, and an estimate of the annual mean wind speed at 80 m provided by Brower (2007)(Figure 3).

Brower (2007) uses results from simulations performed with MASS (Mesoscale Atmospheric Simulation System). The model includes the fundamental physics of the atmosphere including conservation of mass, momentum, and energy, as well as the moisture phases. It also includes a turbulent kinetic energy module that accounts for the effects of viscosity and thermal stability on wind shear. The system creates a wind resource map by simulating weather conditions over 366 days selected from a 15-year period. The days are chosen through a stratified random sampling scheme so that each month and season is represented equally in the sample. Each simulation generates wind and other weather variables (including temperature, pressure, moisture, turbulent kinetic energy, and heat flux) throughout the model domain, and the information is stored at

hourly intervals. The analysis has been performed on a 2. 5 km grid, for the Ocean SAMP study area, and the data provided on a 200 m grid.

A review of the Brower (2007) estimates raises concern that this mean climatology does not adequately represent the wind fields in close proximity to Block Island (within state water boundary) given its topography (mean elevation of 35 m on the southern half of the island) (Figure 4) and surface roughness (Figure 5) and the potential for lee effects from winds from from the W to NE sector. The focus of this paper is to review the available observations to describe the wind fields in the vicinity of the island with a focus on mean annual conditions (Section 2), to apply a high resolution meteorological model (RAMS) (Section 3) to understand the basic flow patterns for eight points of the compass wind directions, and then to use the model predictions, in conjunction with observations, to estimate mean annual wind conditions to the south of the island. The sensitivity of these estimates to the wind rose used to represent the wind distribution and a comparison to Brower (2007) are provided. Finally comparisons are made if an 8 turbine wind farm is located to the SE and S of Block Island on the power generation. In addition, wake models (Section 6) are applied to determine the losses from each wind direction for the two sites and the total loss over the year. Conclusions are provided in Section 7.

2. Wind Observations

There are five sources of wind observations/hindcasts in the vicinity of Block Island. Each is briefly summarized below. These represent the principal observations for winds in the study area.

Army Corp of Engineers Wave Information Studies (WIS)-WIS101 (41 Lat, 71.58 Lon)(WIS101)

The US Army Corp performed a 20 yr hindcast (1980-1999) of the wind and wave conditions for a number of sites located along the southern boundary of the SAMP study area as part of the Wave Information Study (WIS)(http://www.frf.usace.army.mil/cgi-bin/wis/atl/atl_main.html). The locations of the southern New England hindcast sites are provided at the WIS web site. The site of primary interest in this investigation is WIS101, located immediately south of Block Island. Wind time series data are available at 10 m via the internet over the 20 yr hindcast period. Validation of the hindcasts was performed primarily using the NOAA NDBC offshore observations (Stations 44004, 44008, 440017, 440018, and 44025).

WeatherFlow Block Island Jetty (41.199 Lat, 71.593 Long)(BI Jetty)

WeatherFlow (http://www.weatherflow.com/) is a private firm that operates a network of meteorological observation towers in the SAMP study area. Data from their Block Island Jetty (western entrance to Great Salt Pond) station was obtained from WeatherFlow. Data was nominally at an elevation of 11 m. This data is available from December 2005 to 2009.

Department of Energy (DOE) Block Island Meteorological Tower (41.183 Lat, 71.57 Long)(DOE)

DOE made wind measurements at a site just south of Great Salt Pond as part of a feasibility study to investigate the siting of a wind turbine on the island (Renne et al, 1982). Measurements were made at two locations in the vertical (9.1 and 45.7 m). Wind data were available from 1979 through 1982, but with substantial periods of the record missing. The site is located on a hill top in rolling grass land on the southern edge of and overlooking Great Salt Pond.

Block Island Airport AWOS(41.168 Lat, 71.577 Long)(KBID)

An automated weather observation system (AWOS) is located on the northern side of the E-W oriented Block Island Airport runway (Figure 5). The runway is located on the southern end of the island with a mean elevation of approximately 35 m (Figure 4). Data is available from 1997 to present with observations at a 10 m height. The AWOS was located approximately 50 m eastward of the terminal building (peak height of 8.3 m) until the building was demolished and a new terminal constructed further to the west in 2009. The AWOS data collected prior to 2009 is considered suspect for westerly and northwesterly winds because it is in the immediate lee of the terminal building. In addition, there is strong topographic relief and tree cover to the west and northwest of the AWOS site (Figure 5) complicating accurate measurements of the wind.

Ocean SAMP Buoy MDS02 (41.1 Lat, 41.56 Long)(MDS)

The University of Maine, on behalf of the Ocean SAMP study, deployed an offshore buoy with meteorological and oceanographic sensors immediately south of Block Island at the state water boundary line. The buoy collects wind speed and direction and air and sea surface temperature data every 15 minutes. The data is distributed through the Northeast Regional Association of Coastal Ocean Observing Systems web site (www.neracoos.org) and has been in operation from October 1, 2009 to present.

AWS True Winds Block Island Meteorological Tower (41°11'49.96"N Lat, 71°35'30.34"W,Long.) (AWS Met)

AWS True Winds erected a meteorological tower at the western entrance to Great Salt Pond, in close proximity to WeatherFlow's Block Island Jetty Station. Wind speed and direction data are being collected at elevations of 9.9, 32, 47.6, and 57.4 m. Data is available from Aug 2009 to present.

Appendix A provides wind frequency and power density roses, average power rose, and a Weibull fit to the data for all sites in the study area. The reader is cautioned to note the duration of the observation or hindcast product and its elevation.

Figure 6 and 7 show the wind frequency and power density roses, respectively for all stations and the dates noted above. The reader should note that the data have been collected over different time periods and is of varying duration and at different elevations; so care should be taken in interpreting the data sets. The WIS data is a hindcast product and not actual observations. In all cases the data is presented at the lowest elevation of the measurements (typically in the range of 4 to 10 m).

Comparing the longer term data sets (DOE and WIS) it is observed that the wind frequency and power density roses are similar and dominated by winds from the west; NW and SW in particular. The wind data from KBID is substantially different from these two sets, likely due to the impact of the terminal building and the significant roughness elements NW of the measurement site. This data set is clearly not representative of oceanic conditions.

AWS Met and MDS data sets are from the winter of 2009-2010 and collected over the same period of time. Both data sets show that the dominant winds and power density are from the NW, with the next most frequent winds from the NE. A comparison of the both stations was made to the winter average from WIS 101 and showed good agreement (not shown here), with the exception that the NE winds were more frequent in 2009-2010. This is consistent with recent observations throughout the area showing enhanced NE winds during the 2009 to 2010 winter.

Figure 8 shows the average power density rose for each location. These plots are generated by frequency weighting the power density roses shown in Figure 7. The dominant wind power comes from the NW or W, except for KBID, which is SW dominated. The power density for KBID is more lower than any other station because of vegetative roughness effects. It is noted that wind power is particularly strong from the NE in both the AWS Met and MDS locations. This is consistent with strong NE winds occurring during the winter of 2009-2010.

An analysis was performed of the shear, using both the DOE and AWS Met data sets. Figure 9 shows the observed wind speed data at 9 m vs 45 m from the DOE site. The data have been fitted using a least squares regression line, which gives a shear coefficient of 0.228. This compares to a mean value over the record period of 0.245. A line representing the neutral boundary layer assumption is shown for reference. Figure 10 shows the shear coefficient by season and direction. The shear is lowest in the winter for NW winds and highest in both the summer and winter for SW winds. NW winds dominate in the winter and SW in the summer. The picture that emerges is that winter winds are typically unstable and hence the shear is primarily due to topographic relief and roughness of the island. In summer, the winds are stable and island topographic relief and roughness are significant over the steep southern face of Block Island and hence the shear is quite high.

Shear estimates were made from data collected at the AWS Met site from August 2009 to February 2010. The mean values decreased from 0.18 in August to 0.08 in November and remained in the range of 0.06 to 0.07 through February 2010. The shear was approximately the same, no matter which vertical levels were used to perform the analysis. The shear for the winter season at AWS Met is consistent with ocean conditions and stable transitioning to unstable atmosphere from late summer to winter. The impact of topographic relief and roughness is minimal as might be expected based on the station's location.

Grilli and Spaulding (2010) provide a comprehensive analysis of the data using Weibull distribution methodology. They demonstrate the transition from oceanic to land based roughness impacts on the wind field.

3. High Resolution Meteorological Modeling in Study Area

RAMS, the Regional Atmospheric Modeling System (Piekle et al, 1992; Tremback and Walko, 2010; RAMS, 2010), is a highly versatile numerical code developed by several groups over the years, including the scientists at Colorado State University, the *ASTER division of Mission Research Corporation, and ATMET. RAMS is used for simulating and forecasting meteorological phenomena, and for depicting the results.

RAMS is primarily a limited area model, and many of its parameterizations have been designed for mesoscale or higher resolution scale grids. There is no lower limit to the domain size or to the mesh cell size of the model's finite difference grid; microscale phenomena such as tornadoes and boundary layer eddies, as well as sub-microscale turbulent flow over buildings and

in a wind tunnel, have been simulated with this code. Two-way interactive grid nesting in RAMS allows local fine mesh grids to resolve small-scale atmospheric systems such as thunderstorms, while simultaneously modeling the large-scale environment of the systems on a coarser grid.

The atmospheric model is constructed around the full set of non-hydrostatic, compressible equations that include atmospheric dynamics and thermodynamics, plus conservation equations for scalar quantities such as water vapor and liquid and ice hydrometeor mixing ratios. These equations are supplemented with a large selection of parameterizations for turbulent diffusion, solar and terrestrial radiation, moist processes including the formation and interaction of clouds and precipitating liquid and ice hydrometeors, kinematic effects of terrain, cumulus convection, and sensible and latent heat exchange between the atmosphere and the surface, which consists of multiple soil layers, vegetation, snow cover, canopy air, and surface water.

For the present study daily simulations starting at 0Z were performed with RAMS version 6.1. The model employed a 500m horizontal grid spacing on the high resolution grid telescopically nested from 12 km, 6 km and 2 km grids (Figures 11 and 12). A range of horizontal grid resolutions from 4 km to 250 m were tested. In most cases, the convergence of results at the proposed turbine locations occurred at 1-2km. In some cases, where stable conditions existed and the proposed wind farm sites were downwind of the island, differences were apparent down to 500 m. 20 m vertical grid spacing, expanding upward with a geometric ratio of 1.15 was employed. Vertical grid resolutions from 40 m to 5 m were evaluated. Testing showed a loss in wind speed of up to 5 % when the vertical resolution was lowered from 5 to 20 m. 20 m was used in this study in order to complete the hindcasts in a timely fashion.

RAMS was initialized 6 hours prior to the 0Z start time (tau 0), firstly with a 2 grid run (outer grids only) from tau -6 to tau -3 (stage 1), then with all 4 grids from tau -3 to tau 0 (stage 2). Simulations were initialized from the 12 km North American Mesoscale Model (NAM) analysis, with grid 1 bounded by subsequent 6 hourly 12 km NAM analyses. In stage 1, the wind speed and direction, pressure, and air temperature model fields in the interior domain were strongly nudged to the interpolated NAM analysis values. In stage 2, the same variables were nudged, but far less strongly. The atmospheric moisture data was excluded from the nudging. This forces a balance to develop for the mechanical quantities between the model and the NAM analysis, while allowing moisture quantities (clouds and precipitation) to evolve.

The 3D (spatial and depth) soil moisture field was extracted from the 12km NAM analysis files and interpolated to the RAMS grids and soil levels. The 2D (spatial) snow cover field was

also extracted from the 12km NAM analysis files and interpolated to the RAMS grids. Sea surface temperature data was obtained from Operational Sea Surface Temperature and Sea Ice Analysis (OSTIA) which uses satellite data provided by the GHRSST project, together with in-situ observations to determine the sea surface temperature. The analysis is performed using a variant of optimal interpolation (OI) technique. The analysis is produced daily at a resolution of 1/20 degree, (approx. 5km).

Digital elevation data for Block Island was data was provided from ASTER GDEM, which has a 30 m grid resolution and is referenced to the WGS84/EGM96 geoid. Surface roughness, which is a significant factor in the results of this study, is formulated as a function of wind speed over water. Over land, contributions to the surface roughness come from the water bodies, soil, vegetative cover and topographical drag within the grid cell. RAMS partitions the land use effects into contributing patches, whose weighting on the grid scale is proportional the relative dominance of the water and vegetation cover from the MRLC land use dataset.

RAMs was applied to perform high resolution simulations for discrete events that characterized conditions typical of each direction of wind forcing experienced in the area. The dates and directions which they characterize are provided in Table 1. It is noted that from several of the directions (NE, S, and NW) more than one simulation was performed. While an attempt was made to ensure that the wind directions did not change significantly over the simulation period this was not always possible since the simulations represent real events. A detailed description of each simulation and a comparison of model predictions to wind observations at WeatherFlow's Block Island Jetty wind observation station and at the Block Island Airport (KBID) are provided in Titlow and Morris (2010) (Appendix B).

4. Model Application

Case examples

In the interest of space, only three examples are presented here: NW (Oct 30, 2008), SW (July 8, 2008), and NE (September 22, 2008). They have been selected because they are the predominant wind directions in the winter (NW), summer (SW), and during extra-tropical storms (NE), respectively.

For each case a brief description of the event is provided. This is followed by plan view plots of the wind speed and direction at 80 m for grids 3 and 4. Finally a plan view plot of the shear coefficient estimated from the model at 80 m for the highest resolution grid is provided. A

supporting figure is also given showing the wind shear coefficient as a function of elevation for Block Island Jetty, KBID, and sites to the SE and SW. Finally model predictions are compared to observations at Block Island Jetty and KBID. These are the only two stations collecting observations in the immediate vicinity of Block Island during the simulation periods.

October 30, 2008 – NW

Description

High pressure, 1030mb, building into the East Coast from the southwest, following the departure of a low pressure center tracking northeastward across Newfoundland. This is a relatively common synoptic setup. Since the passage of the cold front late on the 28th, wind directions veered into the west then NW through the 29th, becoming a well established northwesterly through Oct 30th. These post cold frontal northwesterly winds exhibit a characteristically gusty signature, with average morning wind speeds around 10 m/sec, with gusts to the upper teens. Through the afternoon, wind speeds ease slightly, in response to weakening pressure gradients. The gust to lull spread appears to remain relatively large irrespective of diurnal solar insolation and air temperatures over the land. Boundary layer mixing is largely occurring as a result of relatively warm sea surface temperatures warming the lower layers of post cold frontal air advecting into the region.

Wind Speed Contours

Wind speed contours for Grids 3 and 4 are shown in Figure 13, upper and lower panels, respectively, at 80 m. The large scale pattern (Grid 3) shows wind speeds progressively increasing with distance offshore. The contour lines are shore parallel. The rate of increase decreases with distance offshore. Immediately south of Block Island the winds reach their maximum speeds. The wind speeds in addition are impacted by the presence of Long Island immediately to the west. This pattern is a direct result of the decreasing surface roughness from land to the coastal ocean. The basic pattern is interrupted by the presence of Block Island. There are two areas to the SE of the island, at the northern and southern ends of the island that show lee effects from the island's topography and surface roughness. The wind speed deficient zones extend approximately 10 km from the island. The southern lee area is more pronounced than its northern counterpart due to the higher surface roughness and topography (Figure 3 and 4).

Shear

Figure 14 shows the wind shear coefficient at 80 m for Grid 4 at stations to the SE, SW, KBID and Block Island Jetty. Figure 15 shows the vertical structure of the shear coefficients at the same stations. Given the late fall conditions, the atmosphere is unstable (air temperatures colder than water temperatures) during this period and the shear coefficient is very low (0.05) for most of the field. The values over Block Island are considerably larger and reach 0.45 at KBID. The shear coefficient is observed to be strongly correlated with the topographic relief and land cover of the island. Block Island Jetty wind station is on the margins of the impacted area. In the lee of Block Island, SE, shear coefficient is predicted to be impacted by the presence of the island extending to the state water boundary.

Comparison with observations

A comparison of model predicted wind speeds and directions with observations as Block Island Jetty (upper left) and KBID (upper right) are shown in Figure 15. The large scale wind field for the US and Northeast are provided in the lower panels. Model predicted directions are in good agreement with observations. The temporal trend in wind speeds is correctly predicted but the model consistently under predicts the speed.

July 8, 2008- SW

Description

For this case a Bermuda high pressure, 1022 mb, established to the southeast with a weak, expansive low pressure system, 1002 mb, centered over Lake Superior, with associated cold front extending southwestward to Nebraska. A warm front extends from the low pressure center to Canadian Maritimes. This is a relatively common summer synoptic set up.

Southwesterly winds are established through the early morning hours with average wind speeds hovering around 5 to 6 m/sec, but unsteady with several periods of < 2.5 m/sec, and a couple of gusts to 7 to 9 m/sec. During the light period, wind directions veered more WSW to W briefly. Wind speeds began to increase after 0900, reaching a plateau between 1300 and 1600 (local time) with averages around 10 m/sec and gusts into the lower to mid teens.

Wind Speed Contours

The model predicted wind speed contours at 80 m for Grids 3 (upper) and 4 (lower) are provided in Figure 17. Compared to the NW case the coastal boundary layer is substantially compressed with speeds increasing to oceanic levels close to the RI shoreline. Areas on the western side of Block Island Sound are in the lee of Long Island. Wind fields NE of Block Island

show a large lee effect, extending at least 15 km. This effect covers the entire shadow zone of the island and is a result of the enhanced roughness and topographic relief at the southern end of the island (Figure 3).

Shear

Figure 18 shows the wind shear coefficient at 80 m for Grid 3. Figure 19 shows the vertical structure at the selected stations noted earlier. Given summer conditions, the atmosphere is very stable during this period and the shear coefficient is relatively high (0.25) for most of the oceanic field. The values over Block Island are considerably larger and reach 0.43 at KBID. The shear coefficient is again observed to be strongly correlated with the topographic relief and land cover of the island. The Block Island Jetty wind station is on the margins of the impact area. In the lee of Block Island, NE, the impact of the island on the shear coefficient is observed to extend a considerable distance from the island and exhibit lower shears (0.20) than in adjacent waters. The vertical structure of the shear is consistent among all locations with values highest at KBID, next highest at Block Island Jetty, and lowest and about the same at SE and SW sites.

Comparison with observations

A comparison of model predicted wind speeds and directions with observations as Block Island Jetty (upper left) and KBID (upper right) are shown in Figure 20. The large scale wind field for the US and Northeast are provided in the lower panels. Model predicted directions are in good agreement with observations. The temporal trend in wind speeds is correctly predicted but the model under predicts the speed at Block Island Jetty and substantially under predicts them at KBID.

September 22 -24, 2008 - NE

Description

Anti-cyclonic NE winds are observed across New England thanks to high pressure becoming established over Quebec following the passage of a cold front from NNW to SSE the previous day. A stationary frontal boundary and trough axis to the east of Cape Hatteras helps to enhance northeasterly pressure gradients across the region.

Northeast winds increase through the morning hours, from 0200: 5.5 to7 m/sec., to 0700: 8.5 to 9.8 m/sec. For the rest of the period northeast winds generally hold around 9 m/sec. mark. The lull-to-gust spread remains relatively small possibly indicating neutral or stable lower layers, and therefore more stratification rather than well mixed lower layers.

Wind Speed Contours

The wind speed contours (Figure 21) for this simulation are similar to those for SW case presented earlier, shore parallel with increasing wind speed with distance offshore. Reduced wind speeds are clearly observed on the western side of Block Island Sound. (The contours in Figure 21 are shown for February 24 not the 22 nd since the basic NE pattern is better depicted on this date.). Once again there is a low speed area in the lee of Block Island (SW). It extends about 10 km.

Shear

Figure 22 shows the wind shear coefficient at 80 m for the high resolution grid. Figure 23 shows the vertical structure at selected stations. Given fall storm conditions, the atmosphere is unstable during this period and the shear coefficient is relatively low (less than 0.10) for most of the field. The values over Block Island are considerably larger and once again reach 0.43 at KBID. The shear coefficient is again observed to be strongly correlated with the topographic relief and land cover of the island. Block Island Jetty wind station is on the margins of the impacted area. In the lee of Block Island, SW, the impact of the island on the shear coefficient is observed to extend a considerable distance from the island and exhibit lower shears (0.10) than in adjacent waters.

Comparison with observations

A comparison of model predicted wind speeds and directions with observations as Block Island Jetty (upper left) and KBID (upper right) are shown in Figure 24. The large scale wind field for the US and Northeast are provided in the lower panels. Model predicted directions are in reasonable agreement with observations and correctly capture the rapidly changing direction. The temporal trend in wind speeds is correctly predicted but the model substantially under predicts the speed at Block Island Jetty and at KBID.

5. Estimated Wind Resources South of Block Island

To estimate the mean annual wind speed (or power) a spatial template based weighting scheme was employed. (Appendix C provides a step by step protocol for the template based method.) This approach requires an estimate of the wind frequency or power rose at one location in the study area (ideally at hub height but more often at 10 m) and meteorological model predictions for each wind direction as function of elevation and location. Assuming that the wind spatial patterns are relatively constant over the 30 hr simulation period (Table 1) and that the

wind patterns scale linearly with speed, the wind speed map can be determined for each speed and direction bin. The dates given in italics were used as the base case in the analysis. Nominally eight (or some even multiple) direction and 10 or more wind speed bins are employed. The individual speed/direction bins are weighted by their occurrence from the wind frequency rose. If the wind rose is at a different elevation than the desired model predictions, the rose can be extrapolated to the appropriate height using the model predicted shear coefficient. This method assumes that the stratification (wind shear) from a given direction is represented in the model simulation. Note that model under or over prediction is not an issue, since we are only using the model spatial structure in the method.

To test the linearity assumption, hindcasts presented in Spaulding et al (2010b) using RAMS for the period from October 1, 2009 to February 28, 2010 were reviewed and 34 instances of NW winds identified. NW winds were selected since they generated the most power south of the island. The spatial patterns of all simulations were averaged to determine a mean wind speed map for all events. The wind speed maps for each individual event were divided by the mean spatial map to develop a scale map for each event. Appendix D provides the maps for each event. The scaling factors vary from a low of about 0.5 to a high of 2.0. For any given map the largest variation (lower to upper value) in scaling factor is on the order of 0.1 or 10% of the mean value. For all events the scale factor variation is +/- 3.3% of the mean value. This analysis confirms that linear scaling is a reasonable assumption.

Figure 25 shows the observed wind speed direction time series for each of the directional cases at the Block Island Jetty station (upper panel, all directions case). For cases with winds from the NW, E, SW, and W the wind direction does not vary significantly over the simulation period. The variations are much larger for the N, S, and SE cases and particularly large for the NE case. For the present analysis the directions of the cases were assumed to be constant as specified in Table 1.

Simulations were performed using the template weighting method described above and the WIS 101 (10 m) (Figure 26) rose to describe the wind speed directional distribution. WIS was selected as most representative of long term winds in the study area. Predictions of the mean annual wind speed and power, left and right panels, respectively are provided in Figure 27. The dots indicate locations E, ESE, SE, SSE, S, SSW, SW, WSW, and W of the island along the state water boundary line (Figure 5). The basic pattern is that the wind speed and power contours are approximately parallel to the RI shoreline with increasing values moving seaward. The presence

of Block Island and the prevalence of winds from the NW and W have resulted in a substantial area in the lee of the island (SE) with lower wind speeds and power levels. This clearly extends to the state water boundary. This area of reduced wind speed and power is a direct result of lee effects from the topographic relief and roughness of the island. Note a similar low power area is seen SE of the northern tip of Block Island.

An inspection of Figure 26 (upper panel) shows the directional variations of the winds was quite large for several of the cases (NE in particular). This will lead to smearing the directionality of the wind resource assessment. To assess the sensitivity of predictions to this issue, simulations were performed using only wind data that was within 15 degrees of the desired direction (Figure 26, lower panel). This is referred to as the "reduced direction" case.

Figure 28 show the wind speed and power contours, respectively at 80 m for the reduced direction case. The wind speeds and power levels are generally higher for this case but the underlying pattern is the same, extended lee effect E and SE of Block Island. The results from both cases are very similar showing the same large scale pattern. The wind resource to the SE is almost identical. SW of the island the all direction case predicts slightly lower wind power density than the reduced direction case (about 20 kW/m^2).

Template based model predictions were also performed using the AWS Met 57 m wind rose (Figure 26). It must be remembered that this rose is based on data from October 1, 2009 to February 28, 2010. Predictions of mean wind speed and power contours are shown in Figure 29. The basic pattern is again similar to the WIS101 case but with enhanced wind speeds and power since the time is restricted to the winter and spring seasons.

Model simulations, in addition, were performed using wind roses from WIS 100 and KBID. The power density contours are shown for each in Figure 30. Results for the WIS101 and AWS Met cases are also provided again to make facilitate comparisons. Model predictions for the WIS 101 and 100 are almost identical. The pattern for AWS Met is very similar to the WIS 101 cases although with stronger winds due to the winter time period. While the wind rose from KBID is not representative of the study area, as noted above (see Figure 26), predicted power contours are very similar to the other cases. All show strong lee effects to the SE of the island from NW and W winds. The lee effects are least pronounced in the KBID simulations and most prominent in the AWS Met case.

Additional simulations were performed to assess model predictions to which NW data case was used (Table 1). Each case was used separately and the average of all cases was used. There was very little difference among them.

Template based model predicted mean wind speeds and power density at selected sites E through W and at KBID, Block Island Jetty, AWS Met, and MDS are shown in Figure 31, using the WIS101 wind rose. The data show increasing speeds and power densities with distance offshore and lower values to the west compared to the east. The mean values for three potential locations for a small wind farm have been determined for sites SE (E, ESE, SE), S (SSE, S, SSW) and SW (SW,WSW,W) of the island. Mean powers are SE- 973 W/m^2, S- 1045 W/m^2, and SW- 994 W/m^2. The power production potentials at the S site are 6.9% and 4.9% greater than the SE and SW sites, respectively.

It is impossible to assess the uncertainty in the above estimates since there are no long term observations at any of the locations south of Block Island. To provide some sense of uncertainties a Weibull distribution was fit to the wind data at AWS Met, 57.4 m. This site was selected since it has the best quality data, at the highest elevation in the study area. Estimates were made of the mean and the upper and lower 95% confidence limits for the Weibull shape and amplitude parameters. The Weibull distribution was then used to estimate the mean and upper and lower 95% confidence limits for power and showed a +/- 2.5% variation around the mean.

Spaulding et al (2010b) applied the template method to predict the mean wind speeds and power density for a hindcast period for which RAMS hindcasts were performed (October 1, 2009 to February 28, 2010). The template method used directional simulations as noted in Table 1. These periods are hence completely independent of the hindcast period. The mean power density was determined directly from the model hindcasts and from the template based method using the wind rose at the AWS Met tower location as input. The template based model predictions were within +/- 5.3% of the hindcast estimates to the south of Block Island.

6. Wake Loss Modeling

Based on the TDI analysis there are two potential sites for a small, five to eight, turbine wind farm south of Block Island: SE and SSW (Figure 32). The spacing between the turbines is nominally 1 km, or about 10 blade diameters (100 m diameter blade). A site to the SW was not considered as it is not likely given the geological impacts on installation of the pile foundation

(Grilli et al, 2010). To assess the impact of wake losses at each site, simulations were performed with the three wake models incorporated in WinSim (www.winsim.com).

Model 1 (Jensen, 1983) is based on momentum deficit theory and expresses the radius of the area spread of momentum deficit behind the turbine as a linear function of the distance to the rotor, modulated by a decay factor. The decay factor increases with increasing levels of turbulence, which is directly related to the surface roughness (order of 10-2-10-4 for sea surface). Model 2 (Larsen, 1988) is based on turbulent boundary layer equations with the turbulence term expressed in terms of Prandtl's mixing length. Model 3 (Ishihara et al, 2004) introduces a semi-empirical term, the turbulent dependent recovery rate, that modulates the wake expansion. Since there is no model that is clearly superior to the others for the present applications simulations were performed with all three and the results averaged.

Figure 33 shows the average of all three models predictions as a function of wind direction. Simulations were performed for a constant wind speed of 9 m/sec at 80 m, with 12, equally spaced 30 degree direction bins. Three separate location cases are shown. Site 1 represents the SE location while Site 2 and 3 represent the SSW location, with Site 3 representing alignment of wind turbines in the E-W direction and Site 2, the same orientation but with staggering of every other turbine. The predicted losses are as large as 13 to 16 % when the wind farm layout is the same as the wind direction (E-W for Site 3 and NE-SW for site 1). Staggering the turbines substantially reduces the losses (compare Site 2 and 3). Slight curvature in the farm layout, as in Site 1, reduces the maximum loss but spreads it directionally.

To estimate the total loss at a site, a wind rose was used to characterize the frequency distribution of wind speed by direction, the wind losses for each direction and speed bin are determined, and the total determined by applying the frequency weighting to each case. The total wake loss was estimated using wind roses from WIS 101, Buzzard Bay CMAN station, and data collected by meteorological observations on Block Island, with 12 direction (30 degree) and 1 m/sec speed bins. The WIS101 represents the closest long term (20 yr) hindcast, the Buzzard Bay station represents the closest long term observation at elevation (23 m), and the data from the Block Island meteorological tower represents the closest observation but is of limited duration (5 months). The results are provided in Table 2, in terms of the minimum, mean, maximum and standard deviation of the three methods. The results are approximately independent of which wind rose is used. The losses are about twice as high at Site 1 (1.7 to 1.8%) than at Sites 2 and 3 (0.8 to 1%). Staggering at the SSW site reduces the losses slightly,

about 0.2% (Compare Sites 2 and 3). In the larger context, wake losses are predicted to be small and are below the uncertainty of the wind resource estimates in the vicinity of the island.

7. Conclusions

Annual wind speed and power roses in the vicinity of Block Island (WIS 101, DOE) are typically dominated by westerly winds: NW in the winter, SW in the summer, and W in the spring and fall. Winds at AWS Met and MDS are dominated by NW followed by NE winds, characteristic of the winter observation period (Oct to Feb). KBID winds are predominantly from the SW and are strongly impacted by land cover (trees) and resulting high roughness for winds from the W and NW. The speeds at KBID are substantially lower than those at DOE or AWS Met again because of roughness effects.

Wind shear at the DOE site showed seasonal and directional dependence. Wind shear was lowest in the winter months (0.15) (NW), highest during the summer (0.28) (SW), and intermediate in other seasons. The shear at this island based site is impacted both by the seasonal stability of the atmosphere and the land cover and topography upwind from the site: stable in the summer and unstable in the winter. Wind shear coefficient at the AWS Met site was consistent with the transition from late summer (0.15) to fall and winter conditions (0.06 to 0.09). These values are lower than at the DOE site for the comparable time of the year since the AWS Met is located much closer to the shoreline.

Simulations from the individual compass directions showed consistent large scale patterns. When the wind blew offshore (NW, N, NE) the wind speed increased with distance offshore reaching maximum values just seaward of Block Island. If the winds were from the west (W, SW) the wind speed contours were once again shore parallel but more closely spaced. Areas on the western side of Block Island were in the lee of Long Island, with lower wind speeds close to the island. Winds from the S and SE were rare. In the immediate vicinity of Block Island, wind speeds demonstrated a lee effect for all wind directions. The impacted area typically extended 8 km or more from the island. Details of the shape of the impacted area were dependent on the wind direction and its orientation relative to high roughness land cover and elevation of the southern and northern end of the island. For winds from the NW, two lee areas are predicted, consistent with higher elevations and greater roughness at the northern and southern end of the island. For winds from the NE and N and from the S and SW only one impacted area is predicted.

The template scaling method was applied using the model predicted wind pattern for discrete compass directions and the WIS 101 wind rose to determine the annual mean wind speed and power density for the study area. The predictions showed a basic pattern of increasing speeds and power with distance offshore. This pattern is altered with lower speed and power to the southeast of the island. This is due to the fact that NW winds dominate the wind power rose. Sites to the S of the island show the highest power production potential, followed by sites to the SW and SE.

Simulations were performed constraining the model predicted wind time series used to define the directional templates to be within 15 deg of the selected direction. The annual mean estimates showed the same general pattern as the prior case with same small alternations in magnitude.

Sensitivity studies were performed using wind rose data from WIS100, AWS Met, and KBID. All gave similar patterns with prominent lee effects to the SE of the island. The smallest lee effects were predicted KBID because of its enhanced SW winds and largest for AWS Met because the wind rose was from the winter spring season when NW winds dominate.

Power production potential was estimated for three sites: SE, S and SW of island. Wind power at the S site was highest and 4.7% and 6.9% lower, respectively, than the S site. This result is consistent with Spaulding et al (2010c) analysis based on a model hindcast of the period from October 1, 2009 to February 28, 2010.

Simulations were performed using three separate wake models to assess the impact of wake losses on siting of a small wind farm. Turbine spacing was nominally 1 km. The losses are highest (14%) when the winds are in alignment with the turbine layout and disappear in the cross wind directions. The results of the individual directional cases and the WIS 101 wind rose were used to estimate total losses. The losses are about twice as high at Site 1 (SE) (1.7 to 1.8%) than at Sites 2 (staggered) and 3 (0.8 to 1%)(SSW). Staggering at the SSW site reduces the losses slightly, about 0.2%. In the larger context wake losses are predicted to be very small and are well below the uncertainty of the wind resource estimates in the vicinity of the island (Spaulding et al, 2010c).

Considering both lee effects from the island and wake effects, the S site is the preferred location for a small wind farm.

References

Brower, M., 2007. Wind resource maps of Southern New England, prepared by True Wind Solutions, LLC, 10 p.

Grilli, A., M. L. Spaulding, C. Damon, and R. Sharma, 2010. High resolution application of the Technology Development Index (TDI) in state waters south of Block Island, Ocean SAMP project report, Ocean Engineering, University of Rhode Island, Narragansett, RI.

Grilli, A. and M. L. Spaulding, 2010. Estimation of offshore wind power resources based on Weibull distribution in Rhode Island coastal and offshore waters, Ocean Engineering, University of Rhode Island, Narragansett, RI.

Ishihara T., Yamaguchi A., Fujino Y., 2004. Development of a new wake model based on wind tunnel experiment, Poster in Global Wind Power, 2004,Tokyo, Japan.

Jensen, N.O., 1983. A note on wind generator interaction. RIS0-M-2411. RIS0 National Laboratory, Roskilde, Denmark, 16pp.

Larsen, G.C., 1988. A simple wake calculation procedure. RIS0-M-2760. RIS0 National Laboratory, Roskilde, Denmark, 58pp.

Hensel, J.V., 2009. Jacket Structures for offshore wind turbines in RI, MS Thesis, Ocean Engineering, University of Rhode Island, Narragansett, RI, 159p.

Pielke, R.A., W.R. Cotton, R.L. Walko, C.J. Tremback, W.A. Lyons, L.D. Grasso, M.E. Nicholls, M.D. Moran, D.A. Wesley, T.J. Lee, and J.H. Copeland, 1992: A comprehensive meteorological modeling system -- RAMS. Meteor. Atmos. Phys., 49, 69-91.

RAMS, 2010, Regional Atmospheric Modeling System Technical Manual, Weather Flow,

Renne, D. S., W. F. Sandusky, and D. L. Hadley, 1982. Meteorological field measurements at potential and actual wind turbine sites, US Department of Energy, Pacific Northwest Laboratory, Richland, WA, PNL -4431, UC-60, September 1982

Roark, T., 2008. Offshore wind energy: An international perspective, Roger Williams University, Marine Law Symposium, October 23, 2008.

Spaulding, M. L., A. Grilli, C. Damon, and G. Fugate, 2010a. Application of Technology Development Index and Principal Component Analysis and Cluster Methods to Ocean Renewable Energy Facility Siting, Marine Technology Society, Special Issue on Marine Technology for Offshore Wind, Vol. 44, No 1, January/ February 2010, pg 8-23.

Spaulding, M. L., M. Bell, J. Titlow, A. Grilli, R. Sharma, L. Decker, and D. Mendelsohn, 2010b. Meteorological model based wind resource assessment in the vicinity of Block Island, Ocean Engineering, University of Rhode Island, Narragansett, RI

Spaulding, M. L., A. Grilli, A. Crosby, and R. Sharma, 2010c, Evaluation of wind statistics and energy resources in southern RI coastal waters, Ocean Engineering, University of Rhode Island, Narragansett, RI

Titlow, J. and D. Morris, 2010. Block Island modeling analysis, WeatherFlow Inc., Poquoson, VA with model simulations by MetLogics, Fort Collins, CO.

Tremback, C. J. and R. L. Walko, 2010. Regional Atmospheric Modeling System, Users Guide-Introduction, Version 6.0, ATMET, Boulder, CO.

Table 1 List of WeatherFlow simulation dates and their associated directions.

1. ***North: January 4th 2008***
2. ***Northeast: September 22nd 2008***
3. ***Northeast 2: April 17th 2008***
4. ***East: September 24th 2008***
5. ***Southeast: October 25th 2008***
6. South: September 6th 2008
7. ***South 2: November 8th 2008***
8. ***Southwest: July 8th 2008***
9. ***West: December 22nd 2008***
10. Northwest 1: October 30, 2008
11. Northwest 2: November 22 2008
12. ***Northwest 3: February 23 2009***

*Sites in **bold italics** were used in the analysis as the base case.*

Table 2 Sensitivity to climatology

Wake effect: Sensitivity to climatology				
	Power loss (%)			
Climatology 1: WIS101	***min***	***max***	***mean***	***std***
Site1 (SE)	1.1	2.3	1.7	0.43
Site2 (SSW, Stag.)	0.6	1.0	0.8	0.14
Site3 (SSW, SE-W)	0.7	1.6	1.1	0.29
Climatology 2: Block Island Tower	***min***	***max***	***mean***	***std***
Site1 (SE)	1.4	2.3	1.8	0.35
Site2 (SSW, Stag)	0.7	1.1	0.9	0.16
Site3 (SSW, E-W)	0.6	1.3	0.9	0.25
Climatology 3: Buzzard Bay	***min***	***max***	***mean***	***std***
Site1 (SE)	1.1	2.4	1.8	0.46
Site2 (SSW,Stag.)	0.6	0.9	0.8	0.13
Site3 (SSW, E-W)	0.7	1.5	1.0	0.26

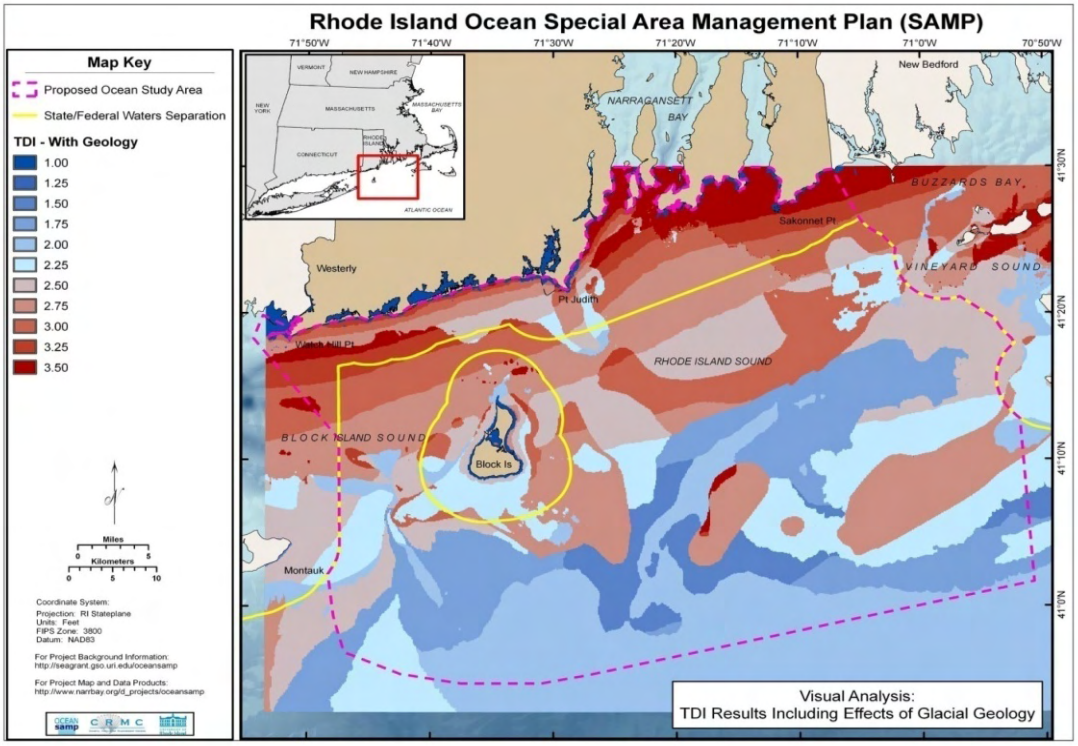

Figure 1 Contours of non-dimensional *TDI* for the Ocean SAMP study area, with glacial geology (Spaulding et al, 2010a).

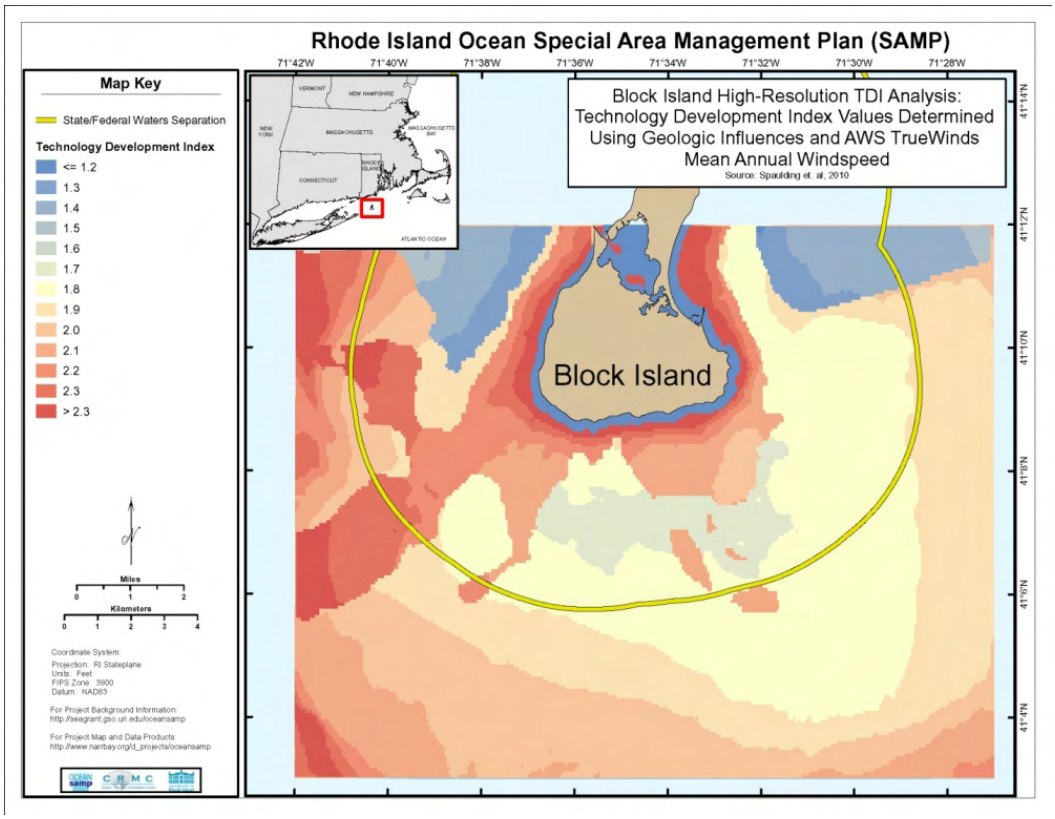

Figure 2 Technology Development Index (TDI) for Block Island Study area with geology (Grilli et al, 2010a) using AWS TrueWinds mean annual winds (Brower, 2007).

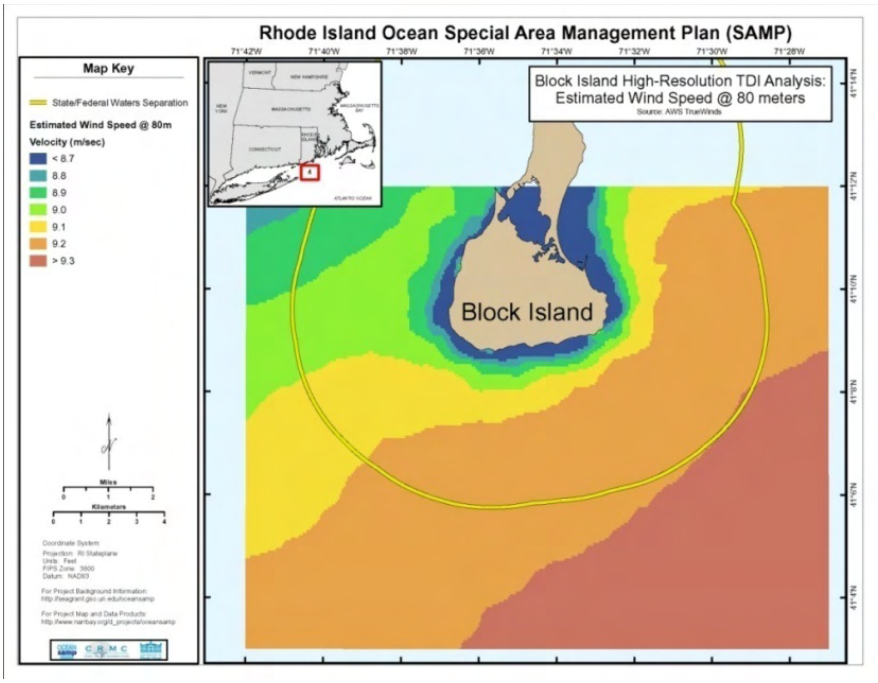

Figure 3 Estimated mean annual wind speed at 80 m from AWS TrueWinds data (Brower, 2007) for Block Island study area.

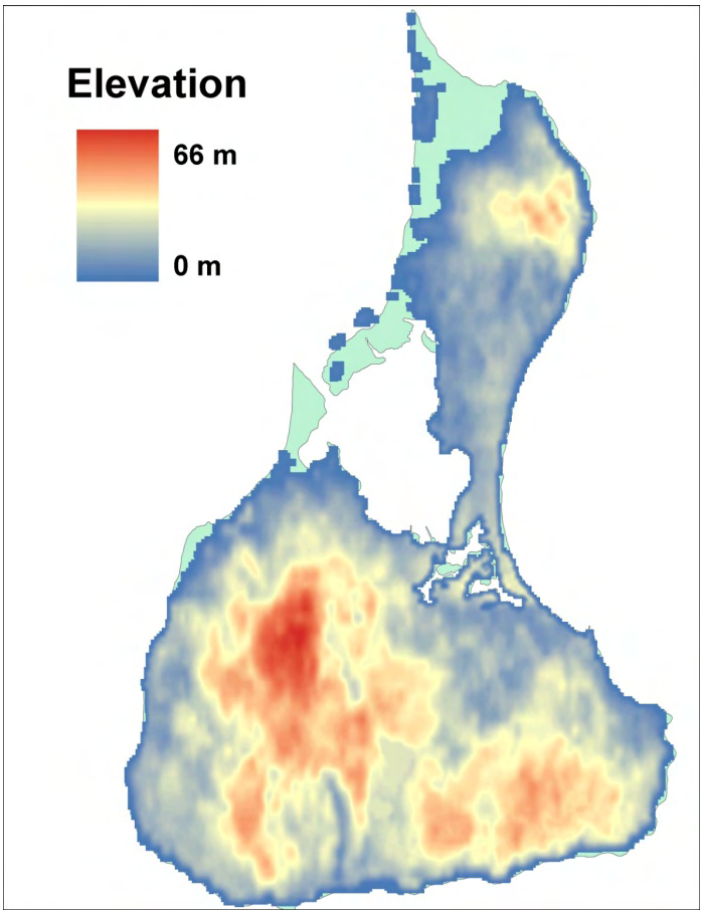

Figure 4 Block Island topography (RI GIS)

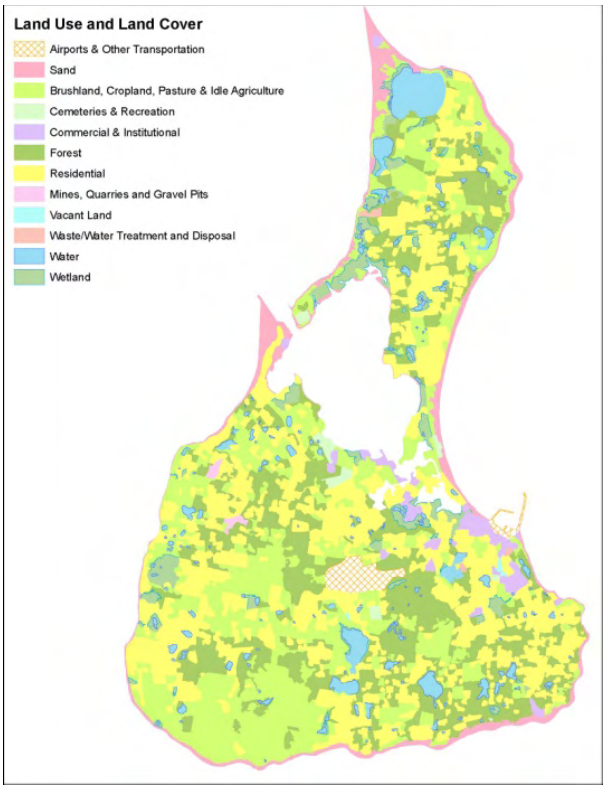

Figure 5 Block Island Land Cover (RI GIS).

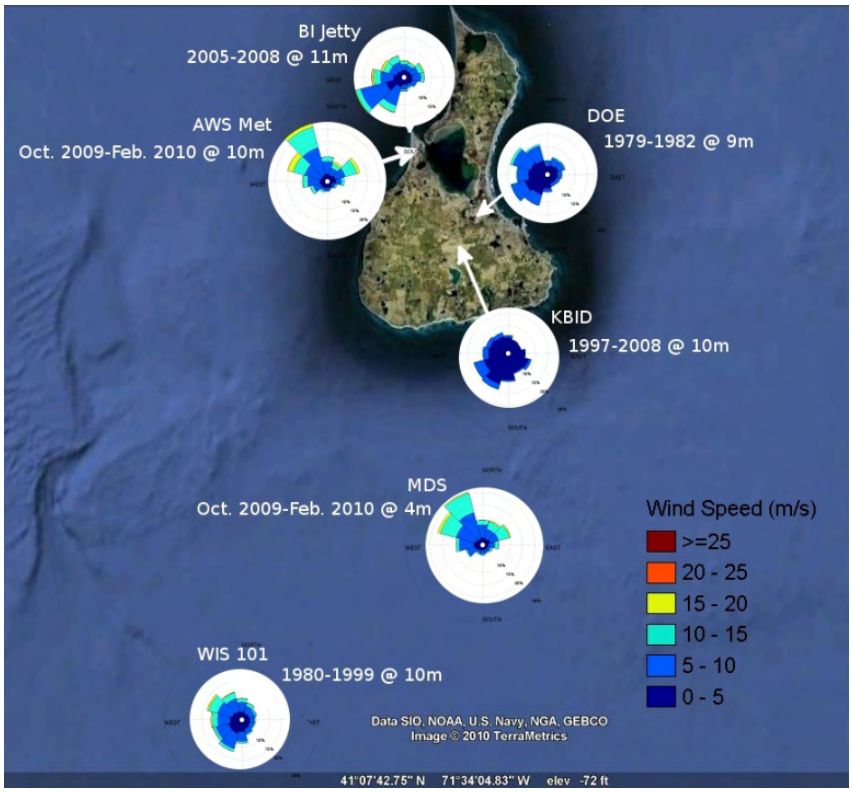

Figure 6 Wind speed frequency roses in the vicinity of Block Island.

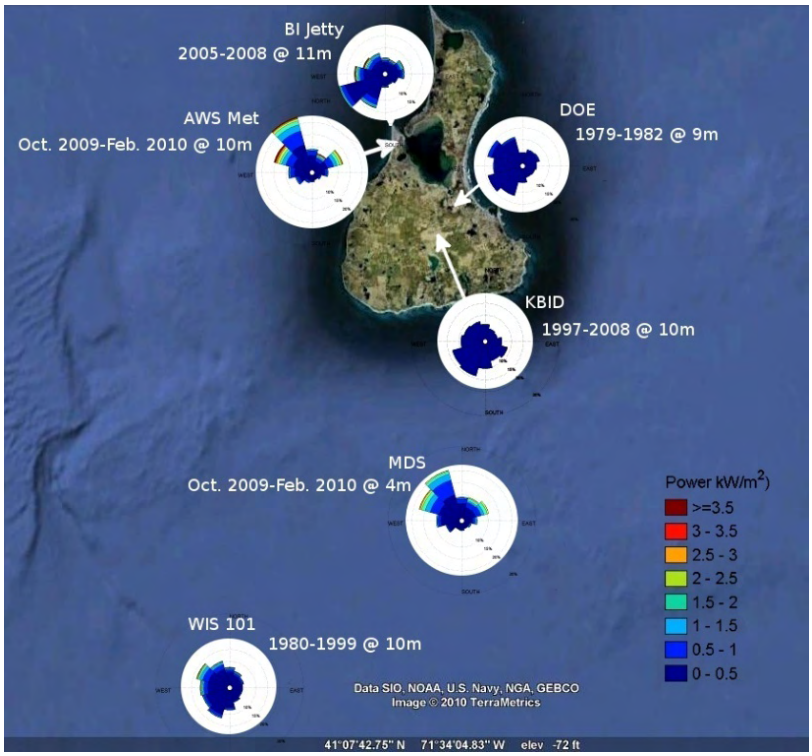

Figure 7 Wind power density roses in the vicinity of Block Island

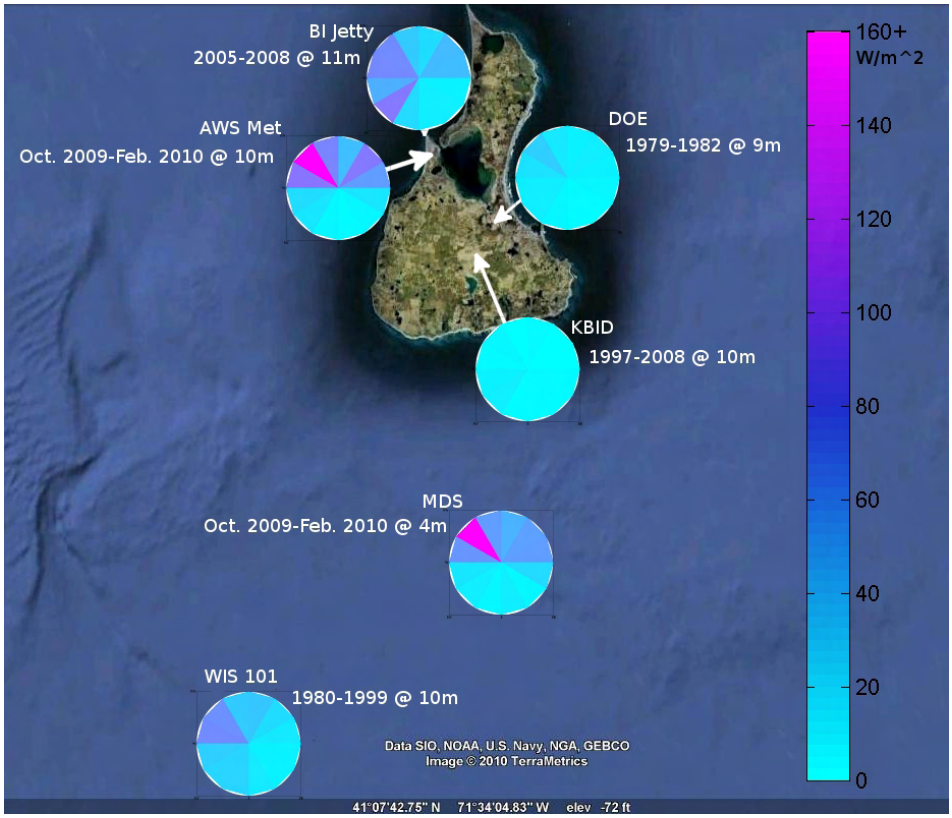

Figure 8 Average wind power density versus direction in the vicinity of Block Island.

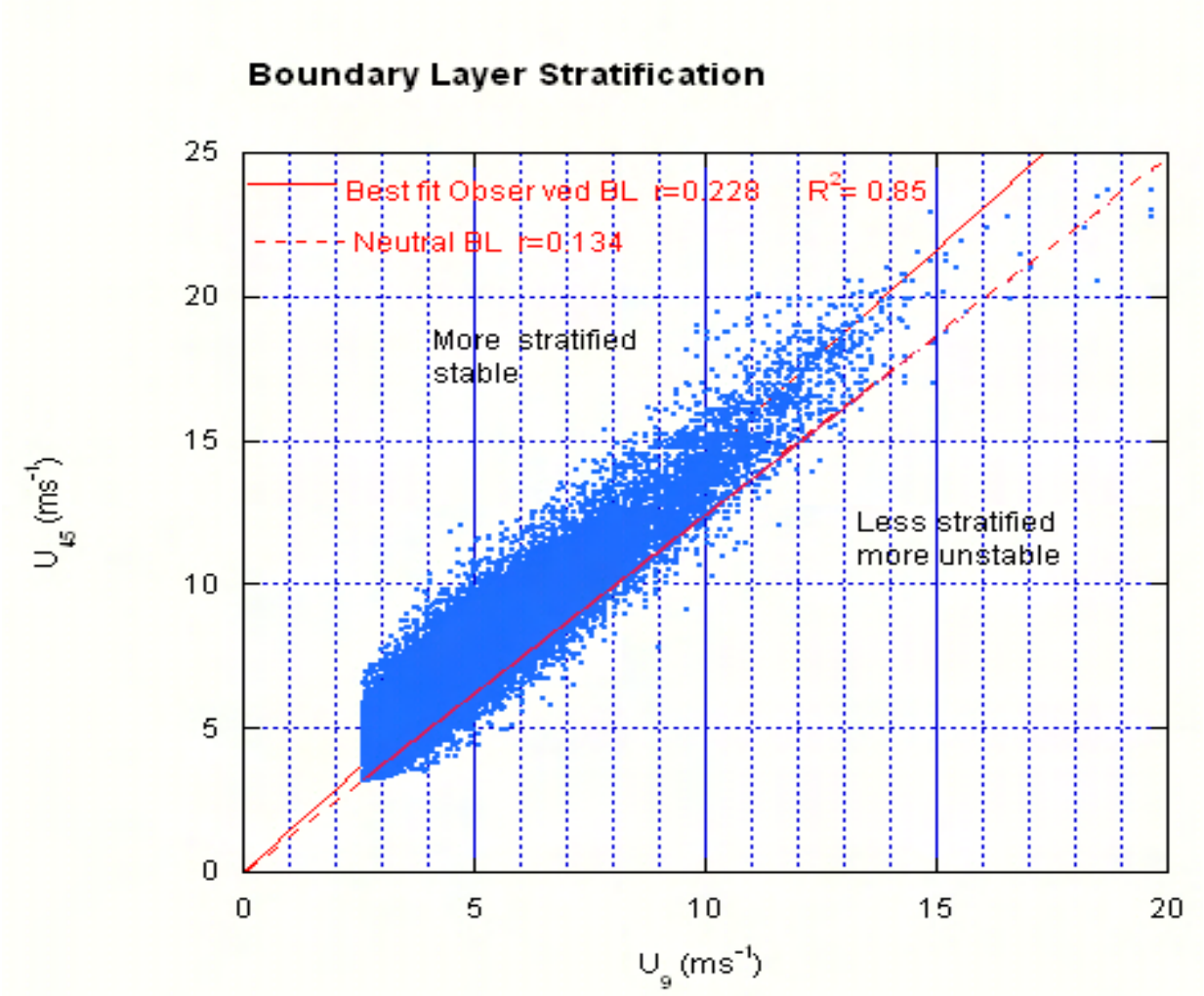

Figure 9 Observed wind speeds at 9 m vs those at 45 m from the DOE observations, 1979 to 1982. A neutral boundary layer is provided for reference and a linear least squares regression line for the shear coefficient is shown.

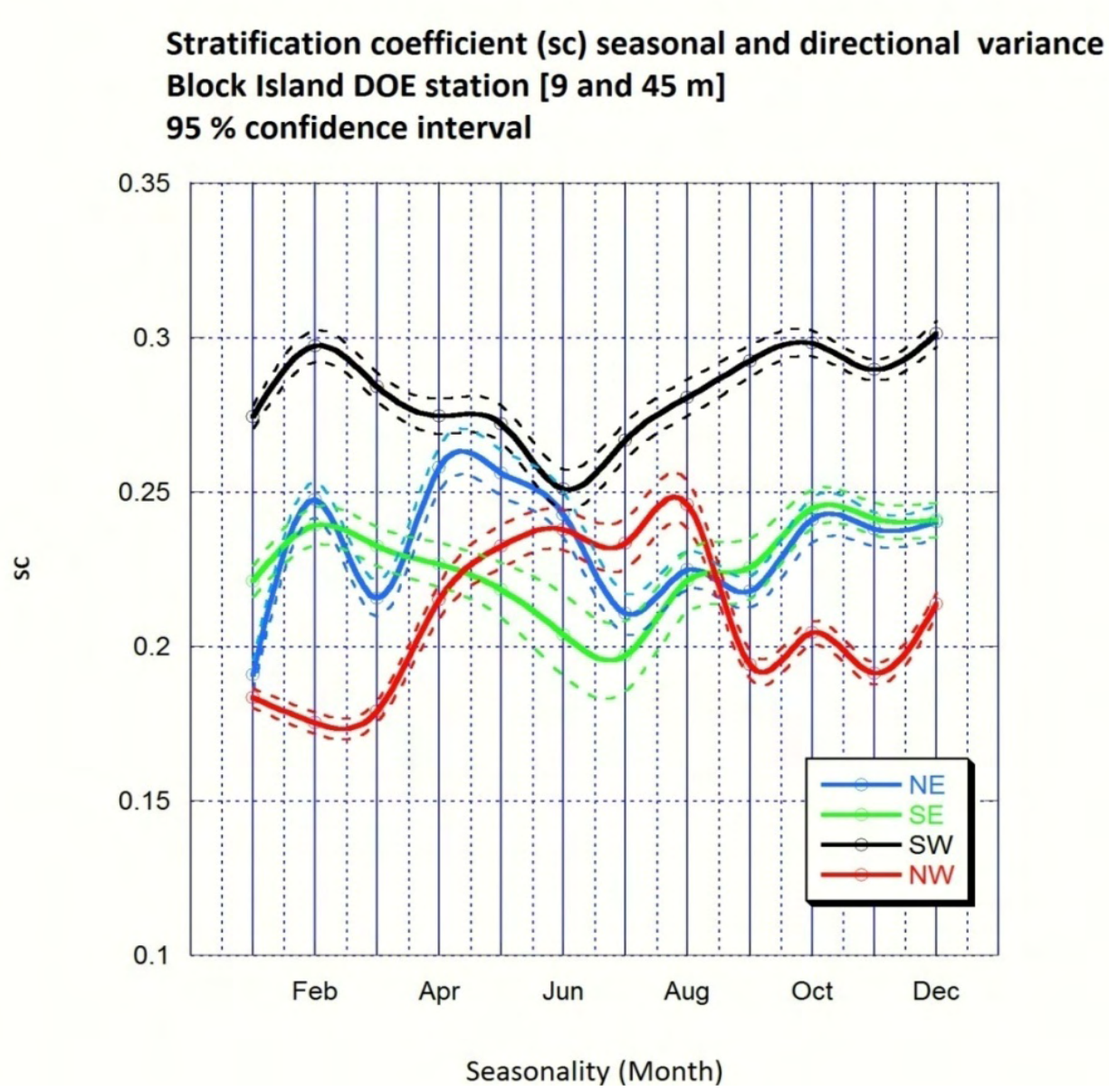

Figure 10 Shear coefficient for the DOE site vs month and direction. The upper and lower 95% confidence limits are shown.

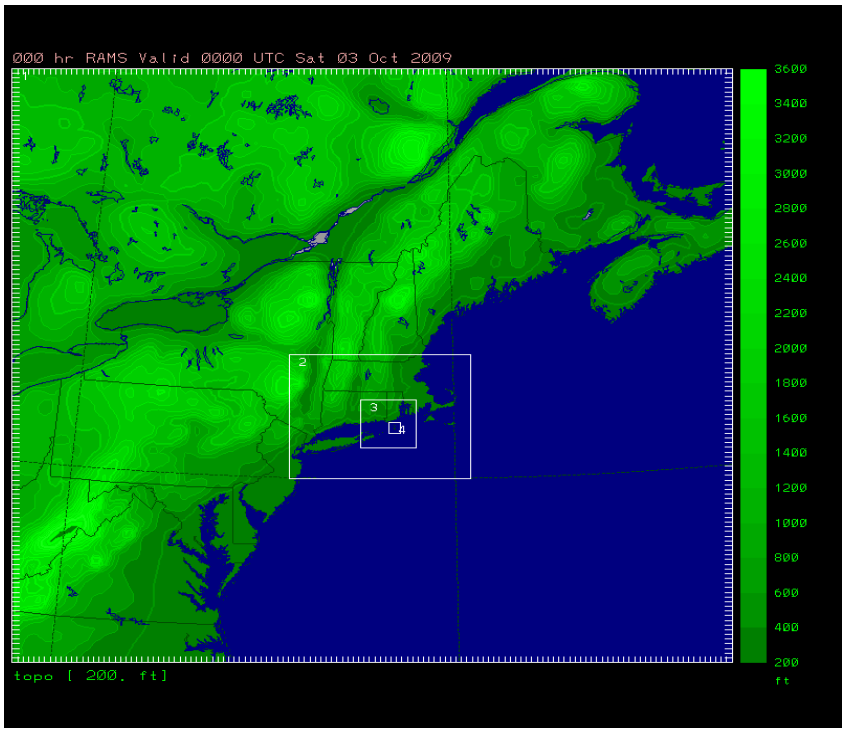

Figure 11 Nested grid system showing 6 km (Grid 2), 2 km (Grid 3) and 0.5 km (Grid 4) grid boundaries.

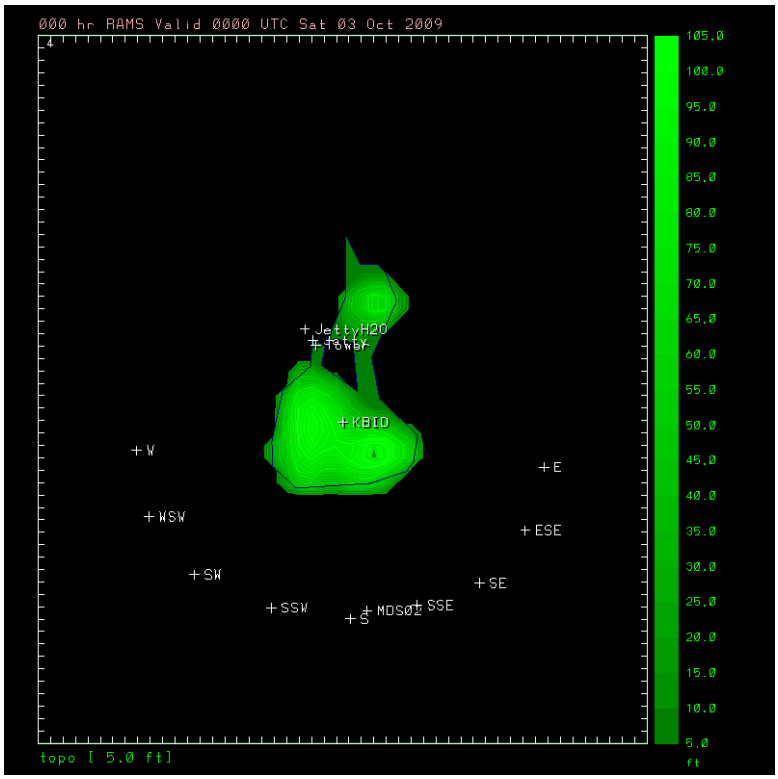

Figure 12 Grid 4 showing topographic relief of Block Island. The locations at which model time series were generated are shown, including E, ESE, SE, SSE, S, SSW, SW, WSW, and W along state water boundary line, and at observation locations KBID, BI Jetty, AWS Met, and MSD.

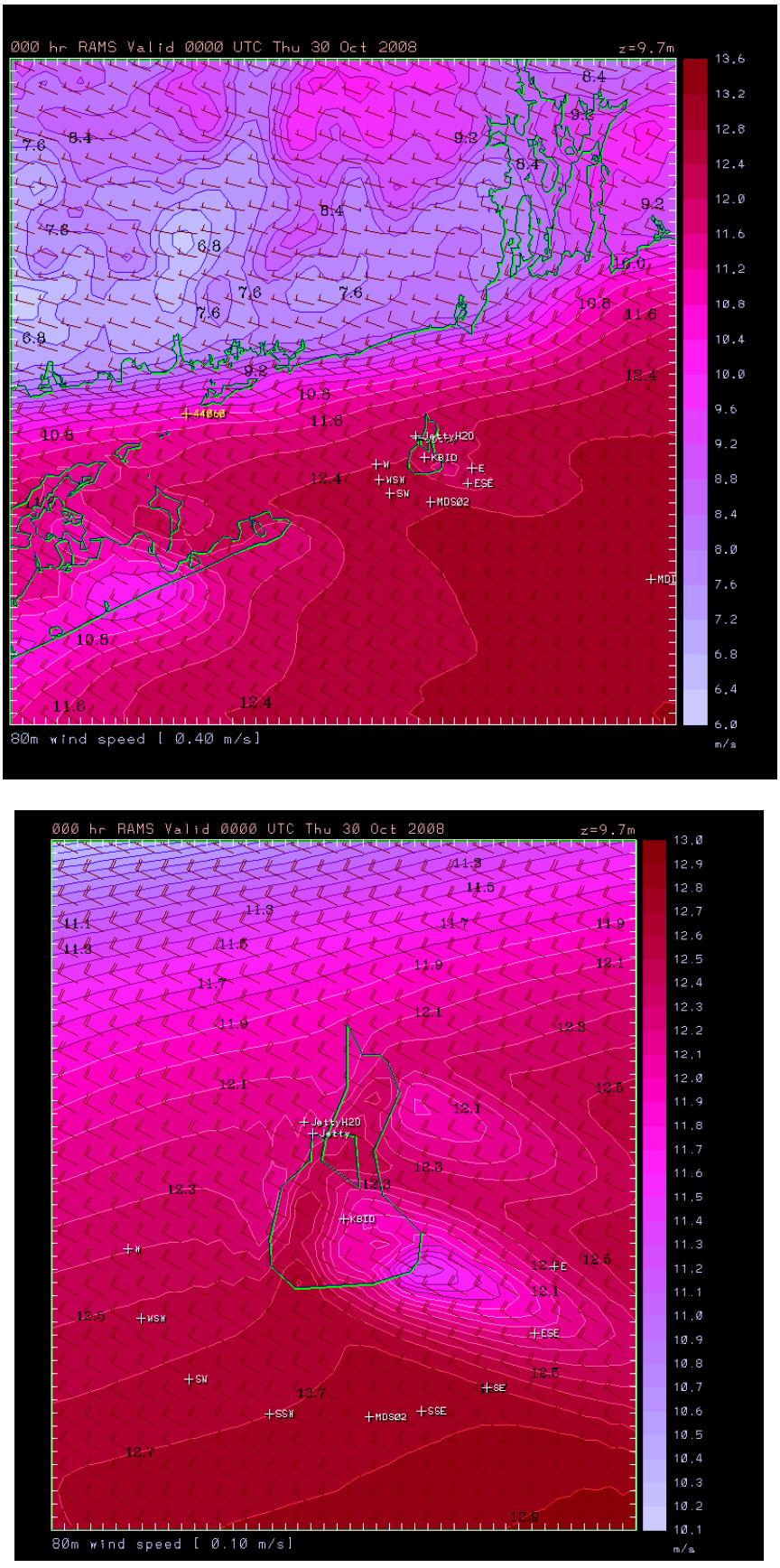

Figure 13 Model predicted wind speeds at 80 m at 0000 UTC on October 30, 2008 (NW). Upper panel Grid 3 and lower panel Grid 4.

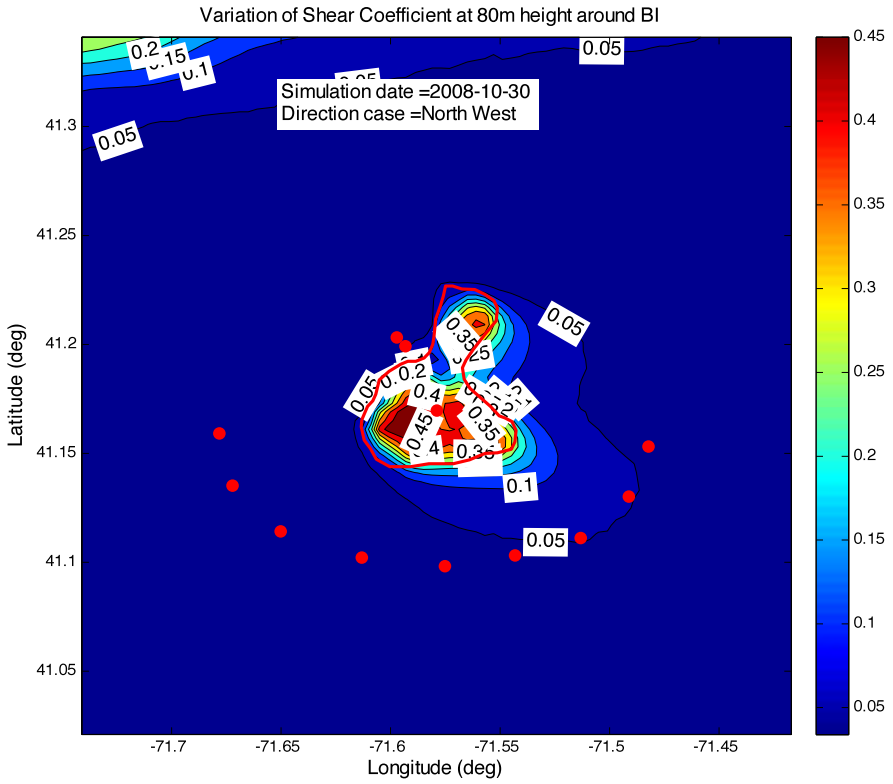

Figure 14 Model predicted shear coefficient for October 30, 2008 simulation.

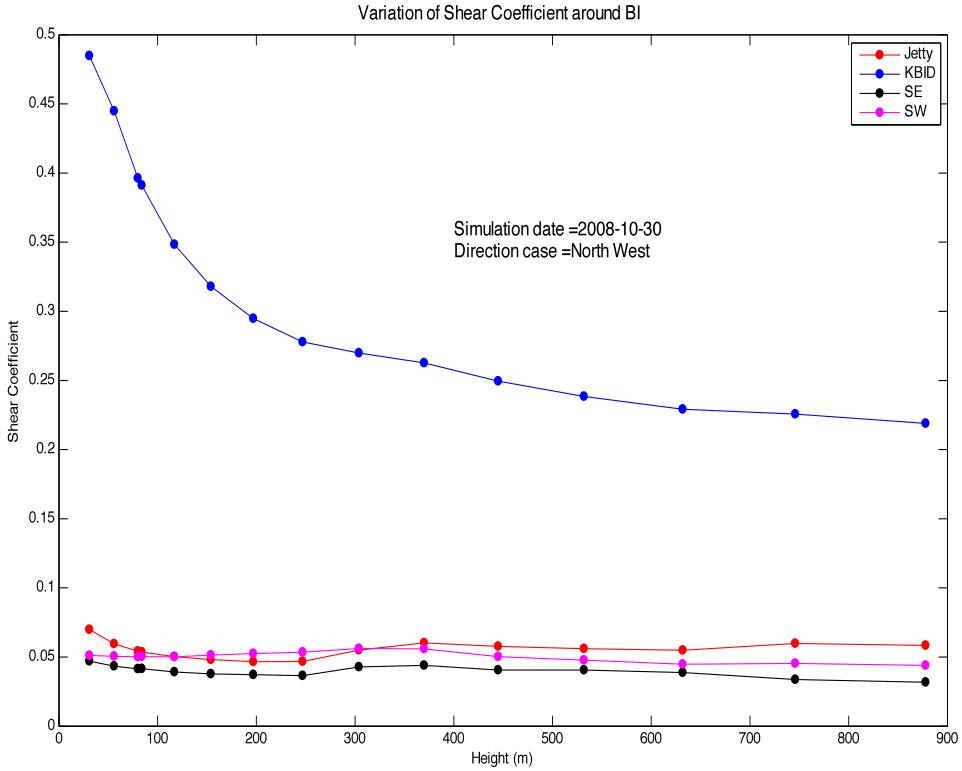

Figure 15 Model predicted shear coefficient at SE, SW, KBID, and Block Island Jetty locations for the October 30, 2008 simulation.

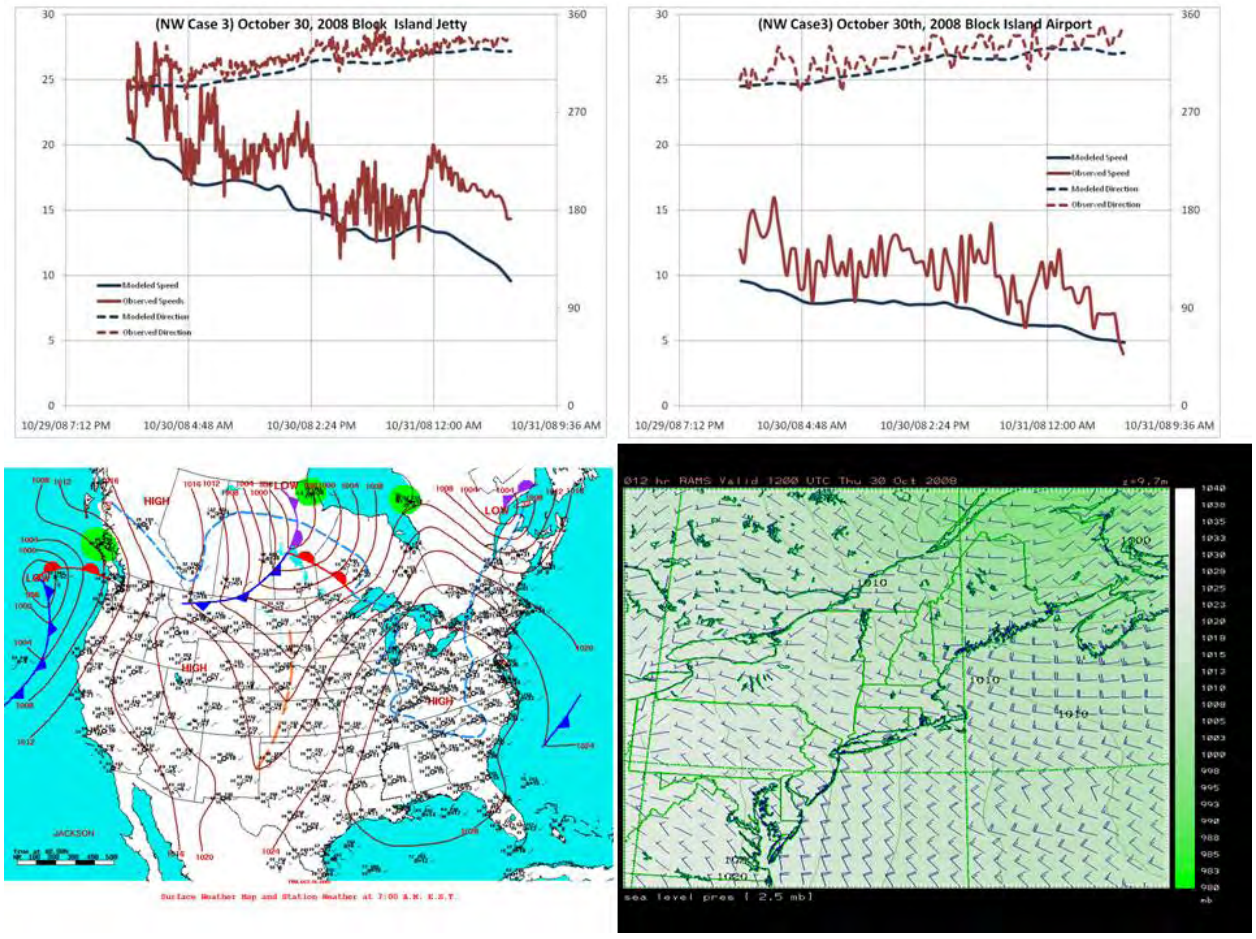

Figure 16 Comparison of model predictions to observations at Block Island Jetty (upper left) and KBID (upper right) on October 30, 2008. Large scale atmospheric forcing field (lower left) and NAM model predictions for Northeastern US (lower right).

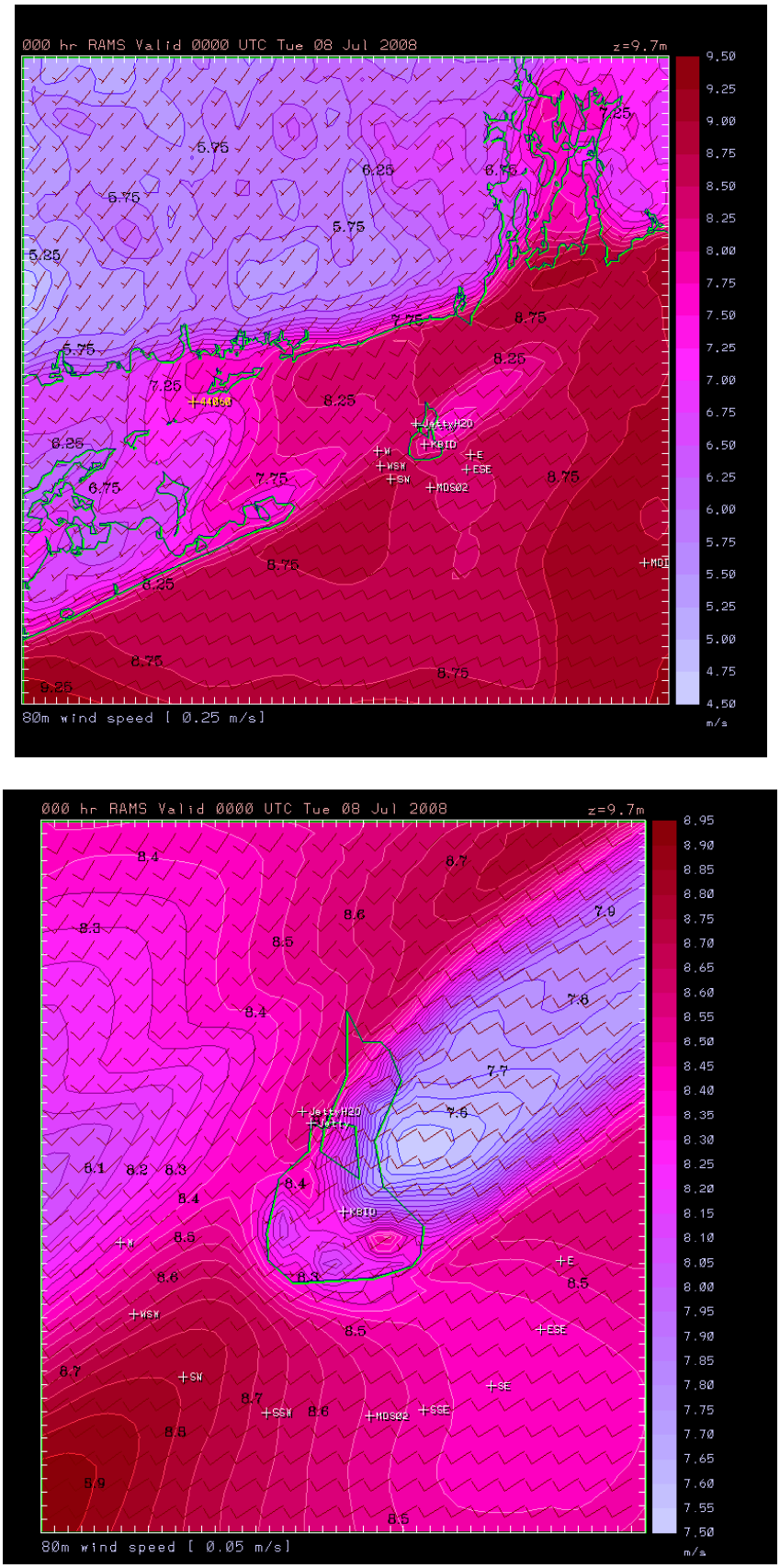

Figure 17 Model predicted wind speeds at 80 m at 0000 UTC on July 8, 2008 (SW). Upper panel- Grid 3 and lower panel - Grid 4.

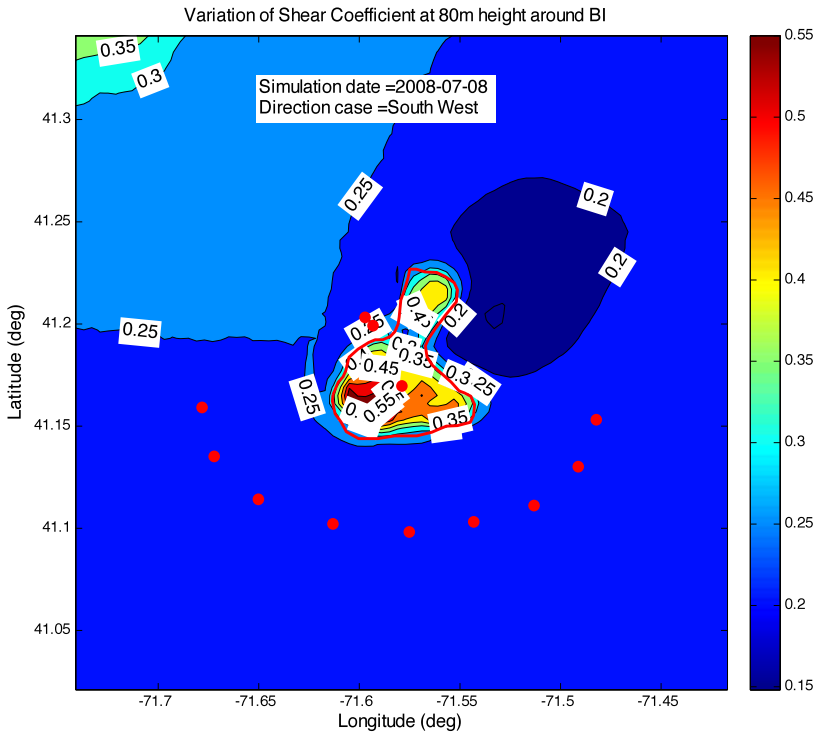

Figure 18 Model predicted shear coefficient for July 8, 2008 simulation.

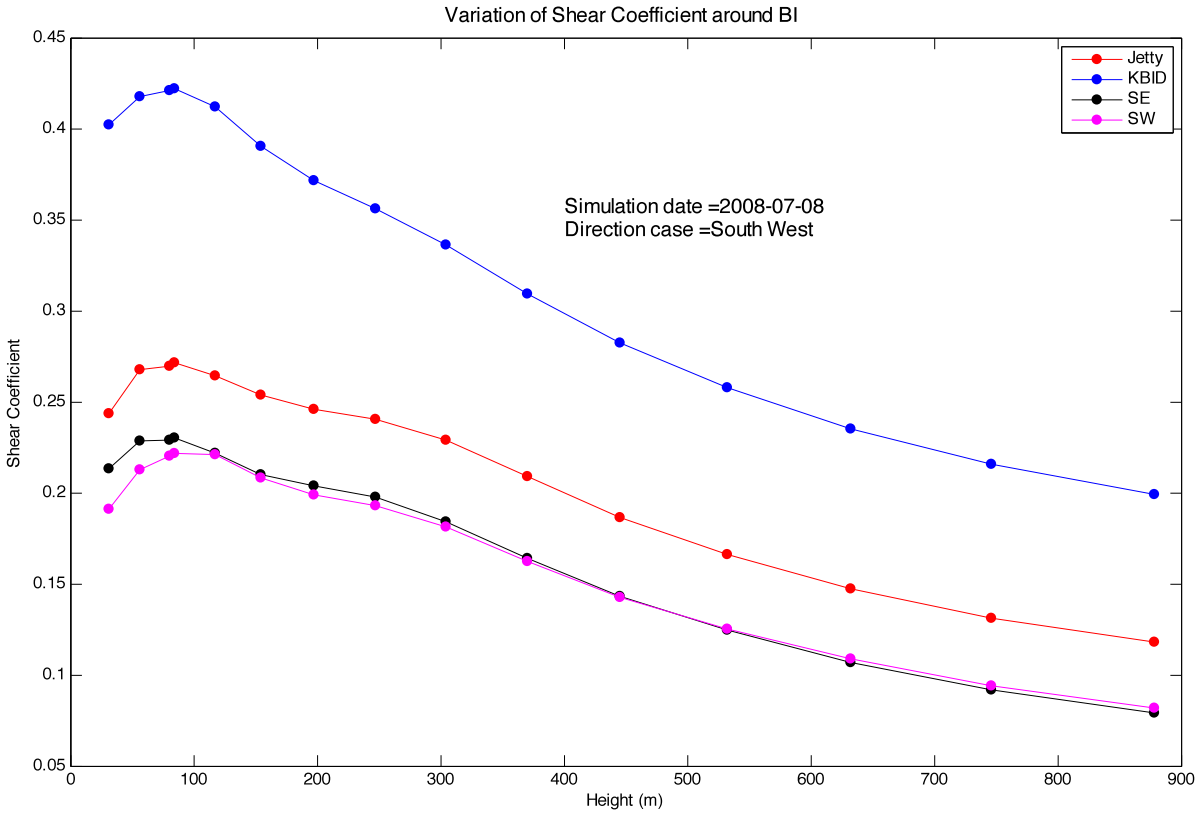

Figure 19 Model predicted shear coefficient at SE, SW, KBID, and Block Island Jetty locations for the July 8, 2008 simulation.

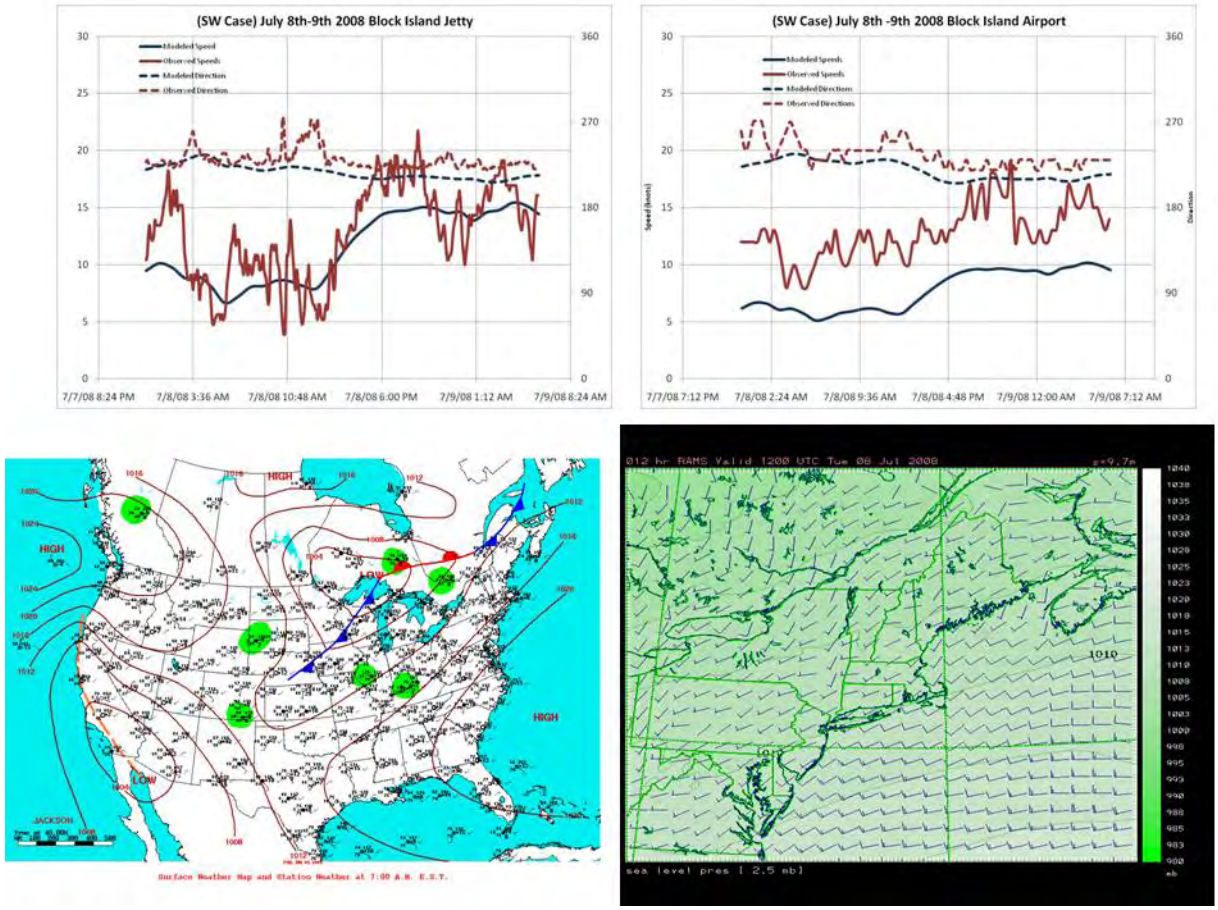

Figure 20 Comparison of model predictions to observations at Block Island Jetty (upper left) and KBID (upper right) on July 8, 2008. Large scale atmospheric forcing field (lower left) and NAM model predictions for Northeastern US (lower right).

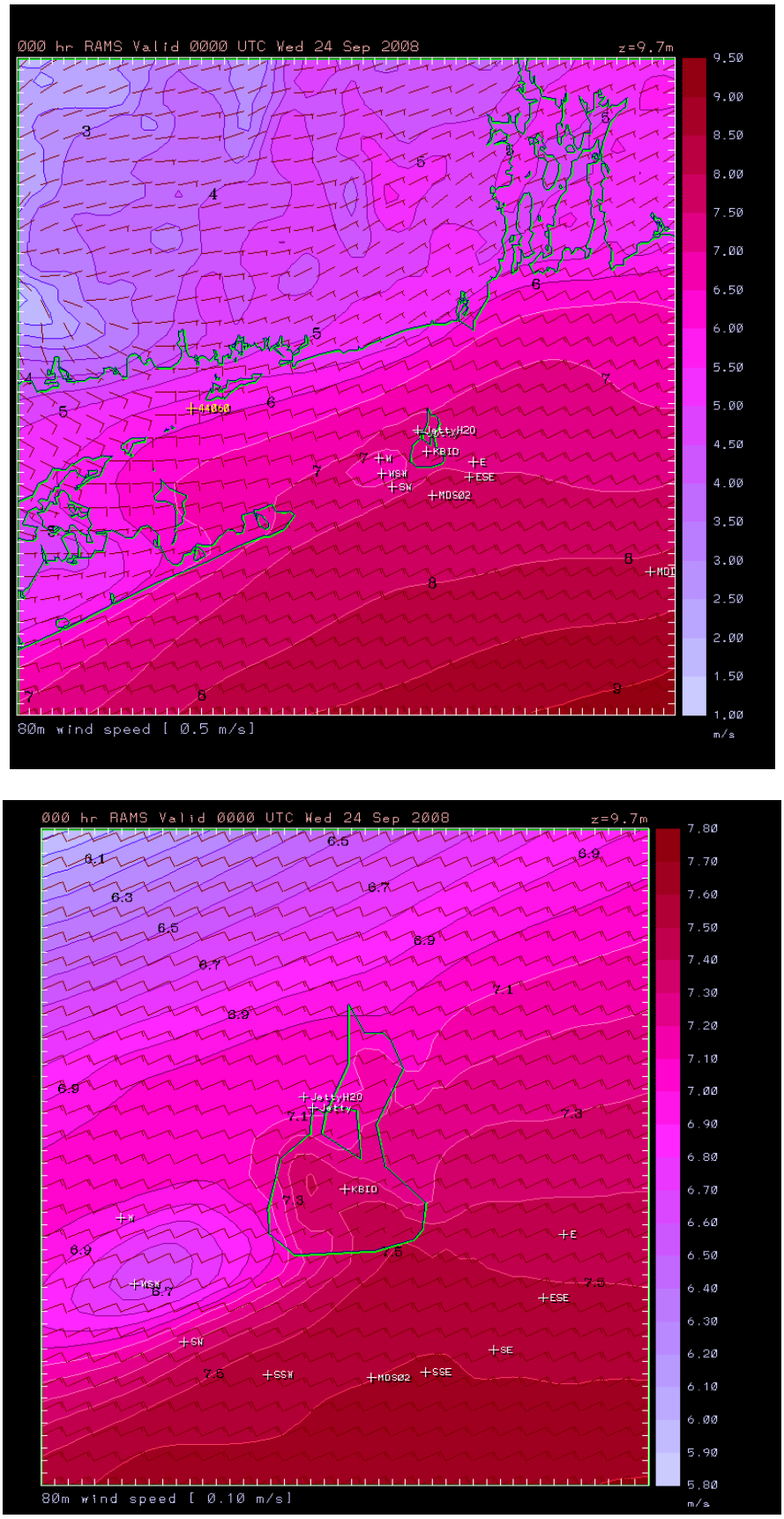

Figure 21 Model predicted wind speeds at 80 m at 0000 UTC on September 24, 2009 (NE). Upper panel - Grid 3 and lower panel - Grid 4.

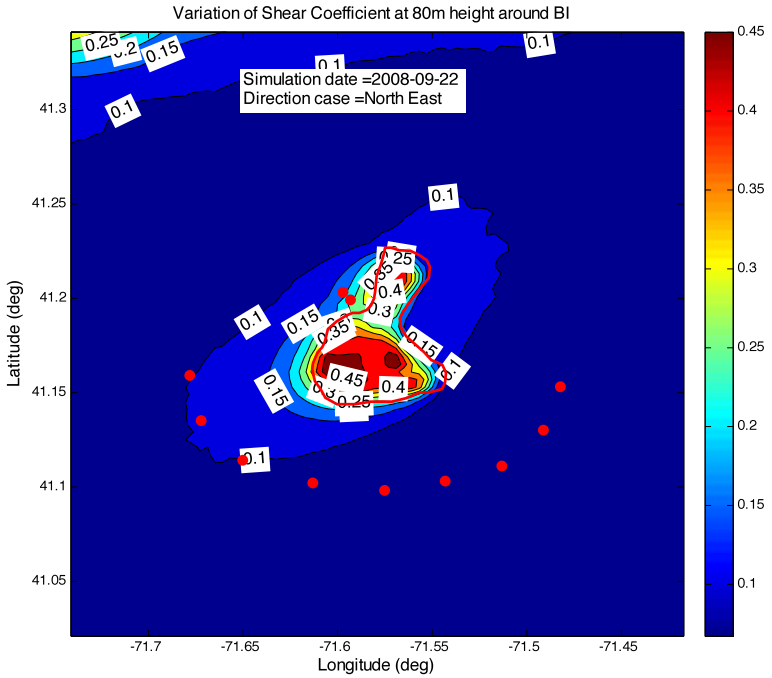

Figure 22 Model predicted shear coefficient for September 22, 2008 simulation.

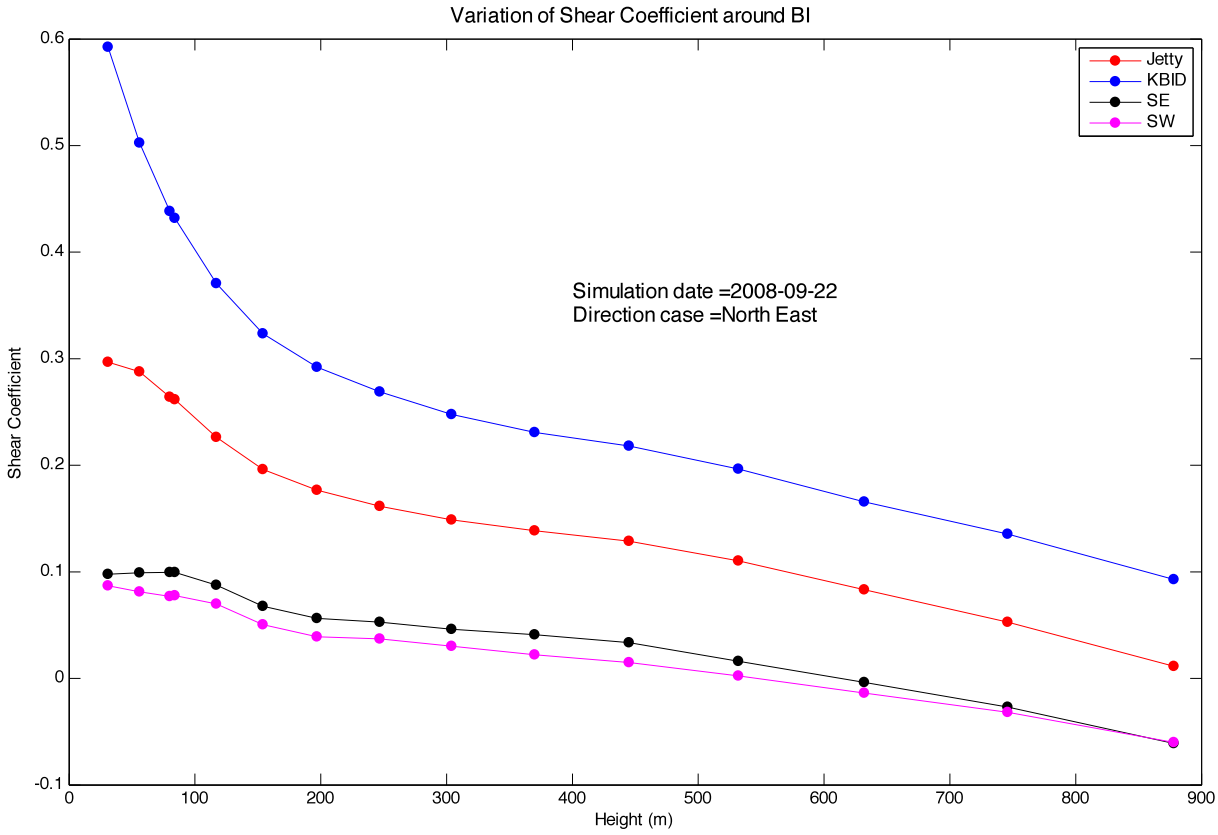

Figure 23 Model predicted shear coefficient at SE, SW, KBID, and Block Island Jetty locations for the September 22, 2008 simulation.

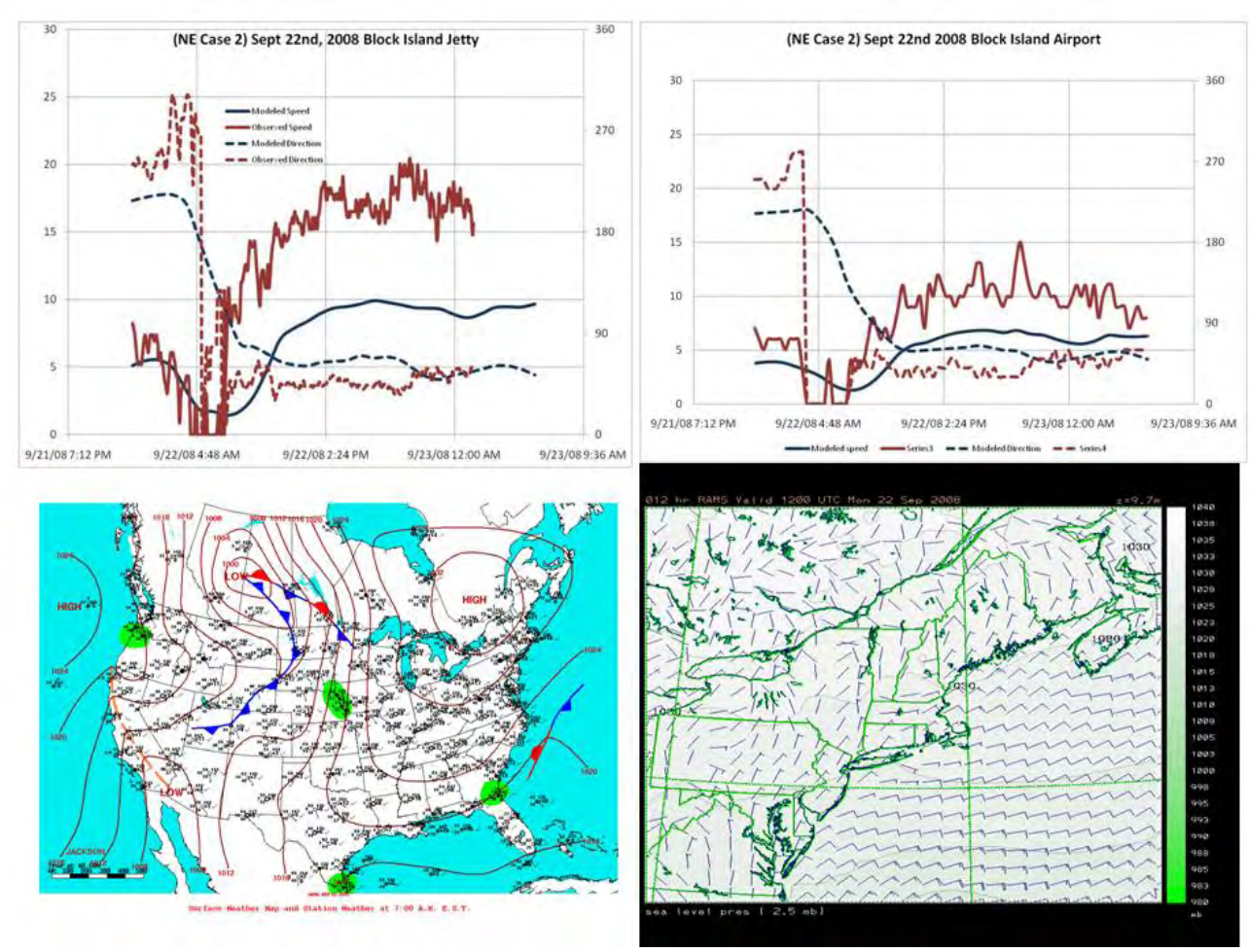

Figure 24 Comparison of model predictions to observations at Block Island Jetty (upper left) and KBID (upper right) on September 22, 2008. Large scale atmospheric forcing field (lower left) and NAM model predictions for Northeastern US (lower right).

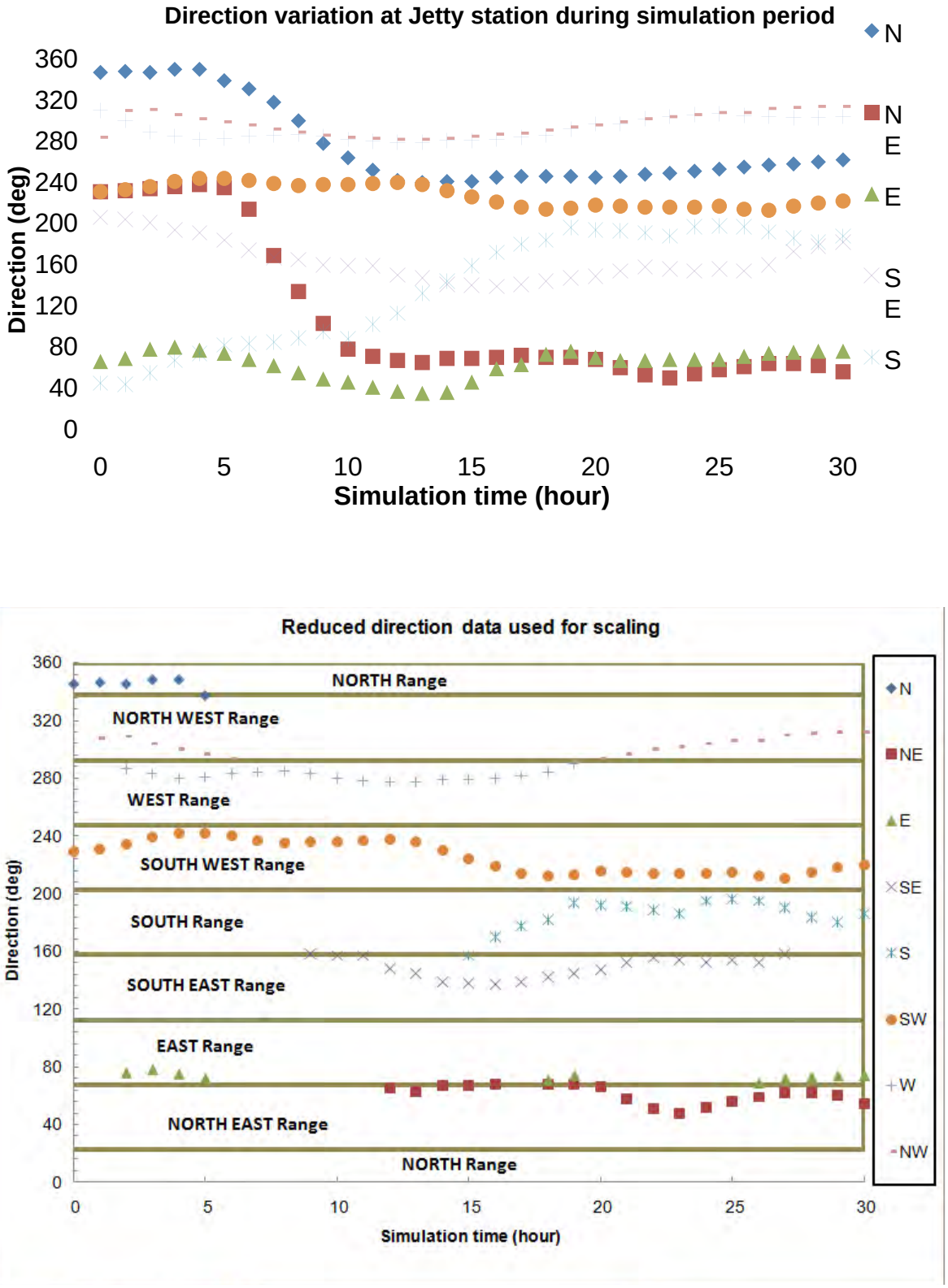

Figure 25 Wind direction as a function of time for the eight directional cases at Block Island, Jetty, upper panel includes all data and the lower panel only data that were within 15 degrees of the desired direction.

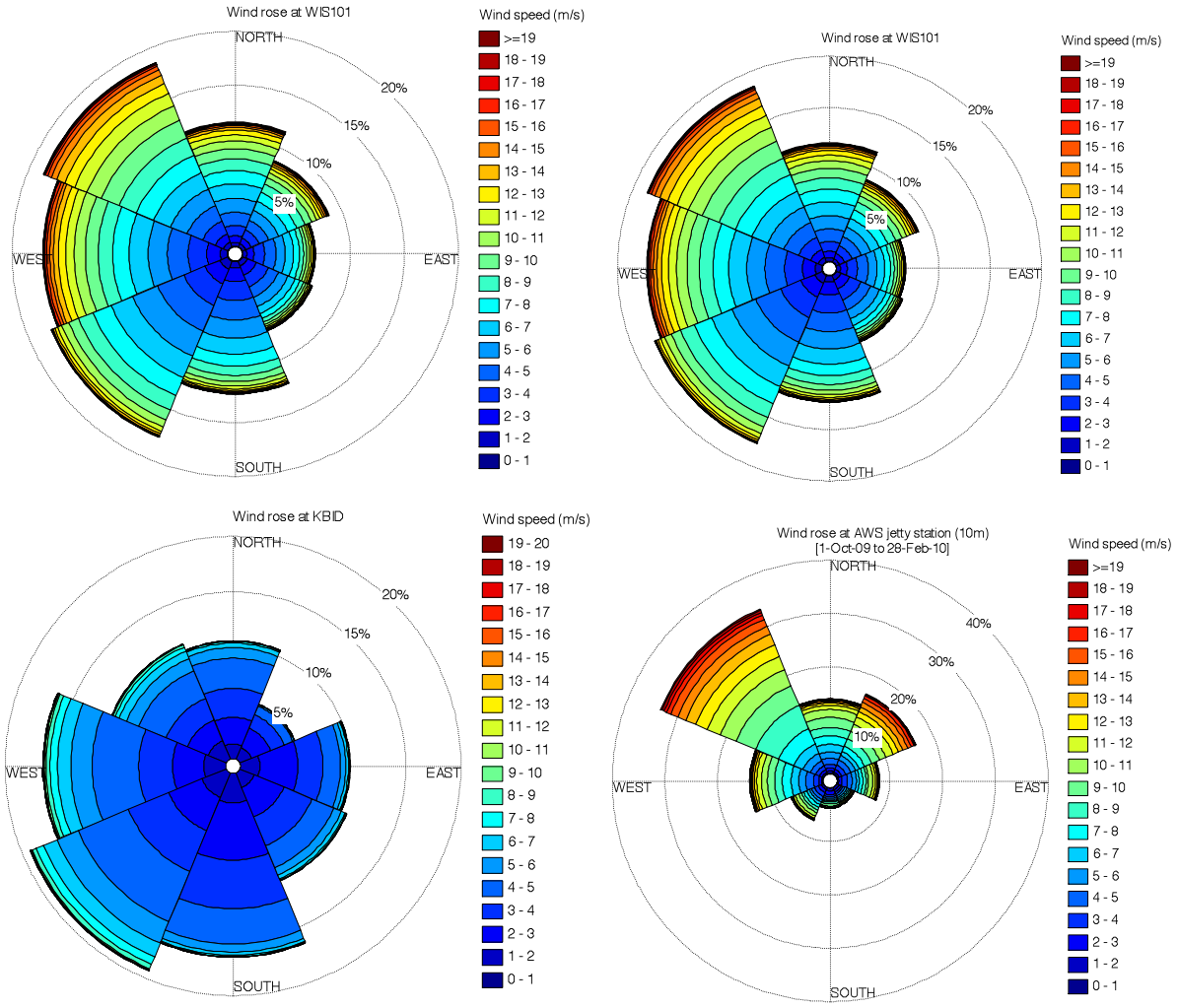

Figure 26 Wind roses at WIS100 and 101, KBID, and AWS Met all at 10 m.

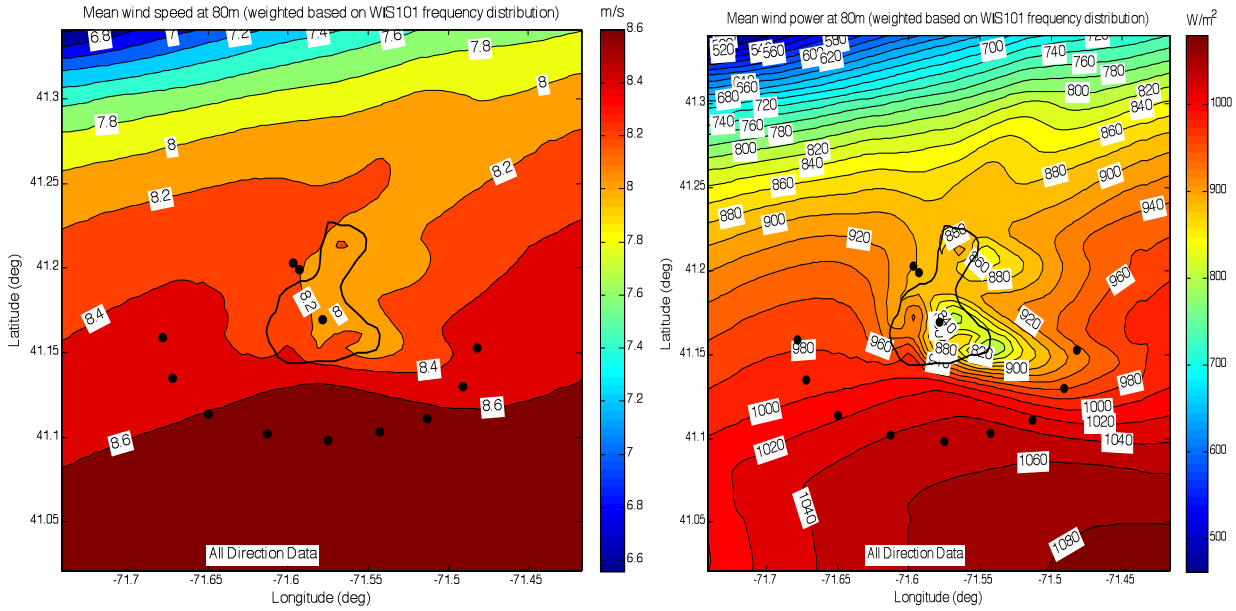

Figure 27 Template based model predictions of the mean annual wind speed (left) and wind power density (right) at 80 m, using the WIS101 wind rose. All direction data.

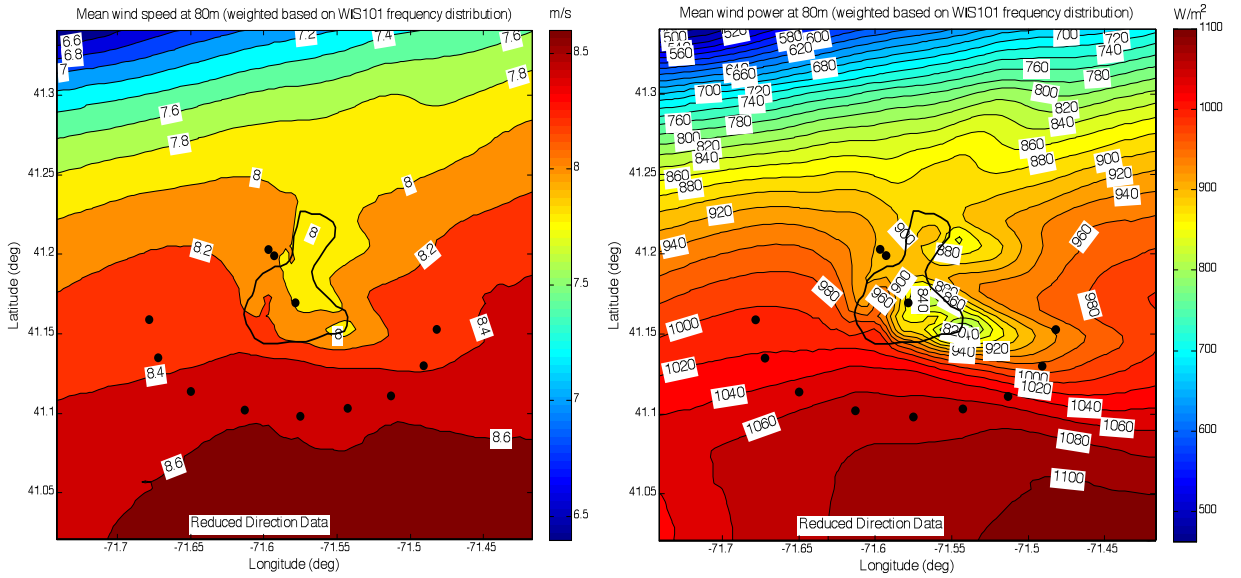

Figure 28 Template based model predictions of the mean annual wind speed (left) and wind power density (right) at 80 m, using the WIS101 wind rose. Reduced direction data.

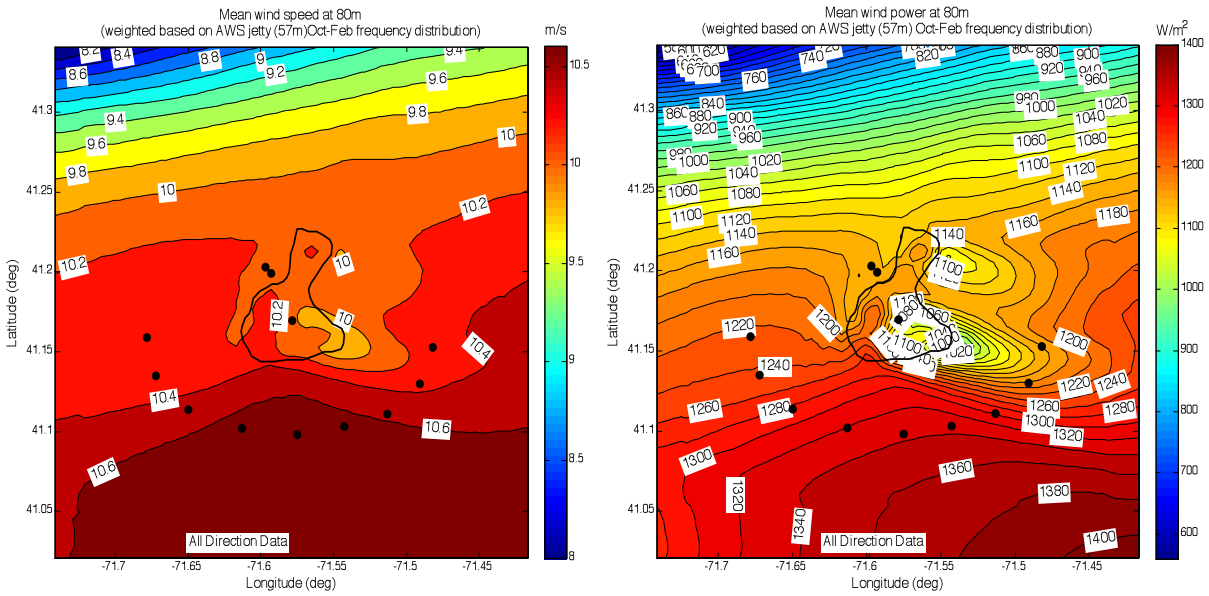

Figure 29 Template based model predictions of the mean annual wind speed (left) and wind power density (right) at 80 m, using the AWS Met 57m wind rose. All direction data.

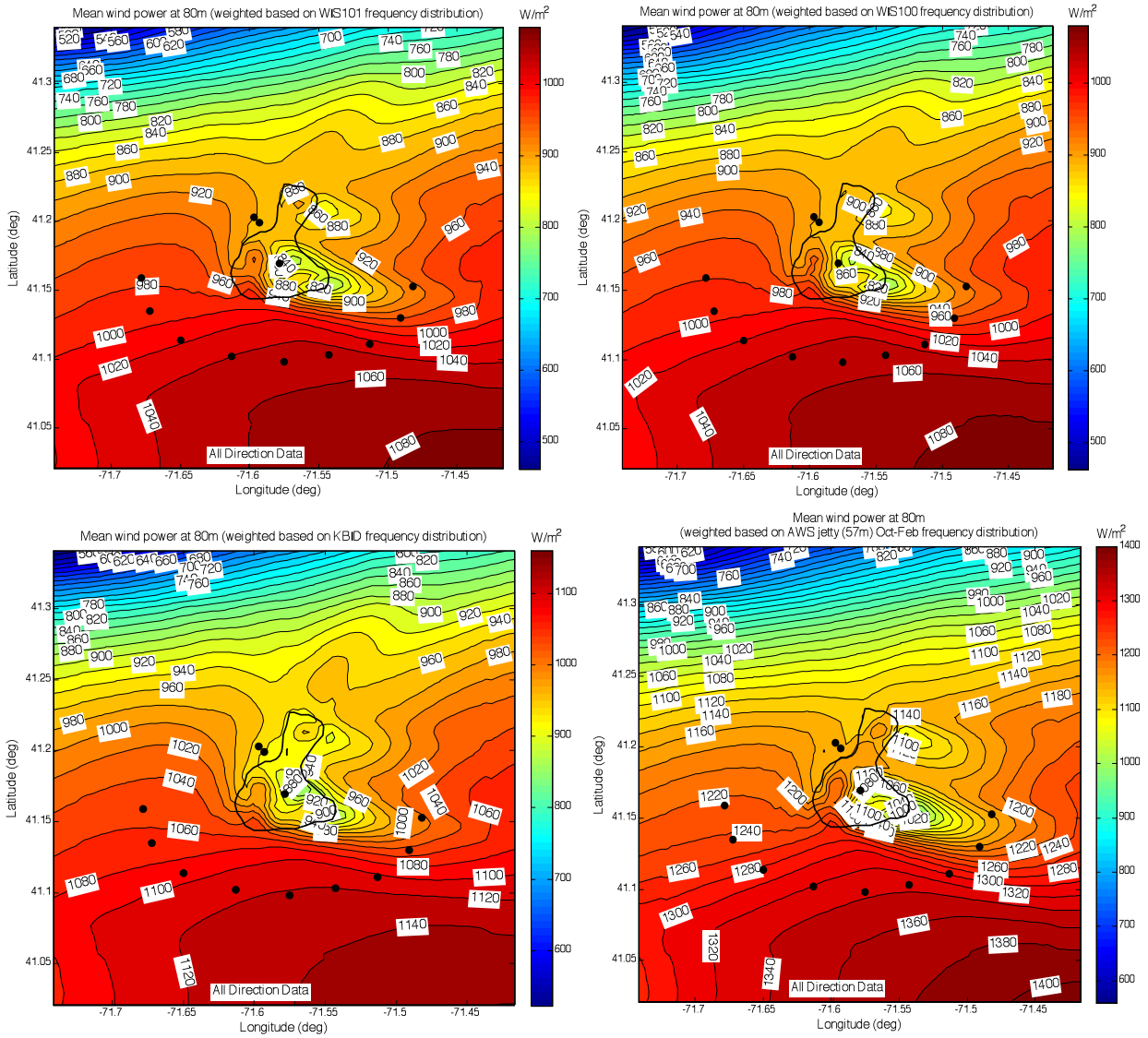

Figure 30 Template based method predictions of wind power density at 80 m using wind roses from WIS 101 (upper left), WIS 101 (upper right), KBID (lower left) and AWS Met (lower right).

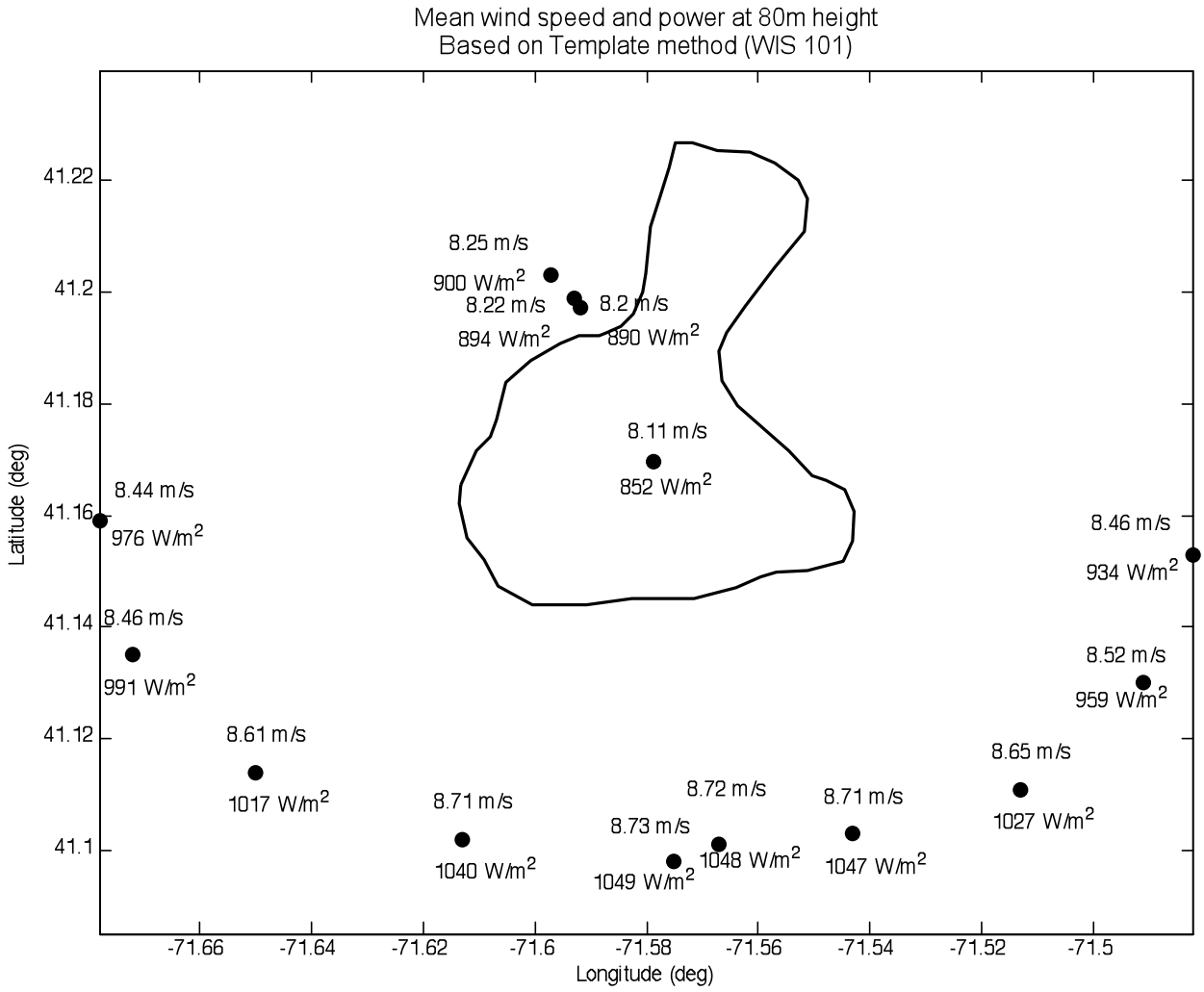

Figure 31 Template model predicted mean wind speed and power at selected locations along the state water boundary line as well as at KBID, Block Island Jetty, MDS, and AWS Met stations using WIS 101 wind rose.

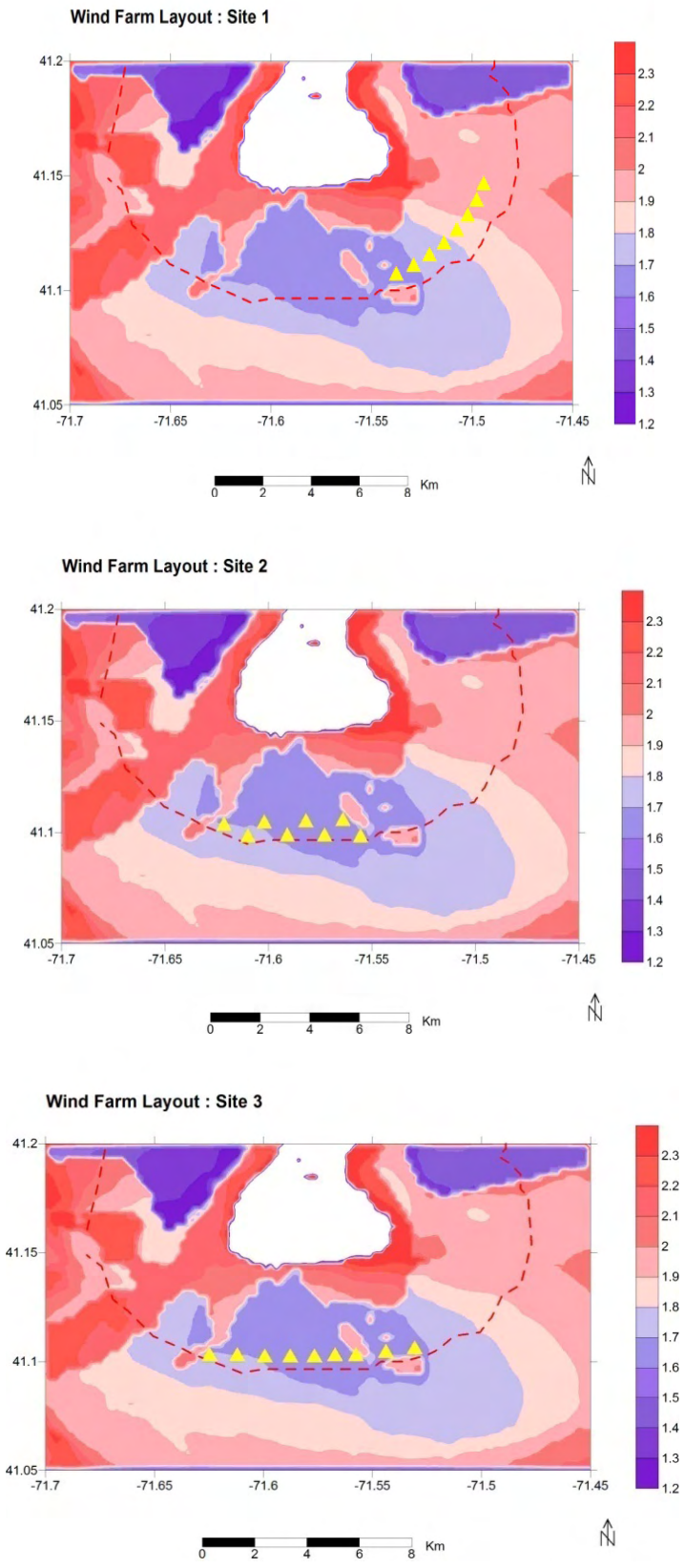

Figure 32 Location of proposed wind farm for wake loss study, SE - Site 1; S- Staggered, Site 2; and S – Un-staggered, Site 3.

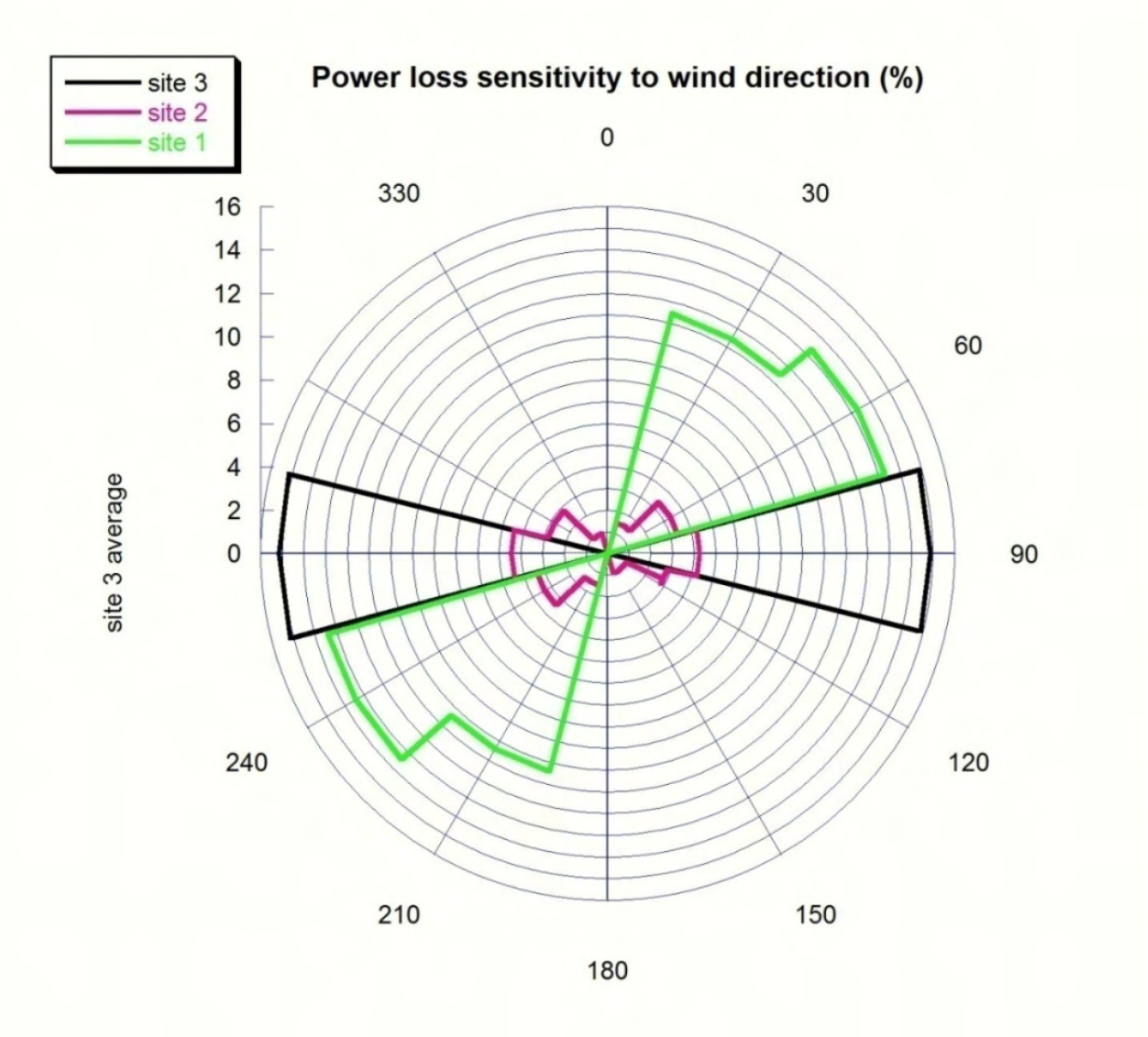

Figure 33 Power loss wind rose due to wake effects (%) for SE - Site 1; S- Staggered, Site 2; and S – Un-staggered, Site 3.

Appendix A

Wind frequency and power density (seasonal and annual) roses and Weibull distribution fits for selected stations in the SAMP study area.

Presented below are wind frequency and power density roses for selected stations in the SAMP study area. Locations are shown in Figures 1 (southern NE) and 2 (In vicinity of Block Island) for seasonal and annual average cases. Also provided are Weibull distribution fits to the data. In each case the data is reported at the elevation at which it was measured or hindcast. The period of observations is noted. In some cases the record lengths are shorter than one year and hence data for all seasons is not available.

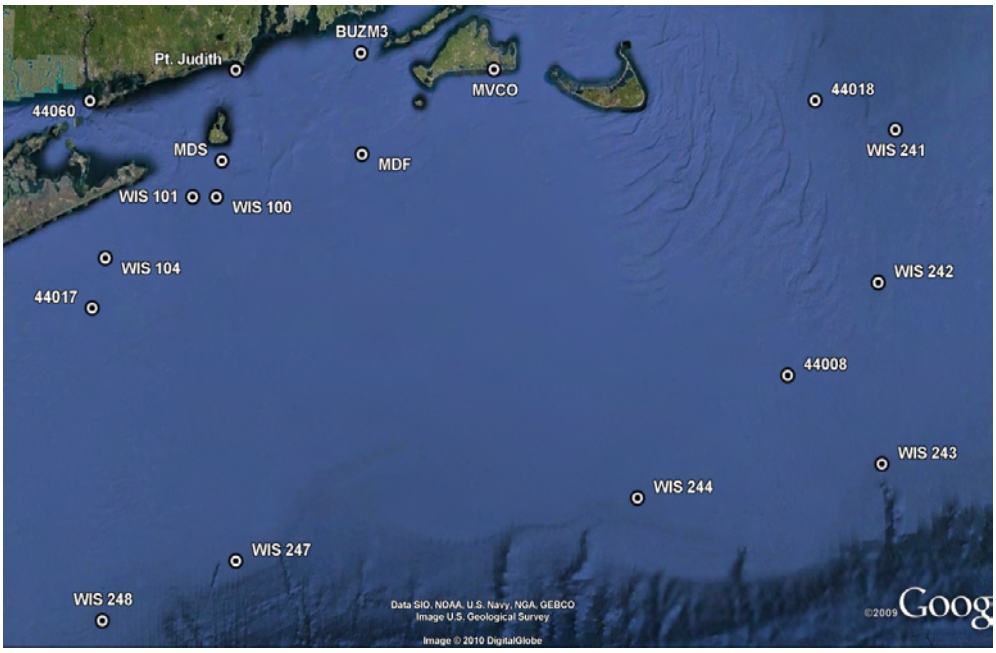

Figure 1 Location of wind observation and hindcast stations in the SAMP study area. US Army Corp of Engineers, WIS; NDBC (44018, 44017, 44060; BUZM3); Ocean SAMP: MDS, MDF; WeatherFlow's Pt Judith; and Martha's Vineyard Coastal Observatory (MVCO).

Figure 2 Location of wind observation stations in the vicinity of Block Island: WeatherFlow's Block Island Jetty, AWS Meteorological Tower, Block Island Airport (KBID), and DOE site.

Weibull distribution fit to the observed data. The start and end dates of the observation are provided as is the elevation of the observation. The Weibull amplitude, c, and shape, k, parameter and their upper and lower 95% confidence interval values are provided.

Wind speed and power density roses are provided. The start and end dates of the observation are provided as is the elevation of the observation. The four corners of the plot show the seasonal results and the center the annual values. The mean wind speed and power density for seasonal and annual results are given.

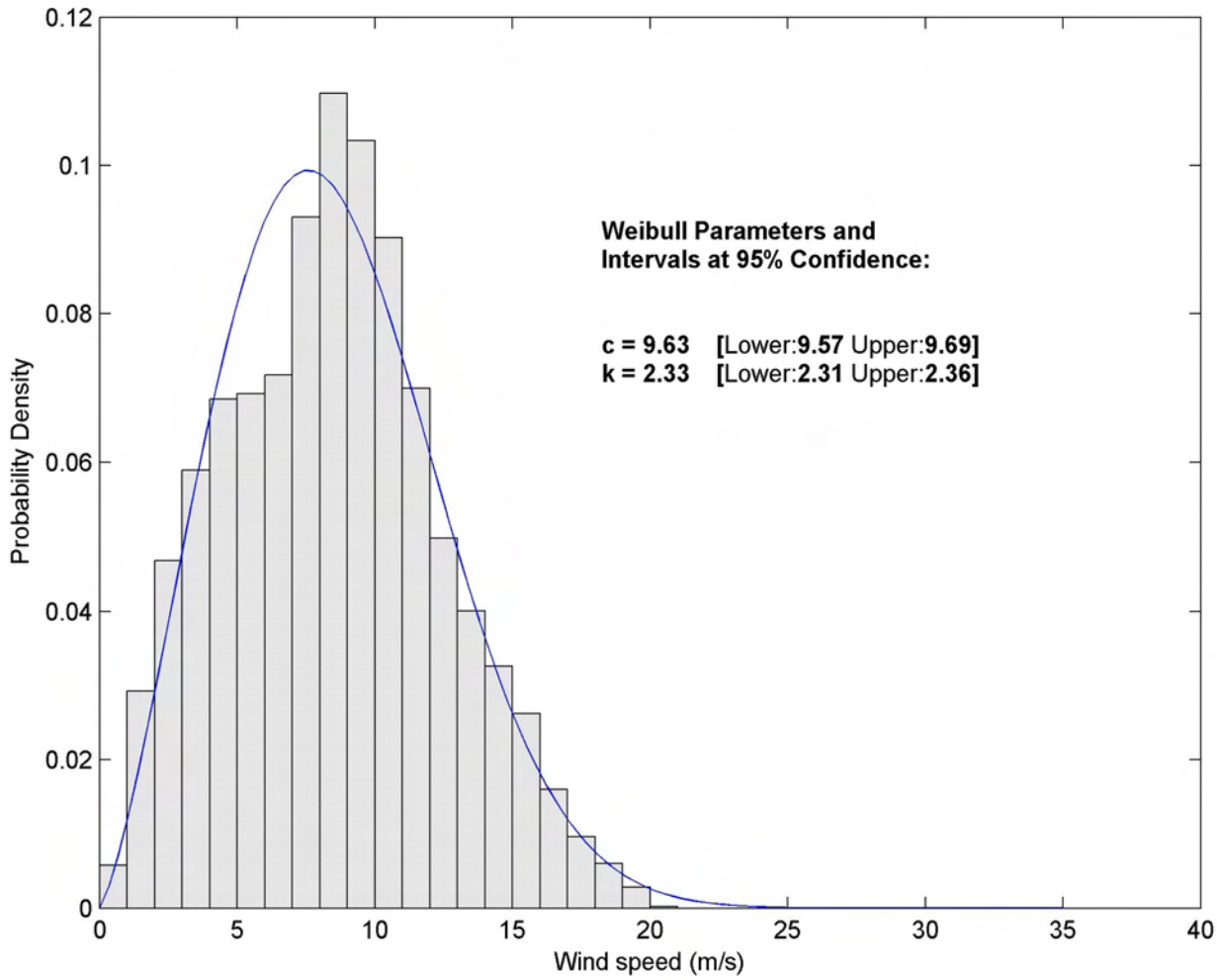
AWS Met Tower Probability Distribution
Dates: October 2009-February 2010
Elevation: 9.9m
Weibull Parameters and
Intervals at 95% Confidence:
c = 9.63 [Lower:9.57 Upper:9.69]
k = 2.33 [Lower:2.31 Upper:2.36]
Probability Density
Wind speed (m/s)
0.12
0.1
0.08
0.06
0.04
0.02
0
0
5
10
15
20
25
30
35
40

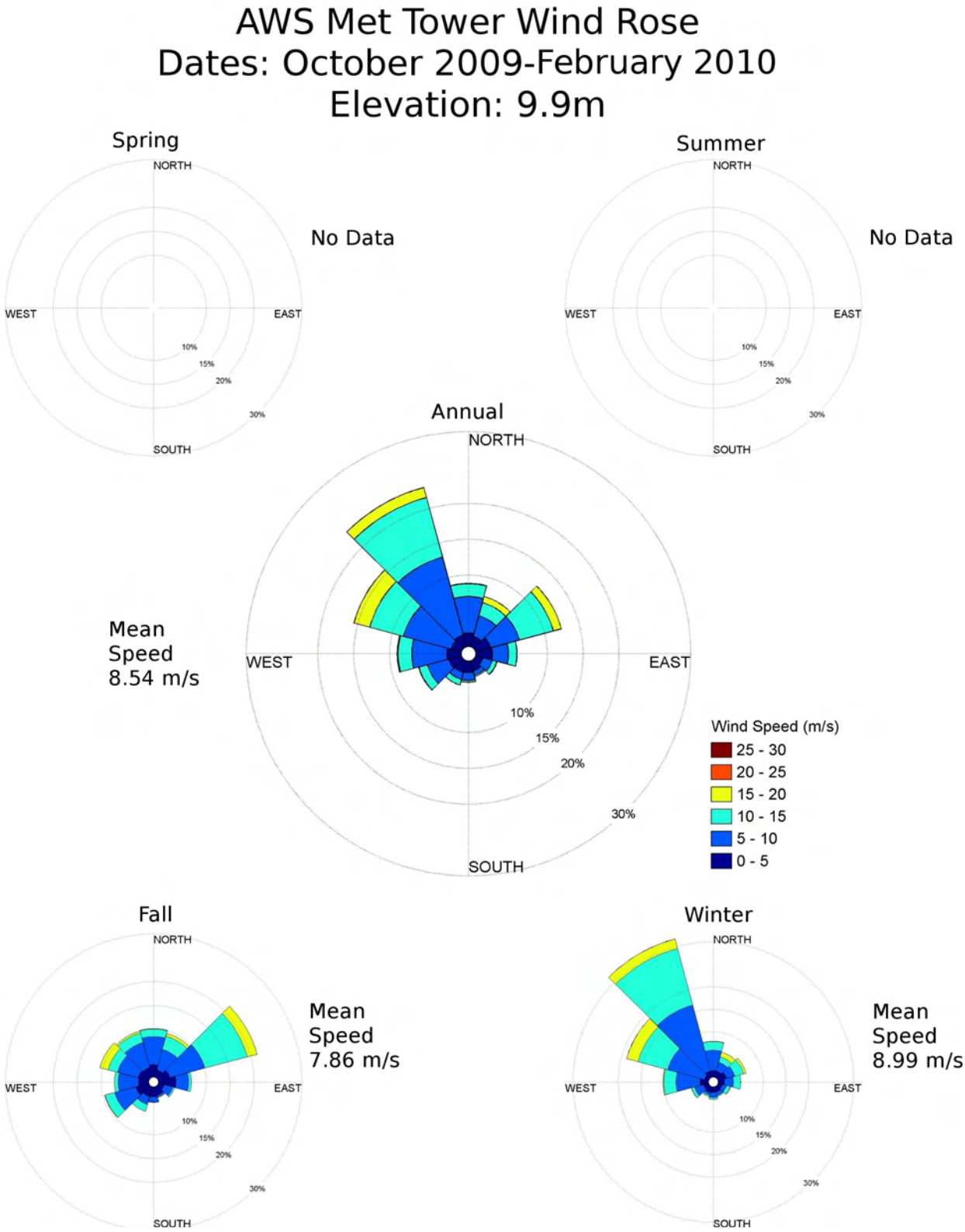
AWS Met Tower Wind Rose
Dates: October 2009-February 2010
Elevation: 9.9m
Spring
No Data
Summer
No Data
Annual
Mean
Speed
8.54 m/s
Fall
Mean
Speed
7.86 m/s
Winter
Mean
Speed
8.99 m/s
NORTH
SOUTH
EAST
WEST
10%
15%
20%
30%
Wind Speed (m/s)
25 - 30
20 - 25
15 - 20
10 - 15
5 - 10
0 - 5

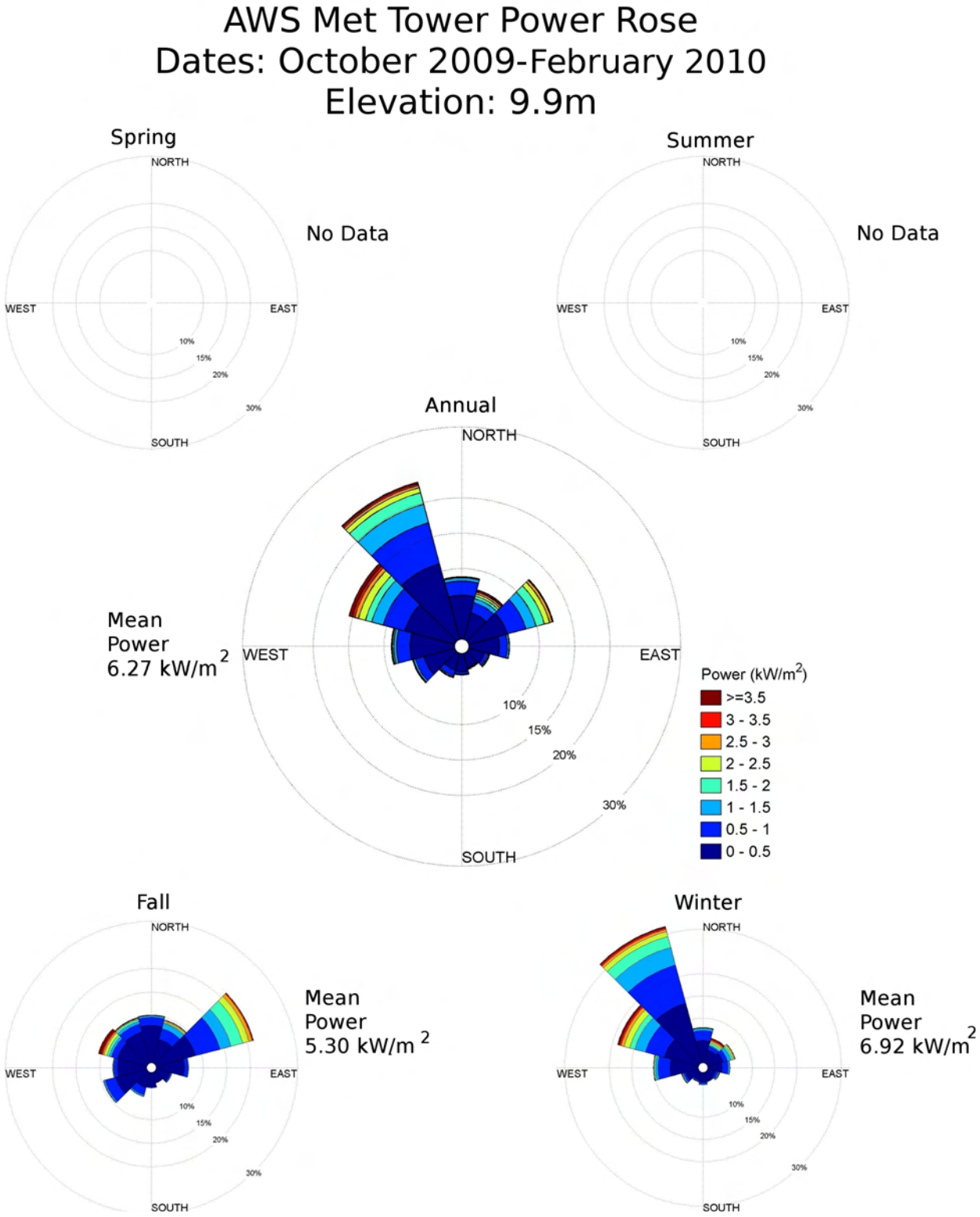
AWS Met Tower Power Rose
Dates: October 2009-February 2010
Elevation: 9.9m
Spring
No Data
Summer
No Data
Annual
Mean
Power
6.27 kW/m 2
Power (kW/m2)
>=3.5
3 - 3.5
2.5 - 3
2 - 2.5
1.5 - 2
1 - 1.5
0.5 - 1
0 - 0.5
Fall
Mean
Power
5.30 kW/m 2
Winter
Mean
Power
6.92 kW/m2
NORTH
SOUTH
EAST
WEST
10%
15%
20%
30%

Block Island Jetty Probability Distribution
Dates: October 2005-September 2008
Elevation: 11m

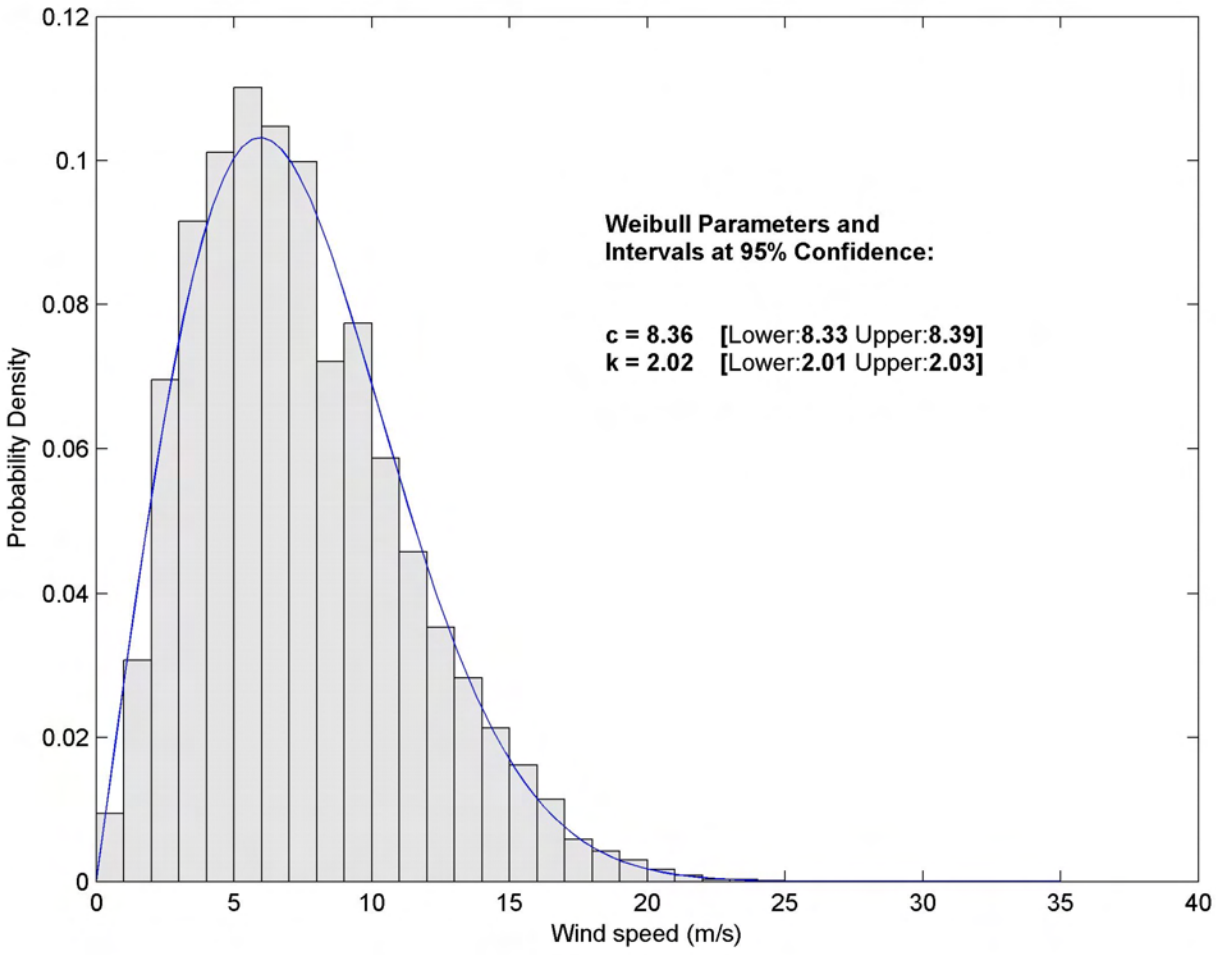

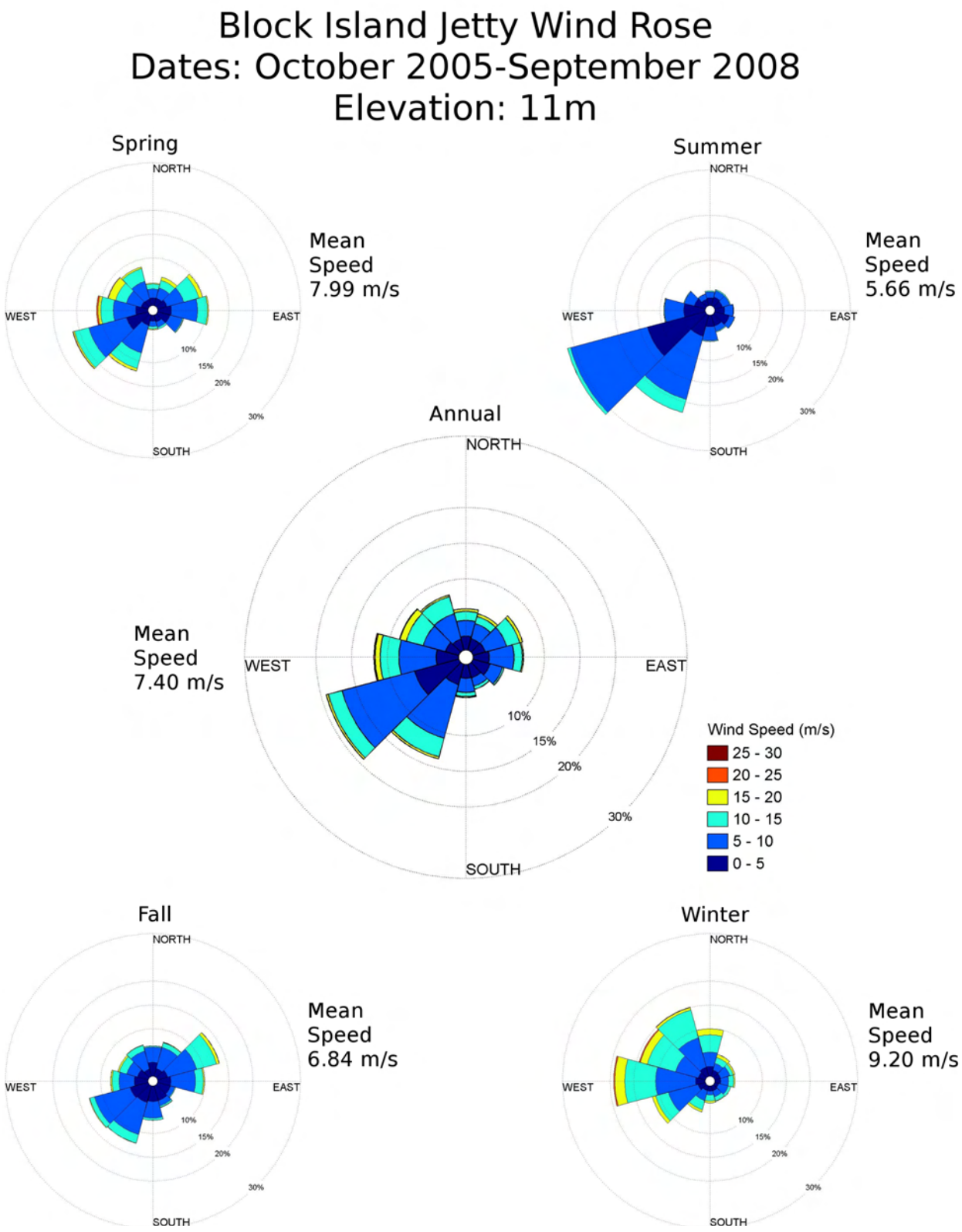
Block Island Jetty Wind Rose
Dates: October 2005-September 2008
Elevation: 11m
Spring
Mean Speed 7.99 m/s
Summer
Mean Speed 5.66 m/s
Annual
Mean Speed 7.40 m/s
Fall
Mean Speed 6.84 m/s
Winter
Mean Speed 9.20 m/s
NORTH
SOUTH
EAST
WEST
10%
15%
20%
30%
Wind Speed (m/s)
25 - 30
20 - 25
15 - 20
10 - 15
5 - 10
0 - 5

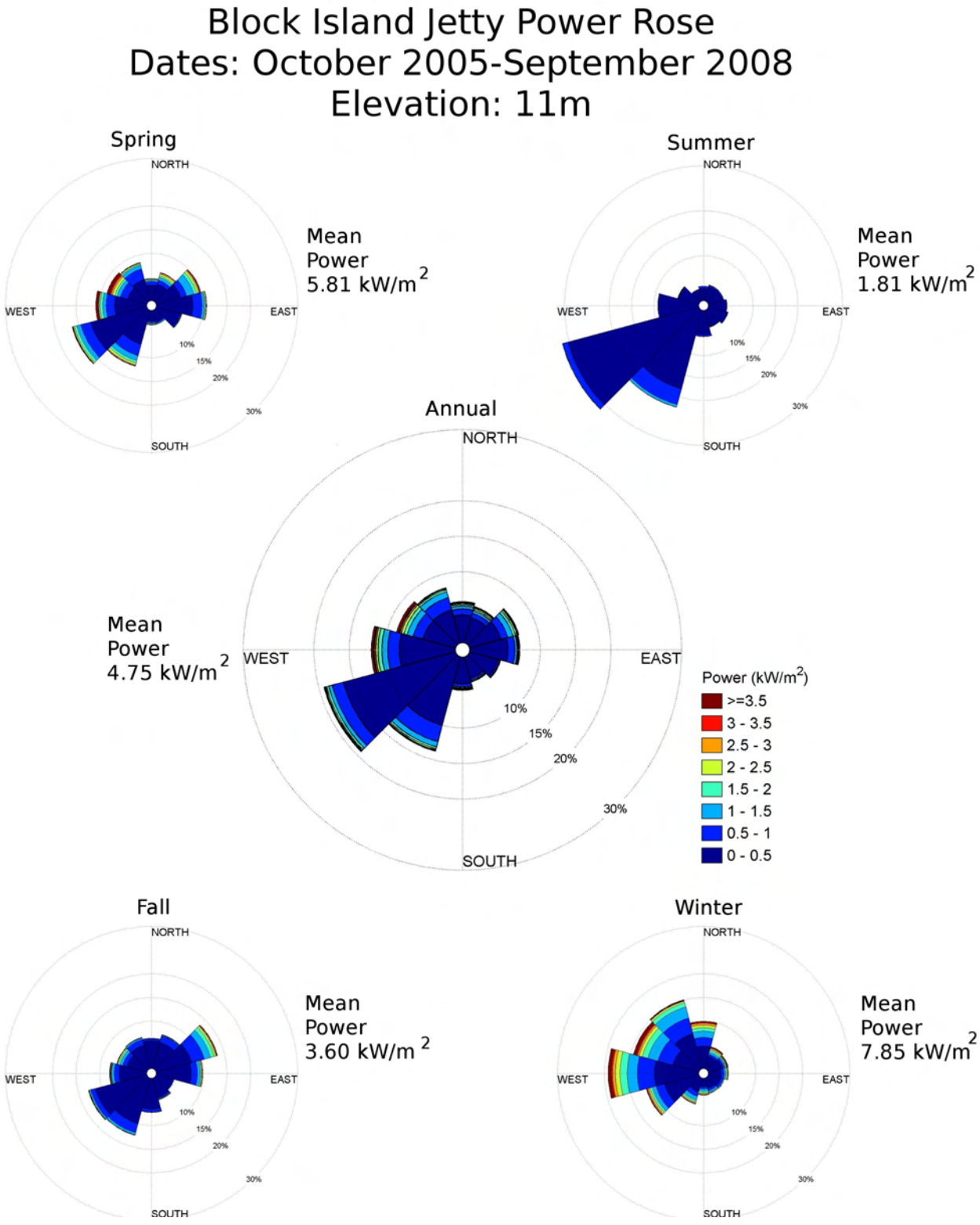
Block Island Jetty Power Rose
Dates: October 2005-September 2008
Elevation: 11m
Spring
Mean Power 5.81 kW/m2
Summer
Mean Power 1.81 kW/m2
Annual
Mean Power 4.75 kW/m2
Fall
Mean Power 3.60 kW/m2
Winter
Mean Power 7.85 kW/m2
NORTH
SOUTH
EAST
WEST
10%
15%
20%
30%
Power (kW/m2)
>=3.5
3 - 3.5
2.5 - 3
2 - 2.5
1.5 - 2
1 - 1.5
0.5 - 1
0 - 0.5

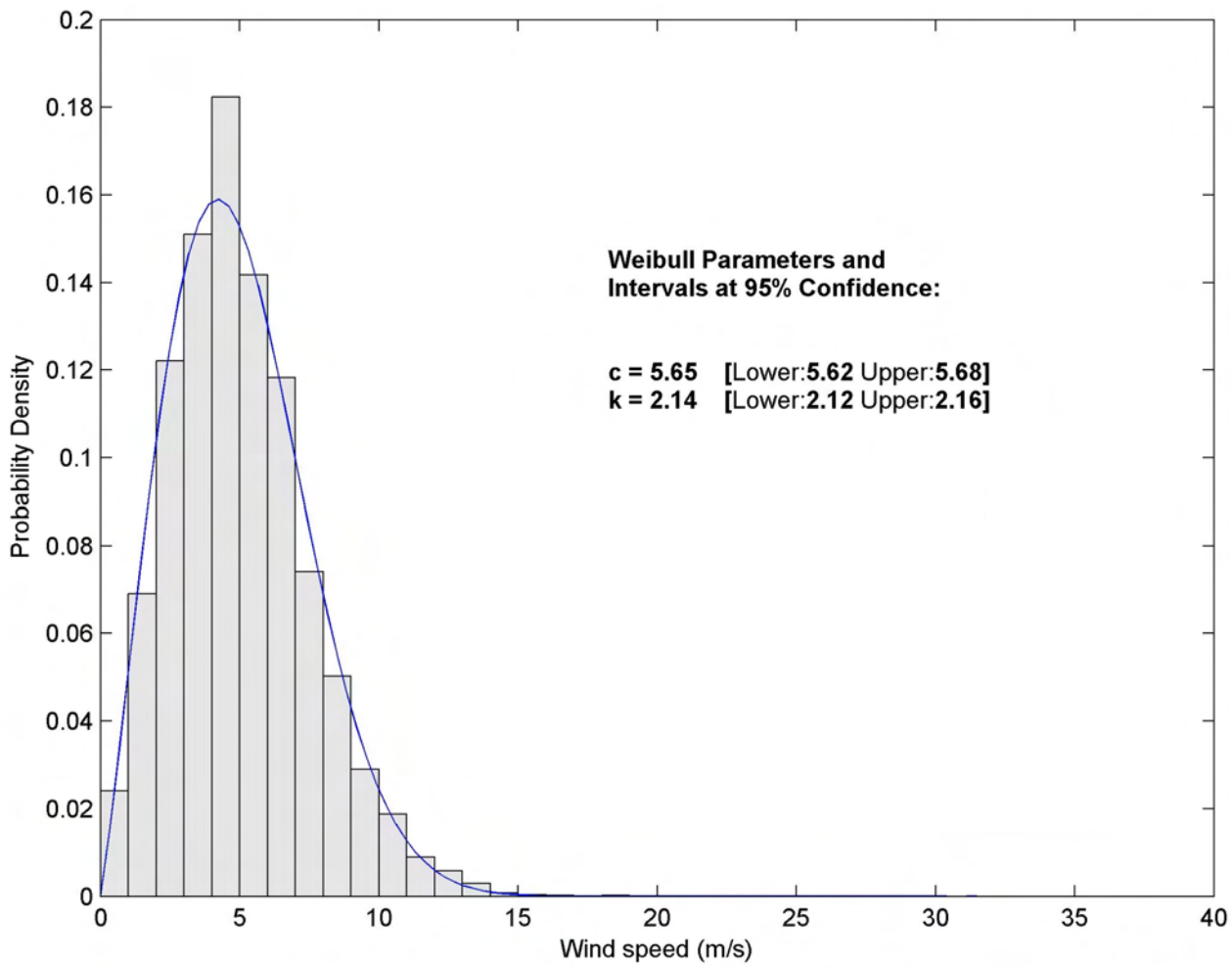
DOE Site Probability Distribution
Dates: 1977-1982
Elevation: 9m
Weibull Parameters and
Intervals at 95% Confidence:
c = 5.65 [Lower:5.62 Upper:5.68]
k = 2.14 [Lower:2.12 Upper:2.16]
Probability Density
Wind speed (m/s)
0
0.02
0.04
0.06
0.08
0.1
0.12
0.14
0.16
0.18
0.2
0
5
10
15
20
25
30
35
40

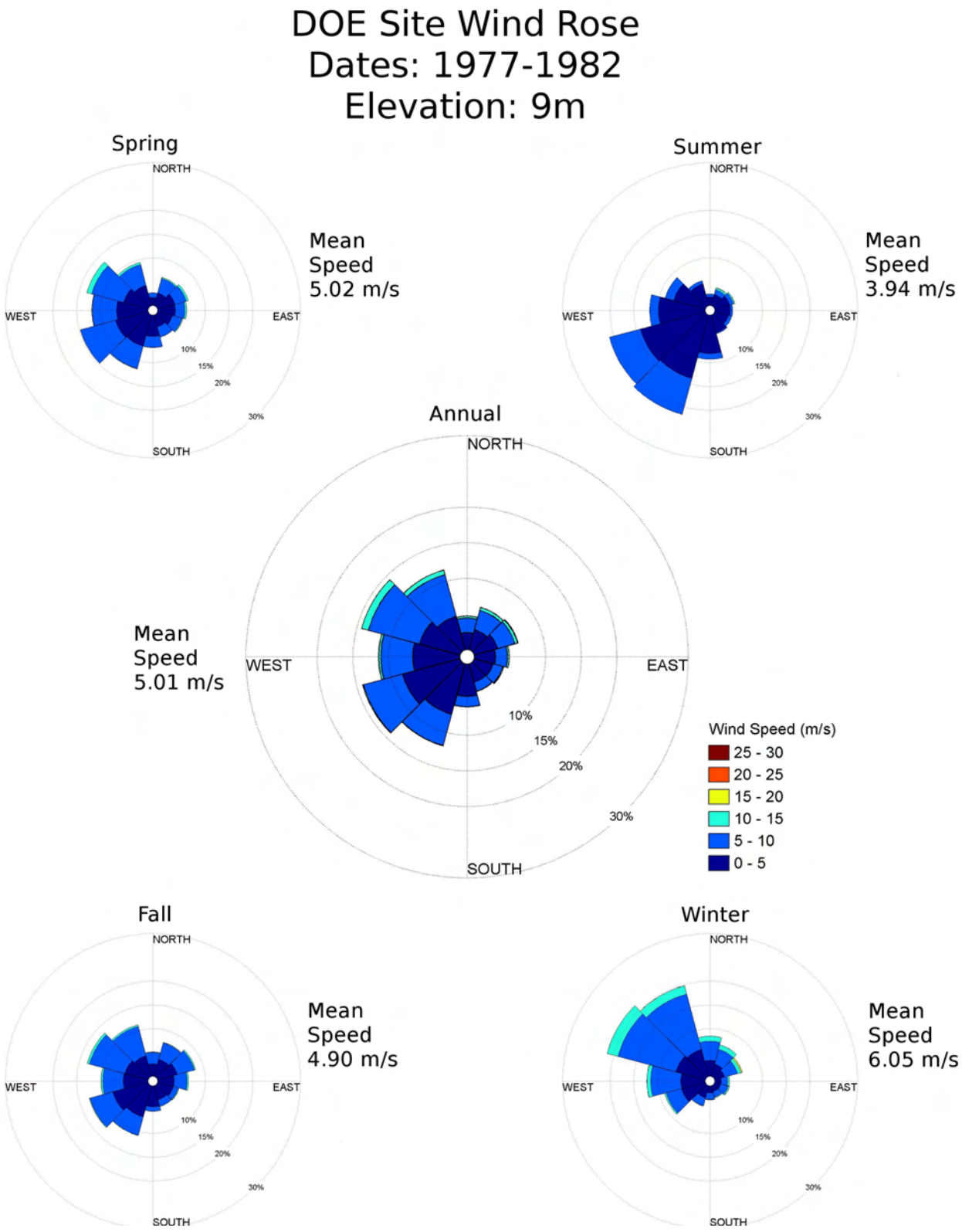
DOE Site Wind Rose
Dates: 1977-1982
Elevation: 9m
Spring
Mean Speed 5.02 m/s
Summer
Mean Speed 3.94 m/s
Annual
Mean Speed 5.01 m/s
Fall
Mean Speed 4.90 m/s
Winter
Mean Speed 6.05 m/s
NORTH
SOUTH
EAST
WEST
10%
15%
20%
30%
Wind Speed (m/s)
25 - 30
20 - 25
15 - 20
10 - 15
5 - 10
0 - 5

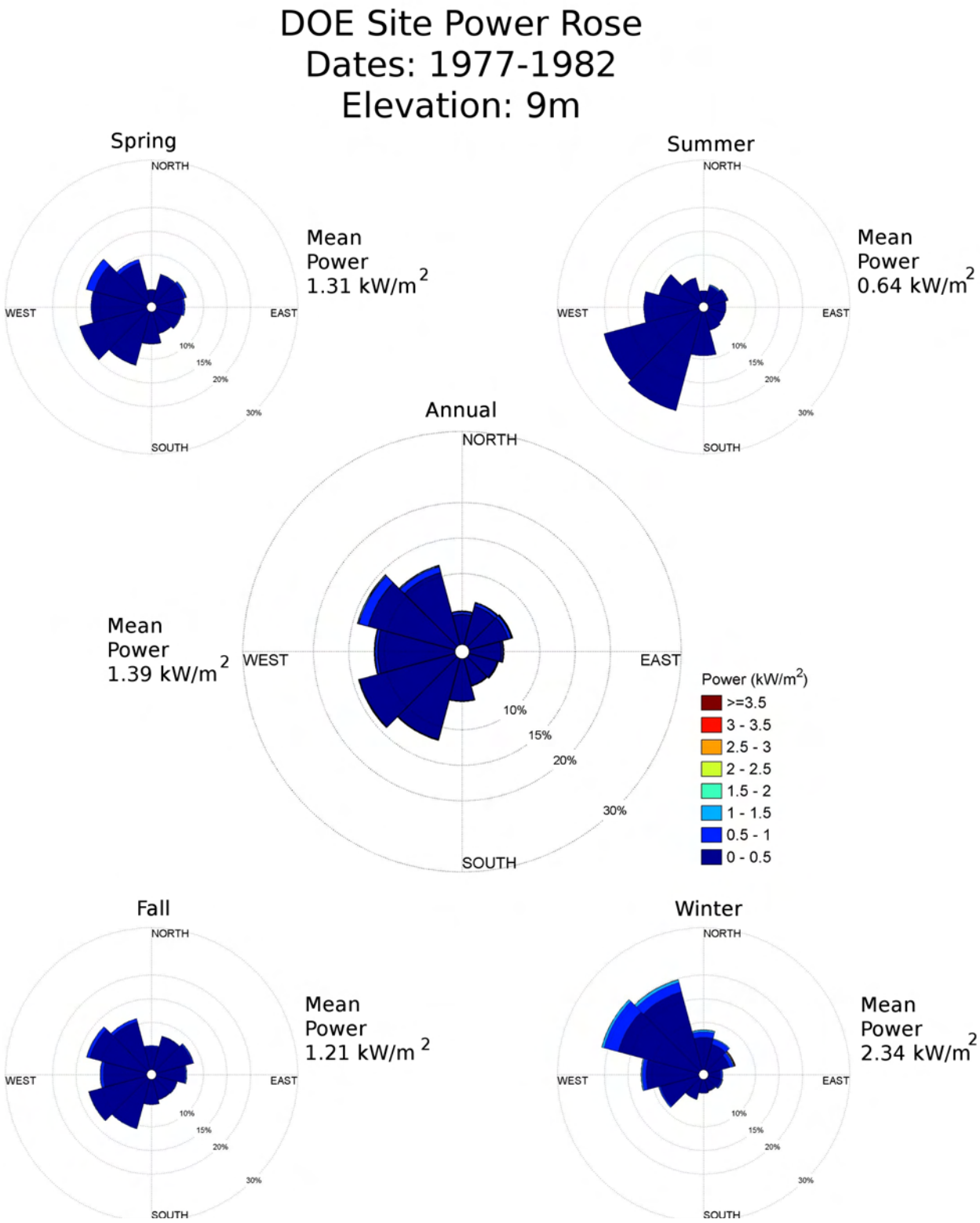
DOE Site Power Rose
Dates: 1977-1982
Elevation: 9m
Spring
Mean Power 1.31 kW/m2
Summer
Mean Power 0.64 kW/m2
Annual
Mean Power 1.39 kW/m2
Fall
Mean Power 1.21 kW/m2
Winter
Mean Power 2.34 kW/m2
NORTH
SOUTH
EAST
WEST
10%
15%
20%
30%
Power (kW/m2)
>=3.5
3 - 3.5
2.5 - 3
2 - 2.5
1.5 - 2
1 - 1.5
0.5 - 1
0 - 0.5

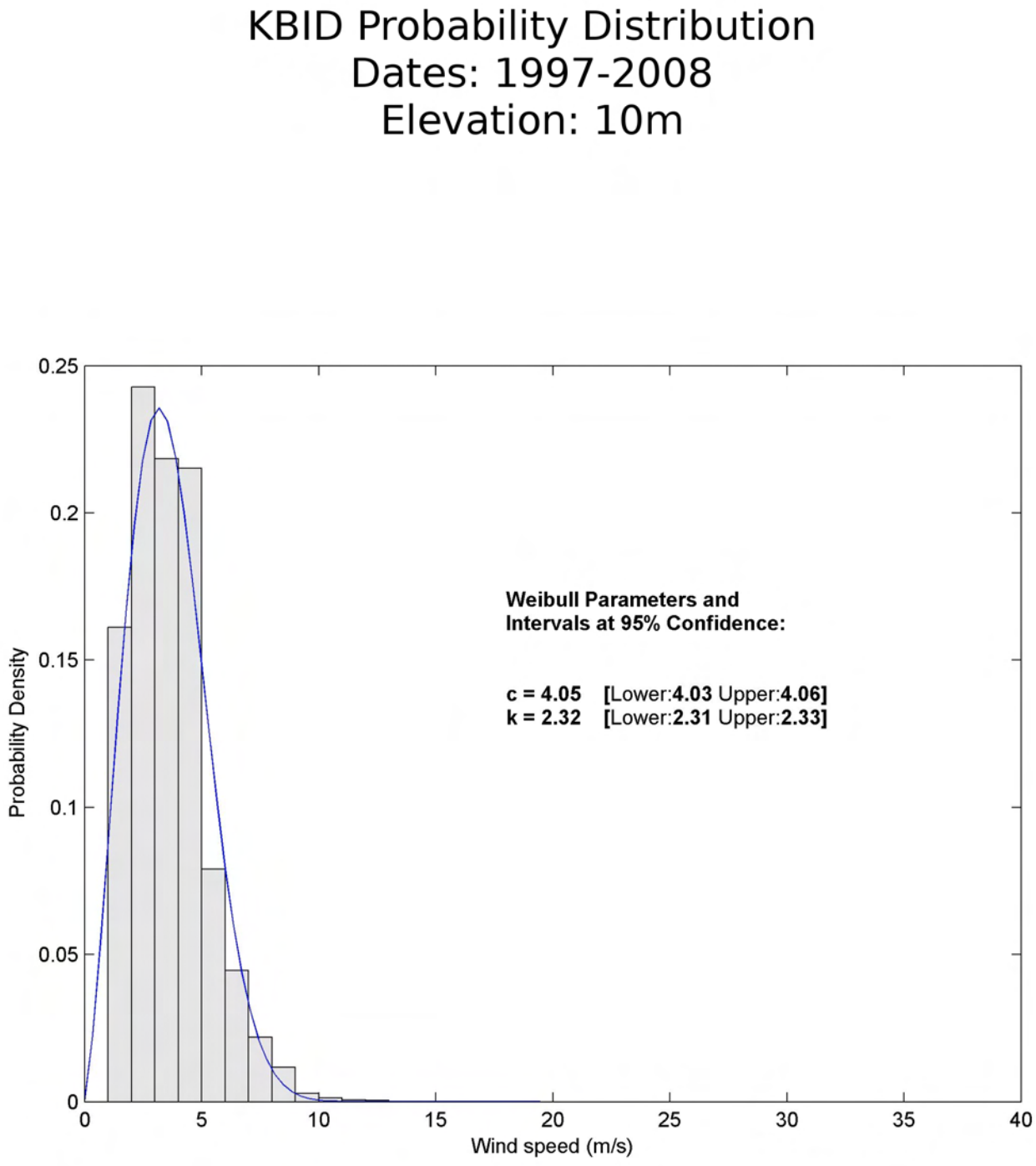
KBID Probability Distribution
Dates: 1997-2008
Elevation: 10m
Weibull Parameters and
Intervals at 95% Confidence:
c = 4.05 [Lower:4.03 Upper:4.06]
k = 2.32 [Lower:2.31 Upper:2.33]
Probability Density
Wind speed (m/s)
0
0.05
0.1
0.15
0.2
0.25
0
5
10
15
20
25
30
35
40

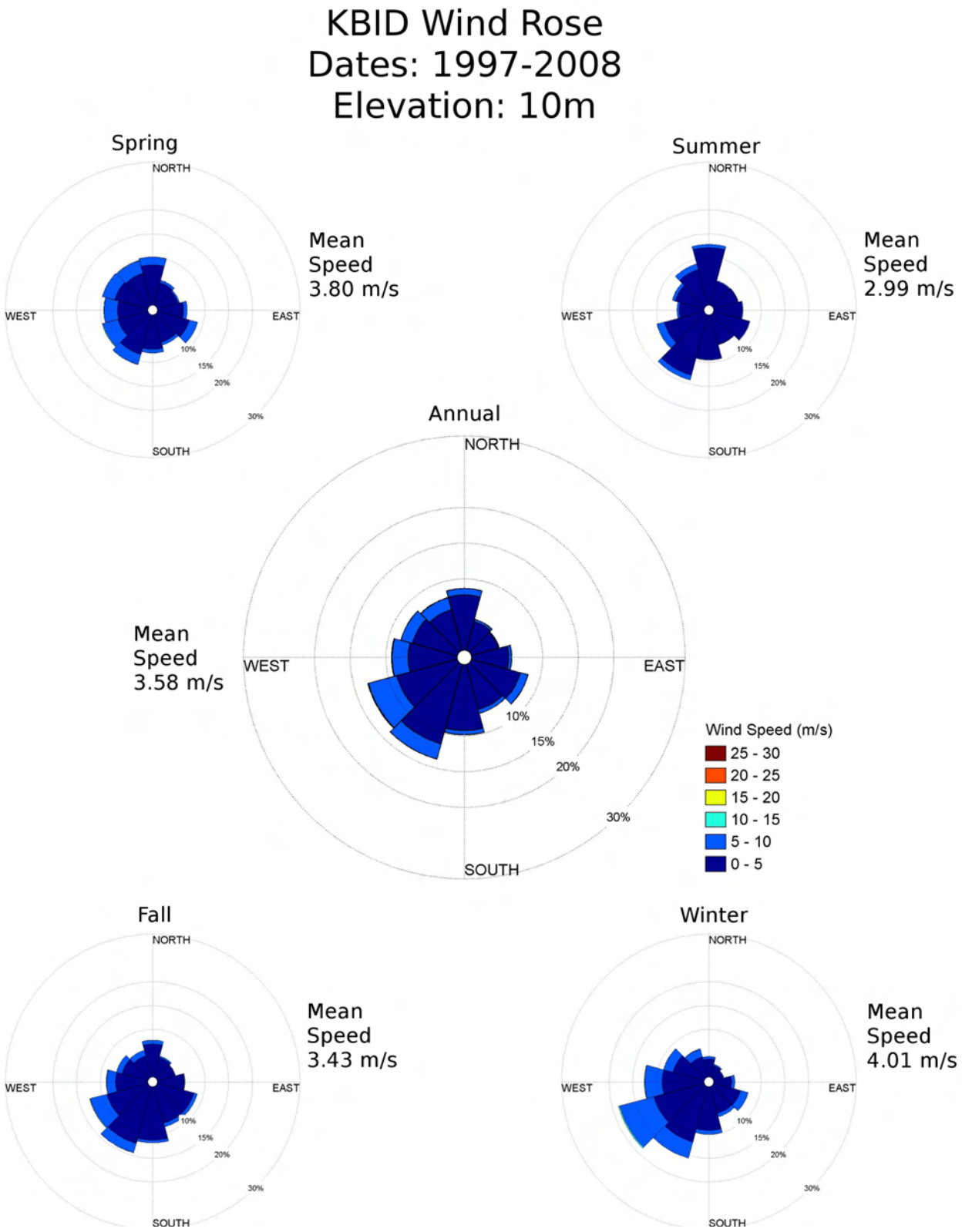
KBID Wind Rose
Dates: 1997-2008
Elevation: 10m
Spring
Mean Speed 3.80 m/s
Summer
Mean Speed 2.99 m/s
Annual
Mean Speed 3.58 m/s
Fall
Mean Speed 3.43 m/s
Winter
Mean Speed 4.01 m/s
NORTH
SOUTH
EAST
WEST
10%
15%
20%
30%
Wind Speed (m/s)
25 - 30
20 - 25
15 - 20
10 - 15
5 - 10
0 - 5

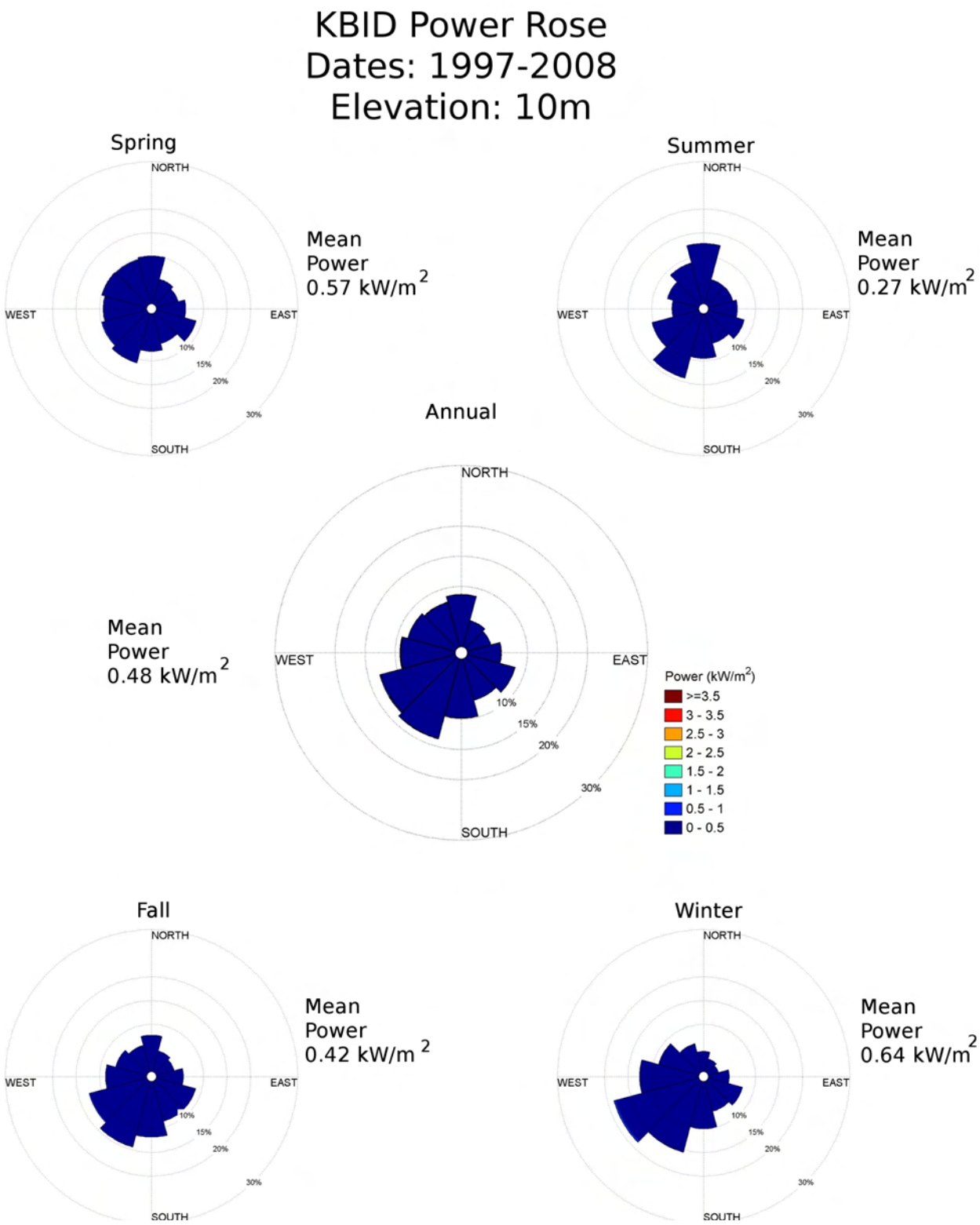
KBID Power Rose
Dates: 1997-2008
Elevation: 10m
Spring
Mean Power 0.57 kW/m2
Summer
Mean Power 0.27 kW/m2
Annual
Mean Power 0.48 kW/m2
Fall
Mean Power 0.42 kW/m2
Winter
Mean Power 0.64 kW/m2
NORTH
SOUTH
EAST
WEST
10%
15%
20%
30%
Power (kW/m2)
>=3.5
3 - 3.5
2.5 - 3
2 - 2.5
1.5 - 2
1 - 1.5
0.5 - 1
0 - 0.5

Martha's Vinyard Coastal Observatory Probability Distribution
Dates: June 2001-May 2010
Elevation: 12.5m

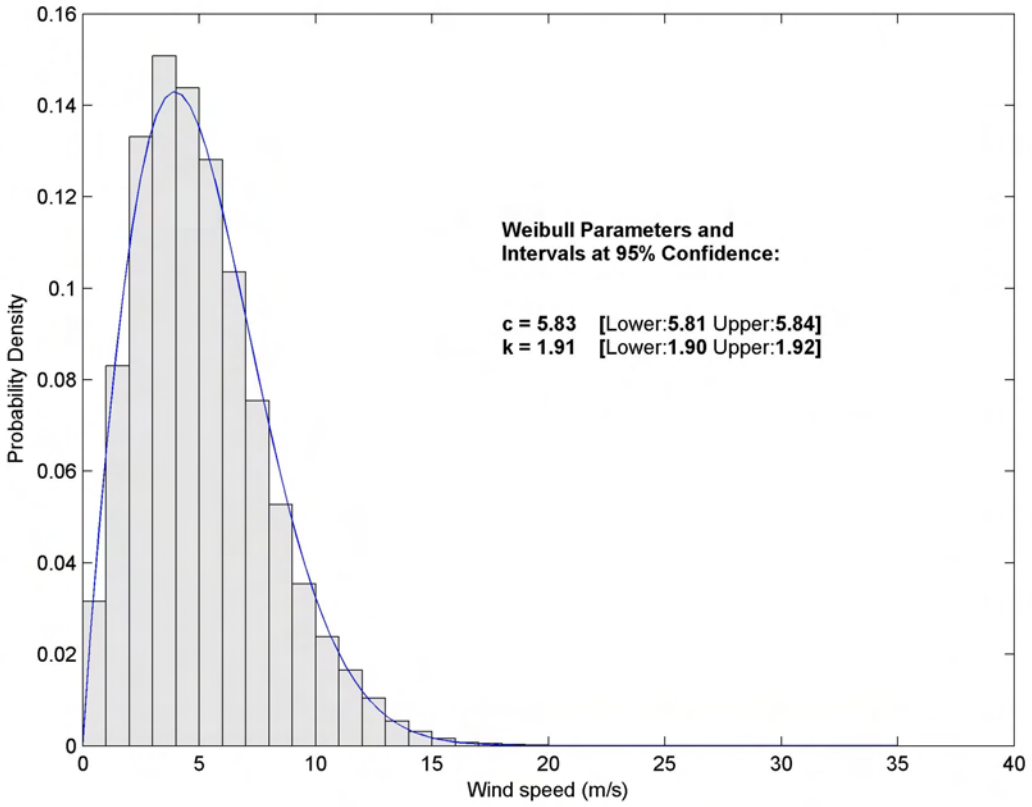

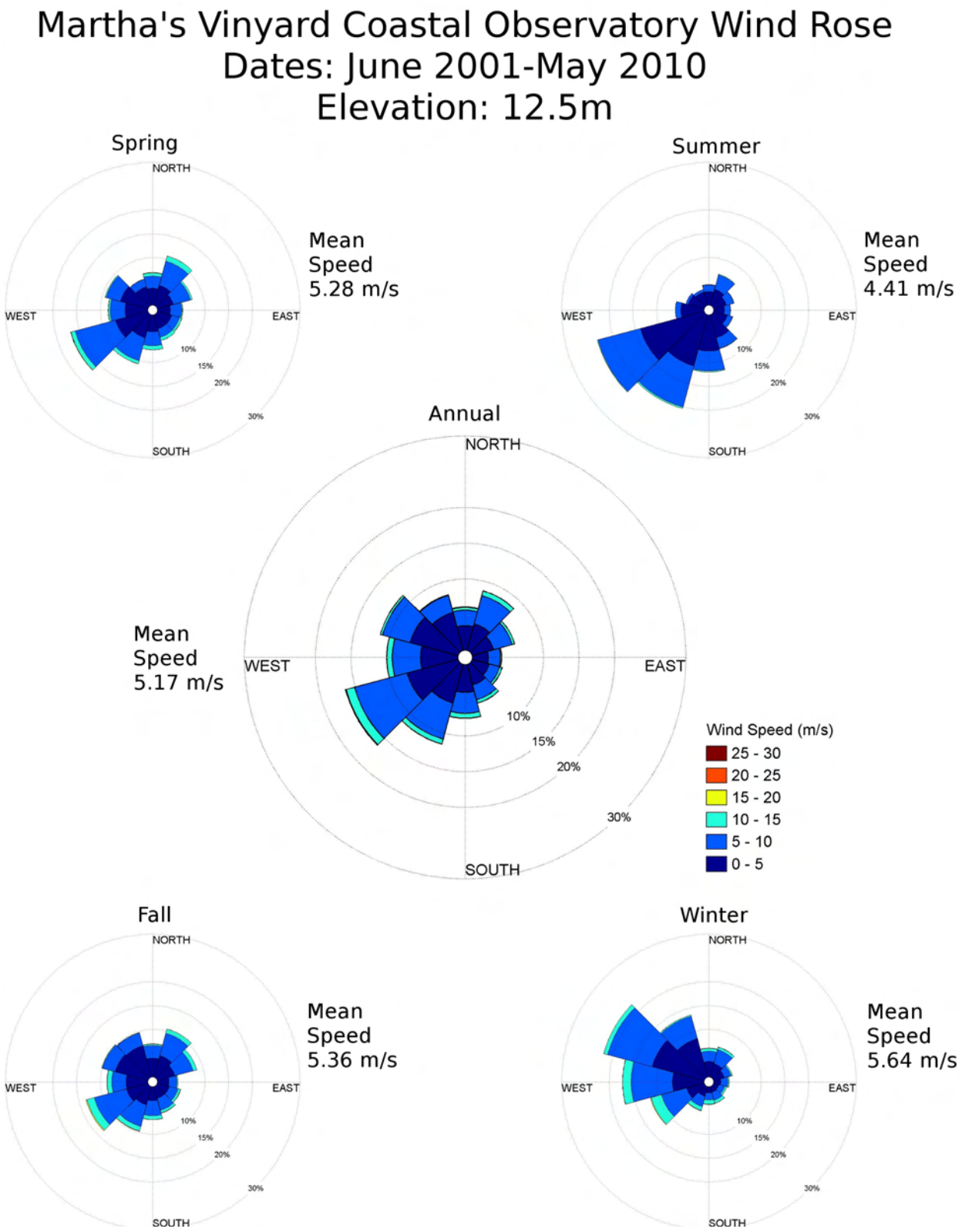
Martha's Vinyard Coastal Observatory Wind Rose
Dates: June 2001-May 2010
Elevation: 12.5m
Spring
Mean Speed 5.28 m/s
Summer
Mean Speed 4.41 m/s
Annual
Mean Speed 5.17 m/s
Fall
Mean Speed 5.36 m/s
Winter
Mean Speed 5.64 m/s
NORTH
SOUTH
EAST
WEST
10%
15%
20%
30%
Wind Speed (m/s)
25 - 30
20 - 25
15 - 20
10 - 15
5 - 10
0 - 5

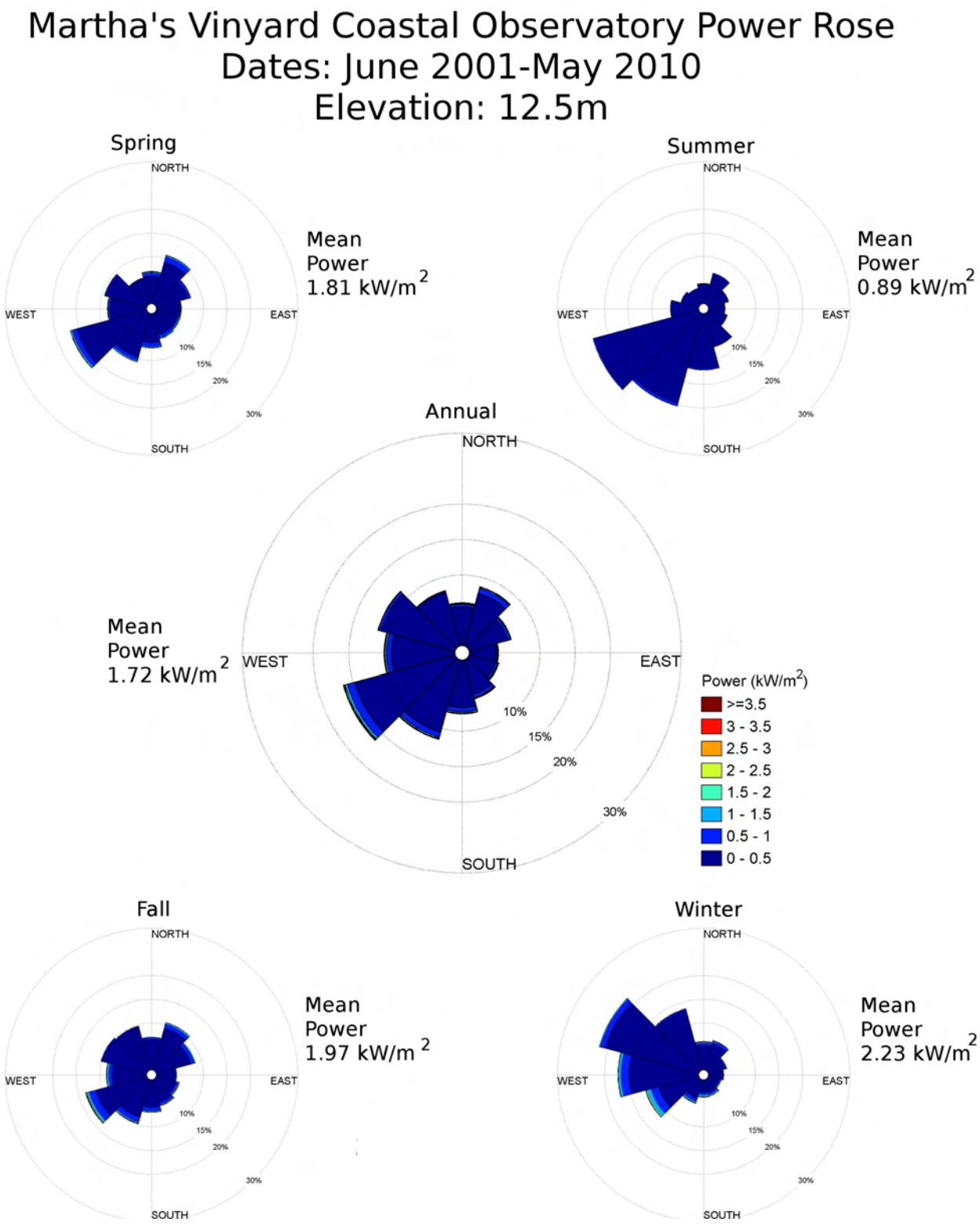
Martha's Vinyard Coastal Observatory Power Rose
Dates: June 2001-May 2010
Elevation: 12.5m
Spring
Mean Power 1.81 kW/m2
Summer
Mean Power 0.89 kW/m2
Annual
Mean Power 1.72 kW/m2
Fall
Mean Power 1.97 kW/m2
Winter
Mean Power 2.23 kW/m2
NORTH
SOUTH
EAST
WEST
10%
15%
20%
30%
Power (kW/m2)
>=3.5
3 - 3.5
2.5 - 3
2 - 2.5
1.5 - 2
1 - 1.5
0.5 - 1
0 - 0.5

NOAA NDBC 44008 Probability Distribution
Dates: 1988-2009
Elevation: 5m

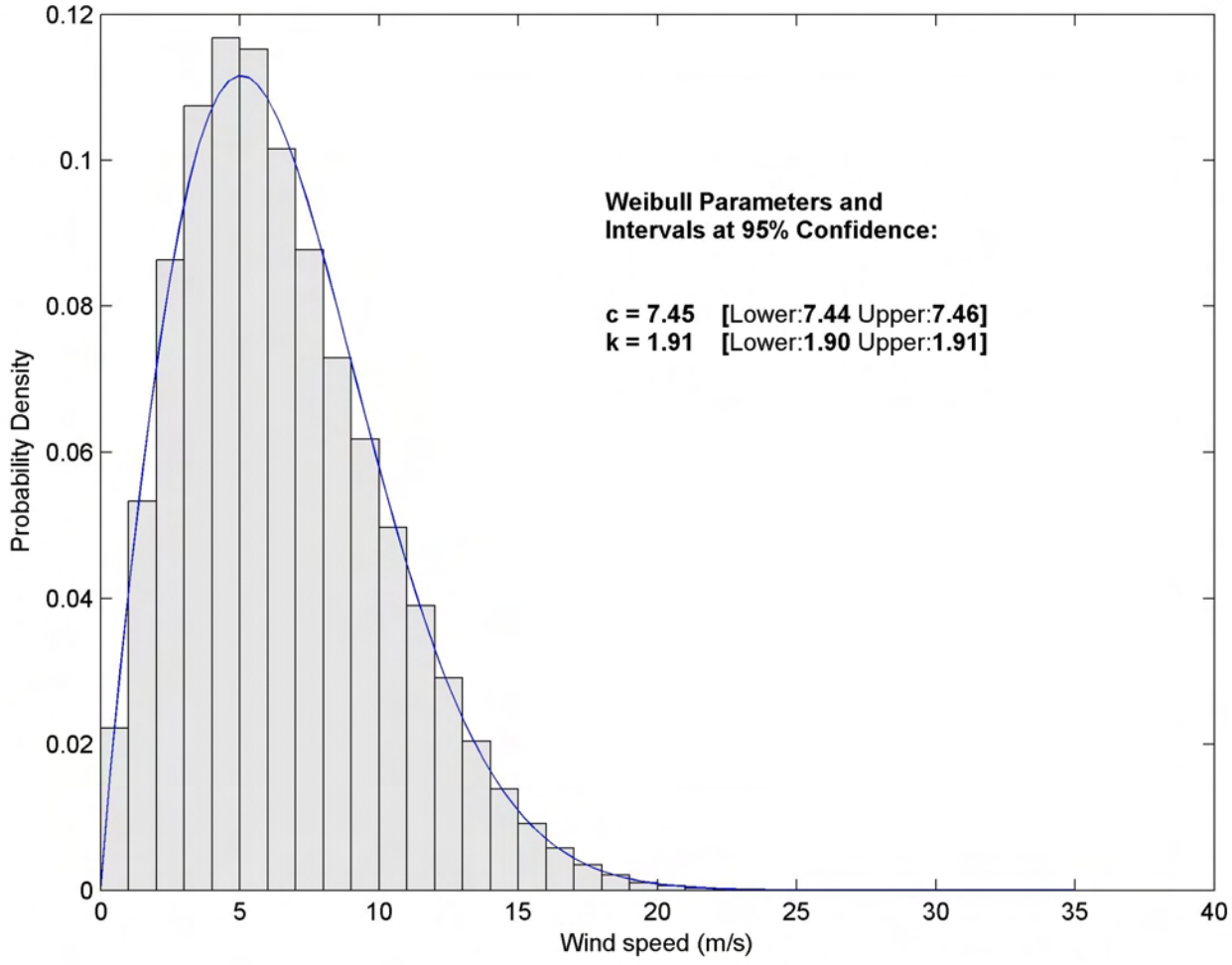

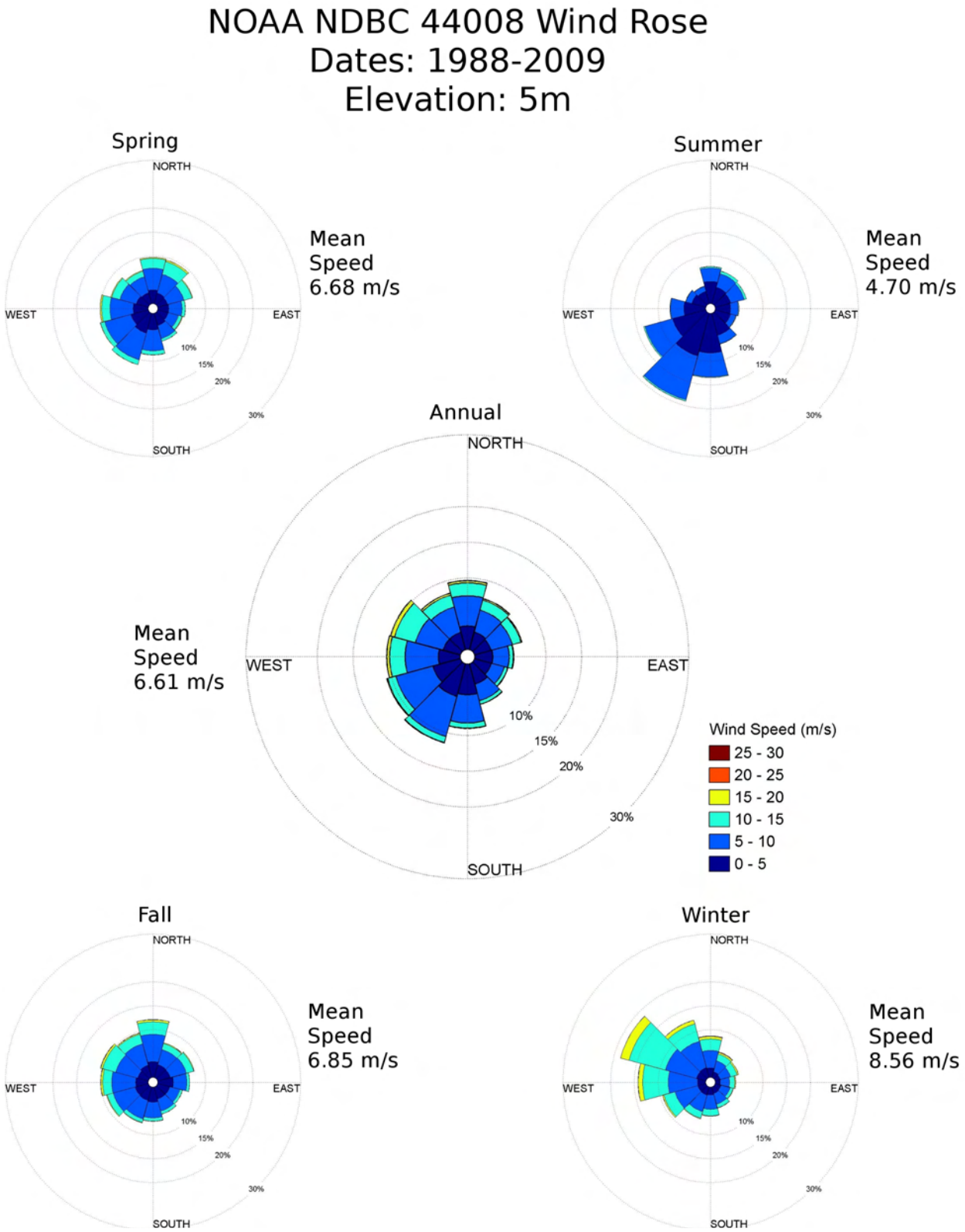
NOAA NDBC 44008 Wind Rose
Dates: 1988-2009
Elevation: 5m
Spring
Mean Speed 6.68 m/s
Summer
Mean Speed 4.70 m/s
Annual
Mean Speed 6.61 m/s
Fall
Mean Speed 6.85 m/s
Winter
Mean Speed 8.56 m/s
NORTH
SOUTH
EAST
WEST
10%
15%
20%
30%
Wind Speed (m/s)
25 - 30
20 - 25
15 - 20
10 - 15
5 - 10
0 - 5

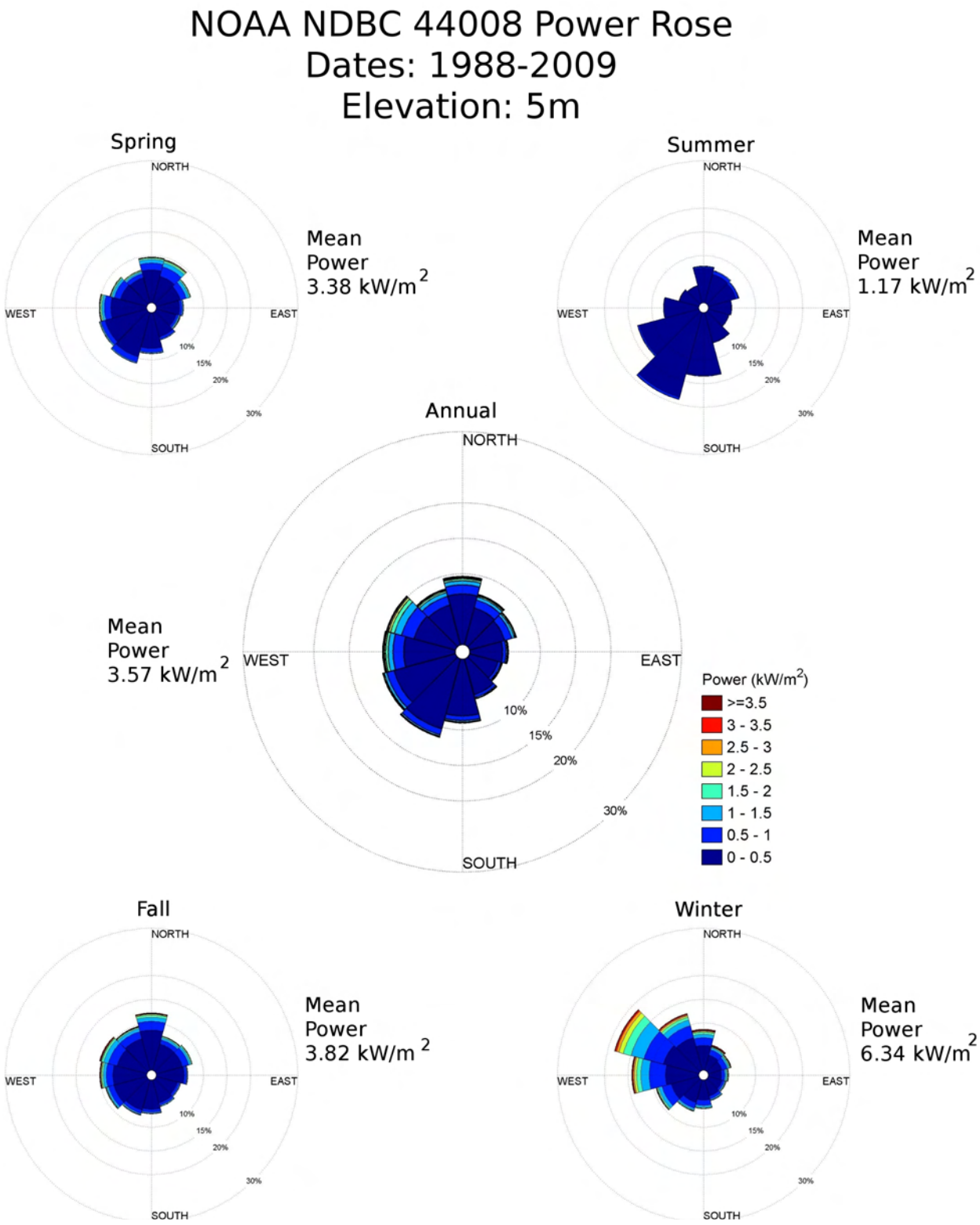
NOAA NDBC 44008 Power Rose
Dates: 1988-2009
Elevation: 5m
Spring
Mean Power 3.38 kW/m2
Summer
Mean Power 1.17 kW/m2
Annual
Mean Power 3.57 kW/m2
Fall
Mean Power 3.82 kW/m2
Winter
Mean Power 6.34 kW/m2
NORTH
SOUTH
EAST
WEST
10%
15%
20%
30%
Power (kW/m2)
>=3.5
3 - 3.5
2.5 - 3
2 - 2.5
1.5 - 2
1 - 1.5
0.5 - 1
0 - 0.5

NOAA NDBC 44017 Probability Distribution
Dates: 2002-2009
Elevation: 5m

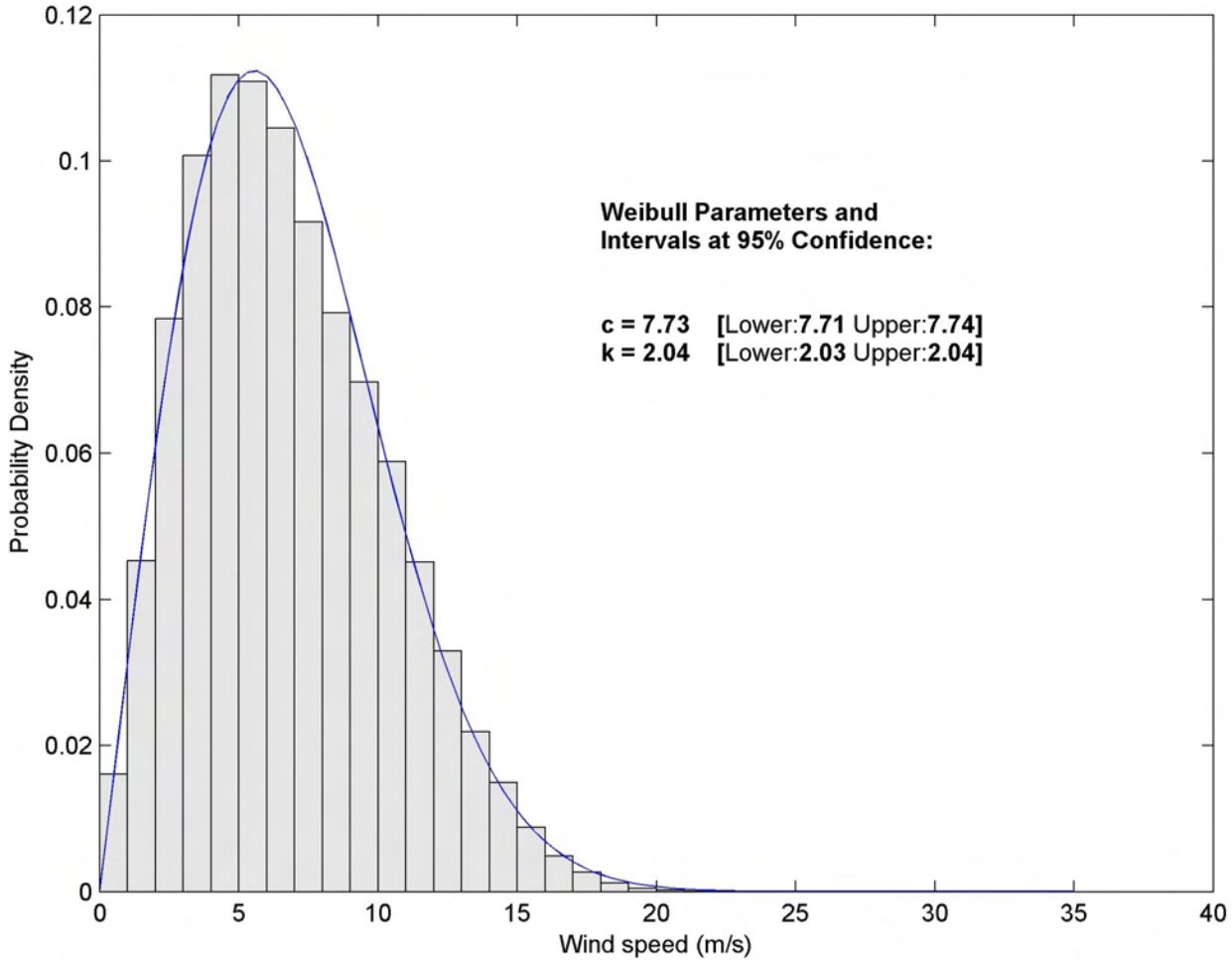

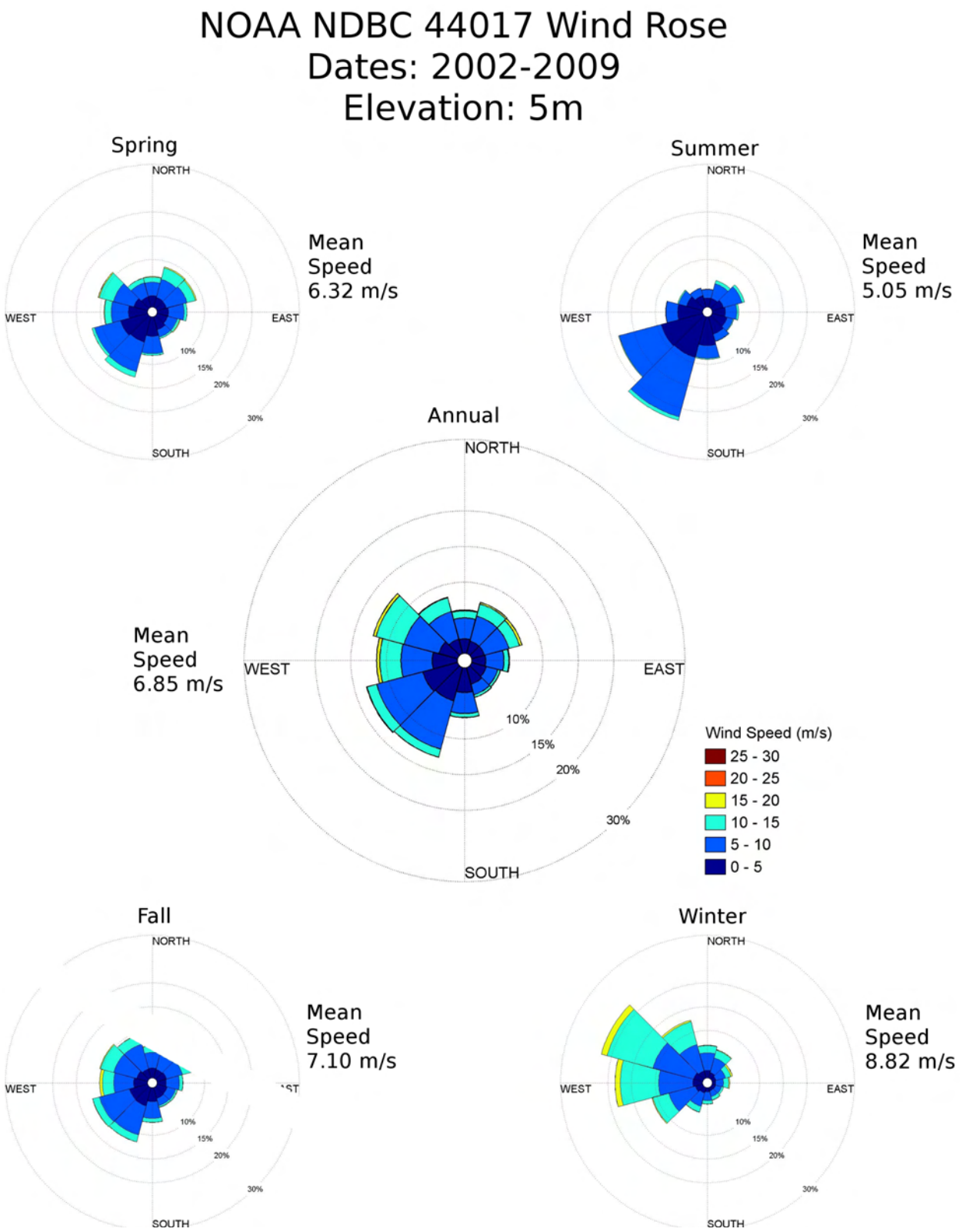
NOAA NDBC 44017 Wind Rose
Dates: 2002-2009
Elevation: 5m
Spring
Mean Speed 6.32 m/s
Summer
Mean Speed 5.05 m/s
Annual
Mean Speed 6.85 m/s
Fall
Mean Speed 7.10 m/s
Winter
Mean Speed 8.82 m/s
NORTH
SOUTH
EAST
WEST
10%
15%
20%
30%
Wind Speed (m/s)
25 - 30
20 - 25
15 - 20
10 - 15
5 - 10
0 - 5

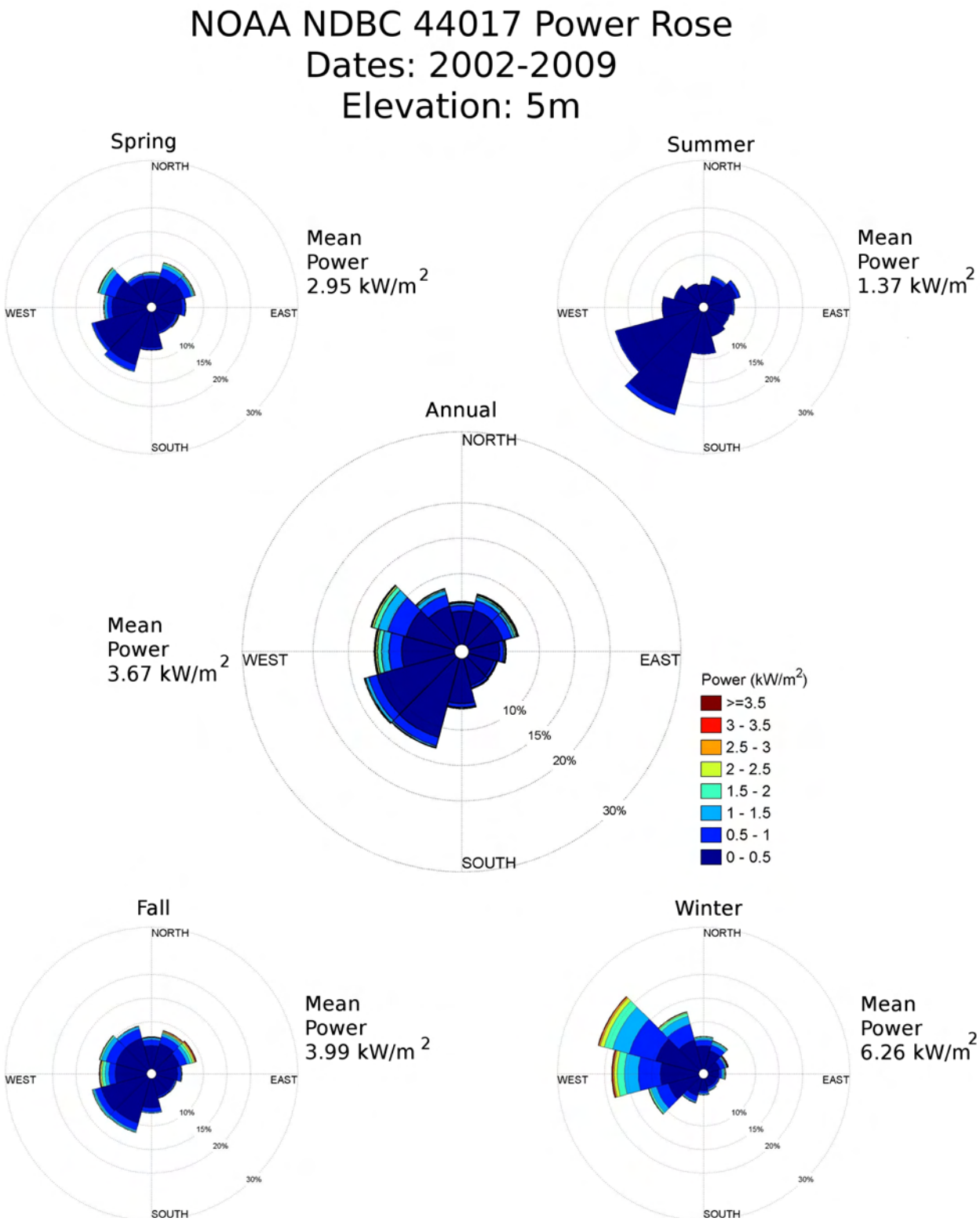
NOAA NDBC 44017 Power Rose
Dates: 2002-2009
Elevation: 5m
Spring
Mean Power 2.95 kW/m2
Summer
Mean Power 1.37 kW/m2
Annual
Mean Power 3.67 kW/m2
Fall
Mean Power 3.99 kW/m2
Winter
Mean Power 6.26 kW/m2
NORTH
SOUTH
EAST
WEST
10%
15%
20%
30%
Power (kW/m2)
>=3.5
3 - 3.5
2.5 - 3
2 - 2.5
1.5 - 2
1 - 1.5
0.5 - 1
0 - 0.5

NOA NDBC 44018 Probability Distribution
Dates: 2002-2009
Elevation: 5m

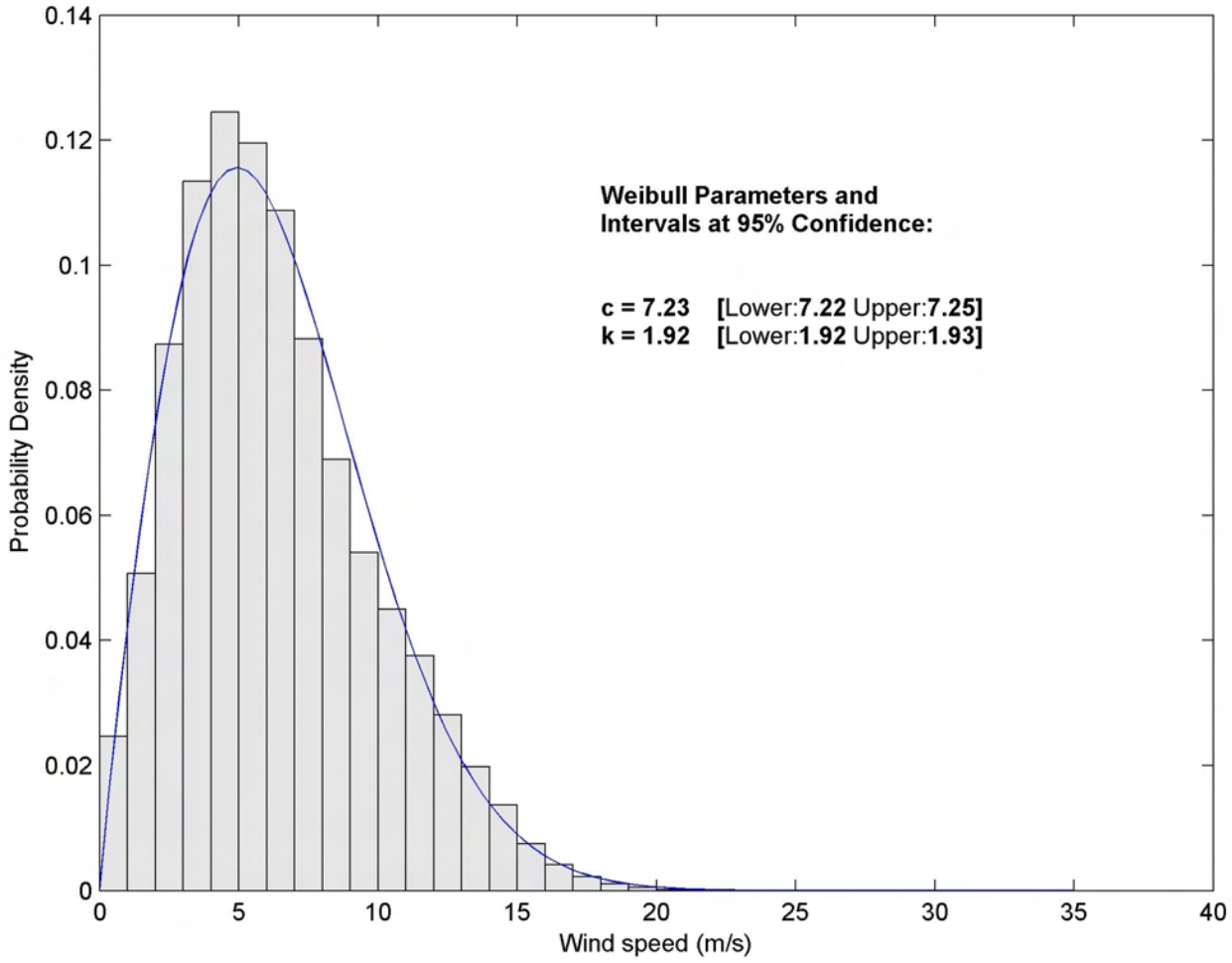

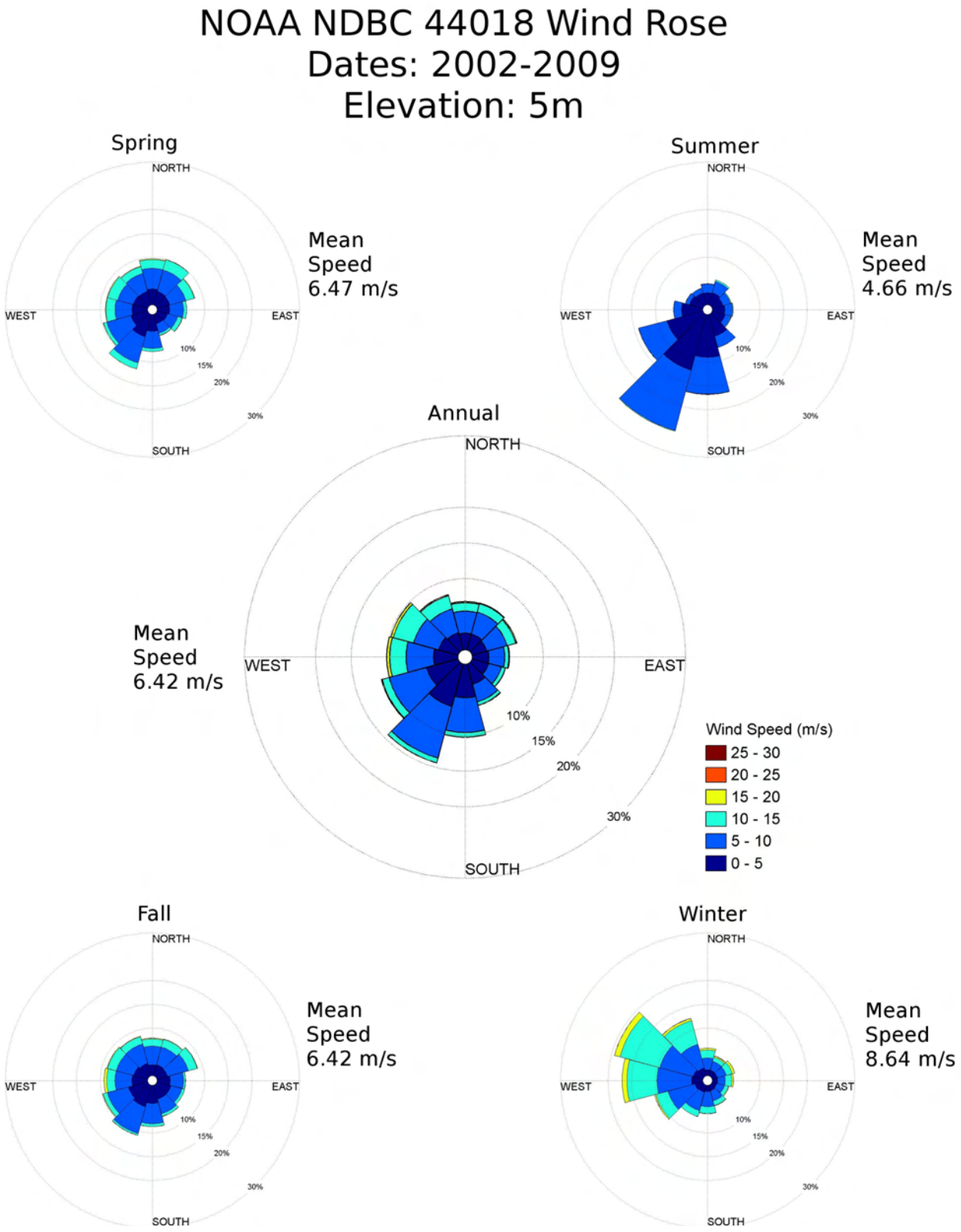
NOAA NDBC 44018 Wind Rose
Dates: 2002-2009
Elevation: 5m
Spring
Mean Speed 6.47 m/s
Summer
Mean Speed 4.66 m/s
Annual
Mean Speed 6.42 m/s
Fall
Mean Speed 6.42 m/s
Winter
Mean Speed 8.64 m/s
NORTH
SOUTH
EAST
WEST
10%
15%
20%
30%
Wind Speed (m/s)
25 - 30
20 - 25
15 - 20
10 - 15
5 - 10
0 - 5

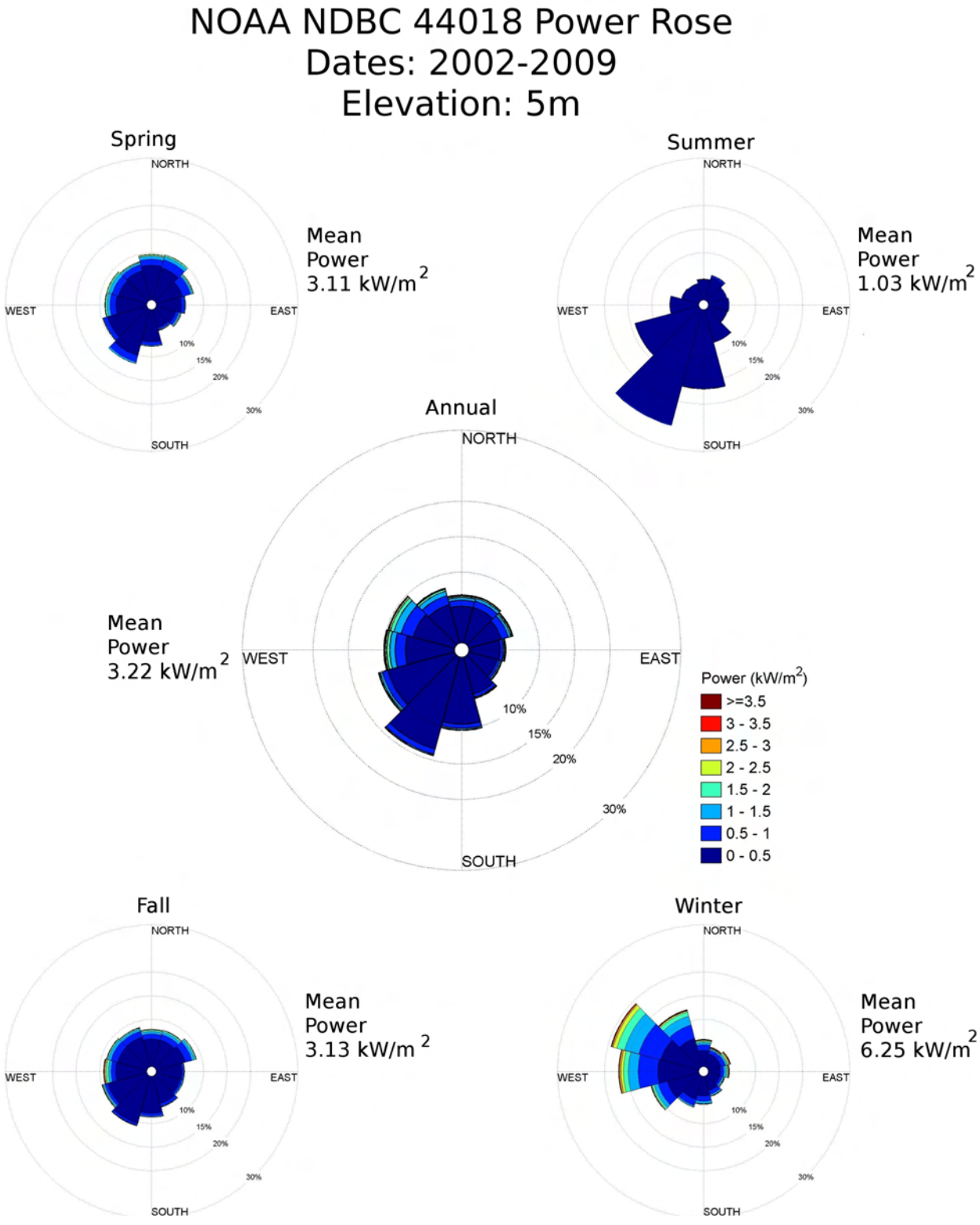
NOAA NDBC 44018 Power Rose
Dates: 2002-2009
Elevation: 5m
Spring
Mean Power 3.11 kW/m2
Summer
Mean Power 1.03 kW/m2
Annual
Mean Power 3.22 kW/m2
Fall
Mean Power 3.13 kW/m2
Winter
Mean Power 6.25 kW/m2
NORTH
SOUTH
EAST
WEST
10%
15%
20%
30%
Power (kW/m2)
>=3.5
3 - 3.5
2.5 - 3
2 - 2.5
1.5 - 2
1 - 1.5
0.5 - 1
0 - 0.5

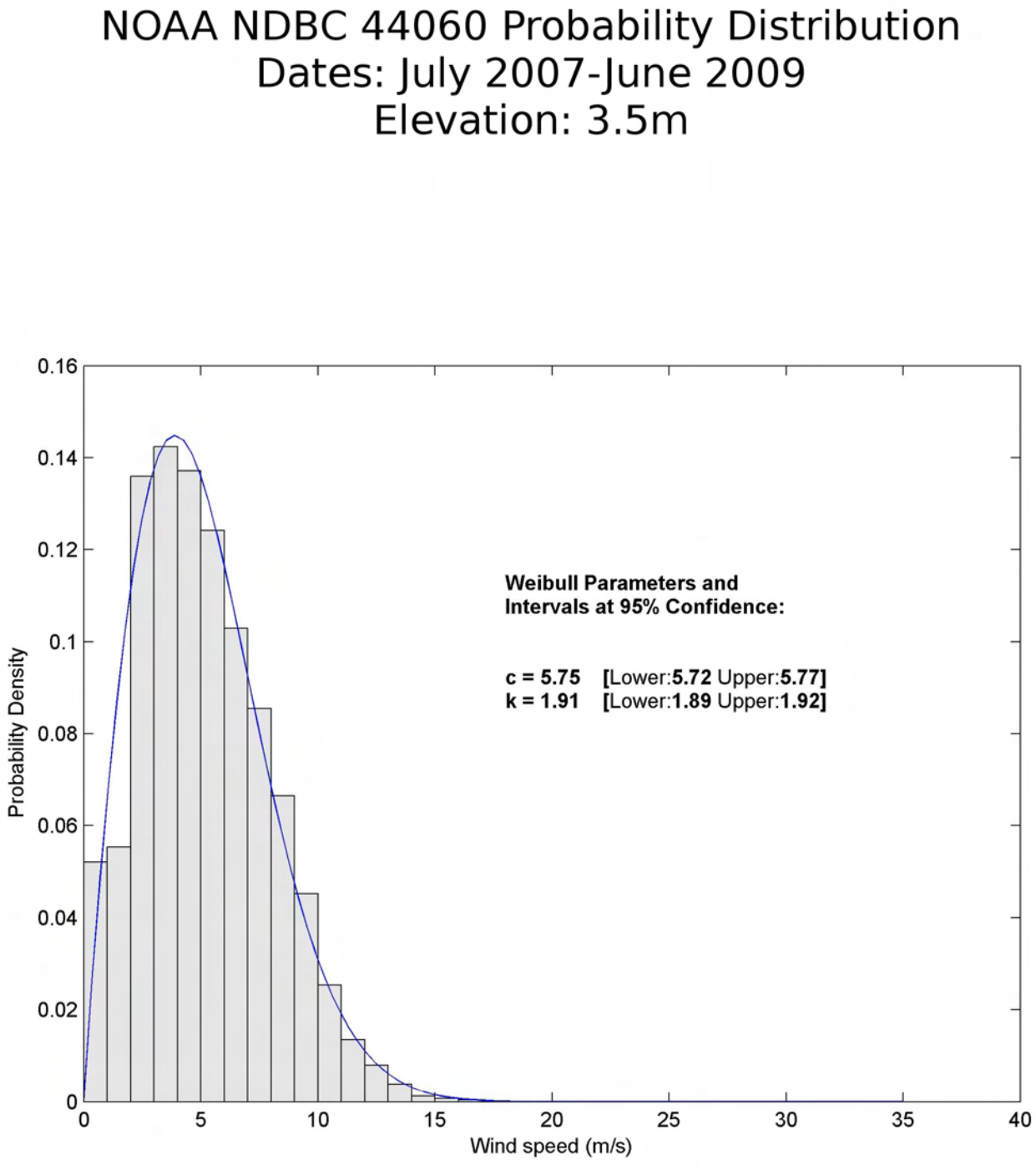
NOAA NDBC 44060 Probability Distribution
Dates: July 2007-June 2009
Elevation: 3.5m
Weibull Parameters and
Intervals at 95% Confidence:
c = 5.75 [Lower:5.72 Upper:5.77]
k = 1.91 [Lower:1.89 Upper:1.92]
Probability Density
Wind speed (m/s)
0
0.02
0.04
0.06
0.08
0.1
0.12
0.14
0.16
0
5
10
15
20
25
30
35
40

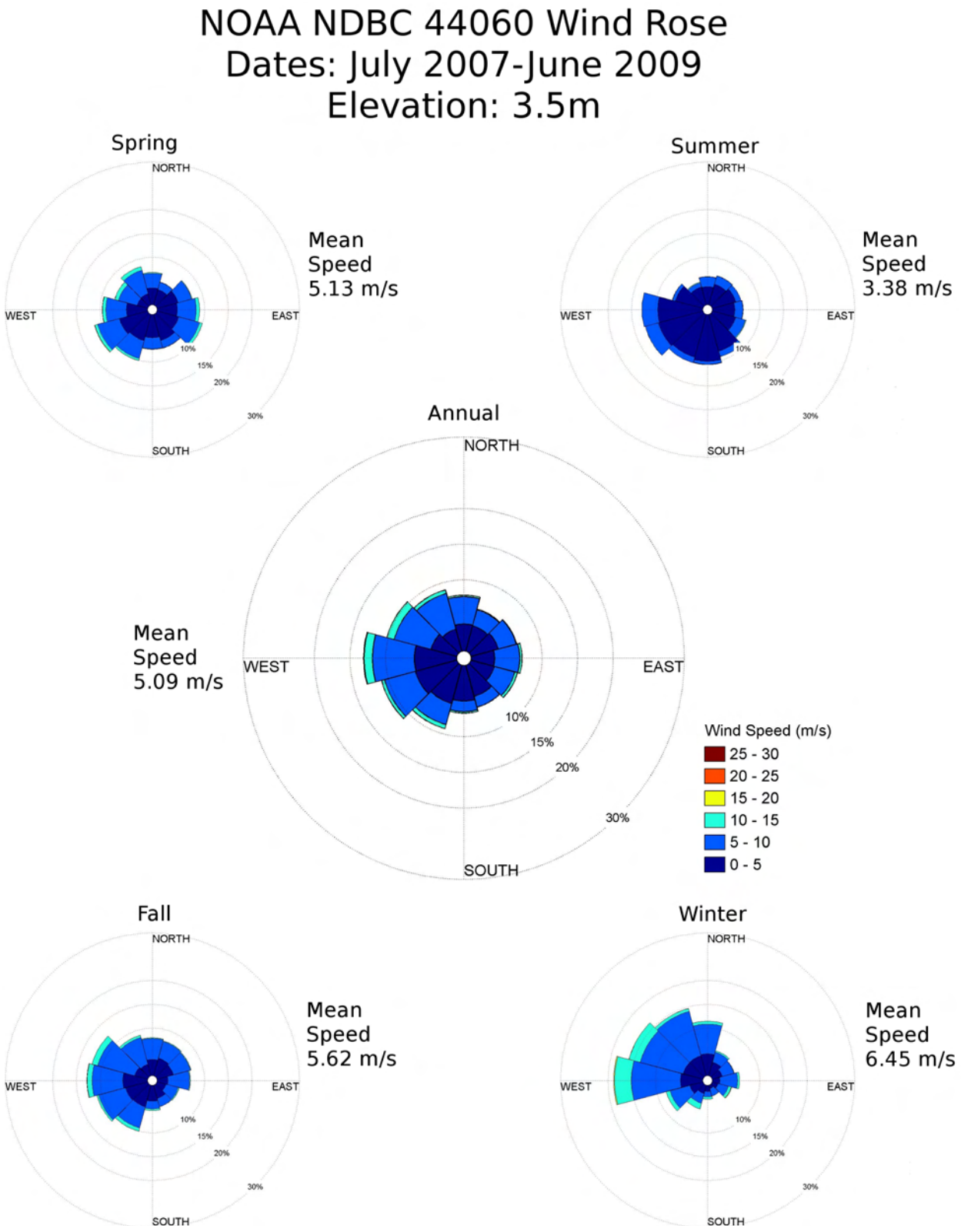
NOAA NDBC 44060 Wind Rose
Dates: July 2007-June 2009
Elevation: 3.5m
Spring
Mean Speed 5.13 m/s
Summer
Mean Speed 3.38 m/s
Annual
Mean Speed 5.09 m/s
Fall
Mean Speed 5.62 m/s
Winter
Mean Speed 6.45 m/s
NORTH
SOUTH
EAST
WEST
10%
15%
20%
30%
Wind Speed (m/s)
25 - 30
20 - 25
15 - 20
10 - 15
5 - 10
0 - 5

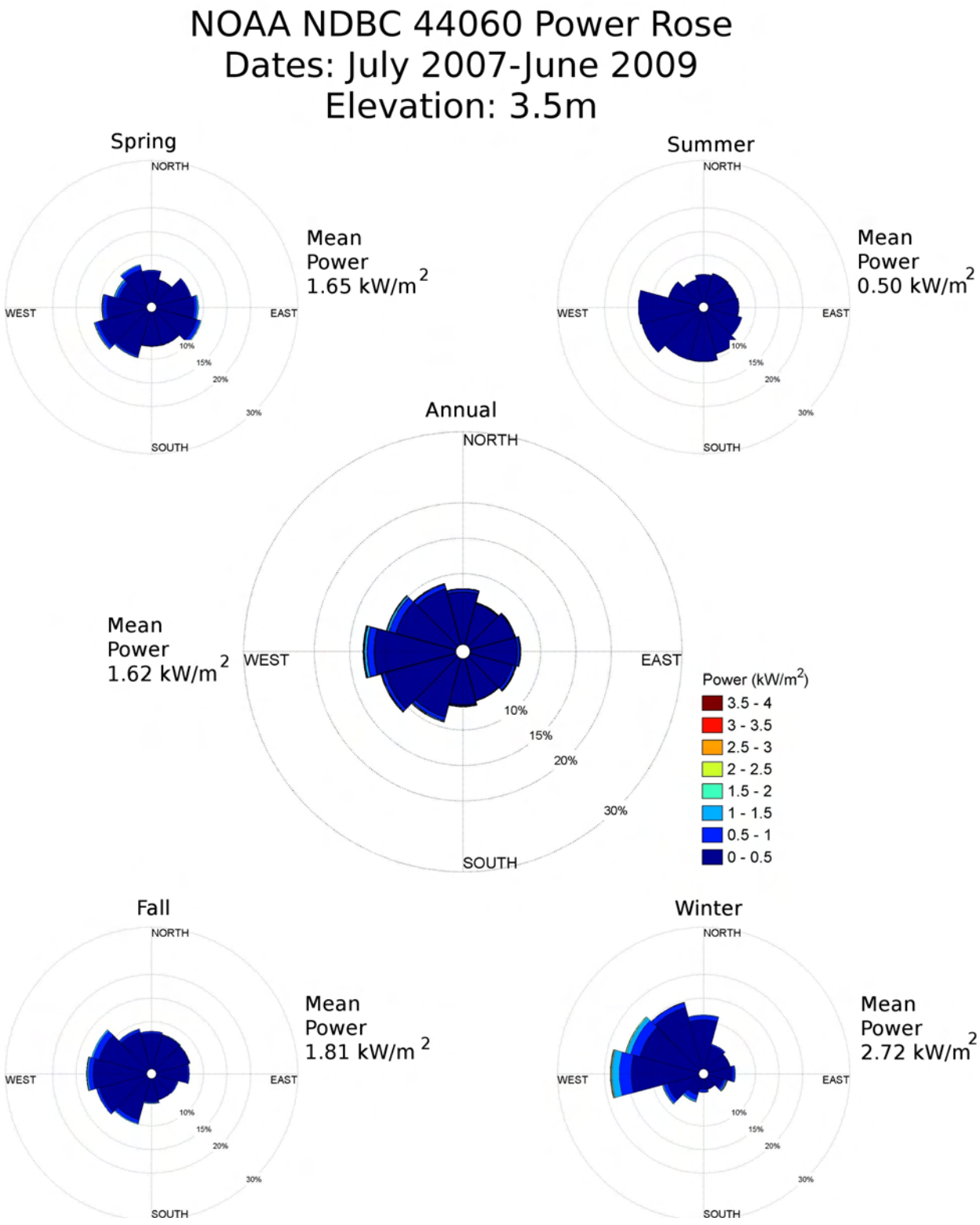
NOAA NDBC 44060 Power Rose
Dates: July 2007-June 2009
Elevation: 3.5m
Spring
Mean Power 1.65 kW/m2
Summer
Mean Power 0.50 kW/m2
Annual
Mean Power 1.62 kW/m2
Fall
Mean Power 1.81 kW/m2
Winter
Mean Power 2.72 kW/m2
NORTH
SOUTH
EAST
WEST
10%
15%
20%
30%
Power (kW/m2)
3.5 - 4
3 - 3.5
2.5 - 3
2 - 2.5
1.5 - 2
1 - 1.5
0.5 - 1
0 - 0.5

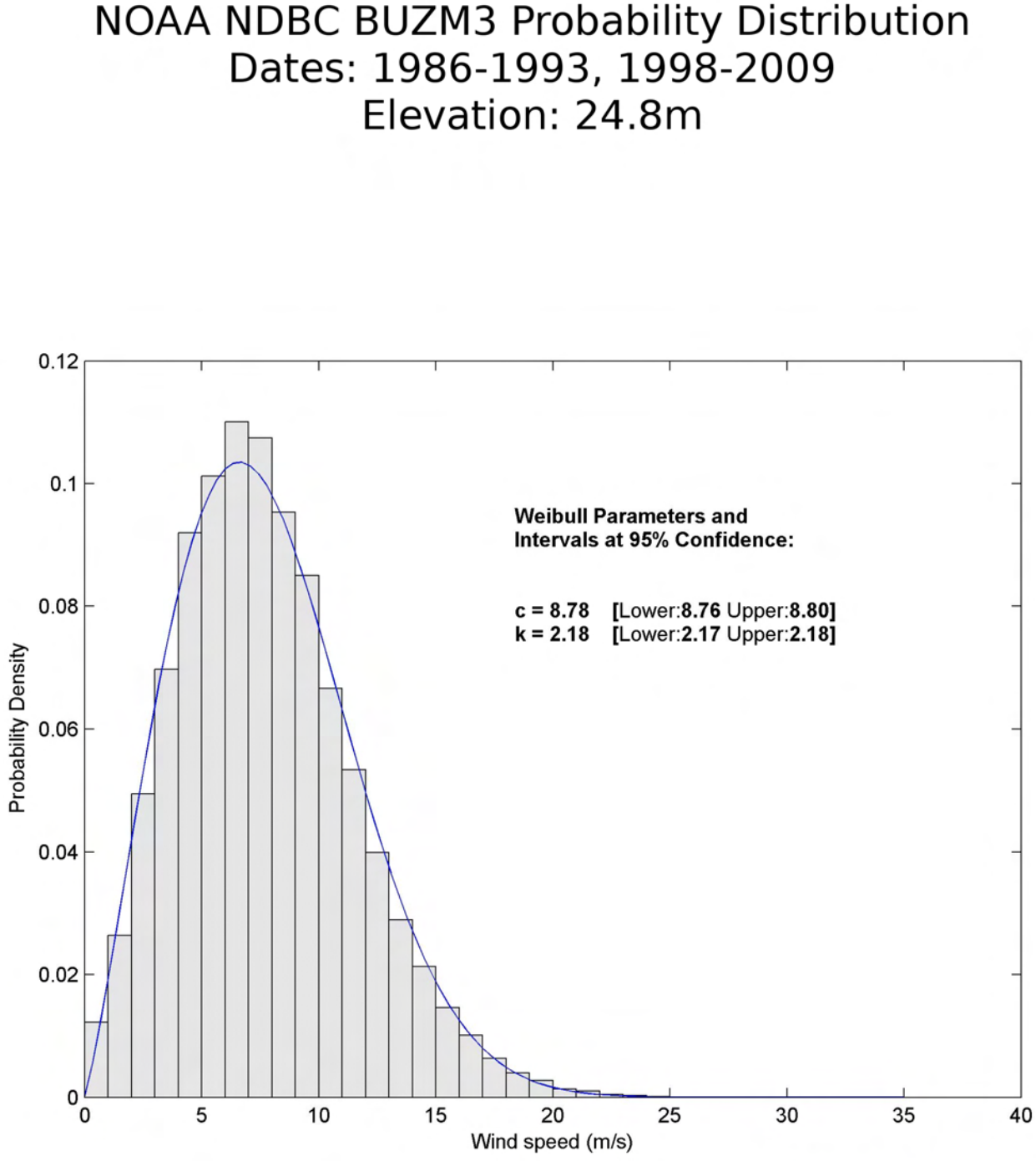
NOAA NDBC BUZM3 Probability Distribution
Dates: 1986-1993, 1998-2009
Elevation: 24.8m
Weibull Parameters and
Intervals at 95% Confidence:
c = 8.78 [Lower:8.76 Upper:8.80]
k = 2.18 [Lower:2.17 Upper:2.18]
Probability Density
Wind speed (m/s)
0.12
0.1
0.08
0.06
0.04
0.02
0
0
5
10
15
20
25
30
35
40

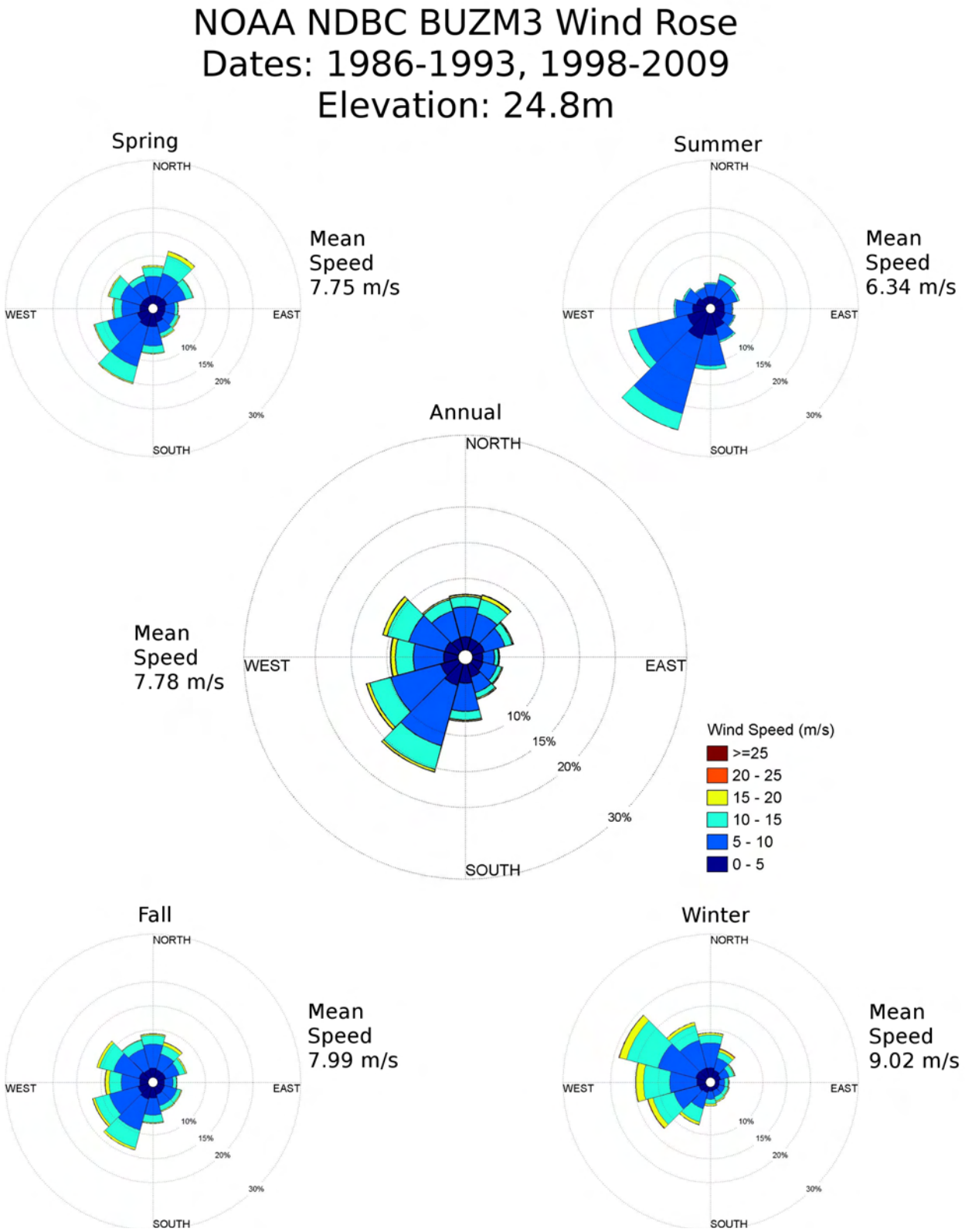
NOAA NDBC BUZM3 Wind Rose
Dates: 1986-1993, 1998-2009
Elevation: 24.8m
Spring
Mean Speed 7.75 m/s
Summer
Mean Speed 6.34 m/s
Annual
Mean Speed 7.78 m/s
Fall
Mean Speed 7.99 m/s
Winter
Mean Speed 9.02 m/s
NORTH
SOUTH
EAST
WEST
10%
15%
20%
30%
Wind Speed (m/s)
>=25
20 - 25
15 - 20
10 - 15
5 - 10
0 - 5

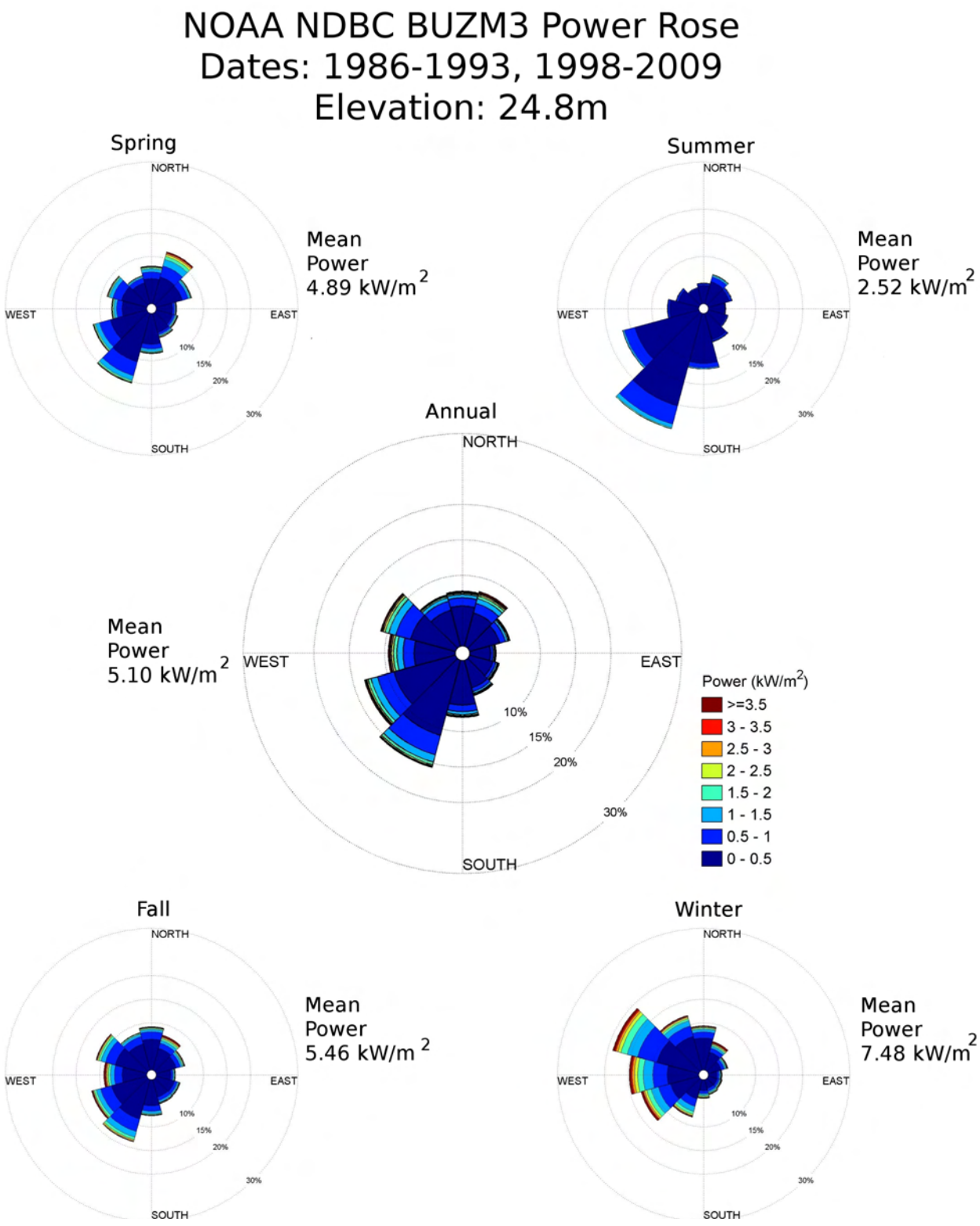
NOAA NDBC BUZM3 Power Rose
Dates: 1986-1993, 1998-2009
Elevation: 24.8m
Spring
Mean Power 4.89 kW/m2
Summer
Mean Power 2.52 kW/m2
Annual
Mean Power 5.10 kW/m2
Fall
Mean Power 5.46 kW/m2
Winter
Mean Power 7.48 kW/m2
NORTH
SOUTH
EAST
WEST
10%
15%
20%
30%
Power (kW/m2)
>=3.5
3 - 3.5
2.5 - 3
2 - 2.5
1.5 - 2
1 - 1.5
0.5 - 1
0 - 0.5

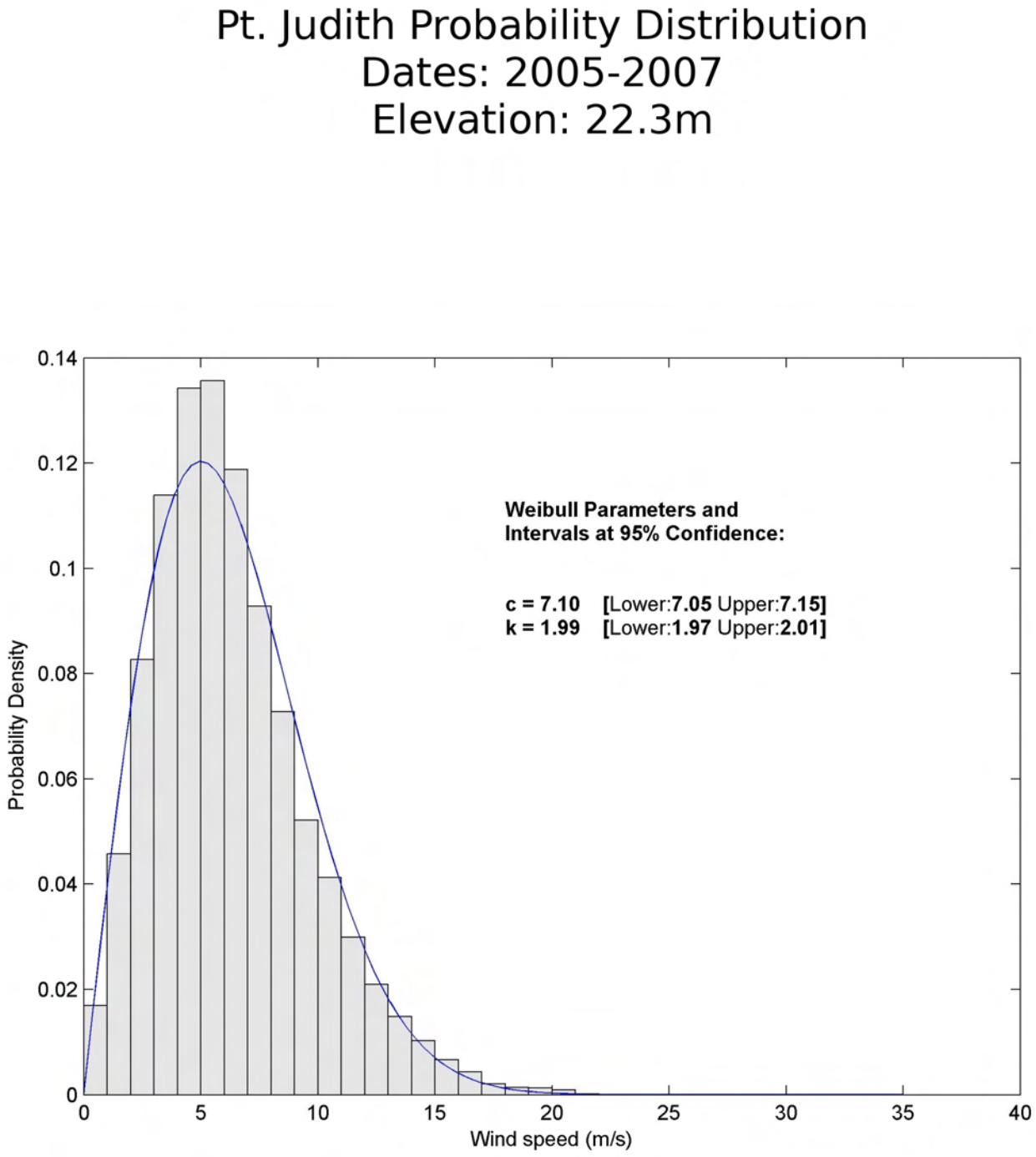
Pt. Judith Probability Distribution
Dates: 2005-2007
Elevation: 22.3m
Weibull Parameters and
Intervals at 95% Confidence:
c = 7.10 [Lower:7.05 Upper:7.15]
k = 1.99 [Lower:1.97 Upper:2.01]
Probability Density
Wind speed (m/s)
0.14
0.12
0.1
0.08
0.06
0.04
0.02
0
0
5
10
15
20
25
30
35
40

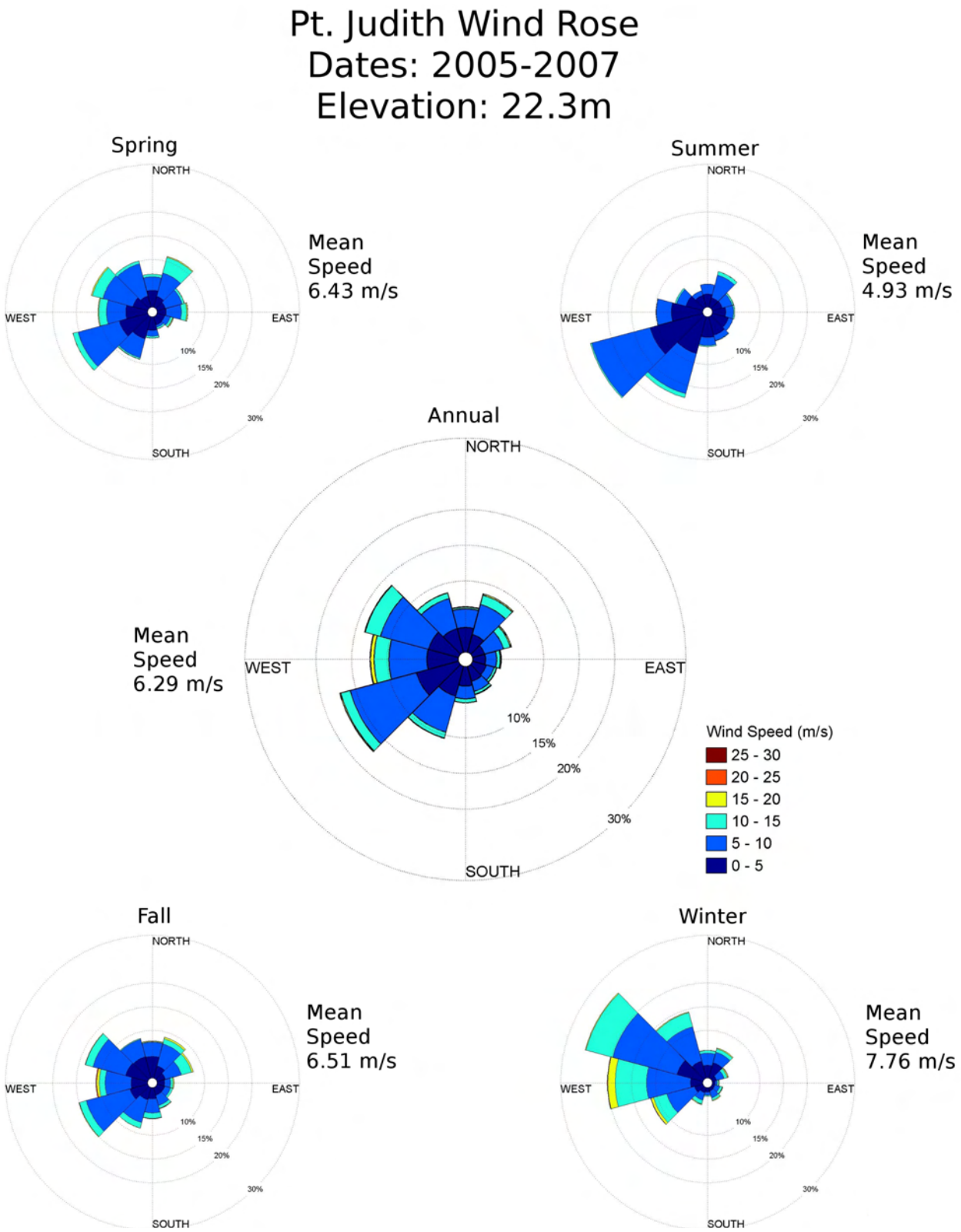
Pt. Judith Wind Rose
Dates: 2005-2007
Elevation: 22.3m
Spring
Mean Speed 6.43 m/s
Summer
Mean Speed 4.93 m/s
Annual
Mean Speed 6.29 m/s
Fall
Mean Speed 6.51 m/s
Winter
Mean Speed 7.76 m/s
NORTH
SOUTH
EAST
WEST
10%
15%
20%
30%
Wind Speed (m/s)
25 - 30
20 - 25
15 - 20
10 - 15
5 - 10
0 - 5

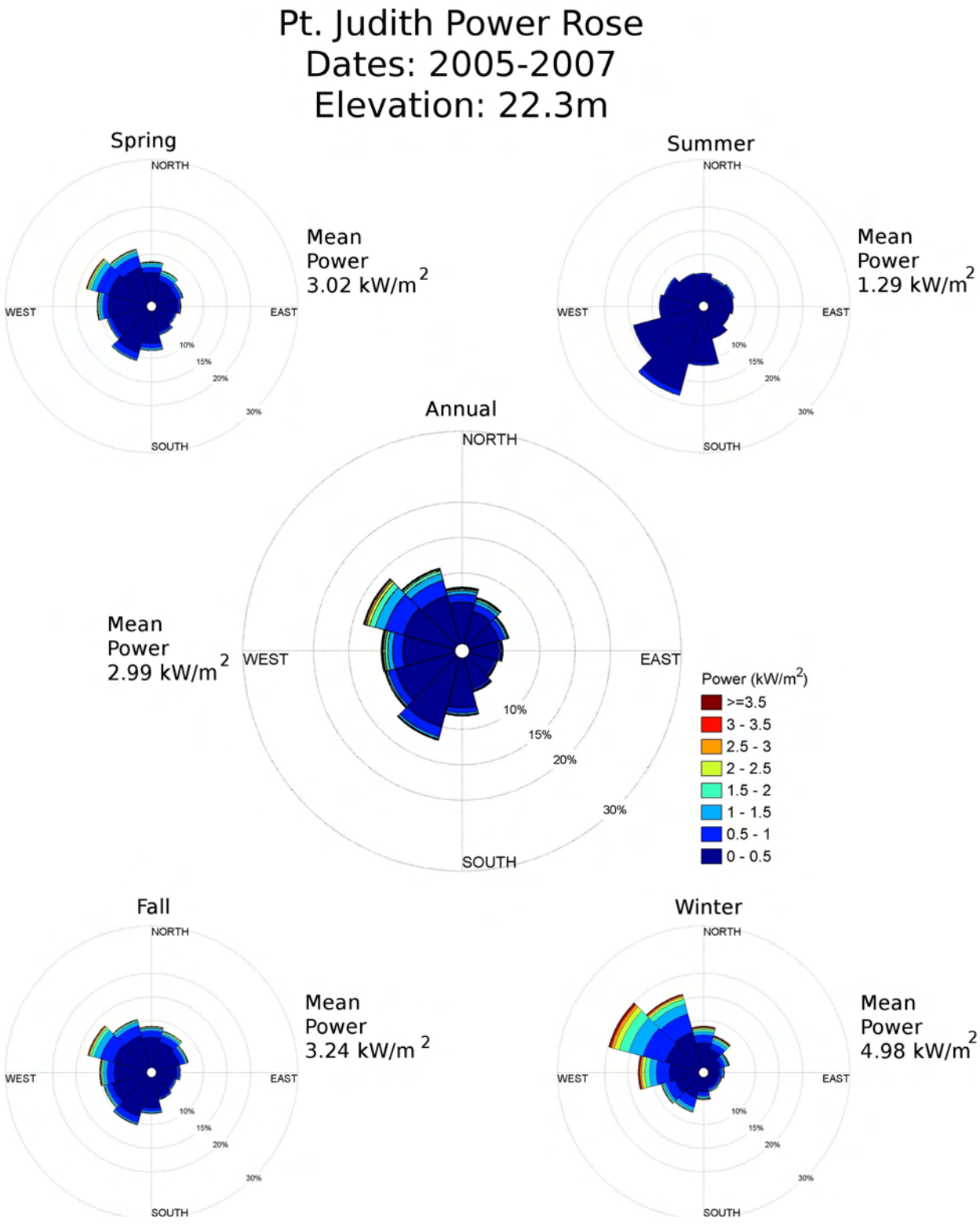
Pt. Judith Power Rose
Dates: 2005-2007
Elevation: 22.3m
Spring
Mean Power 3.02 kW/m2
Summer
Mean Power 1.29 kW/m2
Annual
Mean Power 2.99 kW/m2
Fall
Mean Power 3.24 kW/m2
Winter
Mean Power 4.98 kW/m2
NORTH
SOUTH
EAST
WEST
10%
15%
20%
30%
Power (kW/m2)
>=3.5
3 - 3.5
2.5 - 3
2 - 2.5
1.5 - 2
1 - 1.5
0.5 - 1
0 - 0.5

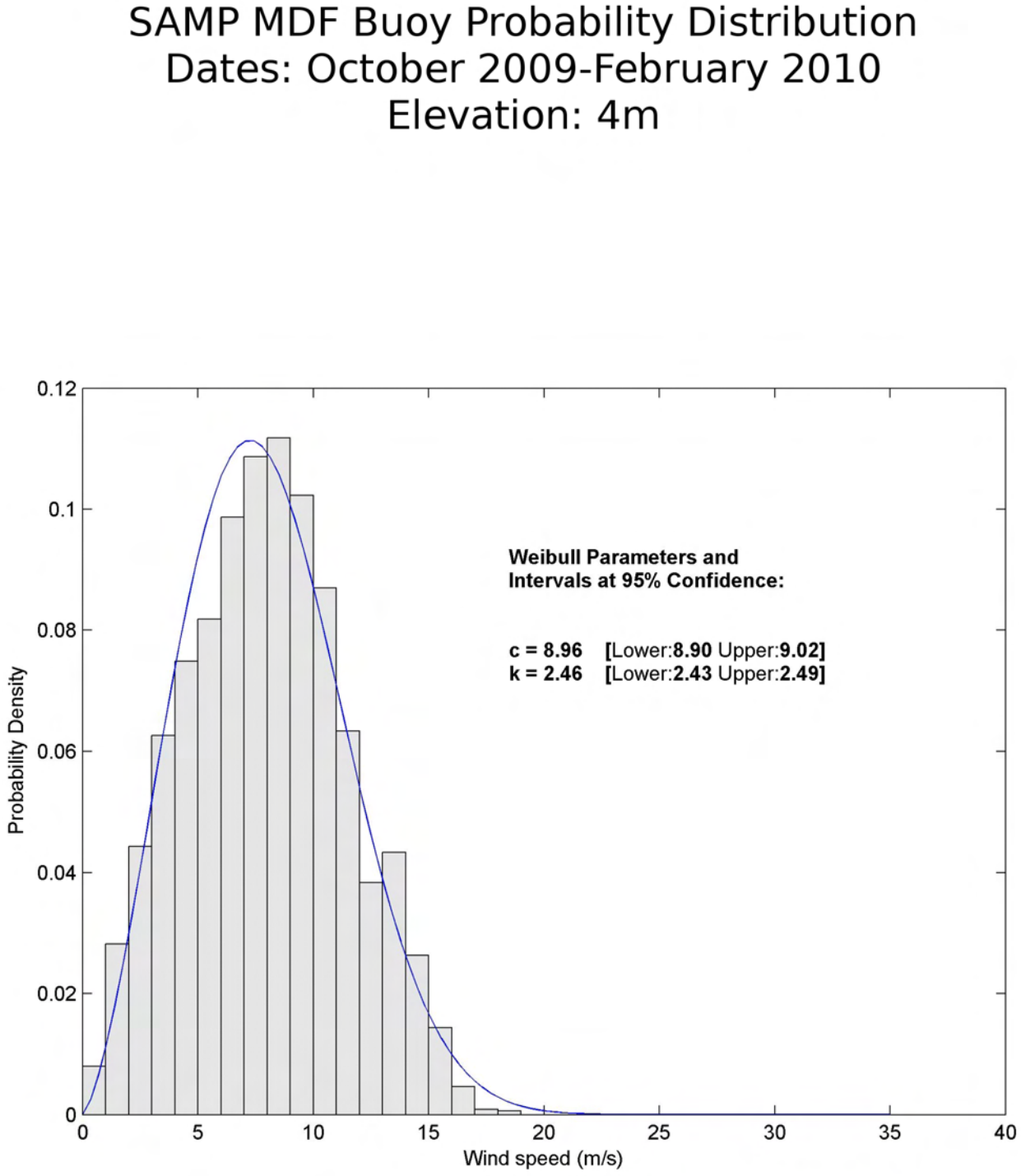
SAMP MDF Buoy Probability Distribution
Dates: October 2009-February 2010
Elevation: 4m
Weibull Parameters and
Intervals at 95% Confidence:
c = 8.96 [Lower:8.90 Upper:9.02]
k = 2.46 [Lower:2.43 Upper:2.49]
Probability Density
Wind speed (m/s)
0.12
0.1
0.08
0.06
0.04
0.02
0
0
5
10
15
20
25
30
35
40

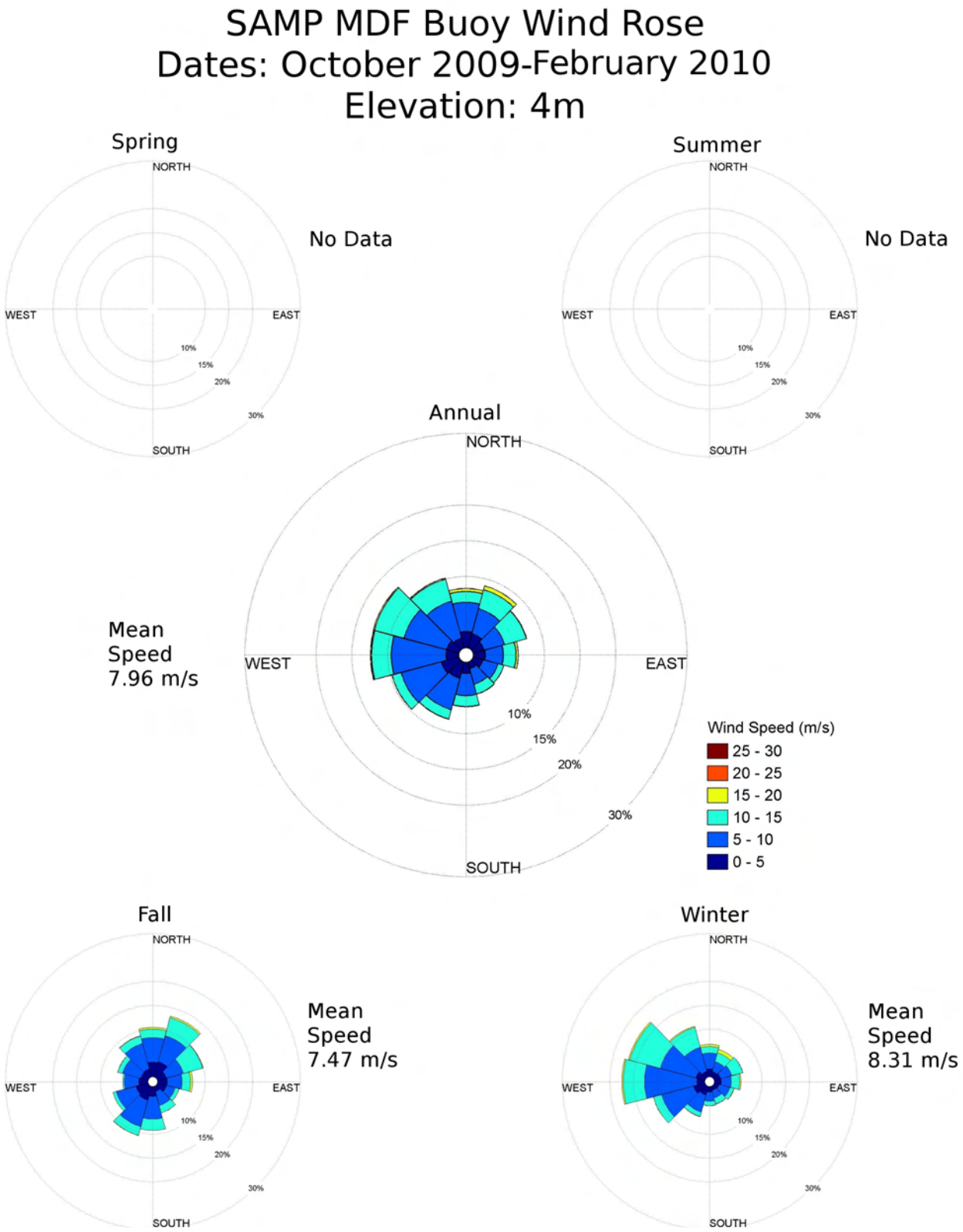
SAMP MDF Buoy Wind Rose
Dates: October 2009-February 2010
Elevation: 4m
Spring
No Data
Summer
No Data
Annual
Mean
Speed
7.96 m/s
Fall
Mean
Speed
7.47 m/s
Winter
Mean
Speed
8.31 m/s
NORTH
SOUTH
EAST
WEST
10%
15%
20%
30%
Wind Speed (m/s)
25 - 30
20 - 25
15 - 20
10 - 15
5 - 10
0 - 5

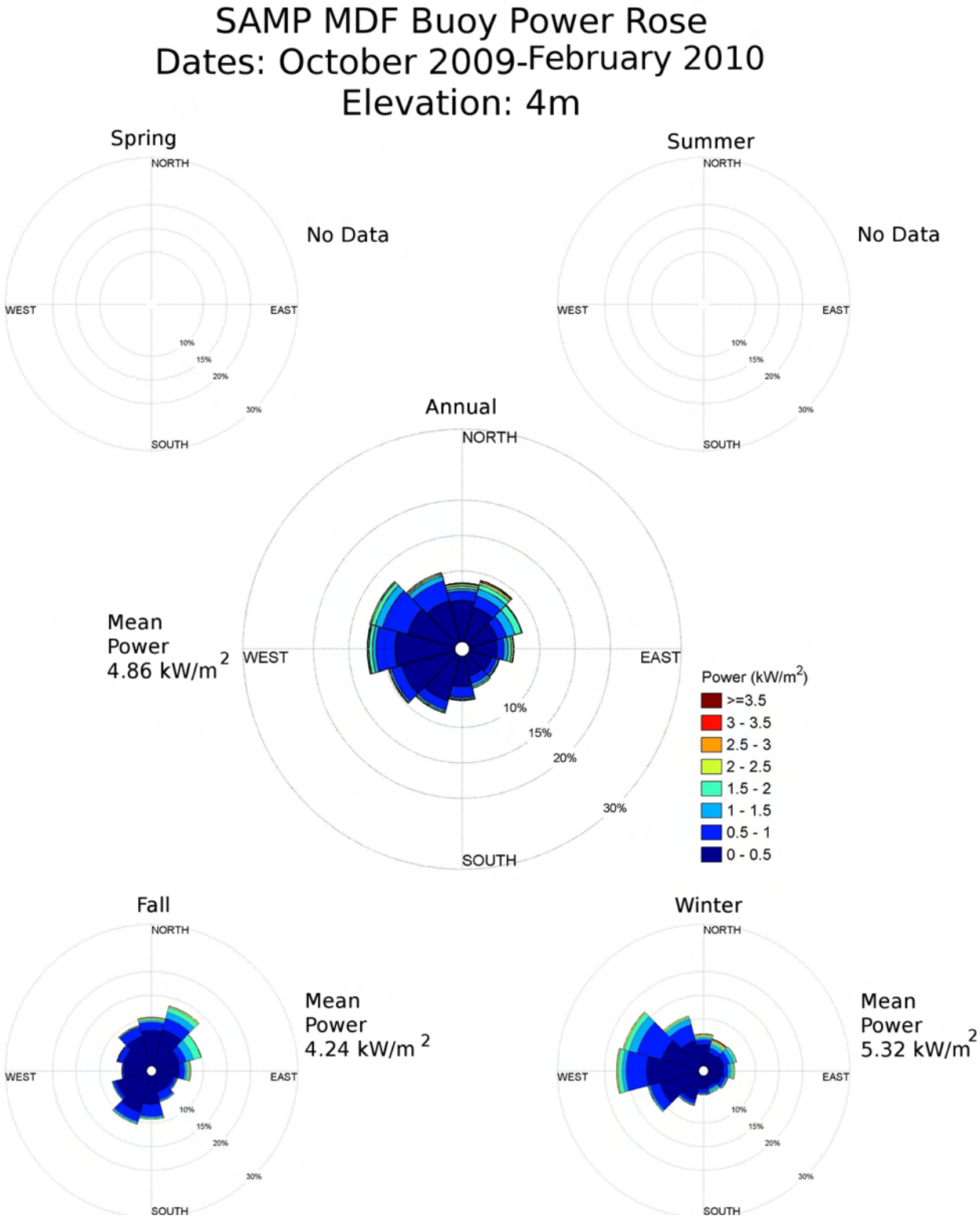
SAMP MDF Buoy Power Rose
Dates: October 2009-February 2010
Elevation: 4m
Spring
No Data
Summer
No Data
Annual
Mean
Power
4.86 kW/m 2
Fall
Mean
Power
4.24 kW/m 2
Winter
Mean
Power
5.32 kW/m 2
NORTH
SOUTH
EAST
WEST
10%
15%
20%
30%
Power (kW/m2)
>=3.5
3 - 3.5
2.5 - 3
2 - 2.5
1.5 - 2
1 - 1.5
0.5 - 1
0 - 0.5

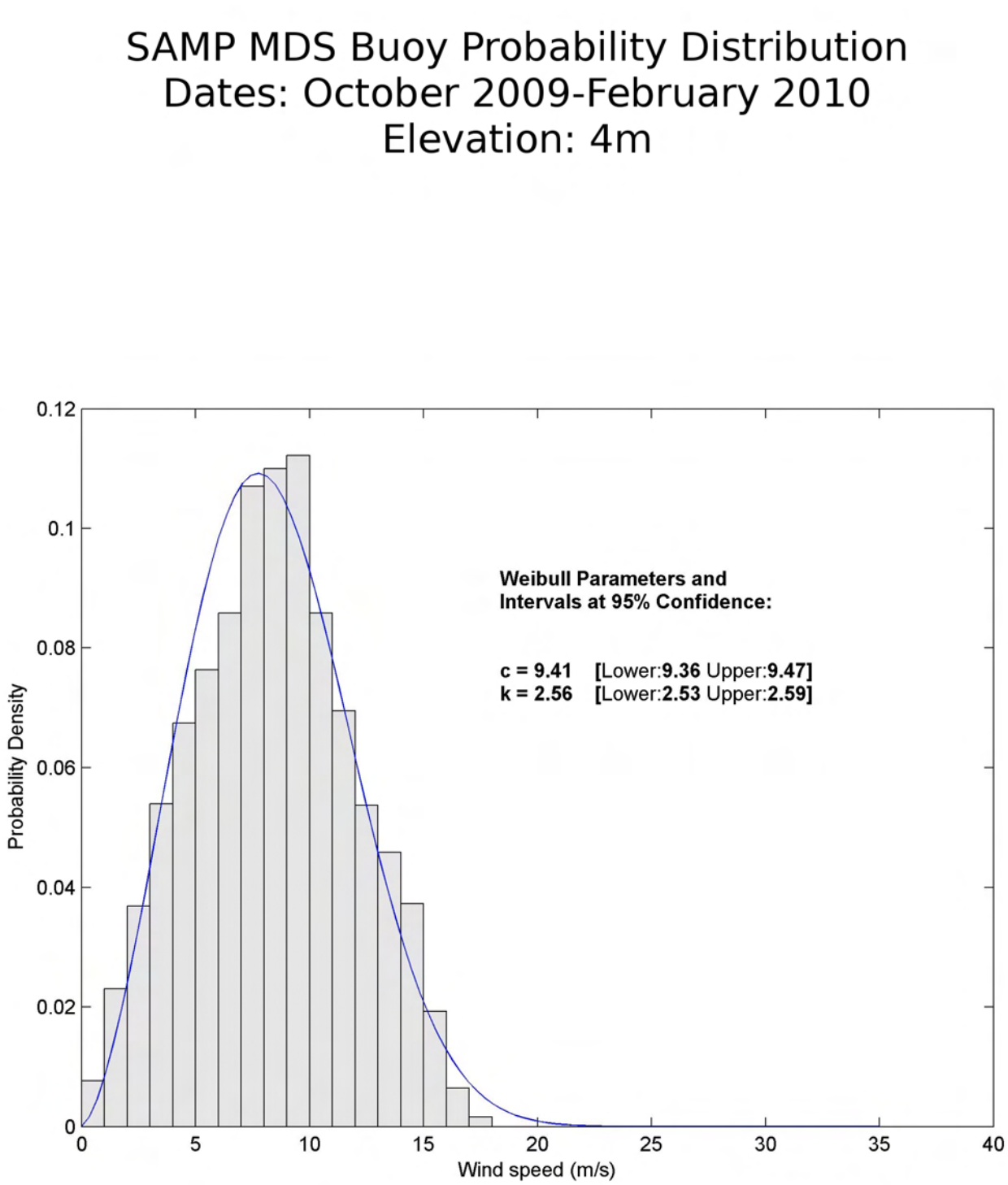
SAMP MDS Buoy Probability Distribution
Dates: October 2009-February 2010
Elevation: 4m
Weibull Parameters and
Intervals at 95% Confidence:
c = 9.41 [Lower:9.36 Upper:9.47]
k = 2.56 [Lower:2.53 Upper:2.59]
Probability Density
Wind speed (m/s)
0
0.02
0.04
0.06
0.08
0.1
0.12
0
5
10
15
20
25
30
35
40

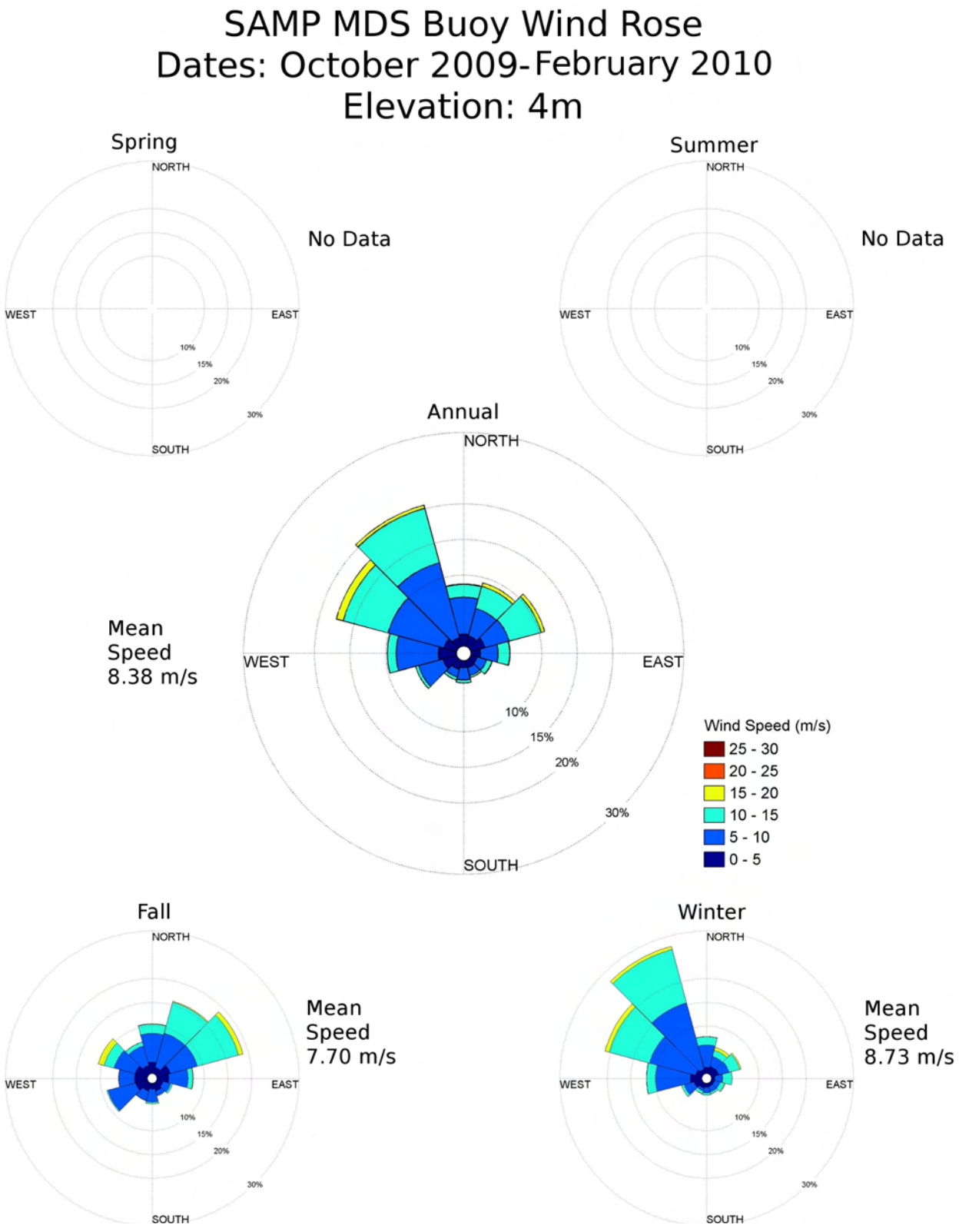
SAMP MDS Buoy Wind Rose
Dates: October 2009-February 2010
Elevation: 4m
Spring
No Data
Summer
No Data
Annual
Mean
Speed
8.38 m/s
Fall
Mean
Speed
7.70 m/s
Winter
Mean
Speed
8.73 m/s
NORTH
SOUTH
EAST
WEST
10%
15%
20%
30%
Wind Speed (m/s)
25 - 30
20 - 25
15 - 20
10 - 15
5 - 10
0 - 5

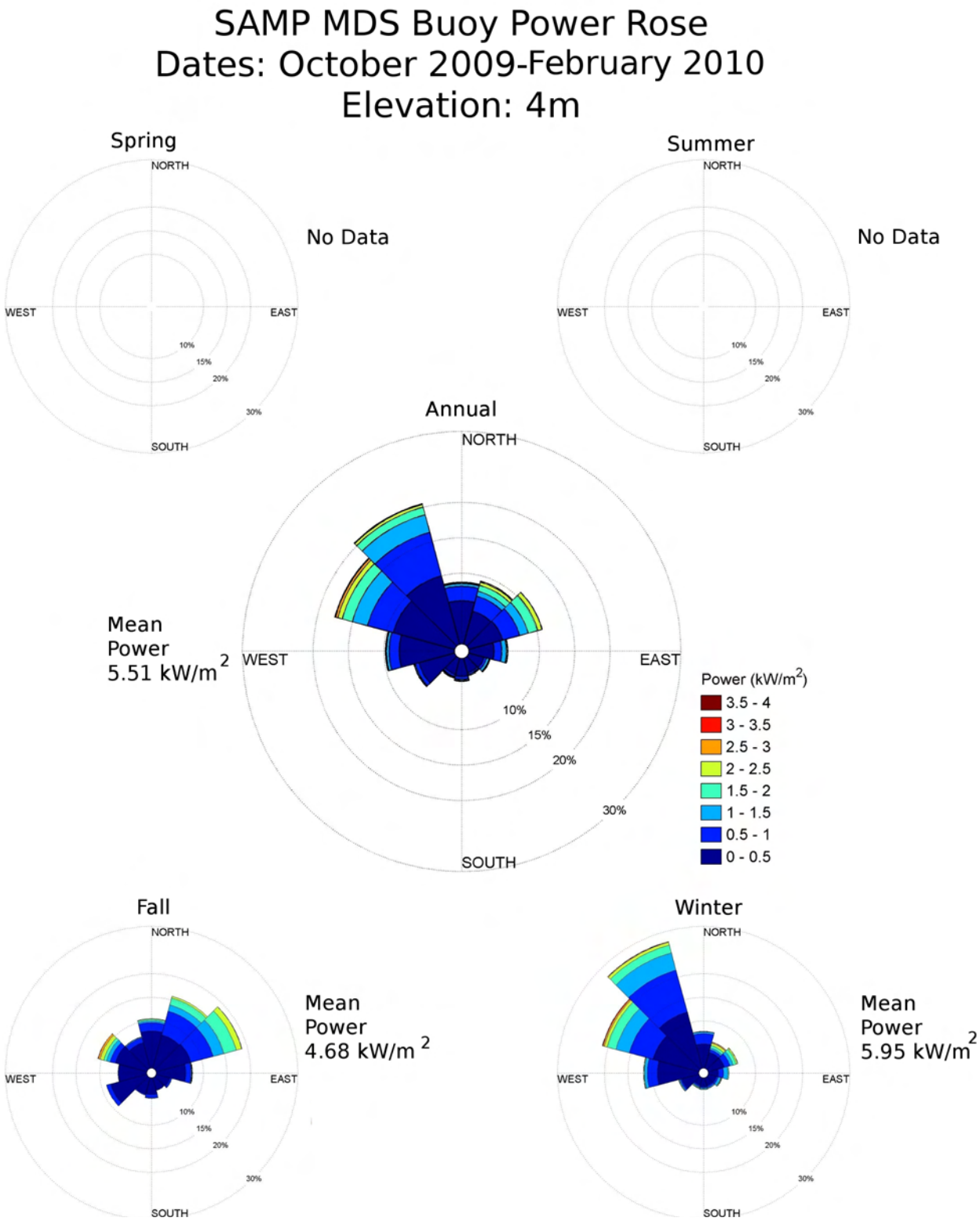
SAMP MDS Buoy Power Rose
Dates: October 2009-February 2010
Elevation: 4m
Spring
No Data
Summer
No Data
Annual
Mean
Power
5.51 kW/m 2
Power (kW/m2)
3.5 - 4
3 - 3.5
2.5 - 3
2 - 2.5
1.5 - 2
1 - 1.5
0.5 - 1
0 - 0.5
Fall
Mean
Power
4.68 kW/m 2
Winter
Mean
Power
5.95 kW/m 2
NORTH
SOUTH
EAST
WEST
10%
15%
20%
30%

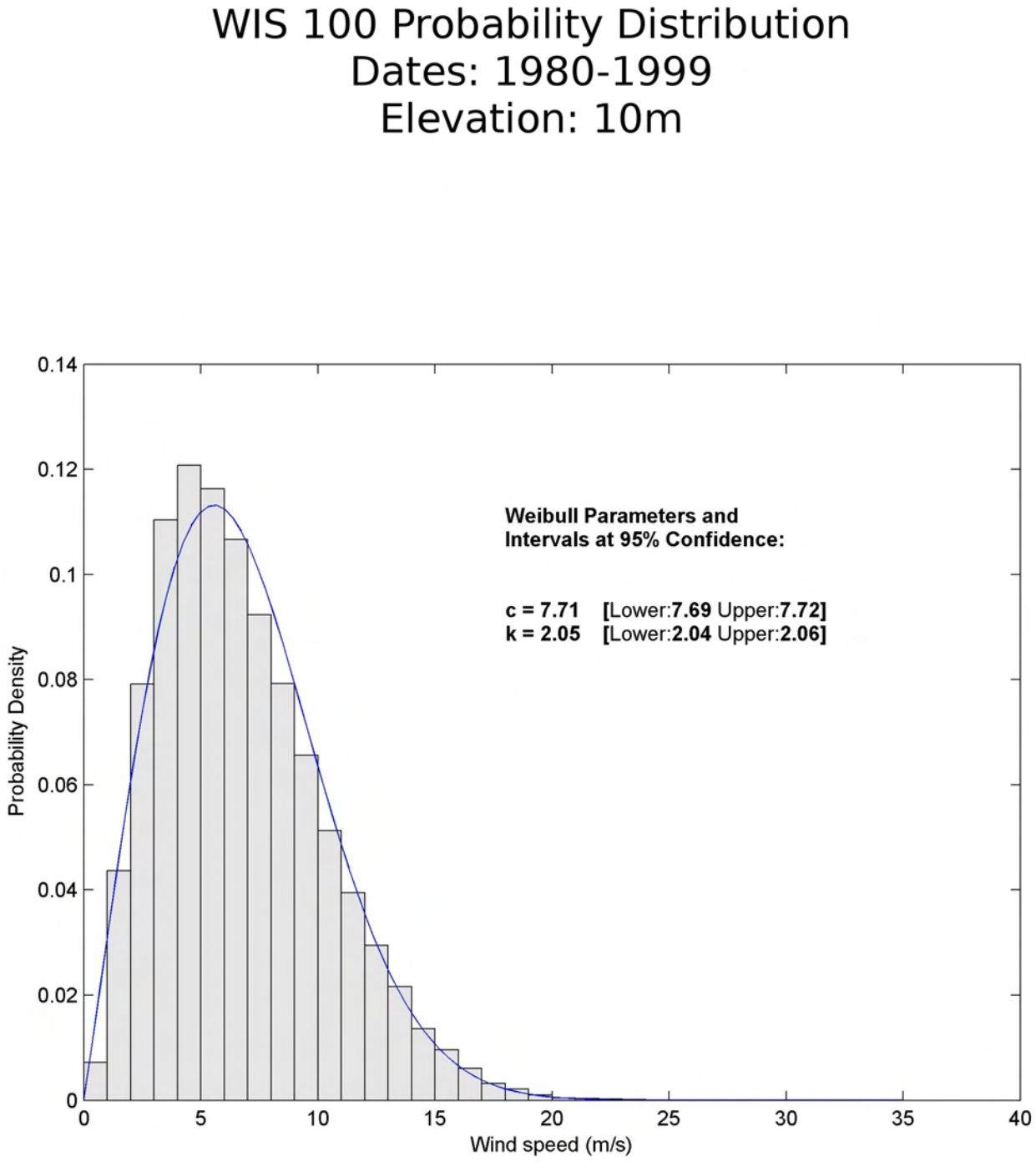
WIS 100 Probability Distribution
Dates: 1980-1999
Elevation: 10m
Weibull Parameters and
Intervals at 95% Confidence:
c = 7.71 [Lower:7.69 Upper:7.72]
k = 2.05 [Lower:2.04 Upper:2.06]
Probability Density
Wind speed (m/s)
0.14
0.12
0.1
0.08
0.06
0.04
0.02
0
0
5
10
15
20
25
30
35
40

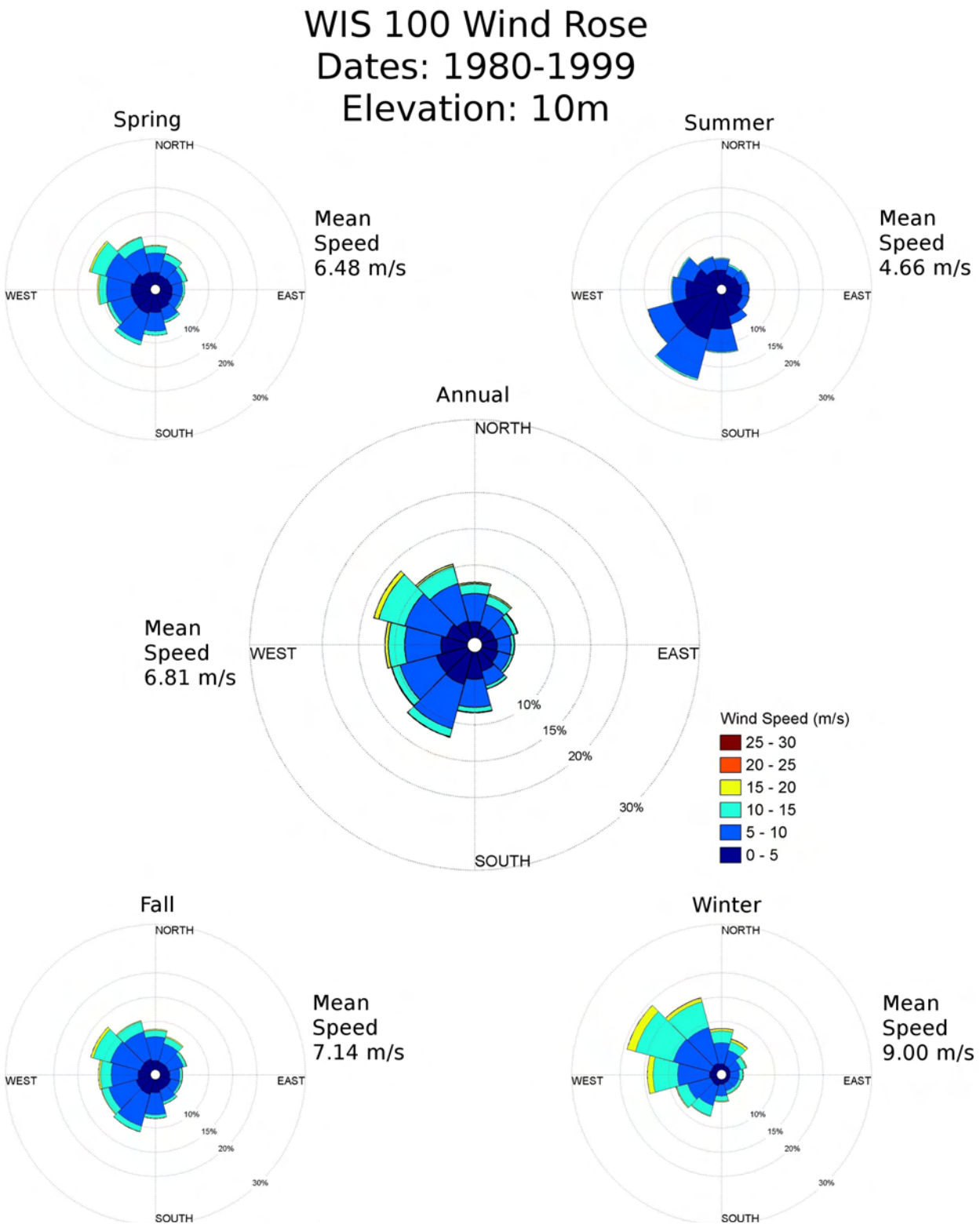
WIS 100 Wind Rose
Dates: 1980-1999
Elevation: 10m
Spring
Mean Speed 6.48 m/s
Summer
Mean Speed 4.66 m/s
Annual
Mean Speed 6.81 m/s
Fall
Mean Speed 7.14 m/s
Winter
Mean Speed 9.00 m/s
NORTH
SOUTH
EAST
WEST
10%
15%
20%
30%
Wind Speed (m/s)
25 - 30
20 - 25
15 - 20
10 - 15
5 - 10
0 - 5

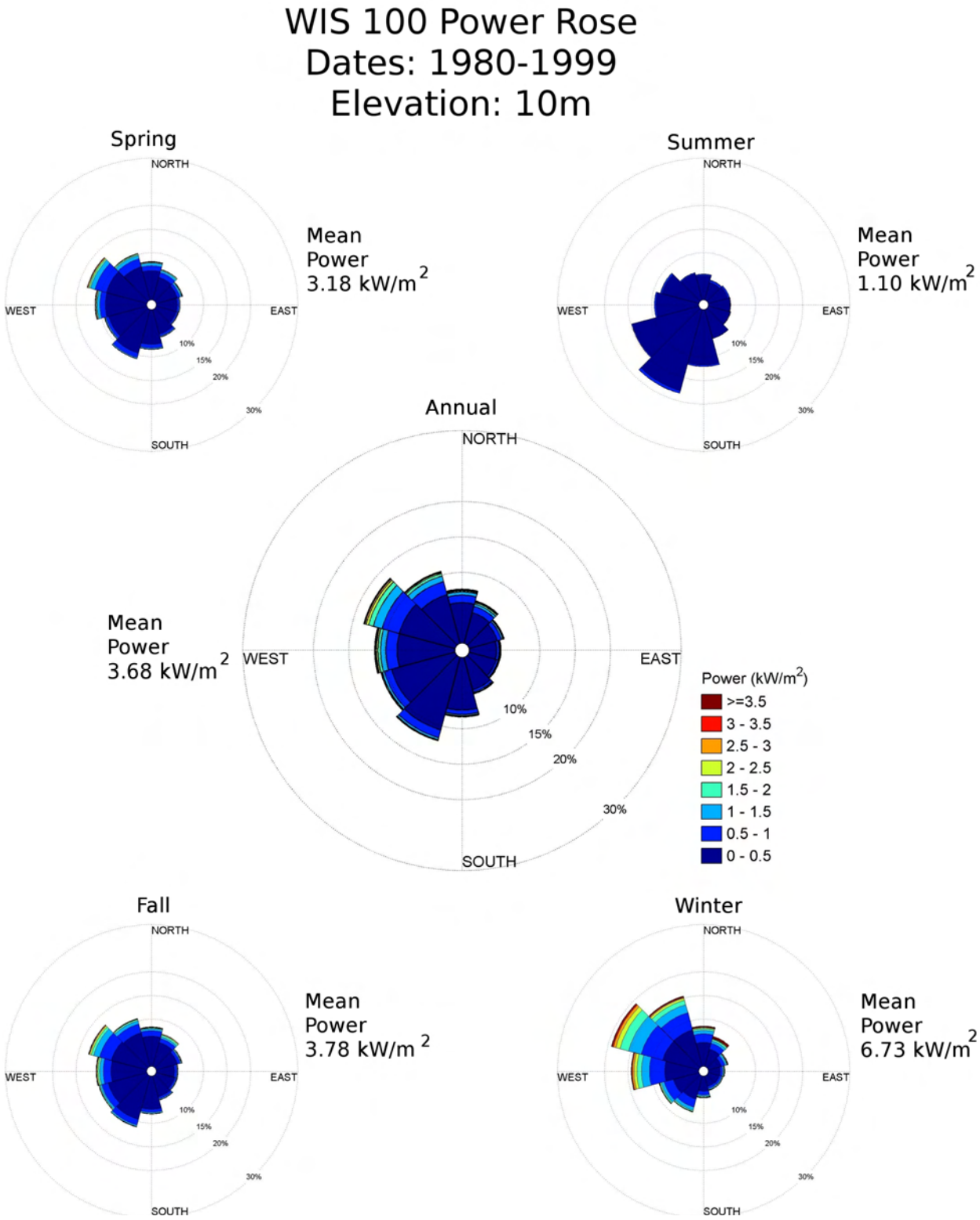
WIS 100 Power Rose
Dates: 1980-1999
Elevation: 10m
Spring
Mean Power 3.18 kW/m2
Summer
Mean Power 1.10 kW/m2
Annual
Mean Power 3.68 kW/m2
Fall
Mean Power 3.78 kW/m2
Winter
Mean Power 6.73 kW/m2
NORTH
SOUTH
EAST
WEST
10%
15%
20%
30%
Power (kW/m2)
>=3.5
3 - 3.5
2.5 - 3
2 - 2.5
1.5 - 2
1 - 1.5
0.5 - 1
0 - 0.5

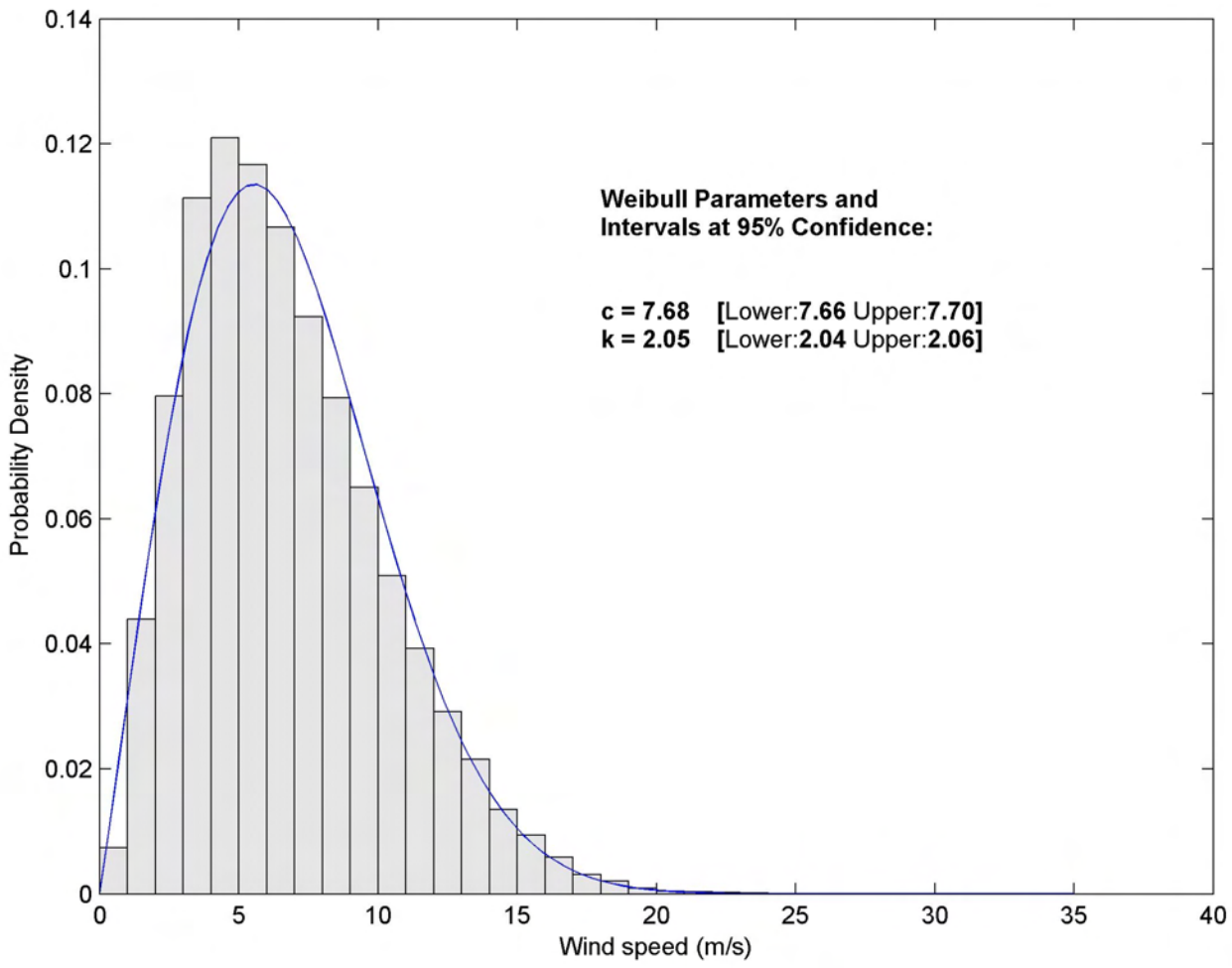
WIS 101 Probability Distribution
Dates: 1980-1999
Elevation: 10m
Weibull Parameters and
Intervals at 95% Confidence:
c = 7.68 [Lower:7.66 Upper:7.70]
k = 2.05 [Lower:2.04 Upper:2.06]
Probability Density
Wind speed (m/s)
0
0.02
0.04
0.06
0.08
0.1
0.12
0.14
0
5
10
15
20
25
30
35
40

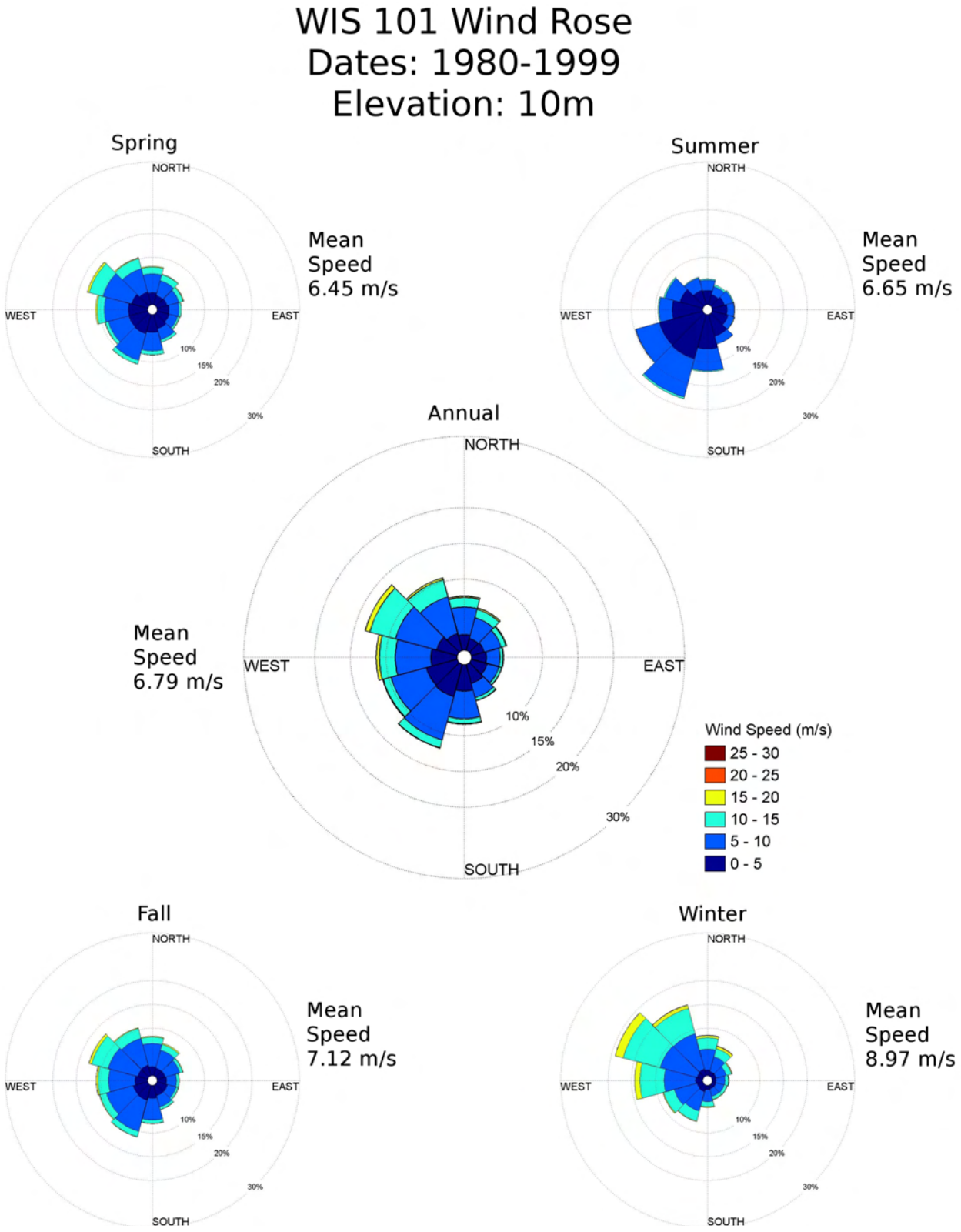
WIS 101 Wind Rose
Dates: 1980-1999
Elevation: 10m
Spring
Mean Speed 6.45 m/s
Summer
Mean Speed 6.65 m/s
Annual
Mean Speed 6.79 m/s
Fall
Mean Speed 7.12 m/s
Winter
Mean Speed 8.97 m/s
NORTH
SOUTH
EAST
WEST
10%
15%
20%
30%
Wind Speed (m/s)
25 - 30
20 - 25
15 - 20
10 - 15
5 - 10
0 - 5

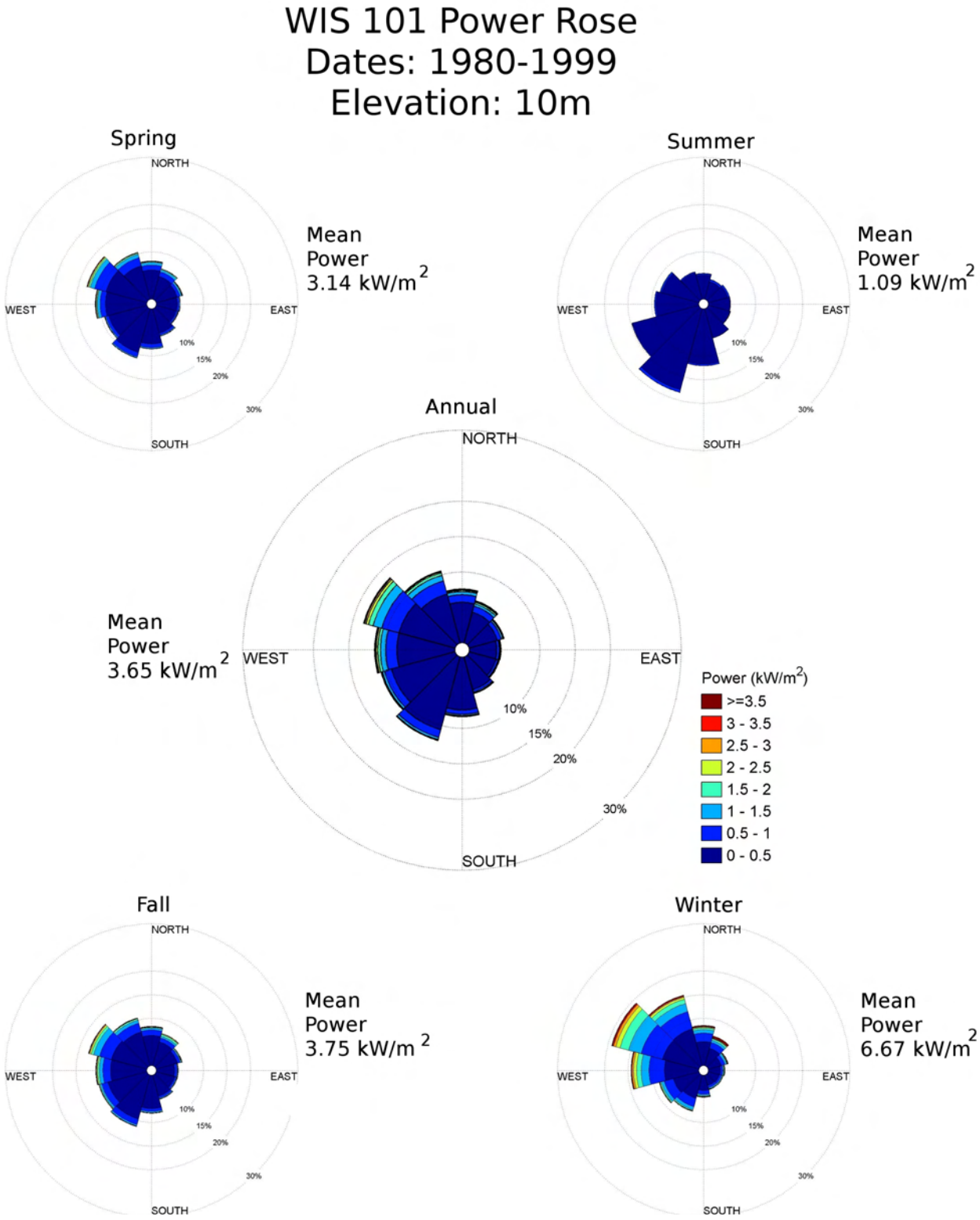
WIS 101 Power Rose
Dates: 1980-1999
Elevation: 10m
Spring
Mean Power 3.14 kW/m2
Summer
Mean Power 1.09 kW/m2
Annual
Mean Power 3.65 kW/m2
Fall
Mean Power 3.75 kW/m2
Winter
Mean Power 6.67 kW/m2
NORTH
SOUTH
EAST
WEST
10%
15%
20%
30%
Power (kW/m2)
>=3.5
3 - 3.5
2.5 - 3
2 - 2.5
1.5 - 2
1 - 1.5
0.5 - 1
0 - 0.5

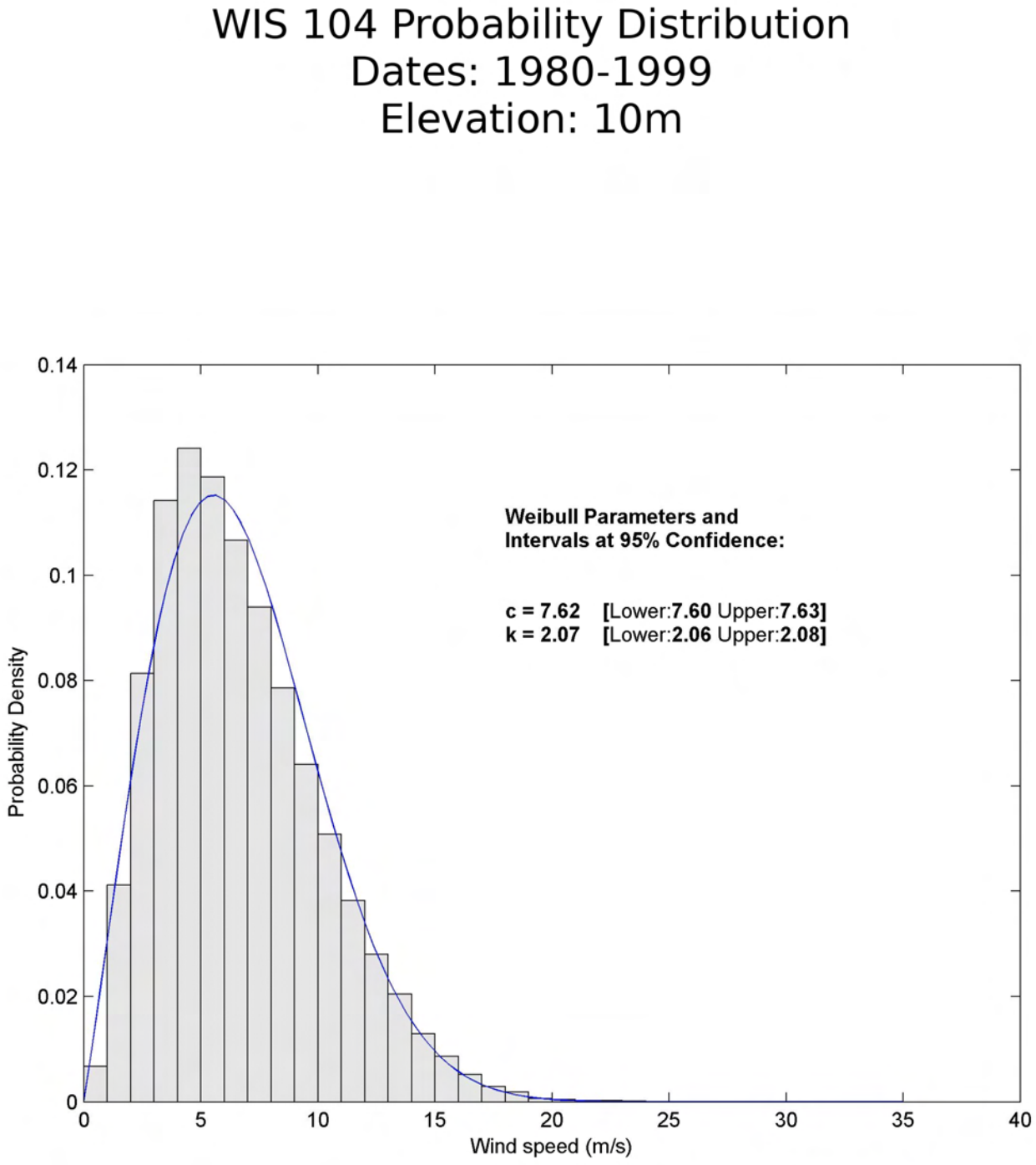
WIS 104 Probability Distribution
Dates: 1980-1999
Elevation: 10m
Weibull Parameters and
Intervals at 95% Confidence:
c = 7.62 [Lower:7.60 Upper:7.63]
k = 2.07 [Lower:2.06 Upper:2.08]
Probability Density
Wind speed (m/s)
0
0.02
0.04
0.06
0.08
0.1
0.12
0.14
0
5
10
15
20
25
30
35
40

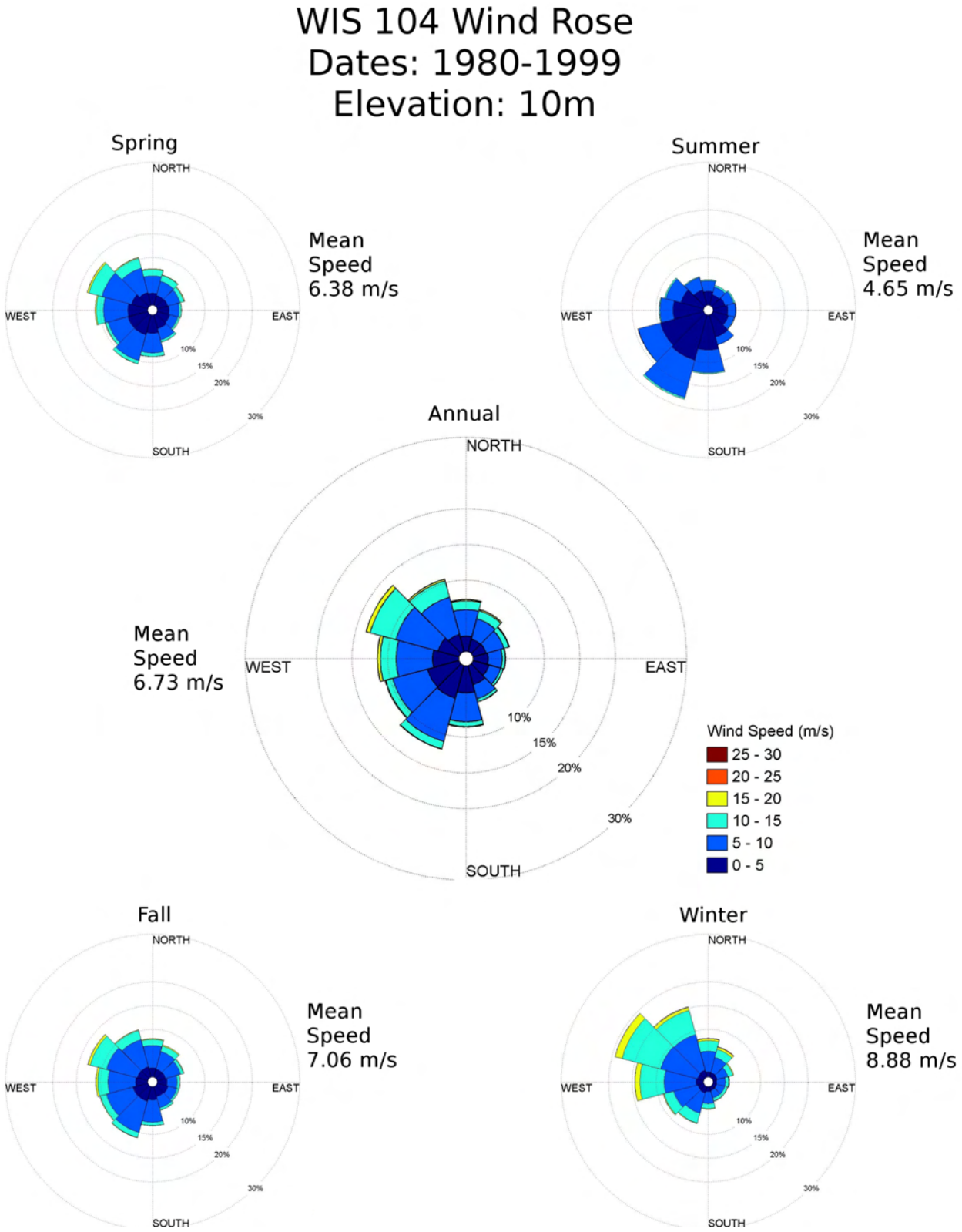
WIS 104 Wind Rose
Dates: 1980-1999
Elevation: 10m
Spring
Mean Speed 6.38 m/s
Summer
Mean Speed 4.65 m/s
Annual
Mean Speed 6.73 m/s
Fall
Mean Speed 7.06 m/s
Winter
Mean Speed 8.88 m/s
NORTH
SOUTH
EAST
WEST
10%
15%
20%
30%
Wind Speed (m/s)
25 - 30
20 - 25
15 - 20
10 - 15
5 - 10
0 - 5

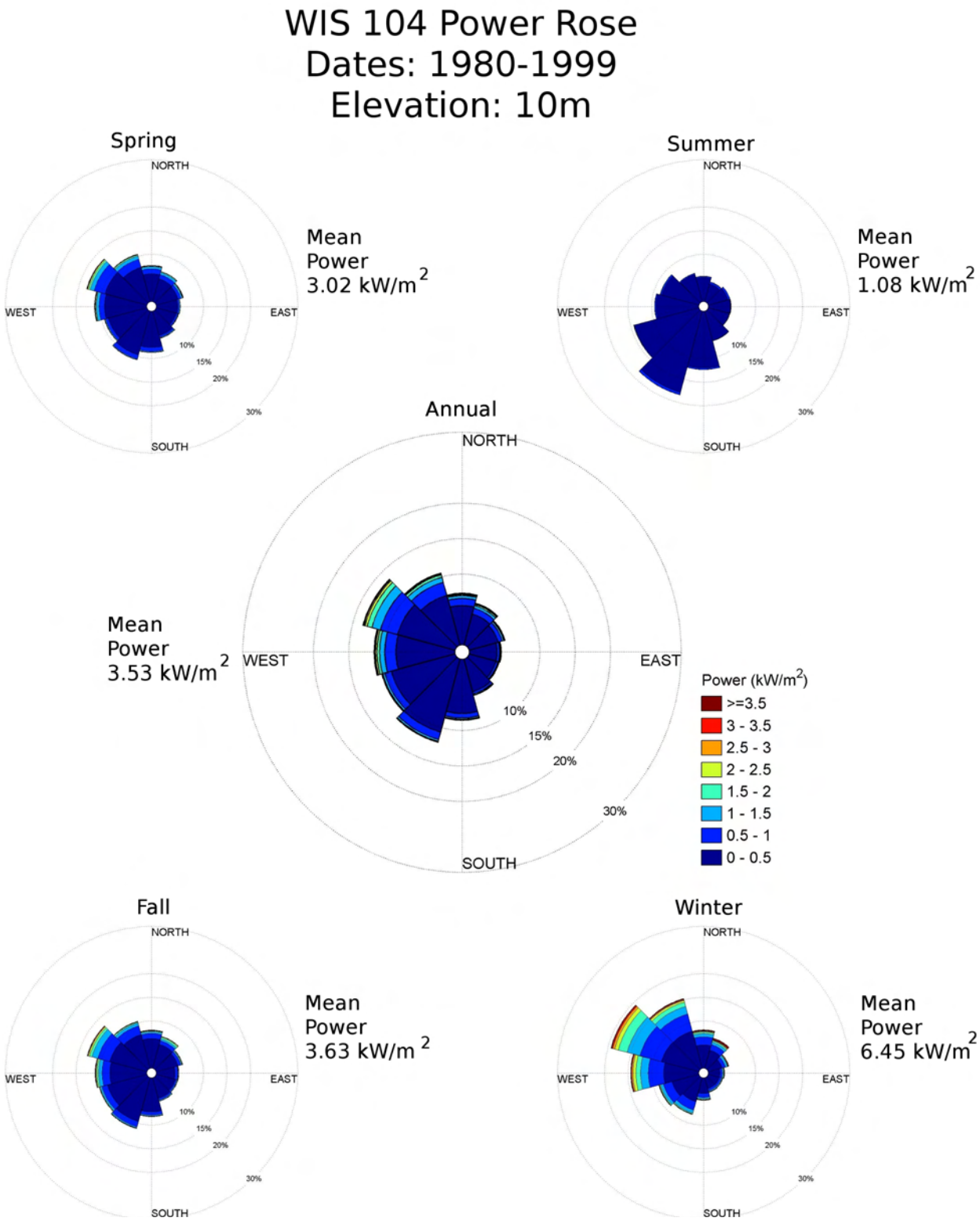
WIS 104 Power Rose
Dates: 1980-1999
Elevation: 10m
Spring
Mean Power 3.02 kW/m2
Summer
Mean Power 1.08 kW/m2
Annual
Mean Power 3.53 kW/m2
Fall
Mean Power 3.63 kW/m2
Winter
Mean Power 6.45 kW/m2
NORTH
SOUTH
EAST
WEST
10%
15%
20%
30%
Power (kW/m2)
>=3.5
3 - 3.5
2.5 - 3
2 - 2.5
1.5 - 2
1 - 1.5
0.5 - 1
0 - 0.5

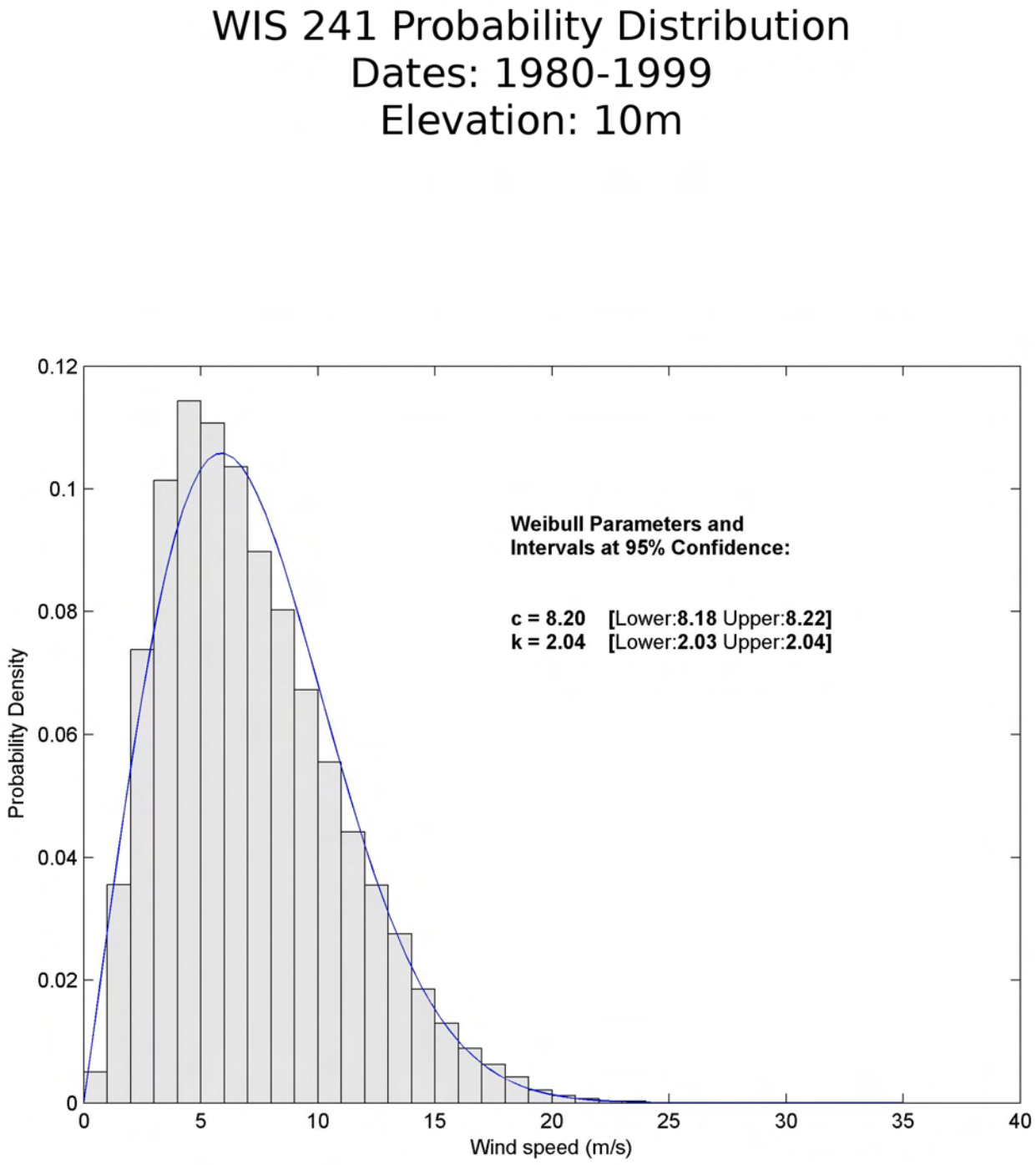
WIS 241 Probability Distribution
Dates: 1980-1999
Elevation: 10m
Weibull Parameters and
Intervals at 95% Confidence:
c = 8.20 [Lower:8.18 Upper:8.22]
k = 2.04 [Lower:2.03 Upper:2.04]
Probability Density
Wind speed (m/s)
0
0.02
0.04
0.06
0.08
0.1
0.12
0
5
10
15
20
25
30
35
40

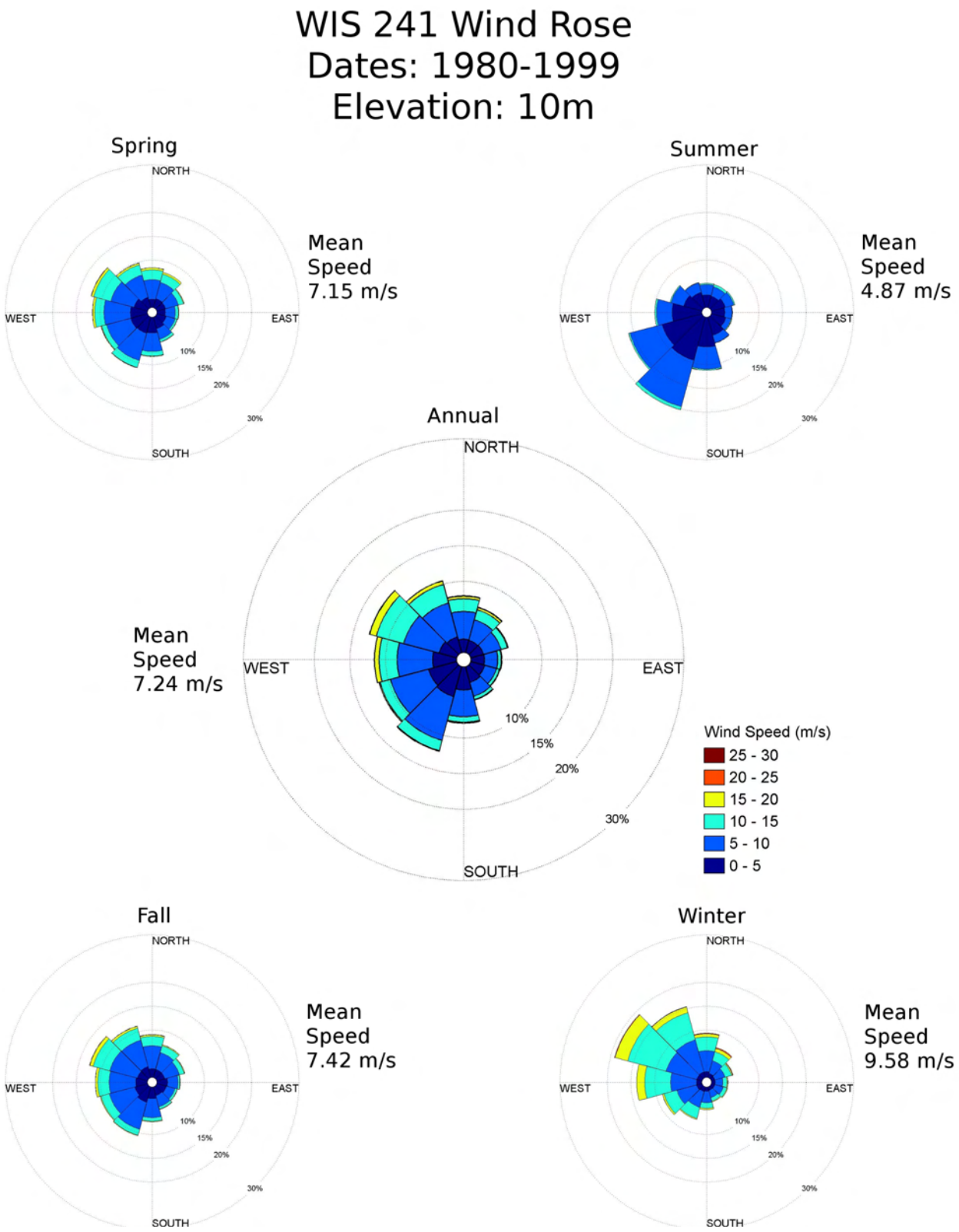
WIS 241 Wind Rose
Dates: 1980-1999
Elevation: 10m
Spring
Mean Speed 7.15 m/s
Summer
Mean Speed 4.87 m/s
Annual
Mean Speed 7.24 m/s
Fall
Mean Speed 7.42 m/s
Winter
Mean Speed 9.58 m/s
NORTH
SOUTH
EAST
WEST
10%
15%
20%
30%
Wind Speed (m/s)
25 - 30
20 - 25
15 - 20
10 - 15
5 - 10
0 - 5

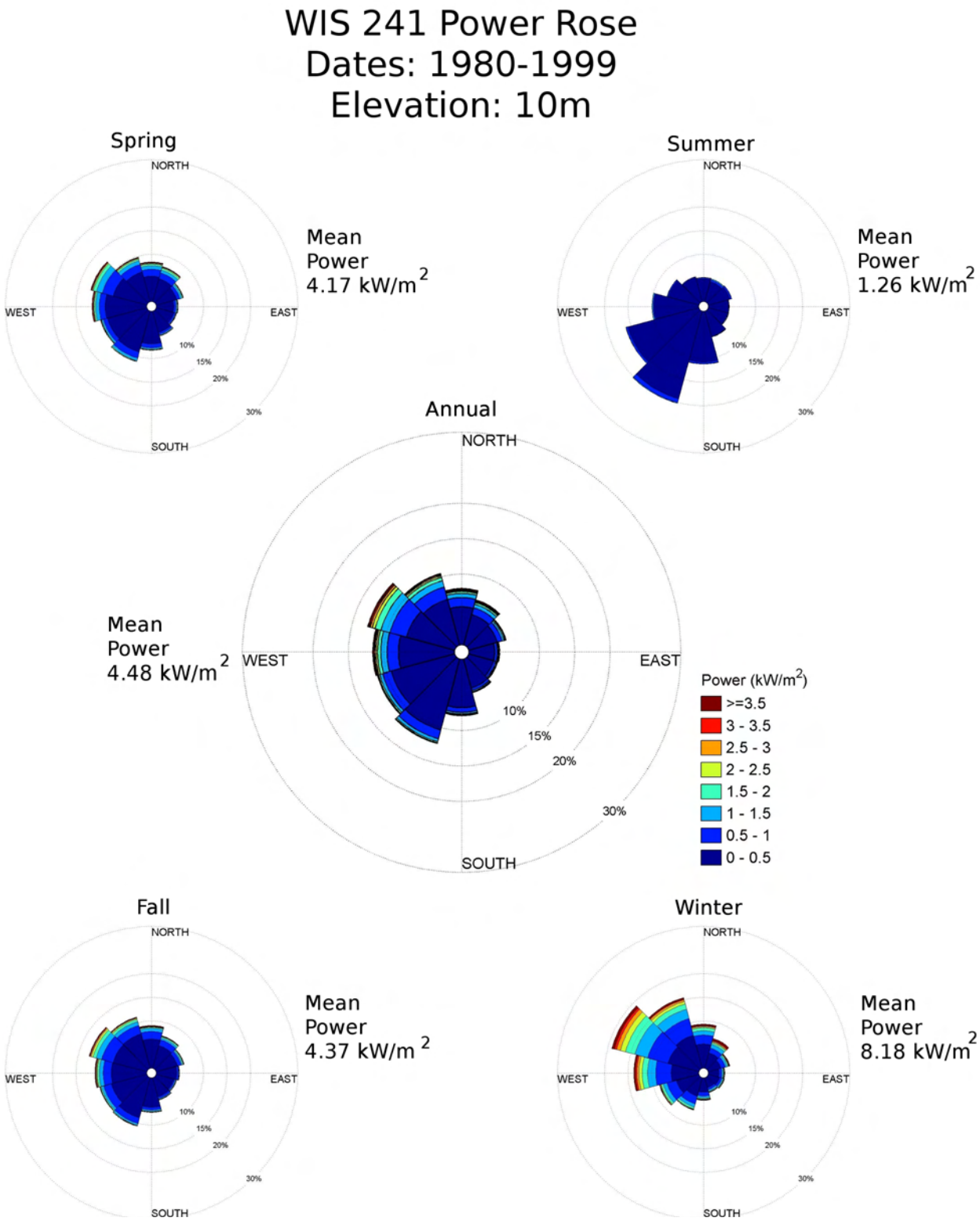
WIS 241 Power Rose
Dates: 1980-1999
Elevation: 10m
Spring
NORTH
WEST
EAST
SOUTH
10%
15%
20%
30%
Mean
Power
4.17 kW/m2
Summer
Mean
Power
1.26 kW/m2
Annual
Mean
Power
4.48 kW/m2
Power (kW/m2)
>=3.5
3 - 3.5
2.5 - 3
2 - 2.5
1.5 - 2
1 - 1.5
0.5 - 1
0 - 0.5
Fall
Mean
Power
4.37 kW/m2
Winter
Mean
Power
8.18 kW/m2

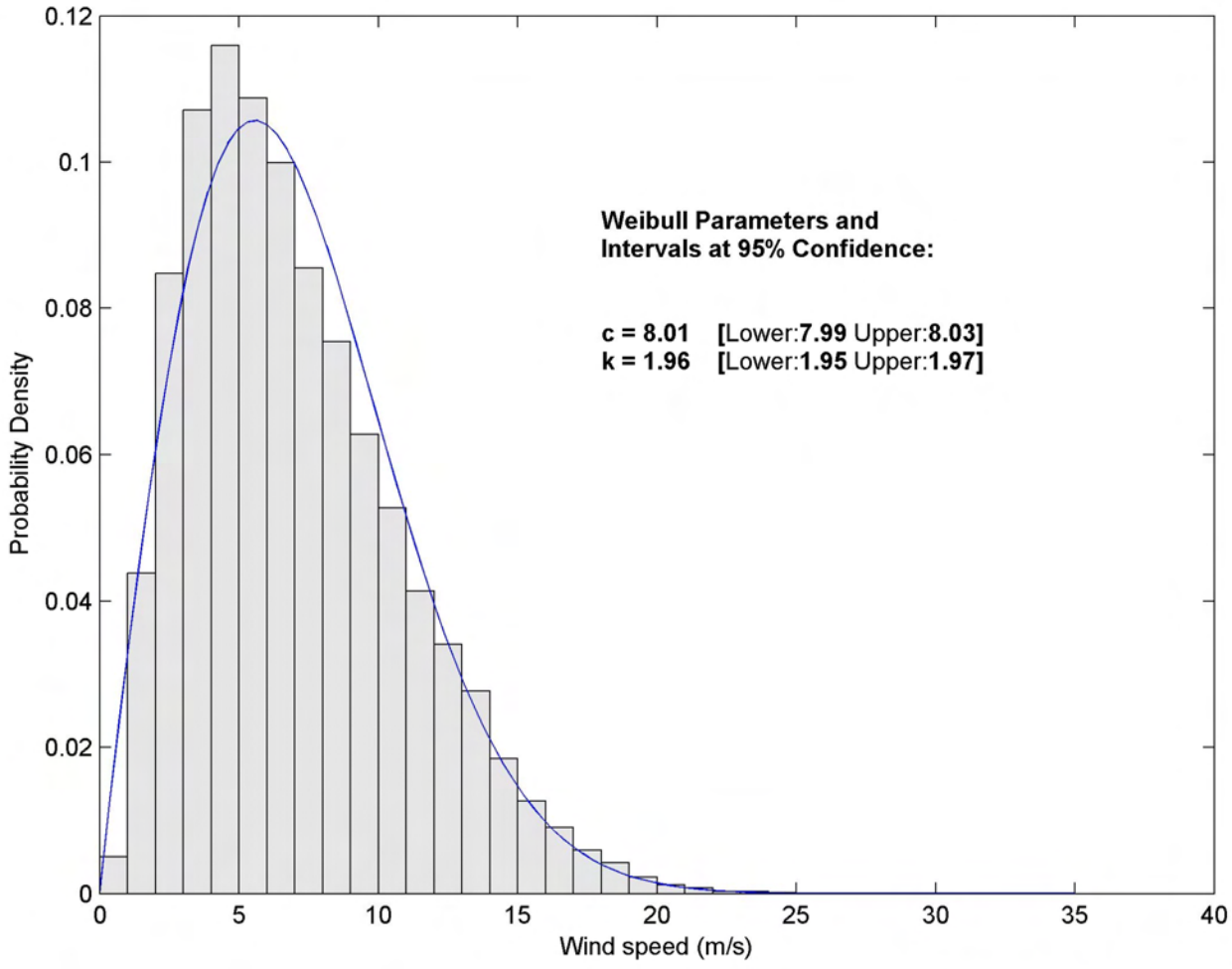
WIS 242 Probability Distribution
Dates: 1980-1999
Elevation: 10m
Weibull Parameters and
Intervals at 95% Confidence:
c = 8.01 [Lower:7.99 Upper:8.03]
k = 1.96 [Lower:1.95 Upper:1.97]
Probability Density
Wind speed (m/s)
0
0.02
0.04
0.06
0.08
0.1
0.12
0
5
10
15
20
25
30
35
40

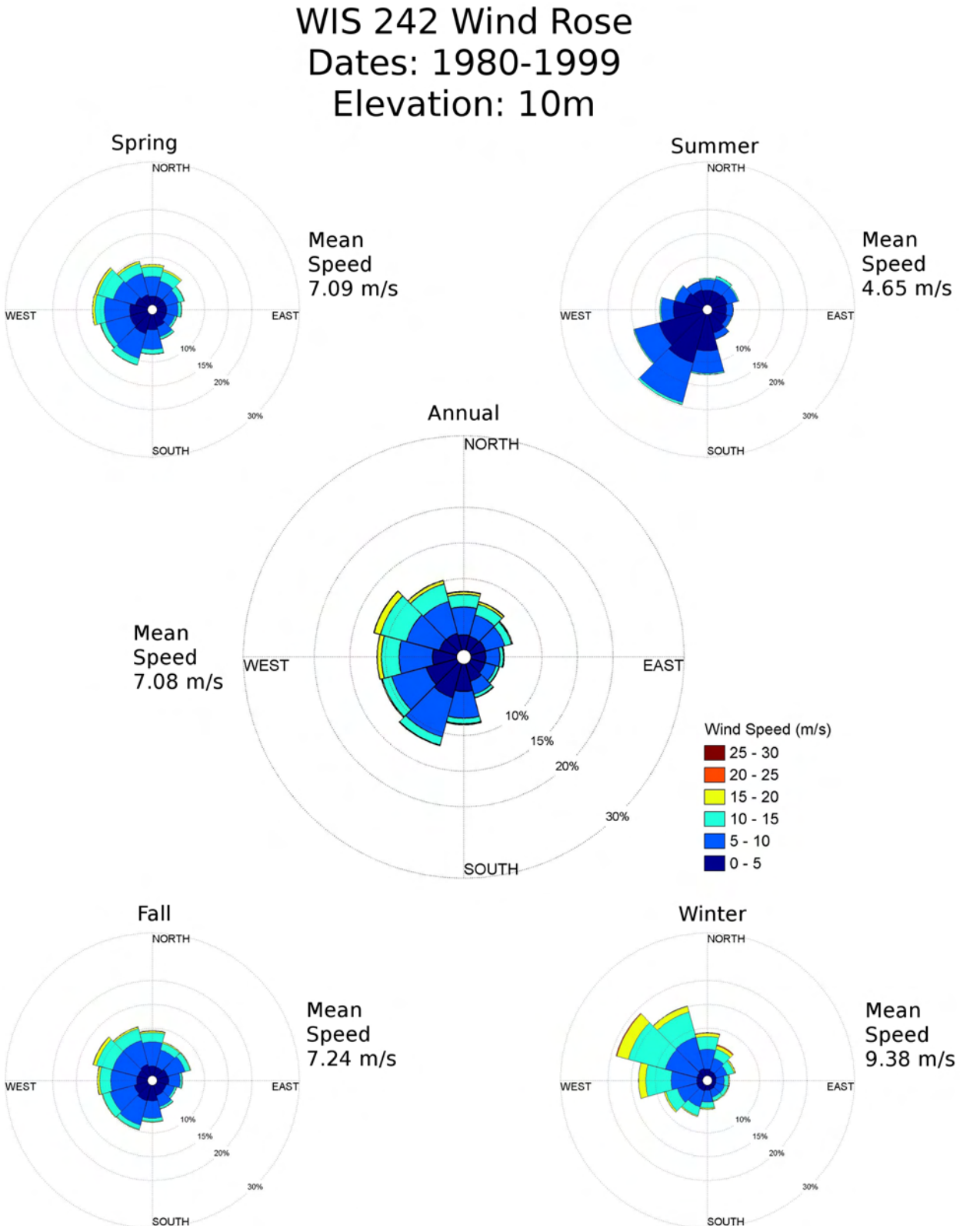
WIS 242 Wind Rose
Dates: 1980-1999
Elevation: 10m
Spring
Mean Speed 7.09 m/s
Summer
Mean Speed 4.65 m/s
Annual
Mean Speed 7.08 m/s
Fall
Mean Speed 7.24 m/s
Winter
Mean Speed 9.38 m/s
NORTH
SOUTH
EAST
WEST
10%
15%
20%
30%
Wind Speed (m/s)
25 - 30
20 - 25
15 - 20
10 - 15
5 - 10
0 - 5

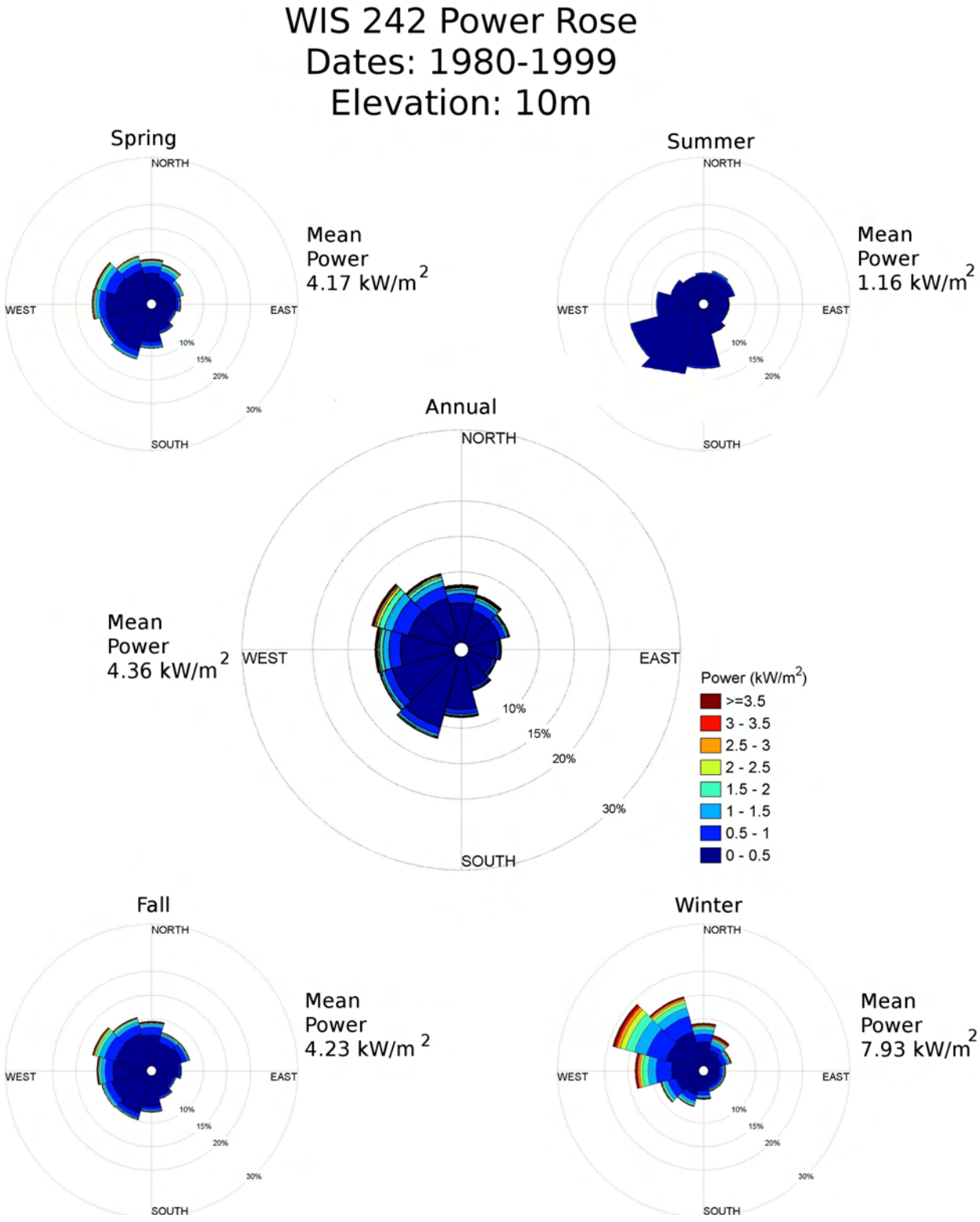
WIS 242 Power Rose
Dates: 1980-1999
Elevation: 10m
Spring
Mean Power 4.17 kW/m2
Summer
Mean Power 1.16 kW/m2
Annual
Mean Power 4.36 kW/m2
Fall
Mean Power 4.23 kW/m2
Winter
Mean Power 7.93 kW/m2
NORTH
SOUTH
EAST
WEST
10%
15%
20%
30%
Power (kW/m2)
>=3.5
3 - 3.5
2.5 - 3
2 - 2.5
1.5 - 2
1 - 1.5
0.5 - 1
0 - 0.5

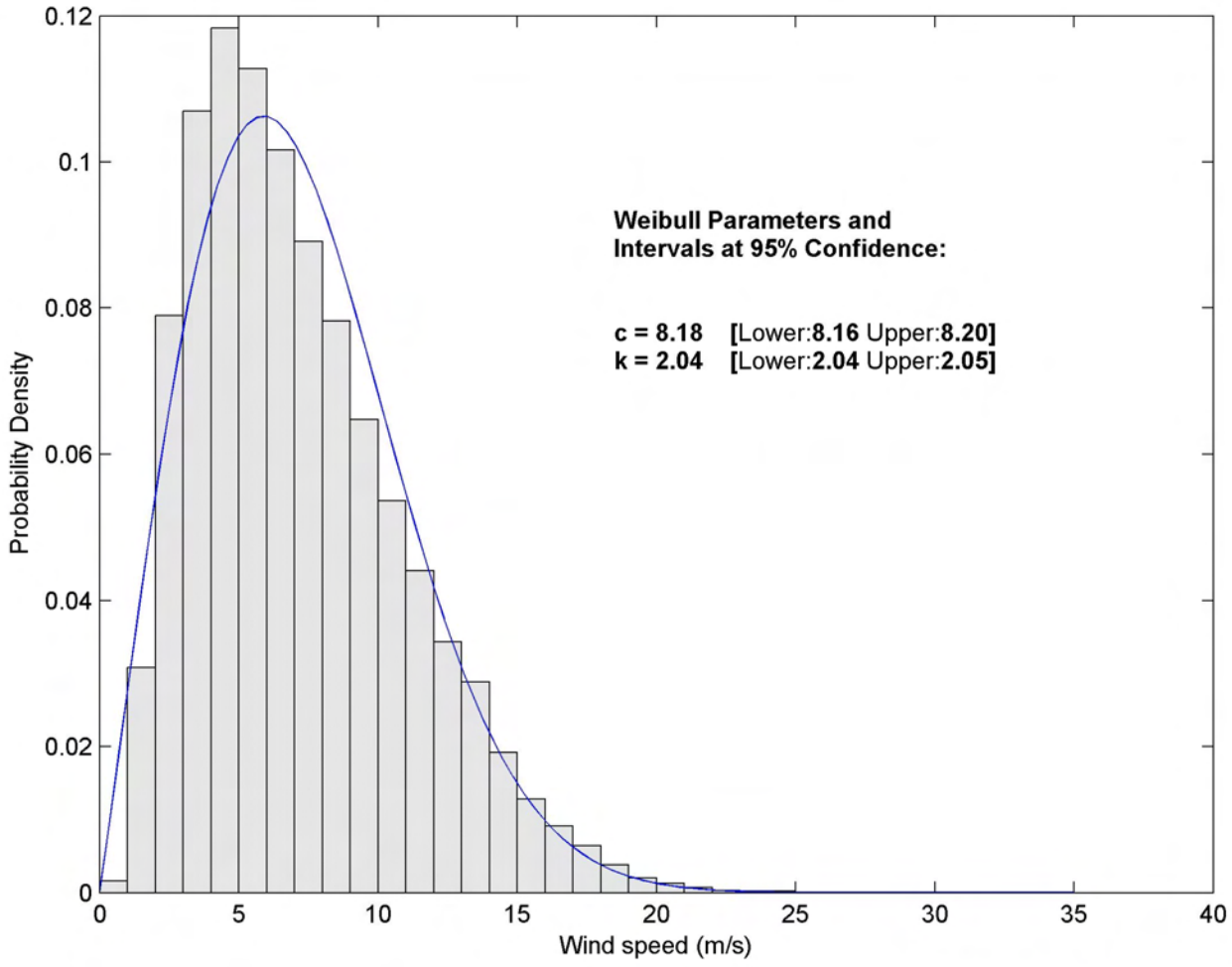
WIS 243 Probability Distribution
Dates: 1980-1999
Elevation: 10m
Weibull Parameters and
Intervals at 95% Confidence:
c = 8.18 [Lower:8.16 Upper:8.20]
k = 2.04 [Lower:2.04 Upper:2.05]
Probability Density
Wind speed (m/s)
0
0.02
0.04
0.06
0.08
0.1
0.12
0
5
10
15
20
25
30
35
40

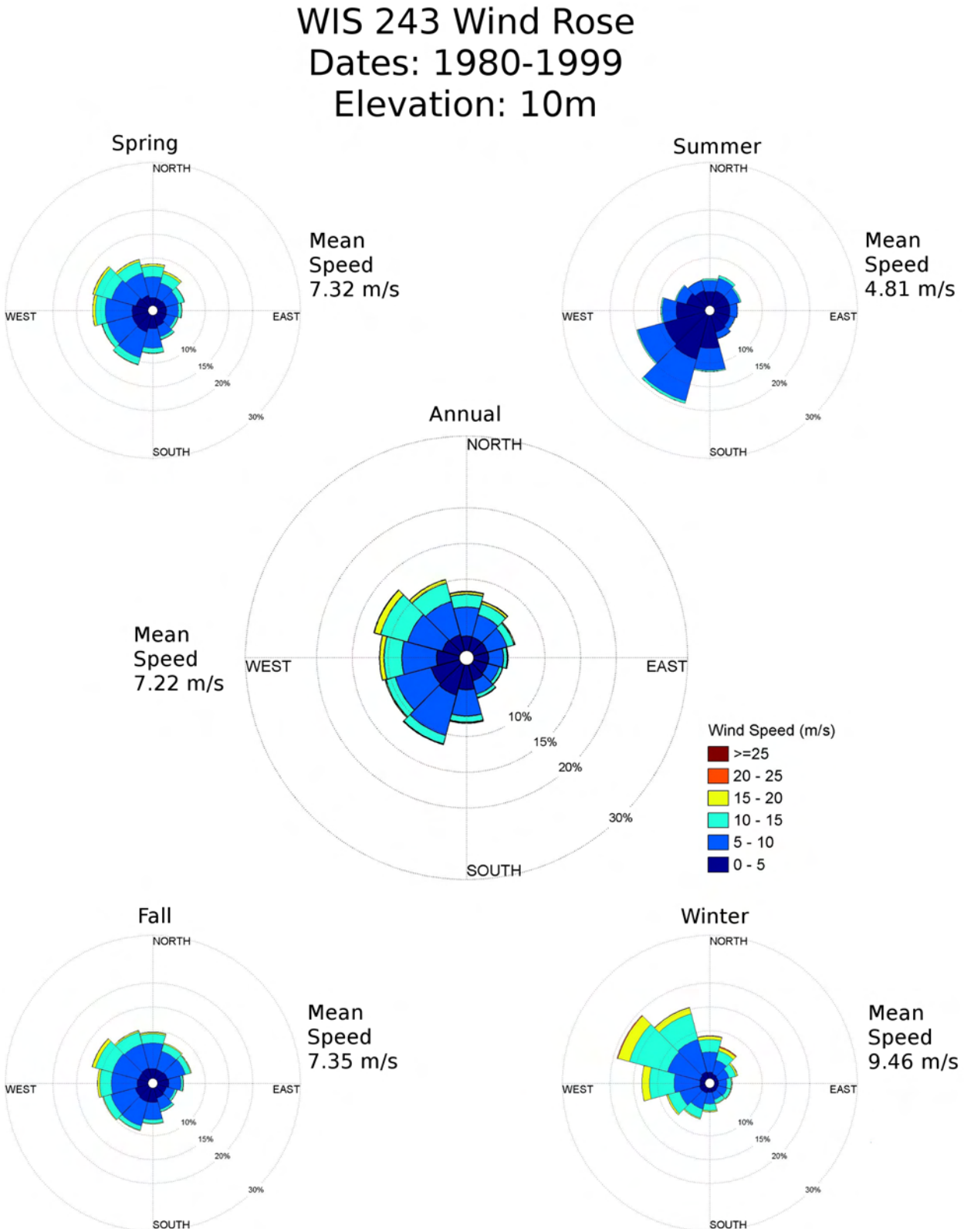
WIS 243 Wind Rose
Dates: 1980-1999
Elevation: 10m
Spring
Mean Speed 7.32 m/s
Summer
Mean Speed 4.81 m/s
Annual
Mean Speed 7.22 m/s
Fall
Mean Speed 7.35 m/s
Winter
Mean Speed 9.46 m/s
NORTH
SOUTH
EAST
WEST
10%
15%
20%
30%
Wind Speed (m/s)
>=25
20 - 25
15 - 20
10 - 15
5 - 10
0 - 5

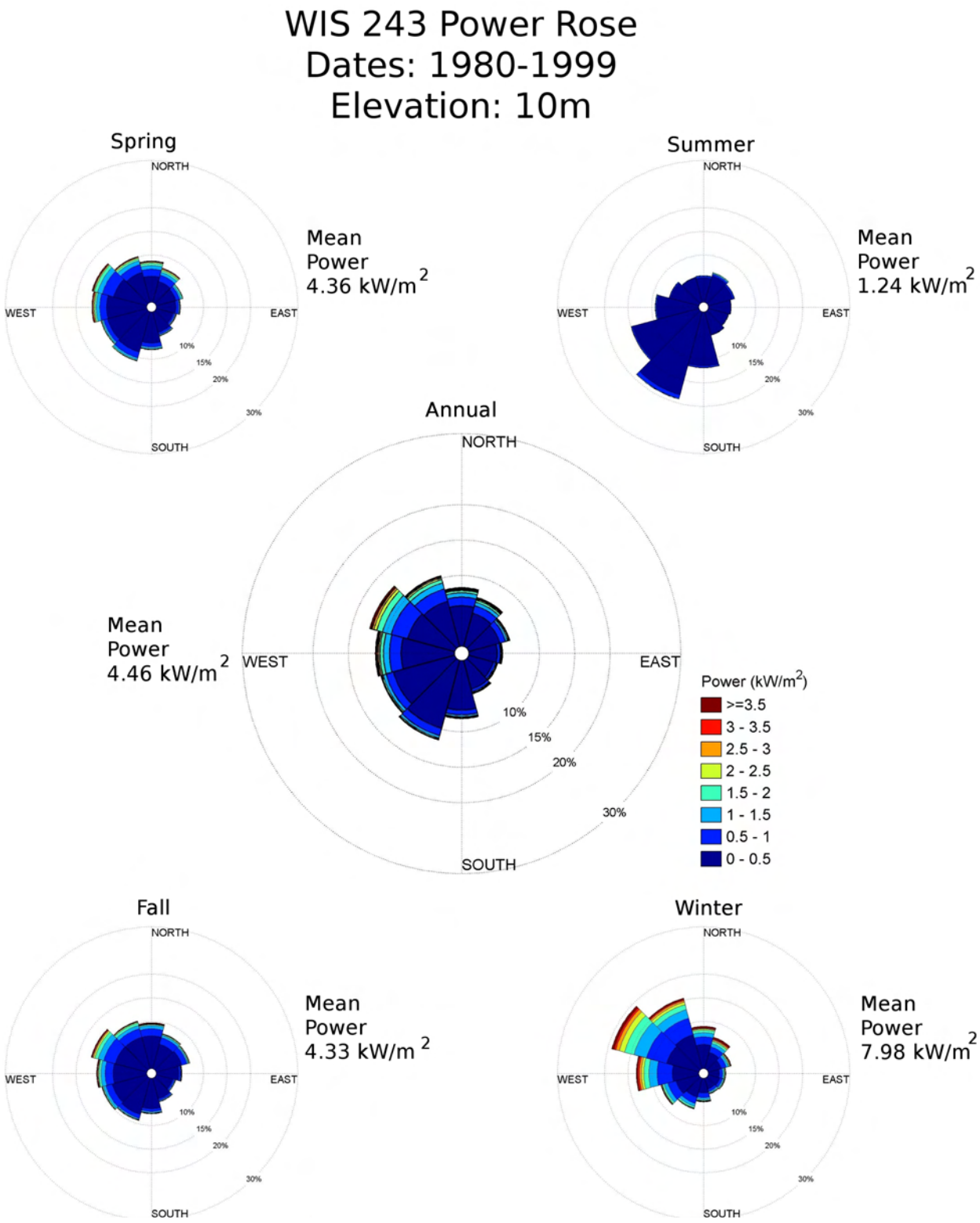
WIS 243 Power Rose
Dates: 1980-1999
Elevation: 10m
Spring
Mean Power 4.36 kW/m2
Summer
Mean Power 1.24 kW/m2
Annual
Mean Power 4.46 kW/m2
Fall
Mean Power 4.33 kW/m2
Winter
Mean Power 7.98 kW/m2
NORTH
SOUTH
EAST
WEST
10%
15%
20%
30%
Power (kW/m2)
>=3.5
3 - 3.5
2.5 - 3
2 - 2.5
1.5 - 2
1 - 1.5
0.5 - 1
0 - 0.5

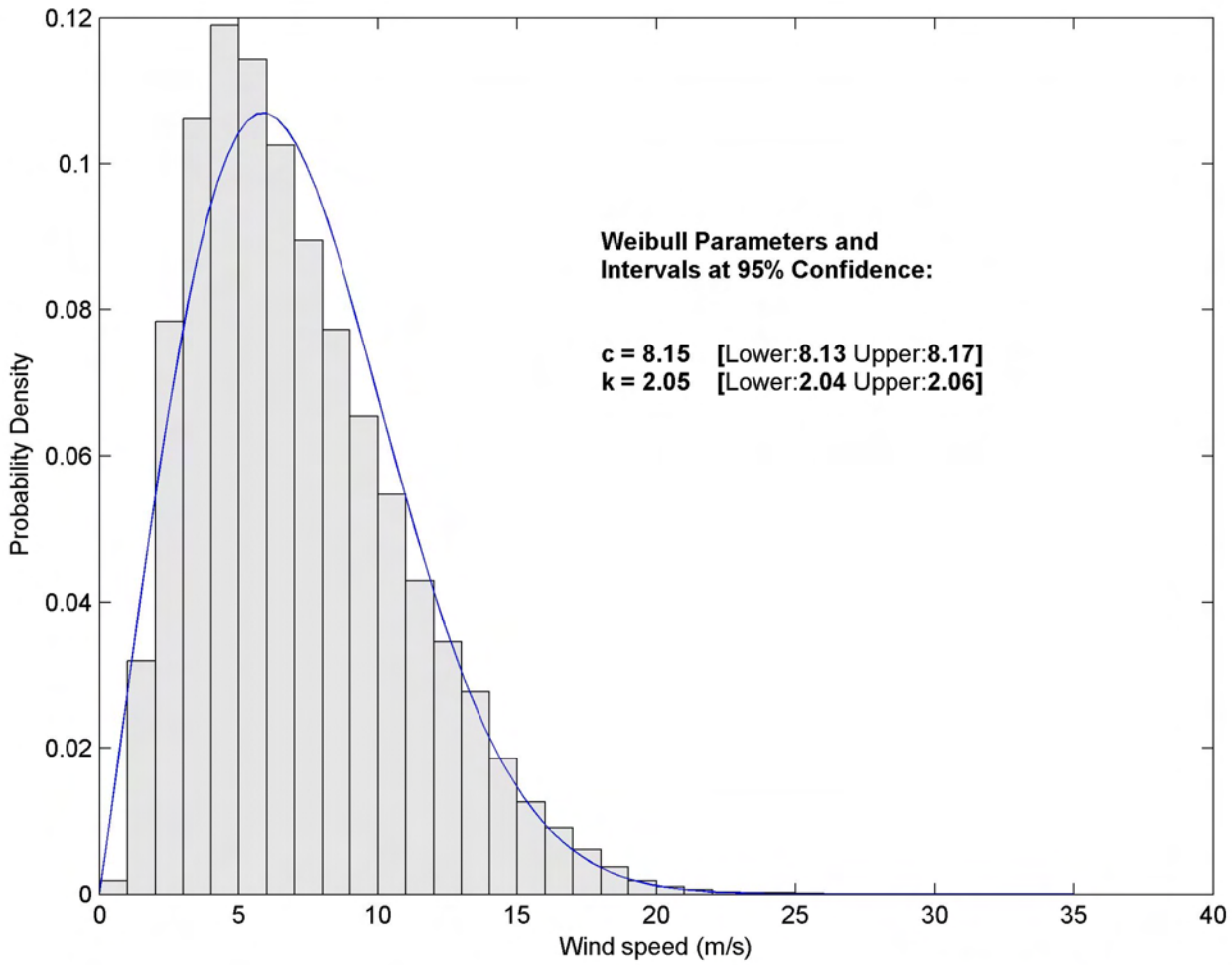
WIS 244 Probability Distribution
Dates: 1980-1999
Elevation: 10m
Weibull Parameters and
Intervals at 95% Confidence:
c = 8.15 [Lower:8.13 Upper:8.17]
k = 2.05 [Lower:2.04 Upper:2.06]
Probability Density
Wind speed (m/s)
0
0.02
0.04
0.06
0.08
0.1
0.12
0
5
10
15
20
25
30
35
40

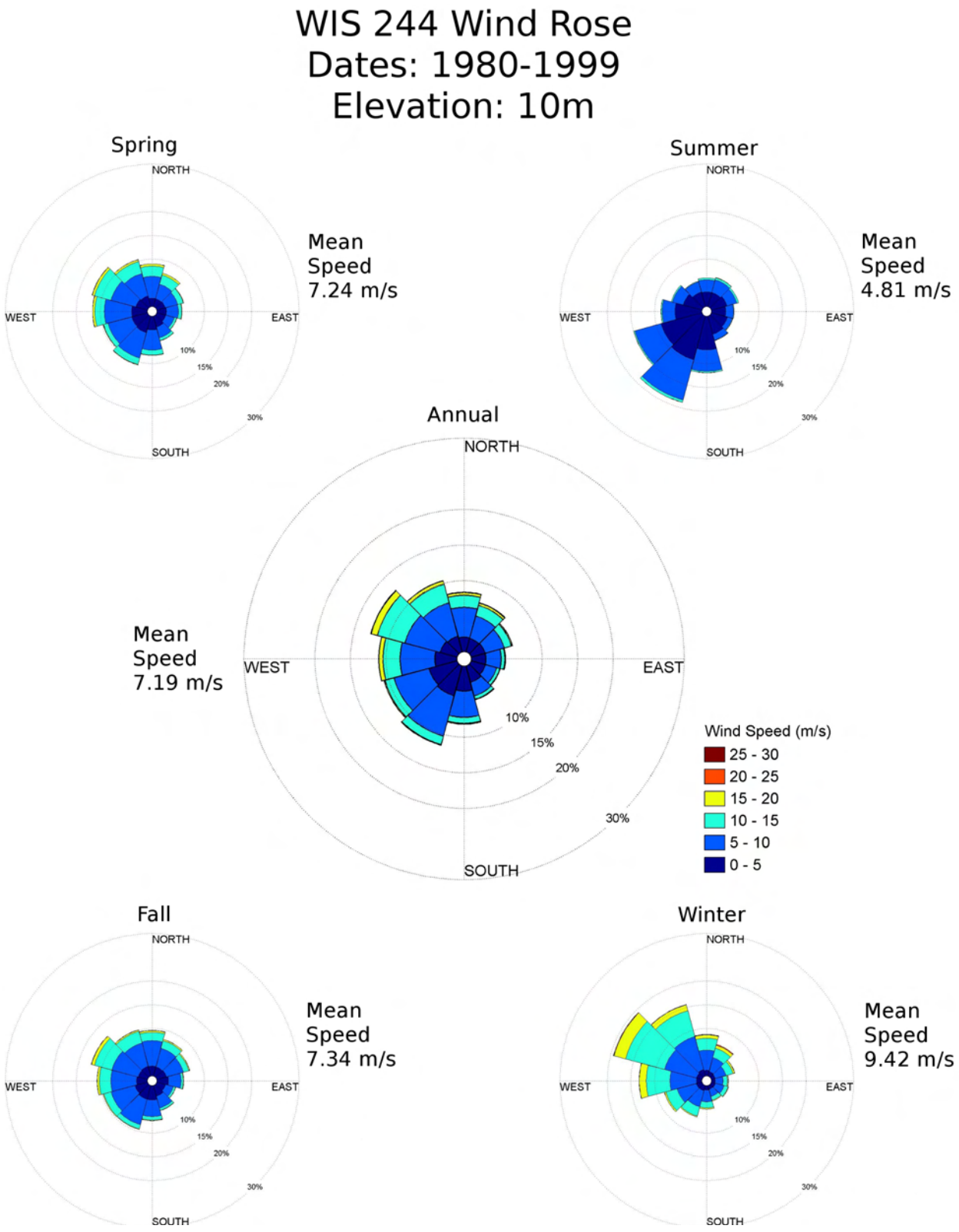
WIS 244 Wind Rose
Dates: 1980-1999
Elevation: 10m
Spring
Mean Speed 7.24 m/s
Summer
Mean Speed 4.81 m/s
Annual
Mean Speed 7.19 m/s
Fall
Mean Speed 7.34 m/s
Winter
Mean Speed 9.42 m/s
NORTH
SOUTH
EAST
WEST
10%
15%
20%
30%
Wind Speed (m/s)
25 - 30
20 - 25
15 - 20
10 - 15
5 - 10
0 - 5

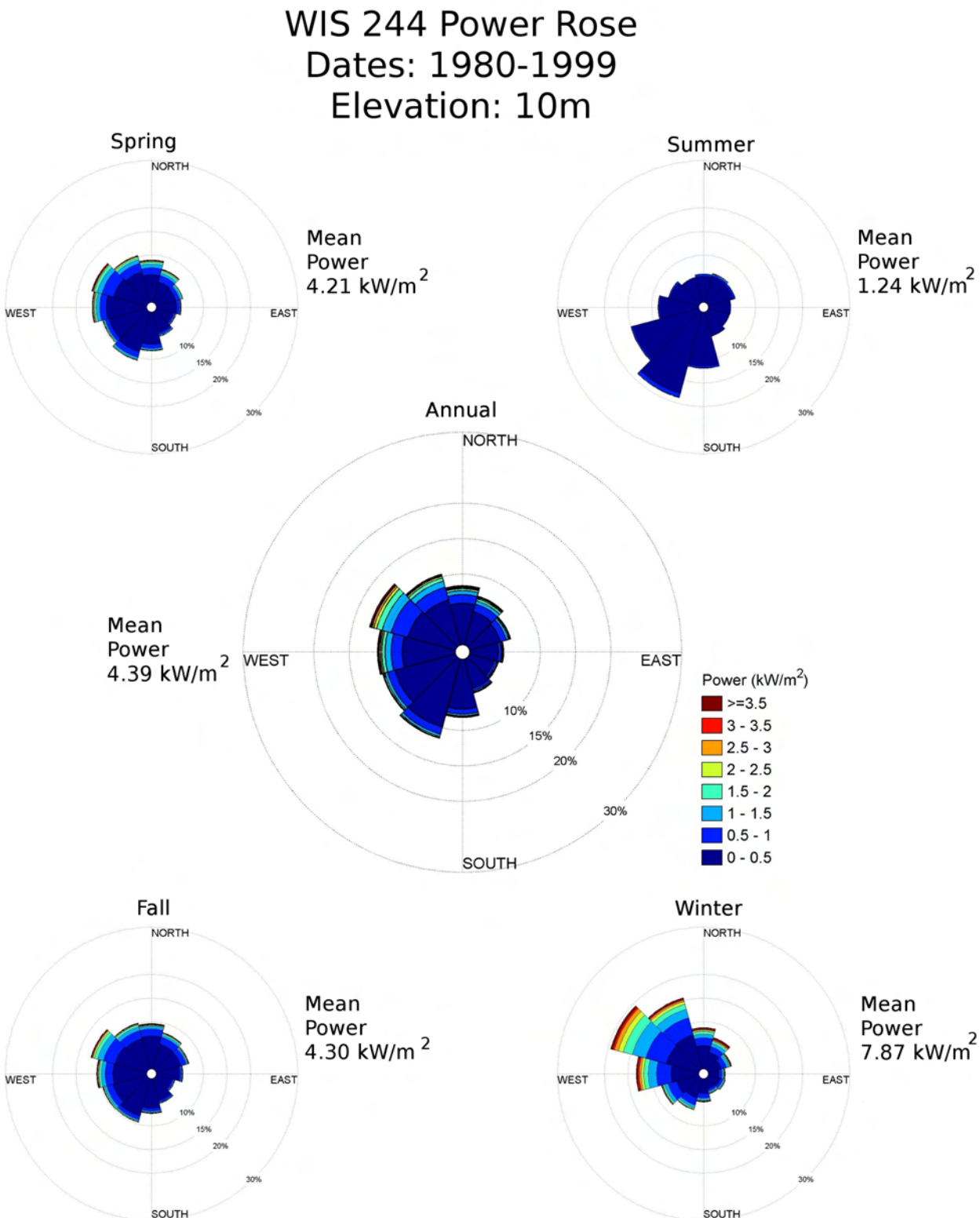
WIS 244 Power Rose
Dates: 1980-1999
Elevation: 10m
Spring
Mean Power 4.21 kW/m2
Summer
Mean Power 1.24 kW/m2
Annual
Mean Power 4.39 kW/m2
Fall
Mean Power 4.30 kW/m2
Winter
Mean Power 7.87 kW/m2
NORTH
SOUTH
EAST
WEST
10%
15%
20%
30%
Power (kW/m2)
>=3.5
3 - 3.5
2.5 - 3
2 - 2.5
1.5 - 2
1 - 1.5
0.5 - 1
0 - 0.5

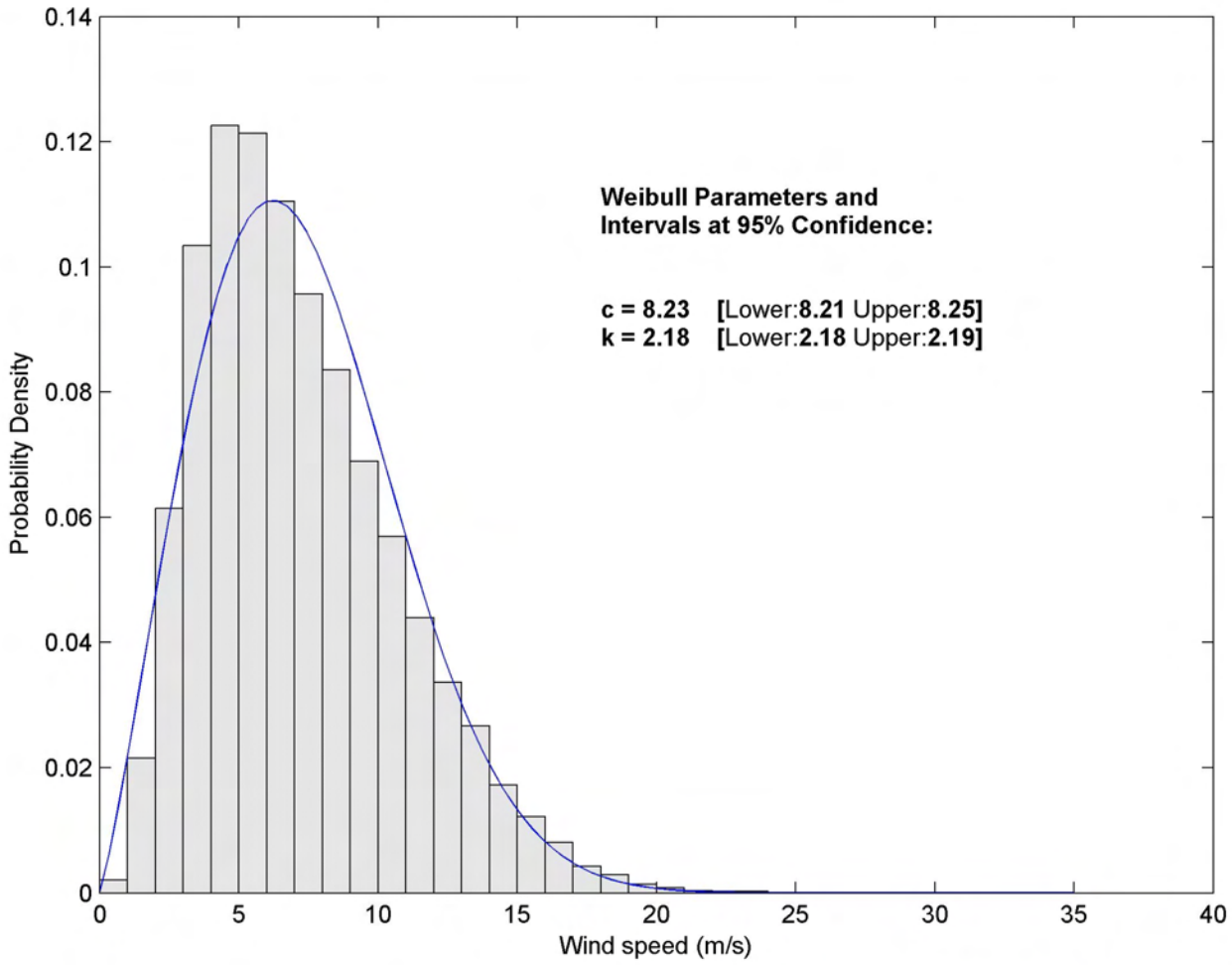
WIS 247 Probability Distribution
Dates: 1980-1999
Elevation: 10m
Weibull Parameters and
Intervals at 95% Confidence:
c = 8.23 [Lower:8.21 Upper:8.25]
k = 2.18 [Lower:2.18 Upper:2.19]
Probability Density
Wind speed (m/s)
0.14
0.12
0.1
0.08
0.06
0.04
0.02
0
0
5
10
15
20
25
30
35
40

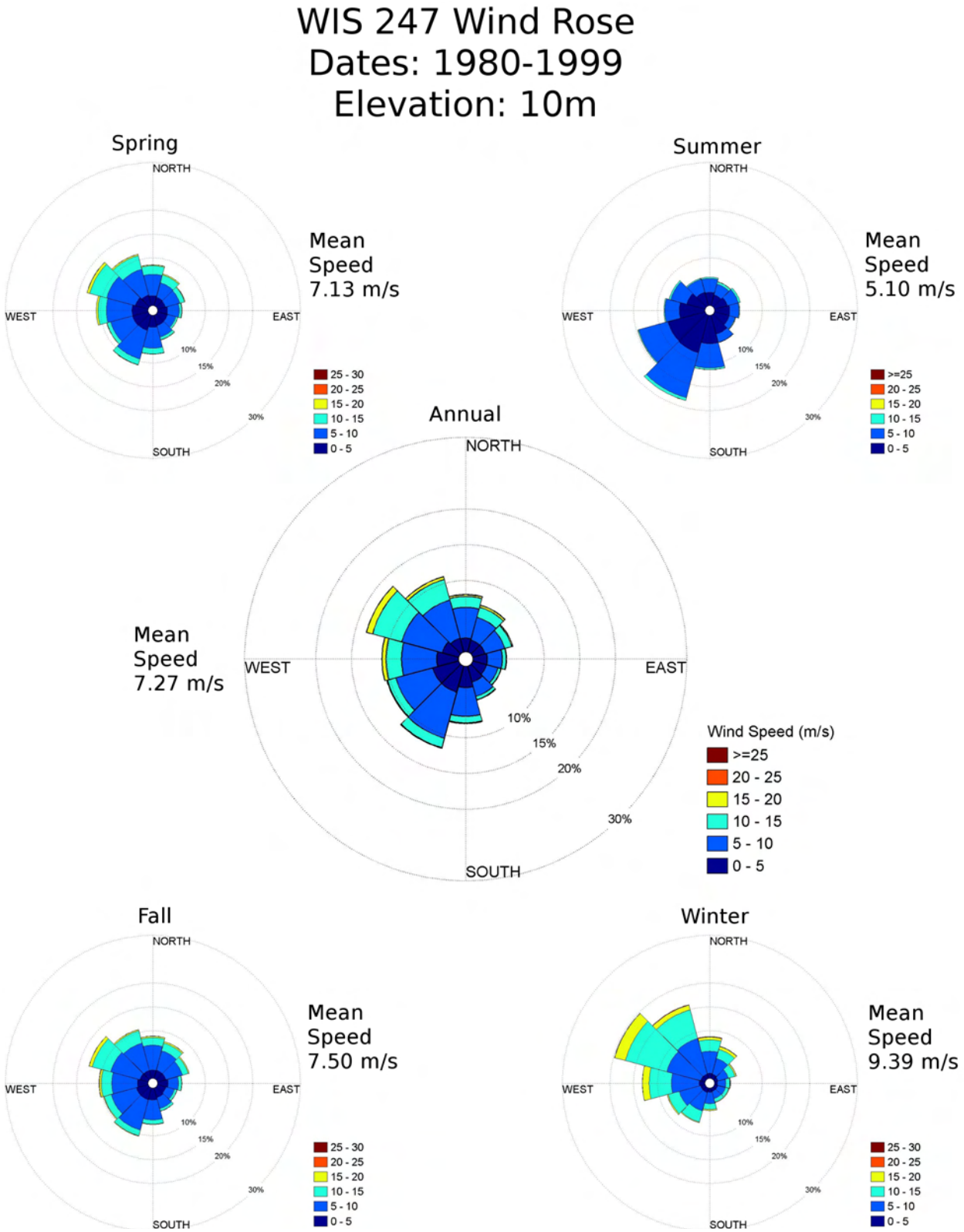
WIS 247 Wind Rose
Dates: 1980-1999
Elevation: 10m
Spring
Mean Speed 7.13 m/s
Summer
Mean Speed 5.10 m/s
Annual
Mean Speed 7.27 m/s
Fall
Mean Speed 7.50 m/s
Winter
Mean Speed 9.39 m/s
NORTH
SOUTH
EAST
WEST
10%
15%
20%
30%
Wind Speed (m/s)
>=25
25 - 30
20 - 25
15 - 20
10 - 15
5 - 10
0 - 5

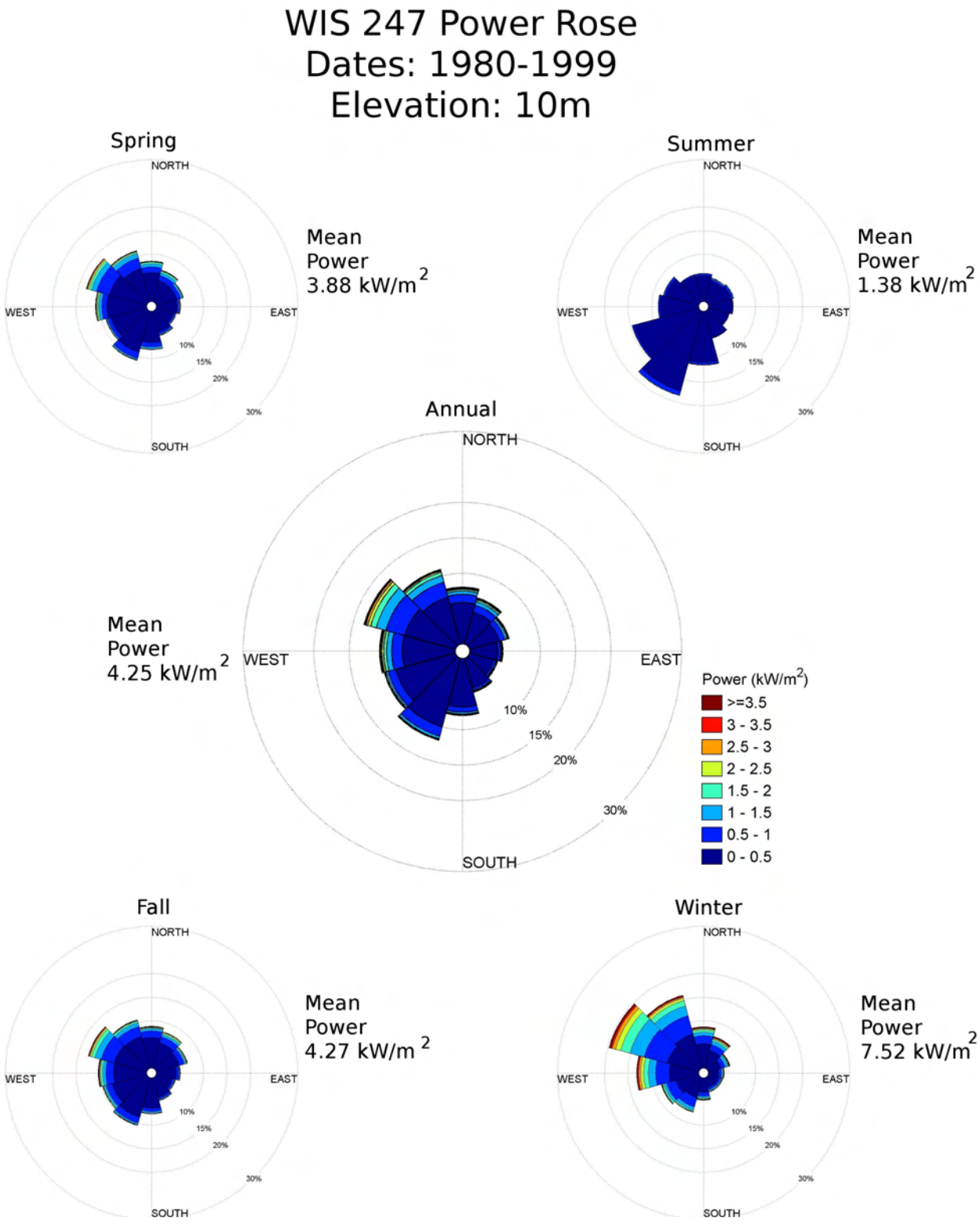
WIS 247 Power Rose
Dates: 1980-1999
Elevation: 10m
Spring
Mean Power 3.88 kW/m2
Summer
Mean Power 1.38 kW/m2
Annual
Mean Power 4.25 kW/m2
Fall
Mean Power 4.27 kW/m2
Winter
Mean Power 7.52 kW/m2
NORTH
SOUTH
EAST
WEST
10%
15%
20%
30%
Power (kW/m2)
>=3.5
3 - 3.5
2.5 - 3
2 - 2.5
1.5 - 2
1 - 1.5
0.5 - 1
0 - 0.5

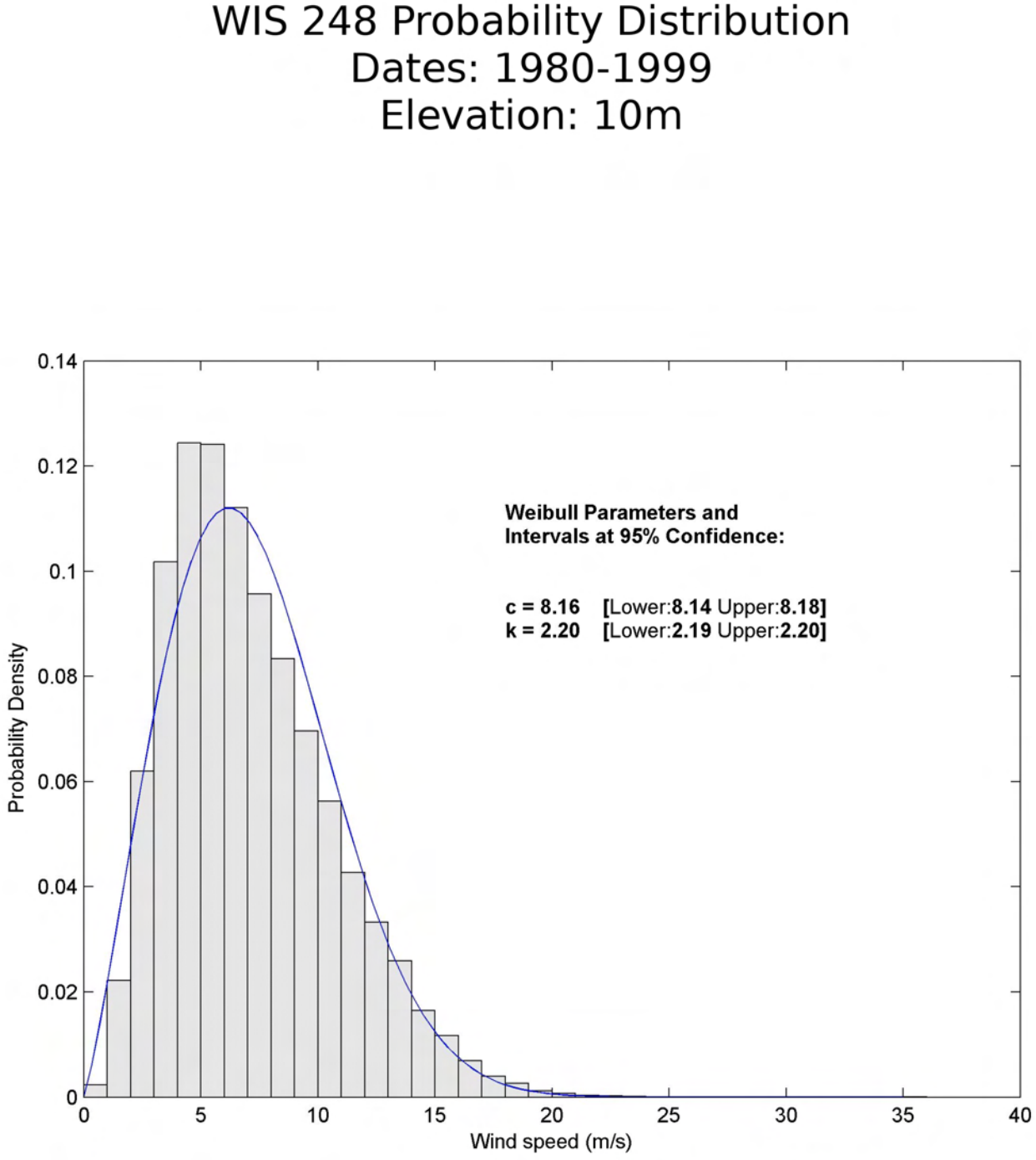
WIS 248 Probability Distribution
Dates: 1980-1999
Elevation: 10m
Weibull Parameters and
Intervals at 95% Confidence:
c = 8.16 [Lower:8.14 Upper:8.18]
k = 2.20 [Lower:2.19 Upper:2.20]
Probability Density
Wind speed (m/s)
0.14
0.12
0.1
0.08
0.06
0.04
0.02
0
0
5
10
15
20
25
30
35
40

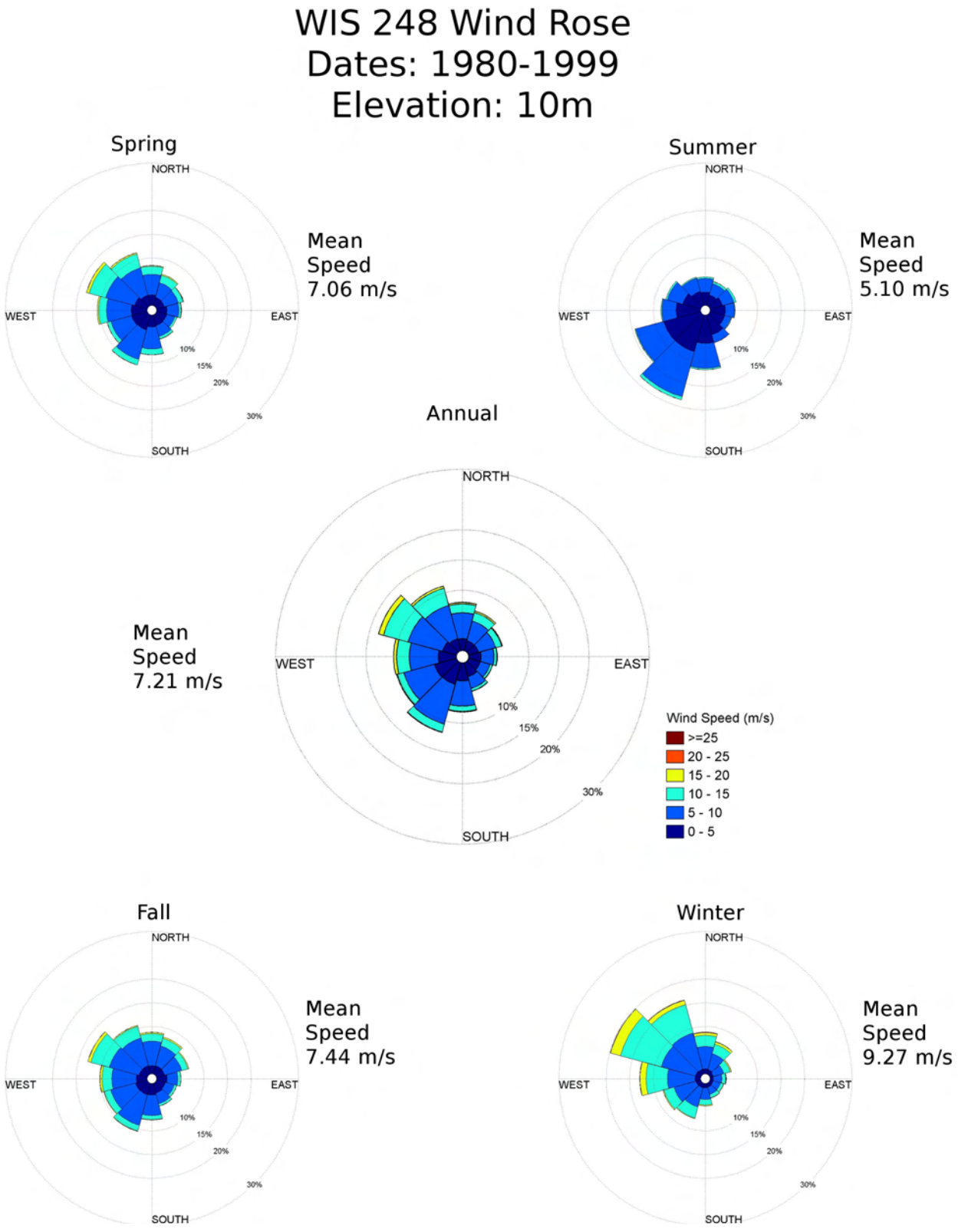
WIS 248 Wind Rose
Dates: 1980-1999
Elevation: 10m
Spring
Mean Speed 7.06 m/s
Summer
Mean Speed 5.10 m/s
Annual
Mean Speed 7.21 m/s
Fall
Mean Speed 7.44 m/s
Winter
Mean Speed 9.27 m/s
NORTH
SOUTH
EAST
WEST
10%
15%
20%
30%
Wind Speed (m/s)
>=25
20 - 25
15 - 20
10 - 15
5 - 10
0 - 5

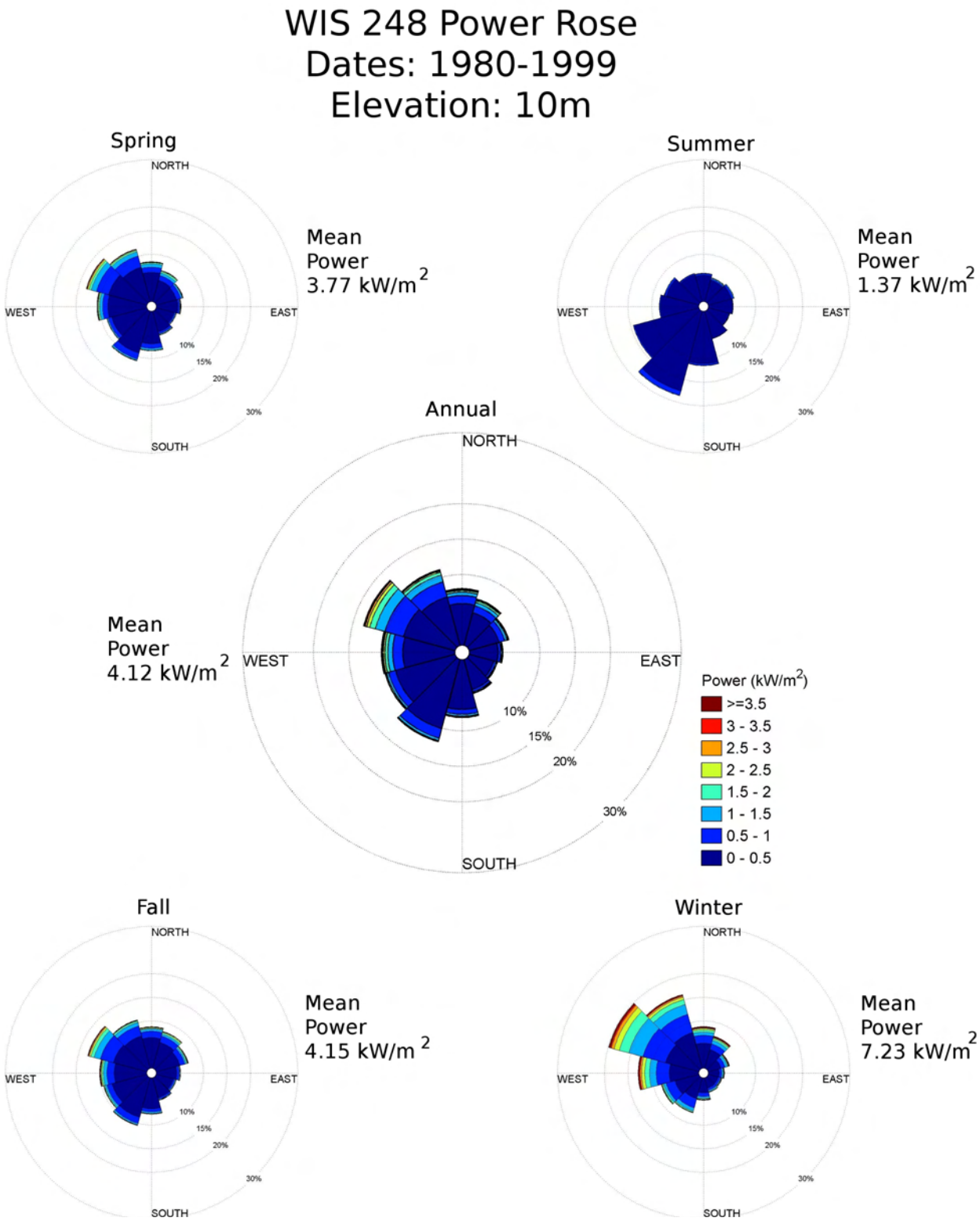
WIS 248 Power Rose
Dates: 1980-1999
Elevation: 10m
Spring
Mean Power 3.77 kW/m2
Summer
Mean Power 1.37 kW/m2
Annual
Mean Power 4.12 kW/m2
Fall
Mean Power 4.15 kW/m2
Winter
Mean Power 7.23 kW/m2
NORTH
SOUTH
EAST
WEST
10%
15%
20%
30%
Power (kW/m2)
>=3.5
3 - 3.5
2.5 - 3
2 - 2.5
1.5 - 2
1 - 1.5
0.5 - 1
0 - 0.5

Appendix B

Block Island Modeling Analysis

Report completed by Jay Titlow and David Morris of WeatherFlow, Inc.

Modeling results produced by MetLogic, Inc.

Project scope:

To complete a set of atmospheric model simulations to reveal flow patterns around Block Island with emphasis on the effect of the Island itself.

Product:

A set of 12 model runs, one for each octant compass direction from North clockwise through Northwest plus 4 additional runs to highlight seasonal variations of the more frequent flow regimes.

Table of Contents

Introduction

The modeling analysis was performed to increase the understanding of wind regimes in the coastal waters surrounding Block Island, Rhode Island. Special emphasis was placed on the influence of the island on surface to hub height flows both upwind and downwind in each particular compass direction.

An overview of the model runs can be found at:

http://rock.metlogic.com/overview.shtml

Results of this analysis can be viewed at the following web site:

http://rock.metlogic.com/index.shtml

Model, Configuration and Input Data

Simulation Details

- Simulations performed with RAMS version 6.1, the latest (unreleased) version from technology partner, ATMET.
- 500m horizontal grid spacing on the high resolution grid telescopically nested from 12km, 6km and 2km grids. A range of horizontal grid resolutions from 4km to 250m were tested. In most cases, the convergence of results at the proposed turbine locations occurred at 1-2km. In some cases, where stable conditions existed and the proposed wind farm sites were downwind of the island, differences with apparent down to 500m.
- 20m vertical grid spacing, expanding upward with a geometric ratio of 1.15. Vertical grid resolutions from 40m to 5m were tested. Most of the energy in the wind is captured at 20m vertical resolution, however, the wind speeds at 80m (hub height) at the wind farm sites are underestimated by up to 20%. It was not feasible within the time frame of the project to run the simulations at the time steps required for 5-10m vertical resolution.
- 0Z start times, simulating for 30 hours, with 6 hours of dynamic initialization prior to the 0Z start.
- Initialized from the 12km NAM analysis, with grid 1 bounded by subsequent 6 hourly 12km NAM analyses.

A complete configuration description can be found at: http://rock.metlogic.com/forecasts/bi/details.bi.shtml.

- *Dynamic Initialization:* RAMS was initialized 6 hours prior to the 0Z start time (tau 0), firstly with a 2 grid run (outer grids only) from tau -6 to tau -3 (stage 1), then with all 4 grids from tau -3 to tau 0 (stage 2). In stage 1, the dynamic model fields (U, V, P and T) in the interior domain were strongly nudged to the interpolated NAM analysis values. In stage 2, the same variables were nudged, but far less strongly. The atmospheric moisture data was excluded from the nudging. This forces a numerical balance to develop for the dynamic quantities (U,V,P and T) between the model and the NAM analysis, while allowing moisture quantities (clouds and precipitation) to evolve independently.

- *3D Soil Moisture Initialization*: The 3D (spatial and depth) soil moisture field was extracted from the 12km NAM analysis files and interpolated to the RAMS grids and soil levels.
- *2D Snow Cover Initialization*: The 2D (spatial) snow cover field was extracted from the 12km NAM analysis files and interpolated to the RAMS grids.

High Resolution Input Data

- *Operational Sea Surface Temperature and Sea Ice Analysis (OSTIA)*

OSTIA uses satellite data provided by the GHRSST project, together with in-situ observations to determine the sea surface temperature. The analysis is performed using a variant of optimal interpolation (OI) technique. The analysis is produced daily at a resolution of 1/200 (approx. 5km). OSTIA data is provided in GHRSST netCDF format every day.

http://ghrsst-pp.metoffice.com/pages/latest_analysis/ostia.html

- *ASTER Global Digital Elevation Model (ASTER GDEM)*

The ASTER GDEM covers land surfaces between 83°N and 83°S and is composed of 22,600 1°-by-1° tiles. Tiles that contain at least 0.01% land area are included. The ASTER GDEM is in GeoTIFF format with geographic lat/long coordinates and a 1 arc-second (30 m) grid of elevation postings. It is referenced to the WGS84/EGM96 geoid. Pre-production estimated accuracies for this global product were 20 meters at 95% confidence for vertical data and 30 meters at 95 % confidence for horizontal data.

http://www.ersdac.or.jp/GDEM/E/index.html

- *National Land Cover Database (NLCD 2001) Multi-zone Download Site*

The Multi-Resolution Land Characteristics Consortium (MRLC) has completed the National Land Cover Database (NLCD) 2001 products for the conterminous United States, Hawaii, Alaska and Puerto Rico at 30 m cell resolution. The NLCD 2001 products (land cover, impervious surface and canopy density) were generated from a standardized set of data layers mosaicked by mapping zone. Typical zonal layers included multi-season Landsat 5 and Landsat 7 imagery centered on a nominal collection year of 2001, and Digital Elevation Model based derivatives at 30 meters spatial resolution. NLCD 2001 used an improved classification algorithm from NLCD 1992, resulting in a more precise rendering of spatial boundaries between 16 classes of land cover (additional classes are available in coastal areas and Alaska only). A

shapefile with the standard NLCD zones as well as a mutlizone attribute is available for download here.

http://www.mrlc.gov/nlcd_multizone_map.php

List of model runs completed:

1. **North: January 4th 2008**
2. **Northeast: September 22nd 2008**
3. **Northeast 2: April 17th 2008**
4. **East: September 24th 2008**
5. **Southeast: October 25th 2008**
6. **South: September 6th 2008**
7. **South 2: November 8th 2008**
8. **Southwest: July 7th 2008**
9. **West: December 22nd 2008**
10. **Northwest 1: October 30, 2008**
11. **Northwest 2: November 22 2008**
12. **Northwest 3: February 23 2009**

Basic Wind Regimes of Block Island and Climatology

Wind behavior over southeastern New England, and in particular, coastal Rhode Island can be best described as progressive west to east flow with embedded mid-latitude synoptic waves, which are more frequent during the spring, fall, and winter. During the summer months basic flow remains westerly, but the jet stream and associated weather lifts northward allowing for periods of lighter flow. During these occasions, mesoscale processes such as sea breezes have a more pronounced effect on the region's weather.

Typical synoptic setups across Southern New England are as follows:

Persistent Bermuda high pressure to the southeast

Very common feature often occurring up to 5 to 7 days a week during the summer months, 3 to5 days a week during the spring and fall and 2 to 4 days a week during the winter.

Consistent SSW to SW synoptic flow is found across the region when this semi-permanent oceanic feature becomes established. From late spring, through summer to early autumn, Southern New England sea breezes enhance prevailing SSW, SW or WSW surface winds. The complex geography of the region from Long Island through to Buzzards Bay and Martha's Vineyard generates multiple convergence zones and varying effects. Examples of this synoptic set-up with mesoscale enhancement include accelerating SW flow into Buzzard Bay and channeled southerly flow into the East and West passages of Narragansett Bay.

High pressure to the west and northwest

The next most common feature, often occurring 1 to 2 days a week during the summer months, 2 to 4 days a week during the spring and fall and 3 to 5 days a week during the winter.

This is often the setup that results following the passage of a low pressure system tracking away to the east. Northwest wind strength depends upon the pressure gradients between the incoming anticyclone to the west and the departing low pressure system. Blocking high pressure can become well established across New England, or slowly migrate eastward and offshore. (In the summer, it is often more common to experience brief surges of NW flow that then die and back to the SW as high pressure weakens and the semi-permanent Bermuda High re-intensifies. Alternately, during the winter and late spring and fall, high pressure often tracks by to the north, veering the flow more NE.

High pressure to the northeast

Right behind B, this pattern is the third most common feature occurring, on average 1 day a week during the summer months, 2 to 3 days a week during the spring and fall and 3 to 4 days a week during the winter.

As previously mentioned, high pressure often becomes well established over the Canadian Maritimes, resulting in NE or ENE winds across Southern New England. This pattern can last a few days and may generate a backdoor cold front. Pressure gradients are sometimes

significantly tightened if an area of low pressure or a trough axis exists to the southeast or south. (Again, this is more frequent during the winter and early spring).

Mid-latitude low pressure systems

Finally, these systems, almost absent from July through mid August, can occur once or twice a month from late August through early October, become much more frequent from mid October all the way to early May, then wind down to one or two a month from mid May through June.

Mid latitude low pressure centers can track toward New England from varying directions. The most common arrive from anywhere between WNW through WSW to SSW. Alberta Clippers, originating in the North Pacific, reform in the lee of the Rocky Mountains and move rapidly across New England. Cyclogenesis also occurs further south, over the Great Plains, and these systems can track directly across Western New England, or push offshore from the Mid-Atlantic states and take a coastal route into Southern New England. Other systems can develop over the Gulf of Mexico or offshore of the Carolinas and approach Southern New England as a potent system. Occasionally, given favorable upper air conditions, a coastal low pressure system may loop back into Eastern New England. (During "normal" progressive patterns, these synoptic events are most responsible for the sporadic ramp-ups and ramp-downs experienced over a several day span).

Mesoscale features

A variety of smaller mesoscale features can also have a significant effect on the wind regimes in the region.

Sea breezes

The geography of Eastern Long Island, Block Island Sound, Buzzards Bay, and Vineyard Sound provides a complex region of sea breeze generation to interact with the overall synoptic flow. The South Coast of Long Island and the Connecticut Coast typically experience independent sea breeze onsets. Given favorable synoptic conditions, these two sea breeze regimes often merge into a larger scale enhanced flow through the course of the day. Typically, as the diurnal flow matures, surface wind directions usually veer from SW through WSW.

Under weak synoptic gradients, a weak thermal trough sometimes develops over Northern Rhode Island and Southeast Massachusetts. This often increases the strength and longevity of sea breeze enhanced SW surface flow into Southern Narragansett Bay, Buzzards Bay and Vineyard Sound. Sea breeze enhancement often begins on a relatively small scale through midday or early

afternoon, but by late afternoon and sometimes well into summer evenings a broad swath of increased SW flow exists across the entire coastline from Western Long Island through Block Island to Nantucket Sound.

The Rhode Island coast usually experiences more of a south or SSW sea breeze onset through East and West Passages and the entrance to the Sakonnet River. Some strengthening, due to channeling through these topographical gaps, is also common. The sea breeze front often shows up well as a distinctive line of Cu on visible satellite imagery. This may be well defined just inland of the Connecticut coast, but becomes less well defined along the Rhode Island coast. The sea breeze front usually propagates inland to the north of Providence and Fall River, a little more rapidly than further east.

The presence of afternoon cloud cover can significantly weaken SW potential on otherwise synoptically favorable days. Conditions in Buzzards Bay are occasionally influenced by the sea breeze from Cape Cod Bay, propagating toward the southwest. The resultant convergence is usually pushed back to the northeast as the dominant SW sea breeze strengthens. The convergence between these two opposing sea breeze onsets, which can extend along the spine of Cape Cod as far as Chatham, is often marked by a distinctive band of Cu.

Mid-latitude low pressure system low level jet

With a low pressure system positioned to the west or northwest, a well defined warm front often slides from south to north across Southern New England. With the associated cold front propagating eastward across Long Island Sound and Southern New England firmly established in the warm sector, a low level jet, associated with warm air advection, can exist for a time. This can commonly generate wind speeds at the 850mb level in the 40 to 70 knot range. This wind mechanism is problematic with respect to wind energy potential as this strong “ribbon of wind” is present aloft but the degree to which it propagates downward towards typical hub heights and to the surface is often related to near surface thermodynamics (if air temperatures are too cool at the surface, the atmosphere becomes too stable for the jet to reach the lower levels) or momentum transfer (in which moderate to heavy precipitation will pull the stronger wind down). Indeed, during a period of “spiked” higher speeds on October 25th, (case 6, SE flow) rain was observed in the area.

Nocturnal low level jet

The nocturnal low level jet is caused by changes in the vertical temperature structure, due to heat exchanges near the surface. This is thought to generate a nocturnal wind maximum a few hundred feet above the ground, at its strongest between 0000 and 0300 local time. When the inversion layer decays upward from the surface due to warming at the surface, the entire layer between the surface and the low level jet becomes more turbulent, increasing wind strengths at the surface and hub height as well as decreasing the strength of the low level jet itself. This effect is thought to be more prevalent during the summer months, however it is difficult to isolate an increase in wind at a station and say that it has been solely generated by a true nocturnal low level jet event, rather than the interaction of other meteorological processes. The nocturnal low level jet can be better visualized as a sheet or ribbon of wind maxima a few hundred feet above the surface.

a. Tropical systems

The winds associated with tropical storms and hurricanes obviously exceed the operational limits for wind turbines, and this region is impacted by these systems, most frequently at tropical storm strength. Consequently, winds of this magnitude must be factored in to project designs. While winds in a nor'easter are rather uniform in the vertical, this is not the case for tropical systems, in which speeds can be much stronger just aloft, introducing shear stresses and other operational issues.

Weather "Wildcard": The effects of Seasonal SST differences

The differing SST regimes found in the different seasons can also have a significant effect on the weather and winds found in the region. For example, in the late spring/early summer, with SSTs around Block Island hovering around the mid 40s F to low 50s F and a warm SW flow, the warmer air aloft usually struggles to mix to the surface resulting in stratification and shear between the lighter winds at the surface and the stronger winds aloft. (To the northeast of Block Island, given a period of solar insolation, there will be less stratification in the immediate lee of the island, and SW winds generally have more success in mixing to the surface). This stratification, or de-coupling effect, becomes much less noticeable with less thermal gradient (i.e. cooler air temps or warmer sea surface temperatures as found in late summer/early autumn).

During post cold frontal northwest winds in late summer and early fall, stronger winds will mix to the surface more readily. Sea surface temperatures at this time will usually be hovering around the upper 60'sF. Unstable conditions over the water generate convection, and result in Cu

or Sc development offshore. The well mixed convective boundary layer maintains strong and gusty conditions (dependent on pressure gradient) irrespective of solar insolation, throughout the night or under a blanket of cloud cover. This is in contrast to the generation of the convective boundary layer over the land, which requires solar insolation to generate diurnal thermal activity. Thus, during an early morning, post cold frontal day, the nocturnal inversion may be keeping surface winds light at Watch Hill and Westerly, whereas stronger NW winds are present on the NW facing shoreline of Block Island. Note that Block Island's nocturnal inversion may keep NW winds off the surface to the southeast of the island.

In addition, autumn NE winds can often have an extra "kick" as cooler air is flowing over relatively warmer waters. For example, case number 3 (NE, on September 22nd) depicts an excellent example of the markedly higher speeds recorded at the jetty location, whereas the airport does not experience the significantly higher speeds. Notice that the model unfortunately does not capture the enhanced speeds at the surface very well. In fact, the model will often perform better at speed forecasts at heights only 10s of meters above the surface, so this inadequacy may be less troublesome for wind energy assessment than for surface operations like Search and Rescue.

Qualitative Analysis of Results

General modeling results:

1. Wind directions verified well. This result is important as the primary focus of this study is to investigate the wind behavior in the Block Island region as a function of wind direction.

2. The model estimates the wind strength trends well, both on land and over water.

3. The model underestimates surface wind speeds on land with what appears to be a rather constant bias of about 5 knots once speeds rise to 5 knots or greater. Surface roughness differences between the model representation of the observation site, and the observation site itself are the primary cause for these differences. The surface roughness differences originate from two sources; deficiencies in the satellite derived land cover dataset used, and the spatial area in the model the observational site data is extracted from (a weighted interpolation from the 4 neighboring grid cells). These effects are minimized as you move vertically up towards elevated hub heights

4. The model also underestimates surface wind speeds over water, but the differences can range from near zero to double digit biases during the course of any particular run. We believe these biases are caused by poorly captured near surface thermal effects. Initial surges of colder air over warmer water associated with frontal passages, nocturnal instability, and interaction with low level jets are examples of events that could cause these thermally driven biases, which are more pronounced at the surface but still may be a factor at hub heights.

5. Finally, precipitation-altered speeds, which in fact, depending on the synoptic conditions, are known to both enhance and diminish speeds. These effects are generally not captured by models.

Event Descriptions and Verifications

1. North Case January 4th 2008

On 3 Jan an intense anticyclone, 1045mb, is established over Tennessee, with a ridge extending across the Great Lakes into Northern Quebec, resulting in cold northerly winds across New England. By Jan 4th, a fast moving low pressure center, propagates eastward across Hudson Bay and into Northern Quebec as the high pressure center to the south shows a weakening tendency and slips eastward across the Carolinas. This results in a steady backing of surface wind directions from northerly to westerly through the period. The high pressure center continues to slide offshore to the east through Jan 5th, resulting in a further backing to SW.

High pressure established inland can be a relatively common occurrence through the winter months, giving several days of N, NW or W winds for New England. During the summer months, high pressure generally becomes better established offshore, giving more days of southwesterly conditions.

Through 3 Jan, N and NNW winds eased slightly from around 30mph during the early hours to 20mph through the afternoon and evening dictated by pressure gradients. For the 4th, westerly winds built back up into the low thirties by 1000 (local time). Westerly winds then hovered around mid to upper twenties (mph) through much of the afternoon, diminishing into the evening.

Well modeled at both the Jetty and Airport.

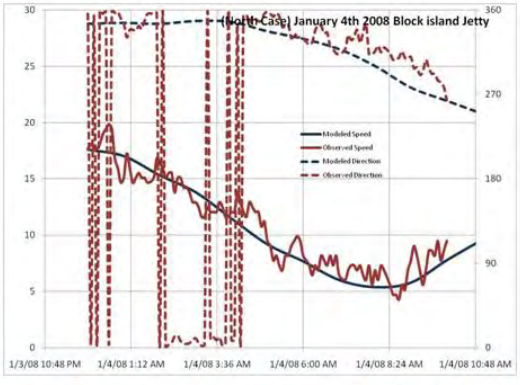

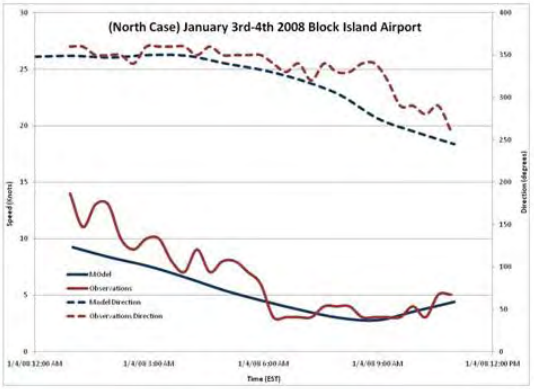

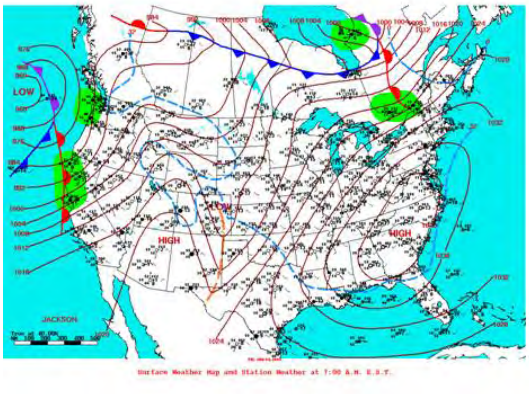

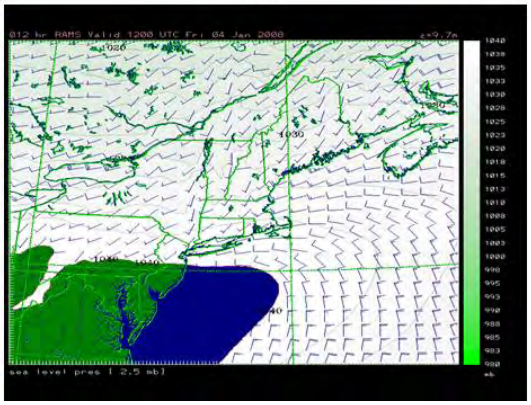

2. Northeast Case September 22nd 2008

Anticyclonic NE winds across New England thanks to high pressure becoming established over Quebec following the passage of a cold front from NNW to SSE the previous day. A stationary frontal boundary and trough axis to the east of Cape Hatteras helps to enhance northeasterly pressure gradients across the region.

Northeast winds increase through the morning hours, from 0200: 11g14mph, to 0700: 19 g22mph. For the rest of the period northeast winds generally hold around the 20mph mark. The lull-to-gust spread remains relatively small possibly indicating neutral or stable lower layers, and therefore more stratification rather than well mixed lower layers.

Directional trends captured well at both the jetty and airport. Speed trends captured well but magnitudes under-predicted at both locations. It is interesting to note that the speed magnitudes captured well with the dying SW flow at the beginning of the simulation, but once the cooler air arrives, the model totally misses the strong initial surge that occurs only over water, but then both locations settles into more of a systematic bias.

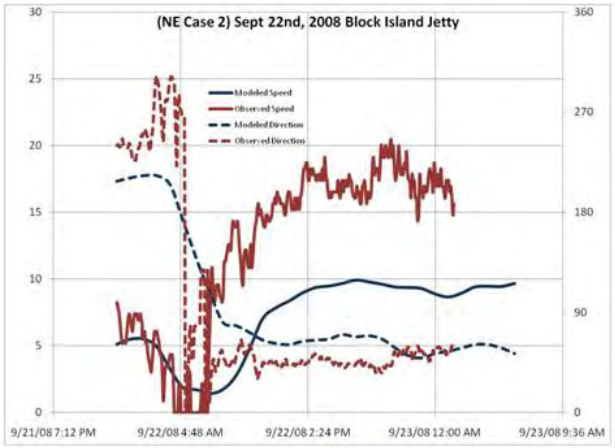

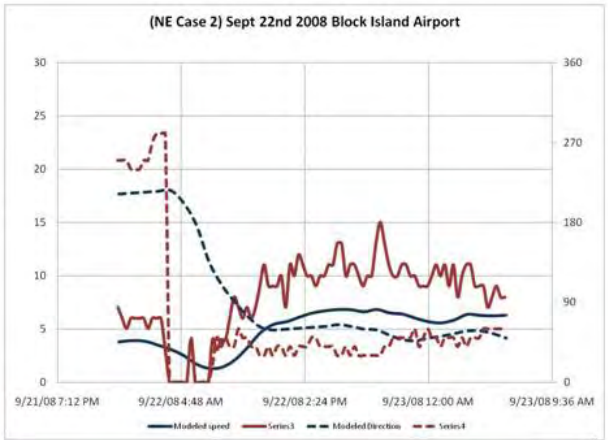

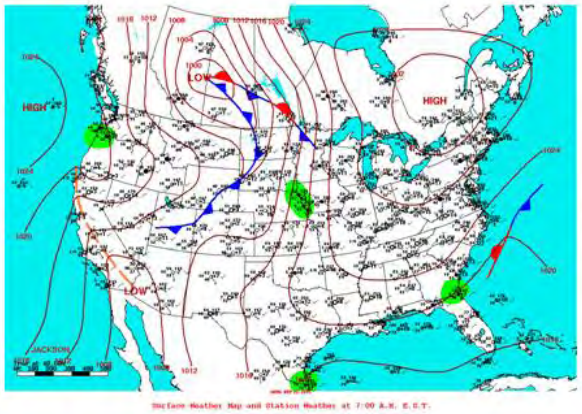

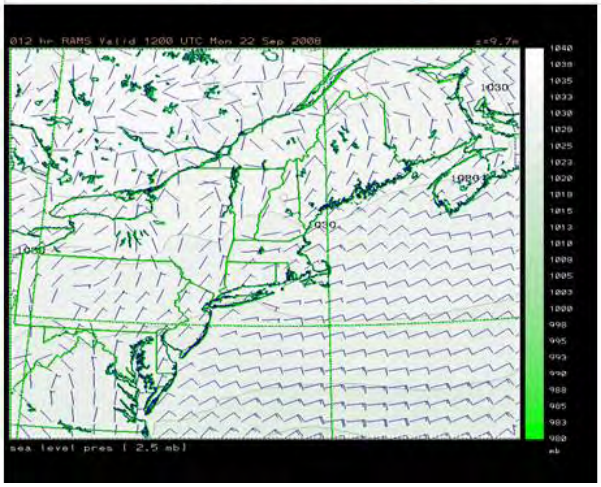

3. Northeast Case 2 April 17th 2008

Ridge of high pressure, 1024mb, extends from Nova Scotia to Florida Panhandle. Low pressure offshore Atlantic, maintaining northeast winds across Cape Cod, Block Island and Eastern Long Island. NE winds increase through the period, builds to 12mph through late morning and to 23mph through the afternoon. This is in response to tightening pressure gradients as low pressure edges westward across coastal New England.

Directional trends again are generally good, although the directional shift pattern at the beginning of the run occurred a couple of hours later than the model predicted, but the model recovered for awhile, only to lag again on a late backing trend. The onset of the speed increases was modeled well at both locations but eventually the prevalent under-prediction in speed occurred at both locations. Notice that the time series for both locations are quite similar with the magnitudes being higher over water.

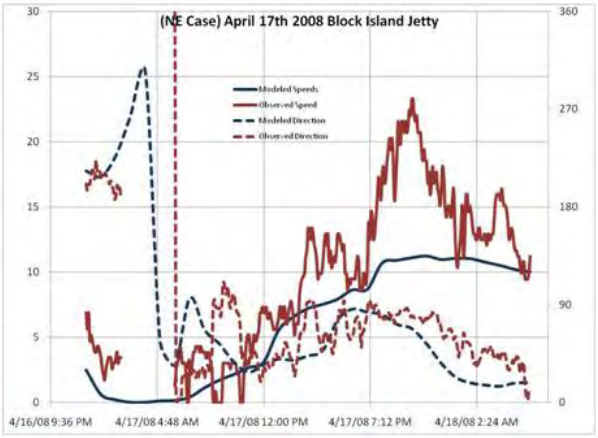

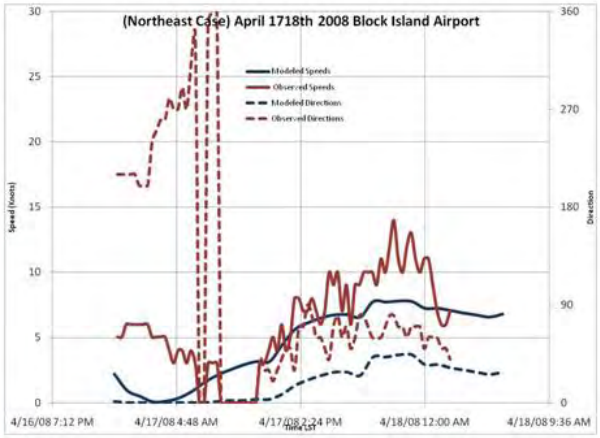

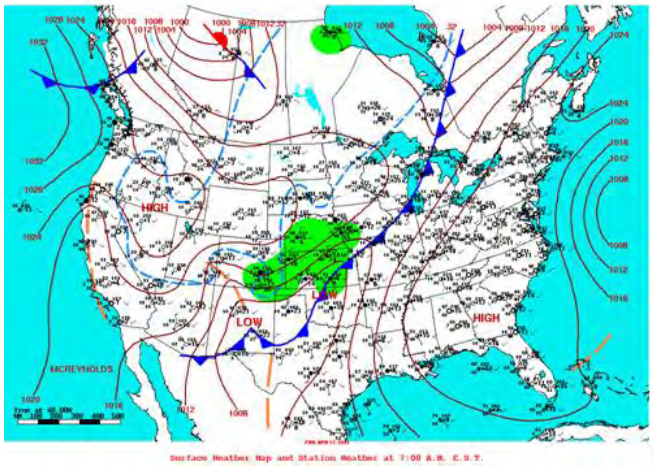

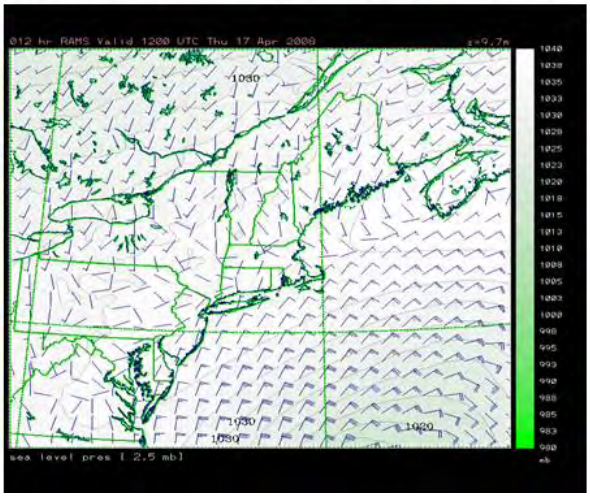

4. East Case September 24th 2008

High pressure, 1032mb, established over Northern New England. Trough axis and cyclogenesis east of Cape Hatteras. NE and ENE pressure gradients across coastal New England, becoming more easterly through the afternoon with some strengthening. Wind strengths through the beginning of the period were in the low teens (mph), building to mid teens by 0900 (local time), followed by a brief diminish through midday to low teens, and then building to mid and upper teens (with gusts to low twenties) by 1400 (local time). Afternoon wind directions become a better established easterly direction, holding into the evening.

This synoptic set up occurs occasionally, but when established (with high pressure and developing coastal low pressure to the south) can last for two to three days.

Directional trends look good, but again, observed speeds are higher at both the jetty and the airport. The differences were significantly higher at the jetty with little overall agreement, whereas the airport observed speed trends generally resemble the model.

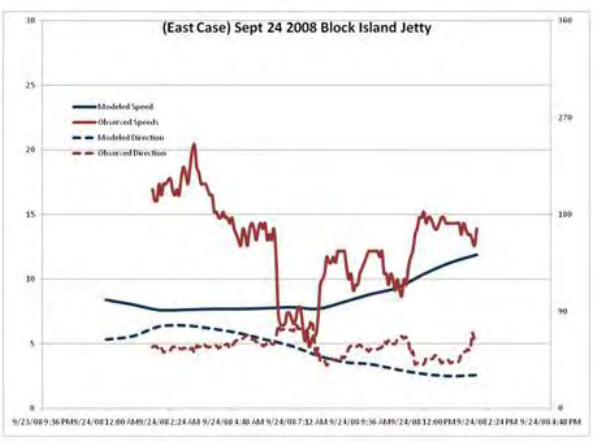

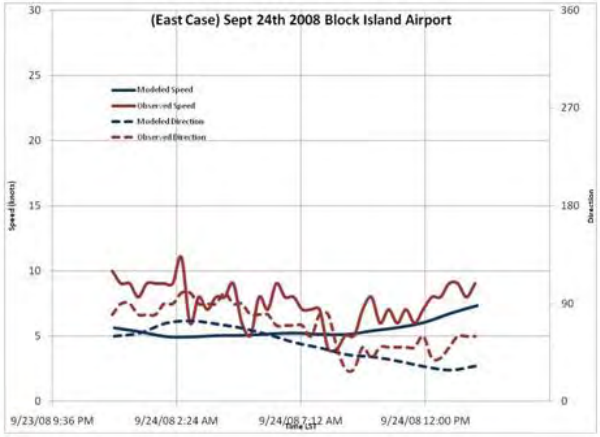

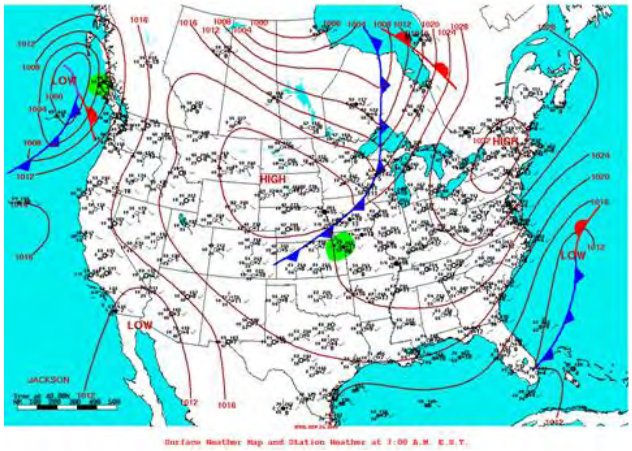

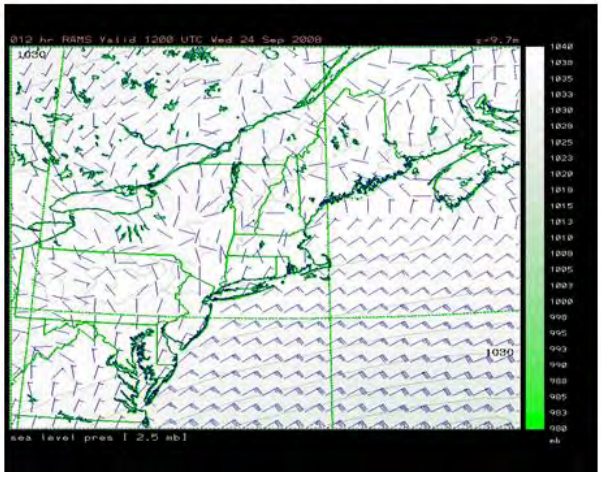

5. Southeast Case October 25th 2008

Quite a rare and short-lived synoptic set up. SE winds established for the day as New England high pressure slips northeastward over Nova Scotia. During the period a trough axis to the west deepens, eventually becoming a vigorous cold front that slides quickly offshore the following day. Through Oct 25th however, SE and SSE winds steadily increase from 14 g18mph at 0600 to 28 g 36 mph by 2300 (local).

Direction verification is quite good at both the jetty and the airport. In addition, observed speed trends also are well modeled. The under-prediction of speed is seen again, with a systematic approximate 5 knot under-prediction throughout most of the model run at the airport. At the jetty, speeds generally agree at both the beginning and end of the run, but during the period where winds backed to the ESE, observed values are significantly higher.

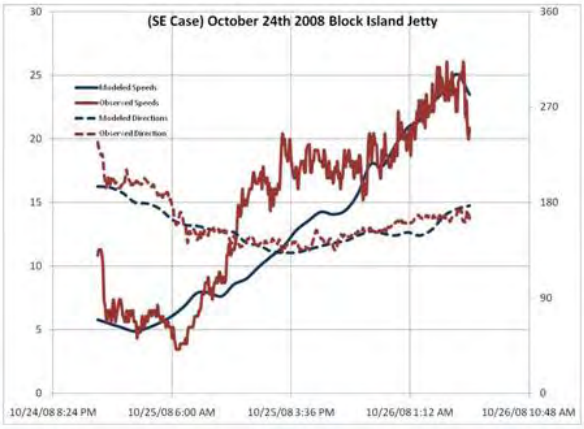

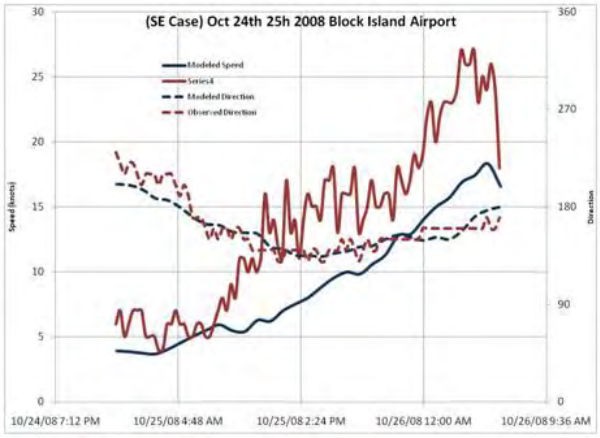

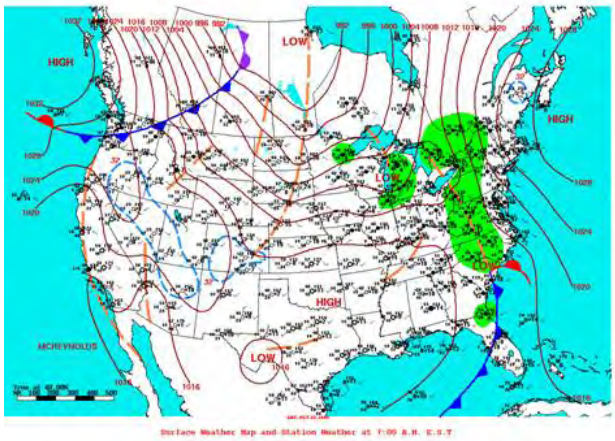

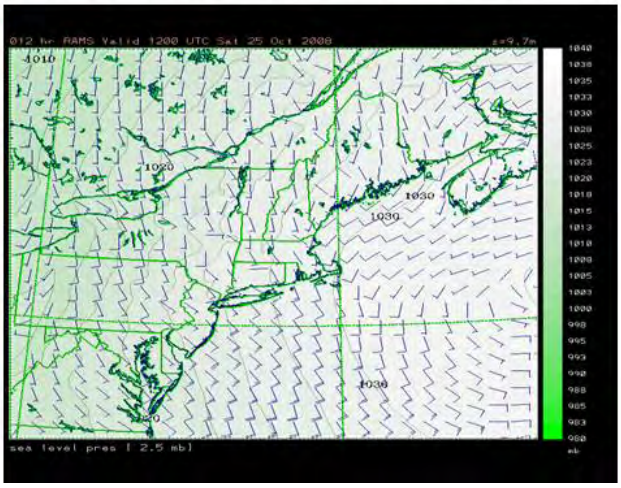

6. South Case September 6th 2008

Tropical Storm Hanna continues on her recurving path to the north, across NC and into VA. High pressure to the southeast of Nova Scotia, with a southerly becoming SE pressure gradient across Block Island. Pressure gradients tighten from 1600 onward (12 g 22mph) as wind directions become a better established SSE to SE. Wind strength maxima are reached between 2030 and 2215 (local time) with averages to 29mph and gusts to mid forties. Once again, southeasterly flow remains a relatively rare occurrence for Block Island, especially in combination with a tropical storm.

Verification for this case is harder to describe simply. This may be due to the complex dynamics associated with a decaying tropical system interacting with a frontal passage. There is general directional agreement during both the beginning and end of the model runs at both locations, but some significant veering and backing is missed mid run at both locales. Speeds are quite different with the most obvious glitch being the model missing the spike in speeds at both locales late in the run.

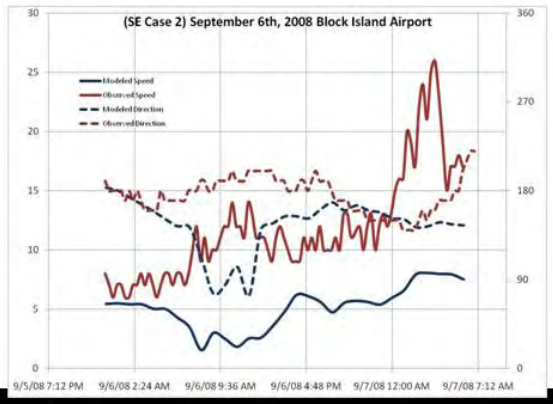

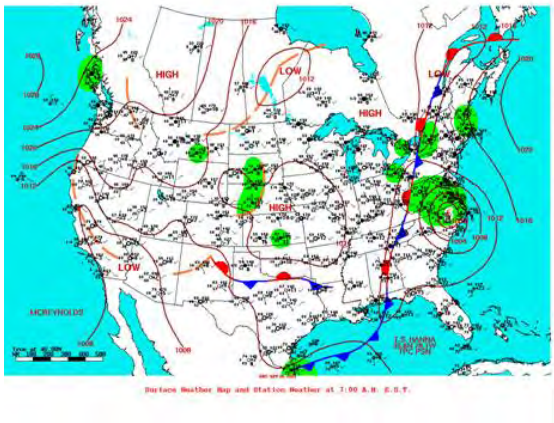

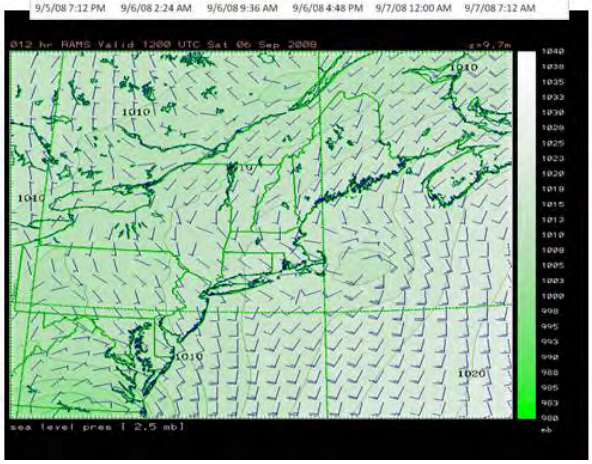

7. South Case 2 November 8th 2008

Low pressure complex, 999mb, over the Great Lakes. Warm front extending from Toronto, eastward across Maine to Nova Scotia. Cold front extending southward from Lake Ontario to Georgia. Warm air advection across New England through the day with tightening SSW to southerly pressure gradients associated with low level jet ahead of approaching cold front to the west. Light winds at Block Island through the early morning, then ramp up begins at 0800 (local time). SW wind maxima at 1415, with average to 18mph and gusts to 20. Wind directions becoming more southerly into the evening. Drops off to around 8mph by 1620, before increasing into the night with 21mph gusting to 27 by 2300. Also veering to SSW and SW by 2300 once again in response to approaching cold front. Cold frontal passage at Block Island eventually occurs around 0400 Nov 9th.

At the airport, some uncaptured directional oscillations. With speeds, an increasing trend is noted, but an under-prediction of speed is also evident, generally about 3 to 5 knots.

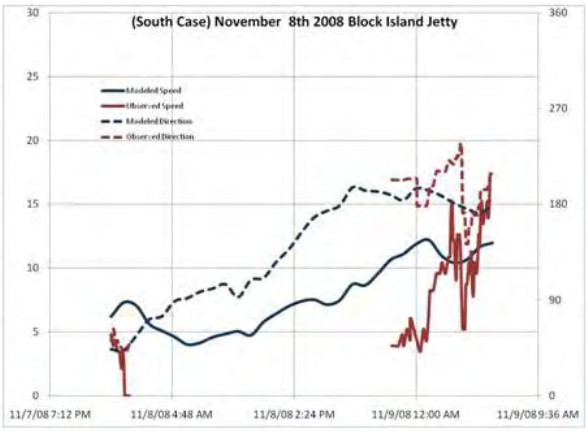

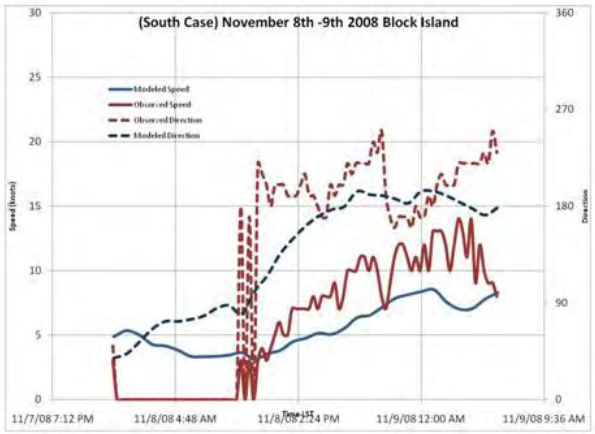

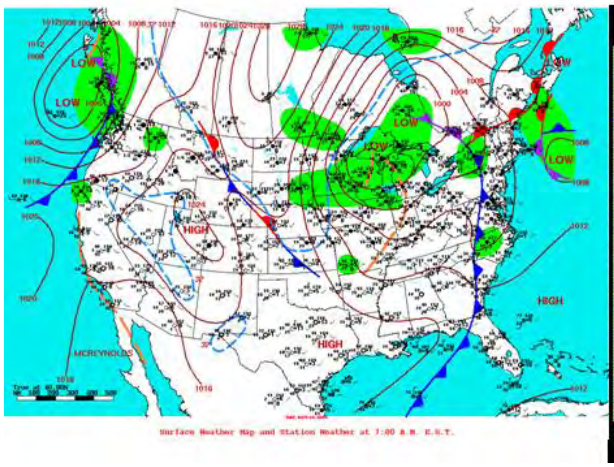

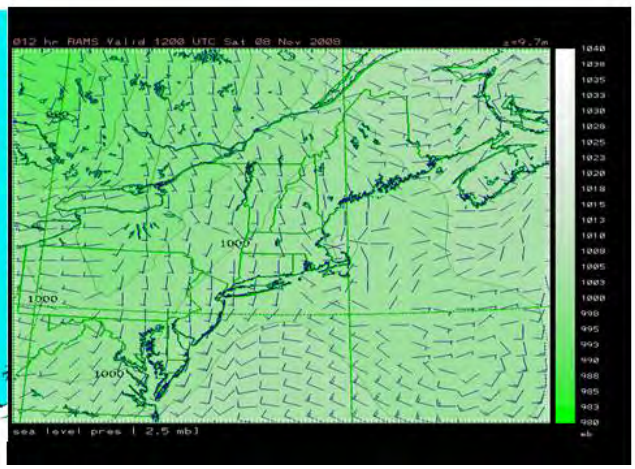

8. Southwest Case July 8th 2008

Bermuda high pressure, 1022mb, established to the southeast. Weak, expansive low pressure system, 1002mb, centered over Lake Superior with associated cold front extending southwestward to Nebraska. Warm front extending from low pressure center to Canadian Maritimes. This is a relatively common summer synoptic set up.

Southwesterly winds are established through the early morning hours with average wind speeds hovering around 10 to 12 mph, but unsteady with several periods of < 5mph, and a couple of gusts to 15 to 18mph. During the light period, wind directions veered more WSW to W briefly. Wind speeds began to ramp up after 0900, reaching a plateau between 1300 and 1600 (local time) with averages around 20mph and gusts into the mid to upper twenties.

Verification trends again very similar with directions in close agreement for both locations. For speeds, the airport exhibits the usual general agreement with trends, but a systematic approximate 5 knot under-prediction bias. Speed verification at the jetty is, at times, quite good with oscillations about near zero difference, but at others times 5 to 10 knots too low. Two such periods are observed during the overnight hours. Although the model does indicate enhanced flow, the model may struggle to capture the full effect of the nocturnal low-level jet.

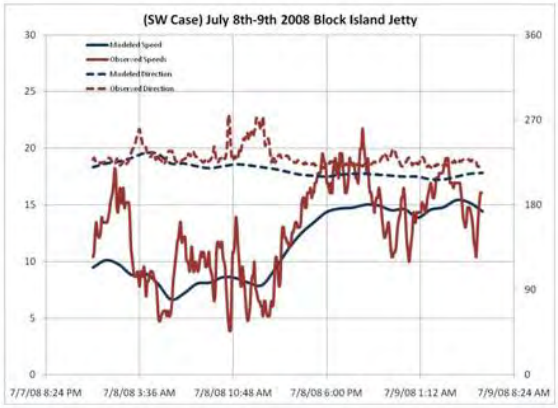

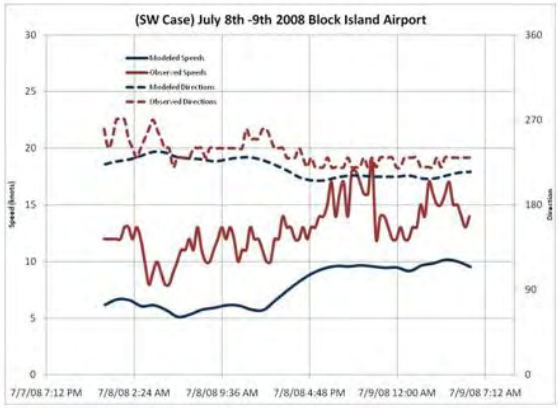

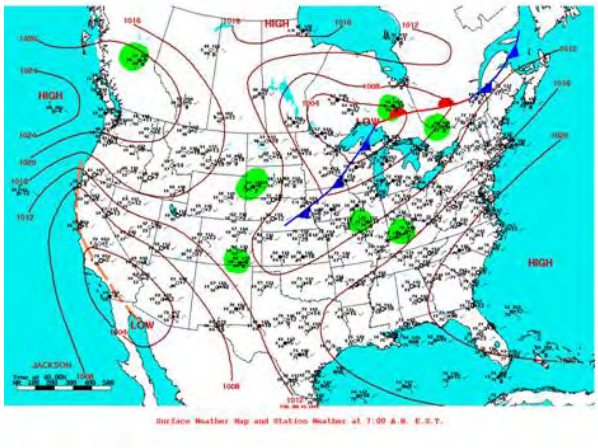

9. West Case December 22nd 2008

Developing low pressure tracks across New England through Dec 21st, deepening over Nova Scotia by Dec 22nd. High pressure, 1038mb, remains established over Missouri, generating northwest pressure gradients across New England and much of the East Coast. WNW winds, becoming NW through the early morning hours with average wind speeds easing from upper forties (mph) to 30mph. Once again, characteristic NW gustiness with a distinctive lull to gust spread throughout the day.

For this case, we were unable to retrieve observations from the airport, and so conducted verification using only the jetty, which reveals directional agreement with exception to a veer and back feature coinciding with lower speeds. This may simply be an embedded wave rotating around a departing deep low pressure system that the model failed to capture. Speed verification looks good although observed stronger flow continues into evening at the end of the model run at similar speeds to afternoon values. This discrepancy is typically problematic for models in near-coastal inland areas as decoupling (stabilization over land due to radiational cooling) may or may not occur based on highly local thermal effects (marsh or urban area may stay relatively unstable whereas an adjacent field may become stable). The vertical depth of the stable area is also difficult to model correctly in these regions.

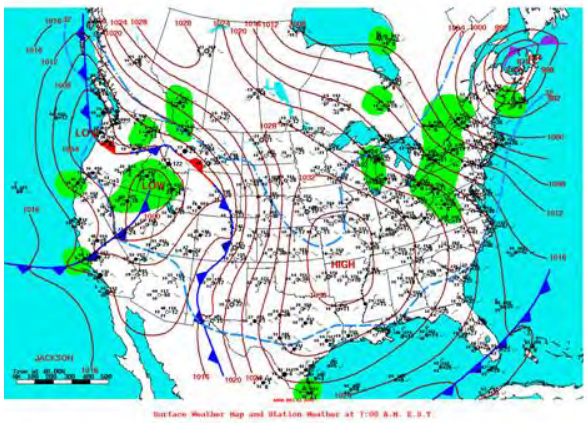

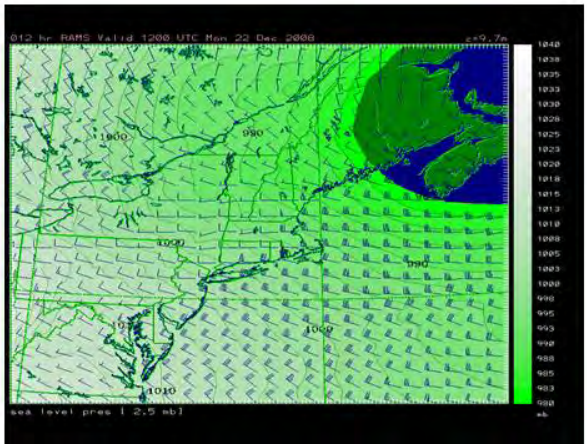

10. Northwest Case October 30th 2008

High pressure, 1030mb, building into the East Coast from the southwest, following the departure of a low pressure center now tracking northeastward across Newfoundland. This is a relatively common synoptic setup. Since the passage of the cold front late on the 28th, wind directions veered into the west then NW through the 29th, becoming a well established northwesterly through Oct 30th. These post cold frontal northwesterly winds exhibit a characteristically gusty signature, with average morning wind speeds around low 20s (mph), with gusts to upper twenties and low thirties. Through the afternoon, wind speeds ease slightly in response to weakening pressure gradients. The gust to lull spread appears to remain relatively large irrespective of diurnal solar insolation and air temps over the land. Boundary layer mixing is largely occurring as a result of relatively warm sea surface temperatures warming the lower layers of post cold frontal air advecting into the region.

Verification behavior is very similar to the other cases. Directional trends and magnitudes are well correlated. Modeled speeds at both locations are too low with the airport exhibiting more of a uniform bias throughout the run, whereas, once again, the jetty trends look good but the bias varies in a generally diurnal fashion, typical for cold air intrusions where both local differences between near-coastal air and water temperatures and nocturnal decoupling are quite sensitive to the resolution of the input fields.

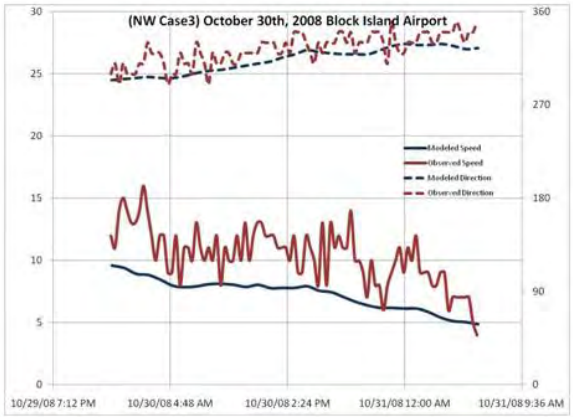

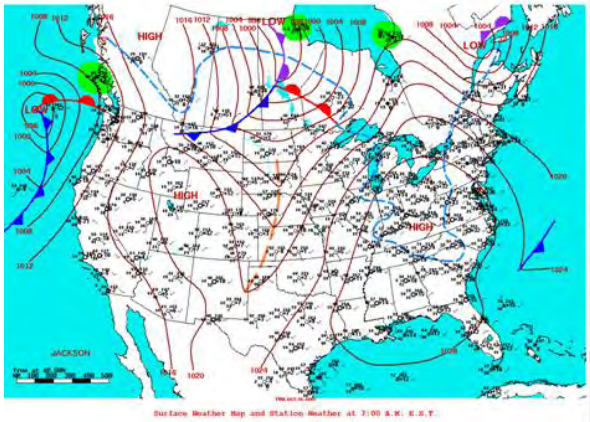

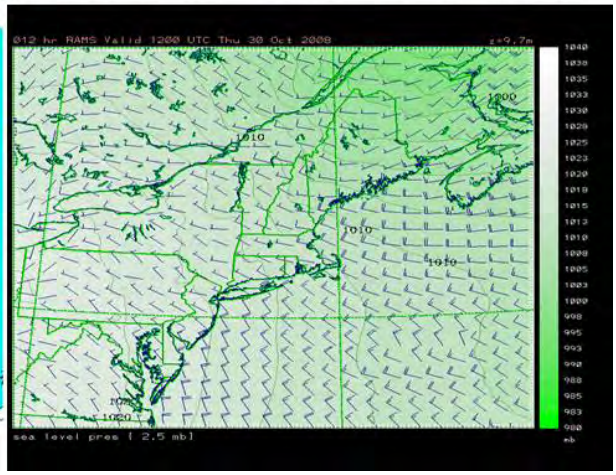

11. Northwest Case 2 November 22nd 2008

Tight NW pressure gradients generated by a low pressure center situated over the Canadian Maritimes and a high pressure system over the Carolinas. Strong and characteristically gusty NW conditions exist through Nov 22nd. Average wind speeds generally between mid twenties and low thirties through the morning hours, with gusts to mid and upper thirties (mph). Through the afternoon generally stronger conditions exist with averages in the low to upper thirties and gusts into the forties. Stronger winds are likely mixing to the surface from aloft as a result of cold air advection over relatively warm sea surface temperatures, as well as a component of mechanical turbulence generated over surface roughness.

Pressure gradients eased dramatically through the morning of Nov 23rd as high pressure built into New England from the southwest and low pressure pushed away to the northeast of the Canadian Maritimes.

Verification trends are similar to the previous northwest case with the only difference being that speeds are actually over predicted at the jetty for a short period and that same stronger speed feature is seen at the airport, yielding the only period during the run where the usual under-prediction bias is reduced to zero. Similar to the west wind case, the model does really "get it right" but more likely is unable to resolve an embedded wave from a departing strong low pressure system.

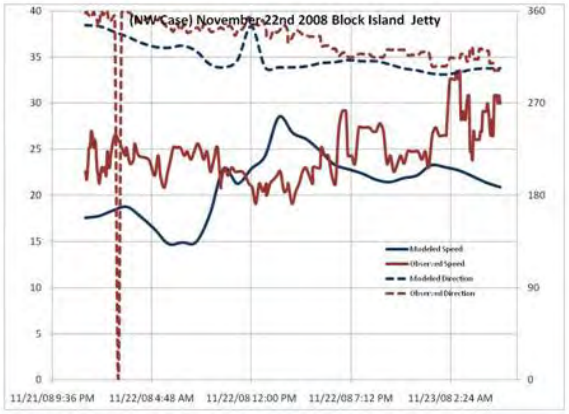

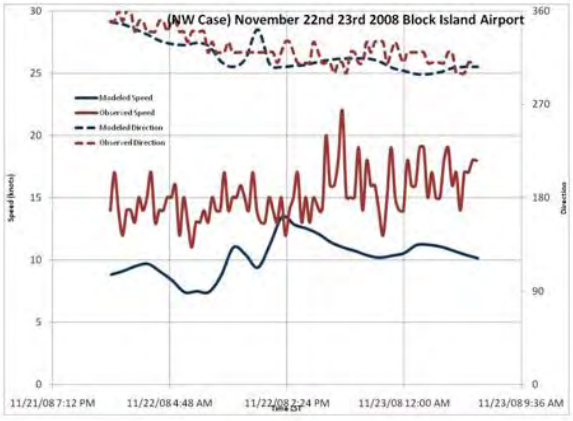

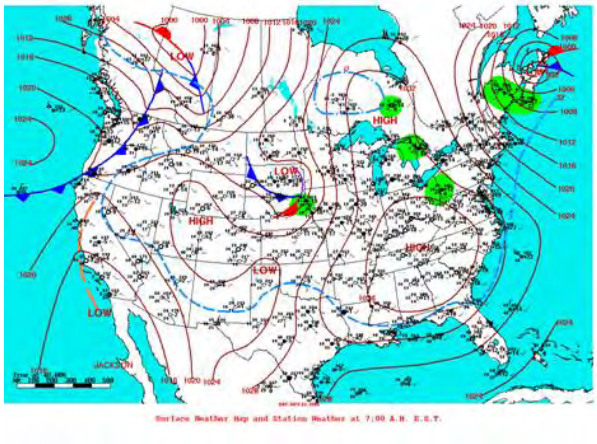

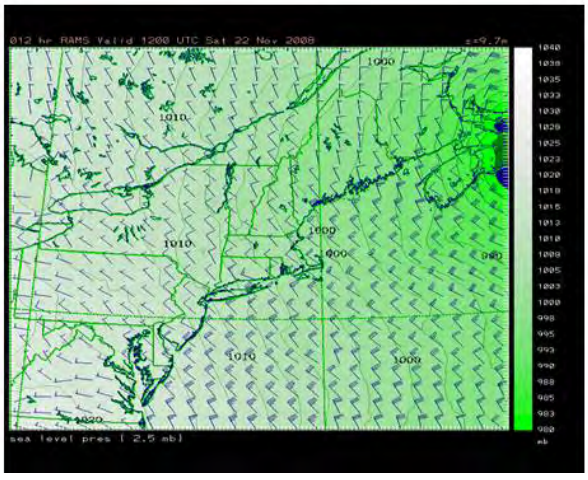

12. NW Case 3 February 23 2009

Low pressure, 992mb, centered over Nova Scotia, maintaining cyclonic flow across New England. Ridge of high pressure established to the west of the Great Lakes and moving gradually eastward. Strong WNW to NW winds throughout the day, starting out with averages to around 40mph and gusts to 50mph. As pressure gradients gradually relax through the day, wind speeds gradually ease into the mid to low thirties. Eventually wind strengths drop into the upper twenties by 2300 (local time).

Finally, for this third northwest case, with only jetty observations available from the archive, the results are roughly the same as with the previous cases - good agreement with observed and modeled direction and an under-prediction of speeds, highest during the initial surge of colder air over a relatively warm, unmixed water column. Of note, as stronger flow persists over time, the water column will mix and cool, thus reducing the difference between air and sea temperatures. The result is less efficient momentum transfer of stronger flow from aloft propagating down to the surface.

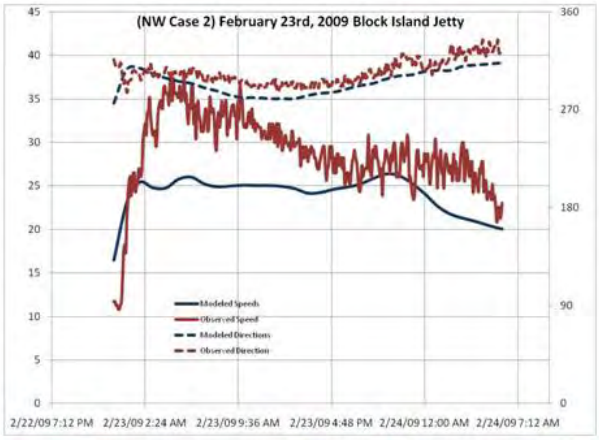

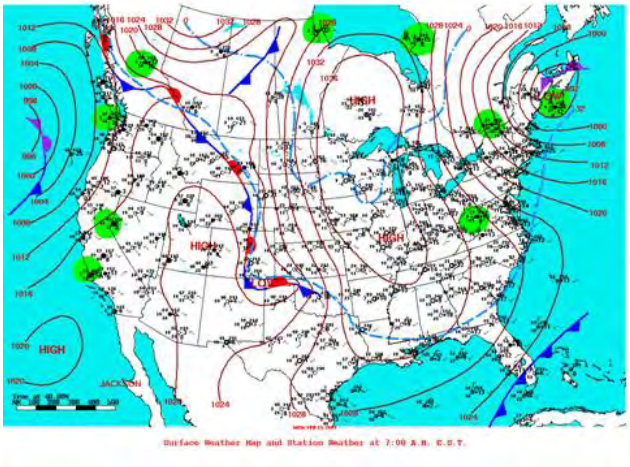

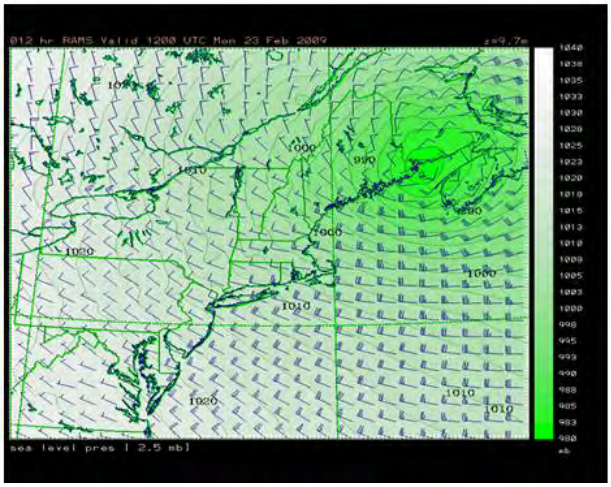

Appendix C

Template Method for Finding Average Annual Wind Speed

The template method for estimating the average annual winds at any point around the area of interest used wind patterns associated with wind fields emanating from the 8 points of the compass. The wind data used for the patterns was developed as hindcasts of 8 different wind regimes using a 3D, fine grid meteorological model of the area. In addition, the template method also used a long term wind speed directional distributions (rose) for determination of the frequency distribution of speeds and directions in the area.

The method for estimating the annual average wind speed is to use the long term wind rose (8 directions and 1 to 20m/s speed bins) from the WIS station and perform a weighted average of the 8 modeled wind regimes using the distributions. From that weighted average, an annual average wind speed is developed for every grid cell of the modeled domain. Using the 3D modeled templates, the estimates can be determined for any height, but the focus here was on the 80m hub height of proposed offshore wind turbines.

The methodology may be summarized as follows:

$$\sum_{w_{dir}=1}^{8} \sum_{w_I=1}^{20} \frac{Winds_{80}(w_{dir})}{SC_{80}(w_{dir})} * wndBin(w_I) * F(WIS_{10} * (80/10)^{\alpha w_{dir}} | (w_I, w_{dir}))$$

w_{dir} is the wind direction (N, NE, E, SE, S, SW, W, NW)

w_I is the wind speed (winds from 1 to 20 m/s)

$Winds_{80}(w_{dir})$ is the average wind speed for a given direction (wdir) at 80 meters based on the meteorological model

$wndBin(w_I)$ is the wind speed used: winds from 1 to 20 m/s

$SC_{80}(w_{dir})$ is the winds near the wind rose at 80 meters in the average meteorological model for a wind direction

WIS_{10}- wind frequency distribution at 10 meters at the wind rose location

$F(WIS_{10} * (80/10)^{alpha\text{-}wdir} | (w_{dir}, w_I))$ is the frequency distribution of rose data extrapolated to 80 meters with a directional alpha, and is dependent on the wind direction and wind speed.

Implementation of the methodology was performed using the following steps:

Build Template:

1) Gather meteorological model results for the 8 different wind directions. Each directional template consisted of a 30 hour hindcast of an actual time period with prevailing winds from the selected direction.

2) Using the location closest to the wind rose, at 80 meters, find the average wind direction for each individual hour of the hindcast. Using the expected wind direction, remove extraneous winds (time steps) that are not in the desired direction.

3) Average all remaining winds from a specific template at 10 and 80 meters.

4) Divide the wind speed values by the velocity in the region of the wind rose.

Determine Shear Coefficient Alpha:

Using the average winds from the template at 10 and 80 meters and the wind shear power law, solve for the wind shear coefficient (alpha):

alpha = (log(Velocity at 80 meters) - log(Velocity at 10 meters)) / (log(80) - log(10));

Find Wind Distribution:

1) Import the wind data to generate the wind rose (if not already available)

2) Using the wind shear equation, project 10m rose winds to 80m hub height. Scale the wind speed from rose location using the power law and the alpha determined in the previous step, to estimate winds at 80 meters:

V80 = V10 (80/10)alpha

Use alpha values as close to the wind rose station as possible.

3) Bin the values into direction and speed sets (8 wind directions and 0 to 20 m/s, 1 meter wind velocities.) Then divide by the number of wind measurements. Summing all values in the table will equal 100% of the data.

Final Annual Average Winds:

The final annual average wind speed estimate is a weighted average of the templates based on the wind distributions at the different speeds. For every wind speed and direction use the appropriate template, multiplied by the current wind speed bin and the distribution value. Then sum all weighted templates. The result is an average wind speed for each cell in the model domain based on the long term speed and direction frequency distribution. A similar strategy can be applied to estimate wind power.

Appendix D

Evaluation of the linear scaling analysis used in the template based method.

In the template based method, it is assumed that for a given wind direction the spatial pattern is similar and that wind speeds scale linearly relative to a reference location. To test this assumption, hindcast simulations for the period from October 1, 2009 to February 28, 2010 (Spaulding et al, 2010b) were reviewed to identify all the time periods for which winds were from the NW. NW winds have been selected since these dominant the hindcast period. These are also winds that dominate the wind power density roses in the vicinity of the renewable energy zone. These events are highlighted in blue in Figure 1. All wind speeds for each NW hindcast period were averaged over the study period to generate an average wind speed and power density map for NW winds (Figure 2). The mean wind speeds over a given event were divided by the average value over all events. The resulting map represents the scaling required to convert the mean wind speed map for all events to the wind speed map for a given event. The scaling maps for each NW event period are provided below. Table 1 (below) summarizes the upper and lower limits for each case. The differences in the scaling values for a given map are the focus here. Ideally the values are all the same, which represents linearly scaling. The scaling values for the various events range from 0.5 to 2, with most of values in the range of 0.8 to 1.2. The variation in the value of scaling parameters for a given time event is typically quite small and never larger than 10%. The average for all cases ranges from 0.979 to 1.05, or 6.6%. Linear scaling hence is a reasonable approximation.

Table 1 Scaling factors by time period for inner scaling of NW wind cases

Start Date	Start Time	End Date	End Time	Scale Factor Lower	Scale Factor Upper	Difference	% Difference
21-Feb	20	22-Feb	16	0.95	1	0.05	5.13
21-Feb	6	21-Feb	11	1.1	1.25	0.15	12.77
20-Feb	22	21-Feb	2	0.85	1.15	0.3	30.00
19-Feb	19	20-Feb	16	1.05	1.15	0.1	0.09
17-Feb	2	17-Feb	9	1.2	1.3	0.1	8.00
18-Feb	10	19-Feb	0	1.05	1.1	0.05	4.65
13-Feb	0	13-Feb	17	0.76	0.8	0.04	5.13
14-Feb	1	14-Feb	8	1.1	1.2	0.1	8.70
11-Feb	21	12-Feb	19	.95	1.05	0.1	10.00
8-Feb	16	9-Feb	16	1.1	1.2	0.1	8.70
7-Feb	14	8-Feb	10	1.09	1.1	0.01	0.91
4-Feb	2	5-Feb	16	0.85	0.9	0.05	5.71
2-Feb	4	2-Feb	16	0.505	0.55	0.045	8.53
29-Jan	4	29-Jan	14	1.55	1.7	0.15	9.23
30-Jan	2	30-Jan	18	1.17	1.2	0.03	2.53
13-Jan	9	14-Jan	7	0.63	0.65	0.02	3.13
12-Jan	4	13-Jan	1	0.68	0.7	0.02	2.90
10-Jan	20	11-Jan	2	0.68	0.71	0.03	4.32
9-Jan	2	9-Jan	22	0.92	1.1	0.18	17.82
8-Jan	3	8-Jan	15	0.45	0.5	0.05	10.53
6-Jan	2	7-Jan	17	0.95	0.95	0	0.00
5-Jan	2	7-Jan	17	0.95	0.95	0	0.00
3-Jan	13	5-Jan	14	1.23	1.3	0.07	5.53
3-Jan	0	3-Jan	9	1.9	2.05	0.15	7.53
29-Dec	14	30-Dec	16	1.35	1.4	0.05	3.54
23-Dec	20	24-Dec	11	1.1	1.15	0.05	4.44
20-Dec	17	23-Dec	9	1.25	1.35	0.1	7.69
17-Dec	2	18-Dec	3	1.25	1.25	0	0.00
16-Dec	2	16-Dec	19	1.06	1.1	0.04	3.70
8-Dec	8	8-Dec	23	0.6	0.6	0	0.00
6-Dec	11	7-Dec	12	0.77	0.8	0.03	3.82
4-Nov	3	4-Nov	17	0.9	0.95	0.05	5.41
19-Oct	19	20-Oct	10	0.45	0.5	0.05	10.53
8-Oct	6	9-Oct	5	1	1	0	0.00
1-Oct	0	1-Oct	11	0.95	0.9	0.05	5.71
			Avg.	0.98	1.04	0.066	6.19

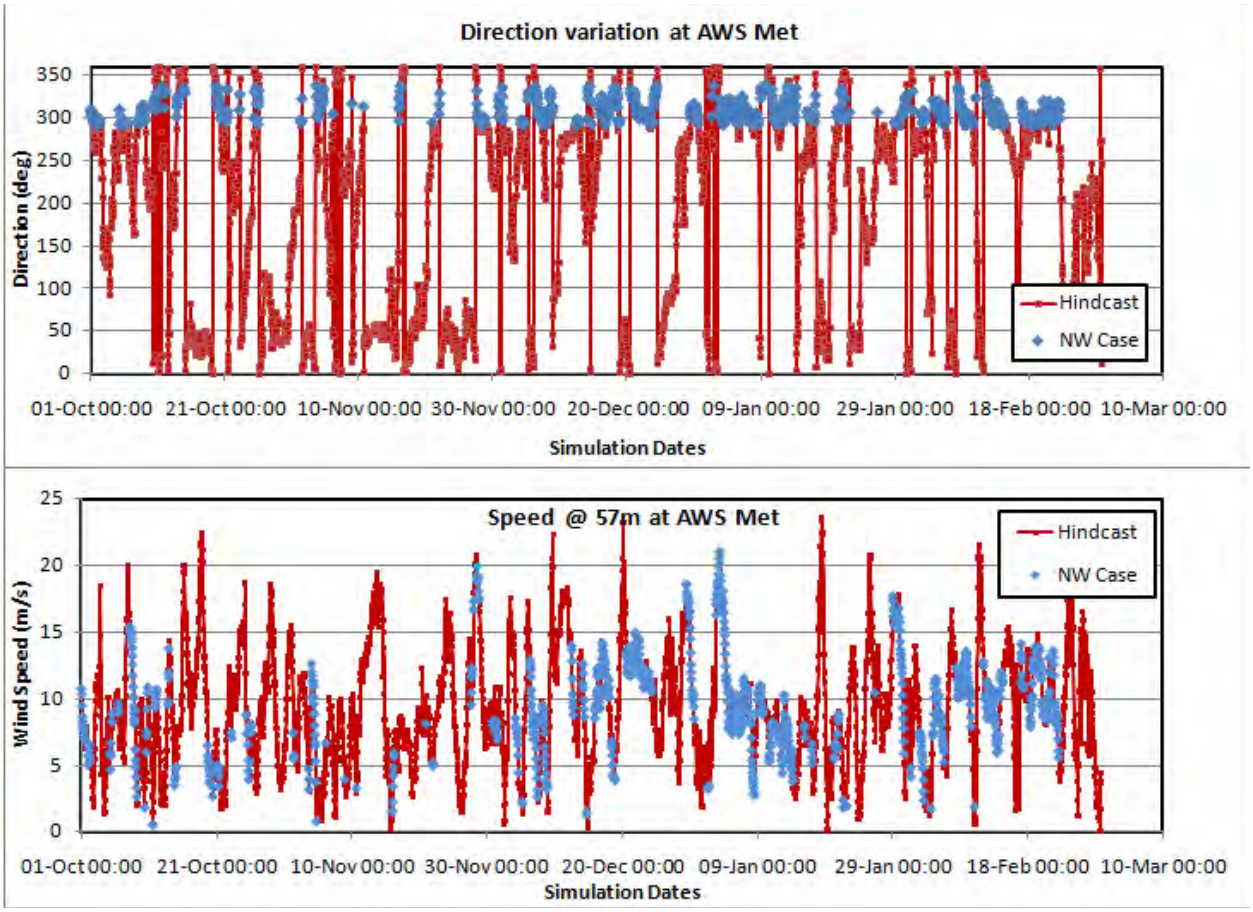

Figure 1 RAMS model predicted winds direction (upper panel) and speed (lower panel) at AWS Met, at 57 m elevation from October 1, 2009 through February 28, 2010.

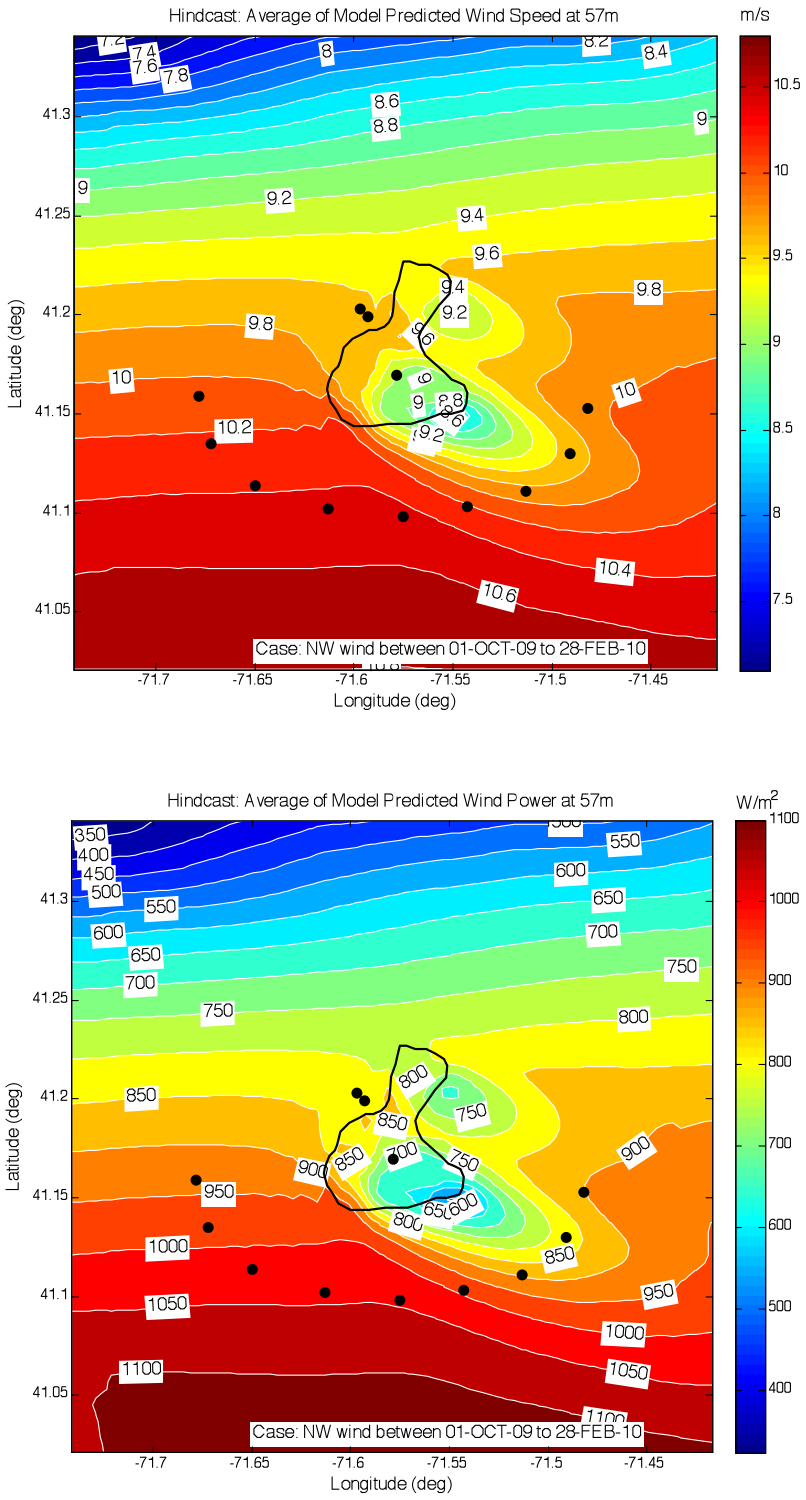

Figure 2 Model predicted average wind speed (upper panel) and wind power density (lower panel) at 57 m for all NW wind cases.

Figures that follow show model predicted scaling parameter, relative to the mean value over each individual event.

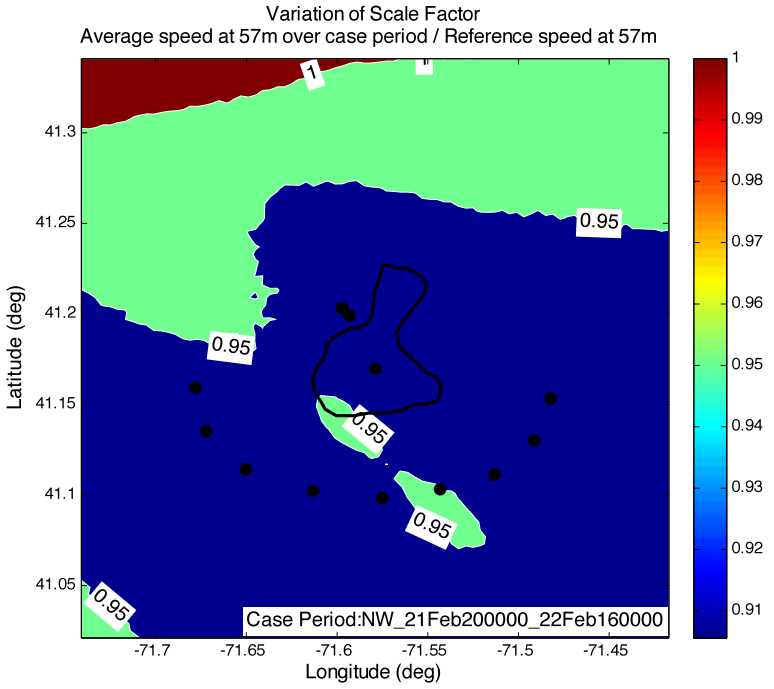
Variation of Scale Factor
Average speed at 57m over case period / Reference speed at 57m
1
0.95
0.95
0.95
0.95
Case Period:NW_21Feb200000_22Feb160000
Latitude (deg)
Longitude (deg)
41.3
41.25
41.2
41.15
41.1
41.05
-71.7
-71.65
-71.6
-71.55
-71.5
-71.45
1
0.99
0.98
0.97
0.96
0.95
0.94
0.93
0.92
0.91

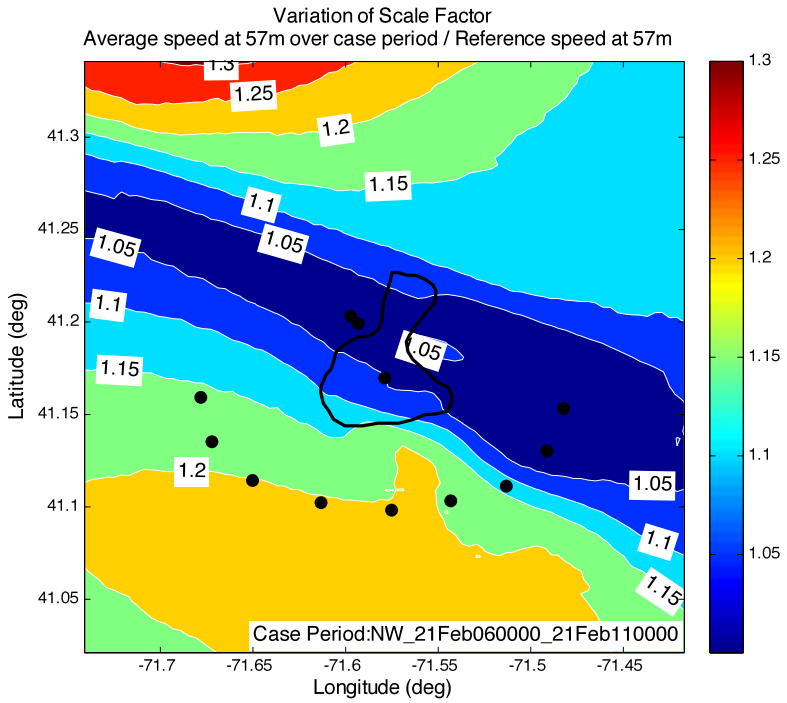
Variation of Scale Factor
Average speed at 57m over case period / Reference speed at 57m
1.25
1.2
1.15
1.1
1.05
1.05
1.1
1.15
1.2
1.05
1.1
1.15
1.05
Case Period:NW_21Feb060000_21Feb110000
Latitude (deg)
Longitude (deg)
41.3
41.25
41.2
41.15
41.1
41.05
-71.7
-71.65
-71.6
-71.55
-71.5
-71.45
1.3
1.25
1.2
1.15
1.1
1.05

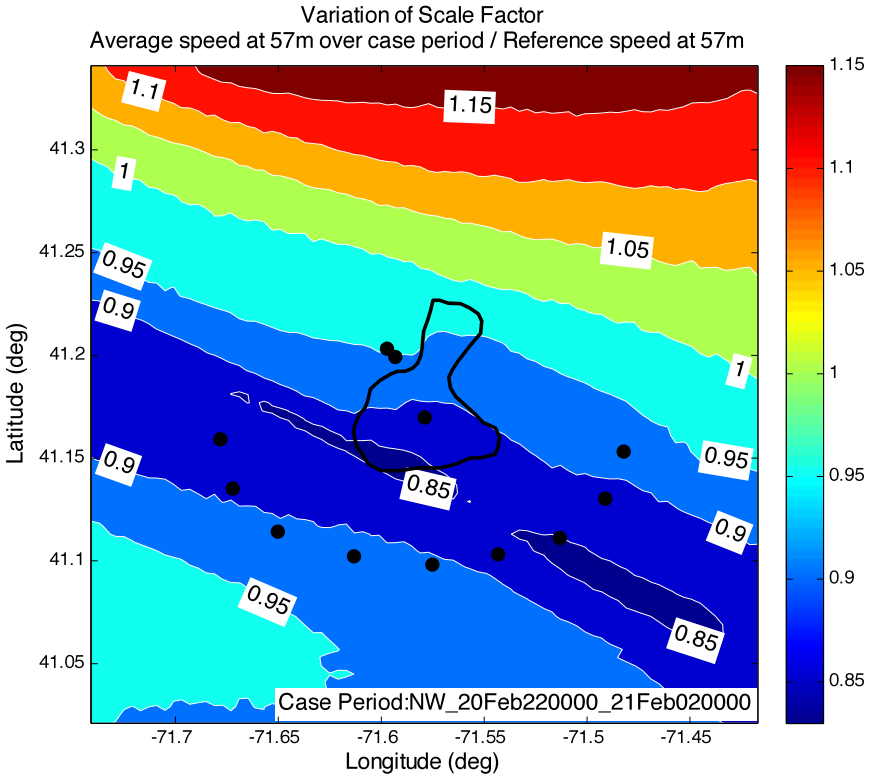
Variation of Scale Factor
Average speed at 57m over case period / Reference speed at 57m
1.1
1.15
1
1.05
0.95
0.9
0.85
Case Period:NW_20Feb220000_21Feb020000
Latitude (deg)
Longitude (deg)
41.3
41.25
41.2
41.15
41.1
41.05
-71.7
-71.65
-71.6
-71.55
-71.5
-71.45
1.15
1.1
1.05
1
0.95
0.9
0.85

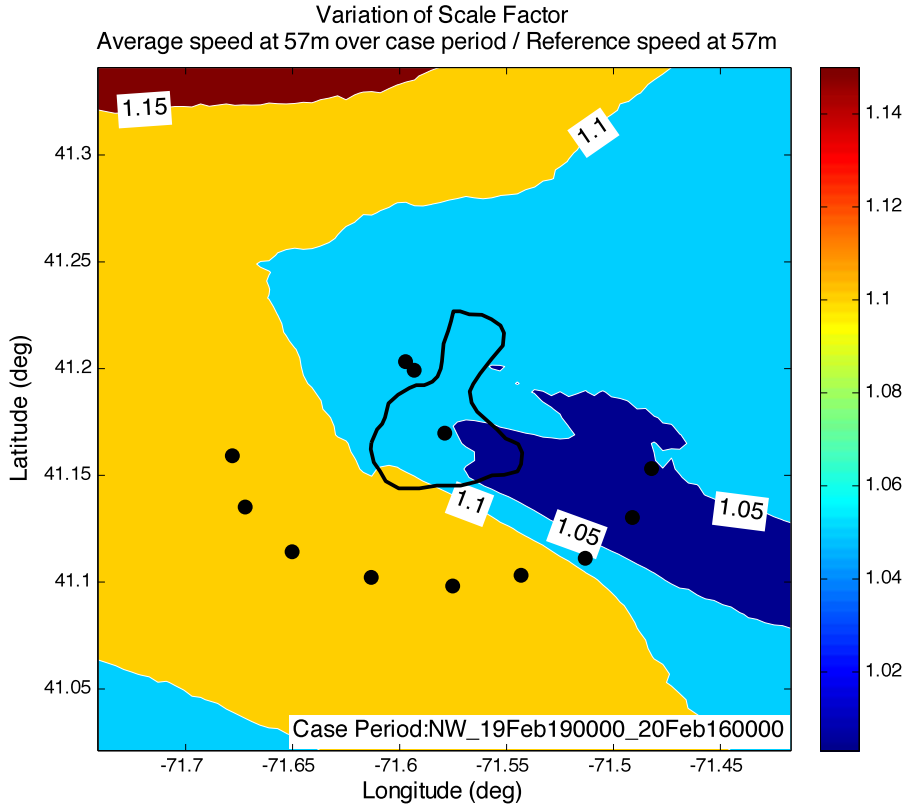
Variation of Scale Factor
Average speed at 57m over case period / Reference speed at 57m
1.15
1.1
1.05
Case Period:NW_19Feb190000_20Feb160000
Latitude (deg)
Longitude (deg)
41.3
41.25
41.2
41.15
41.1
41.05
-71.7
-71.65
-71.6
-71.55
-71.5
-71.45
1.14
1.12
1.1
1.08
1.06
1.04
1.02

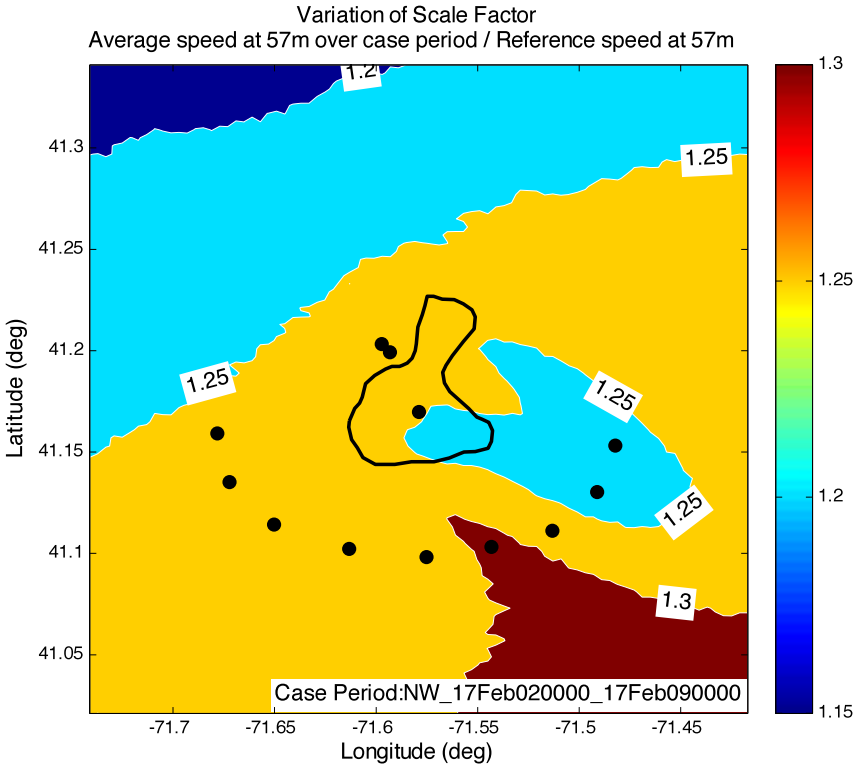
Variation of Scale Factor
Average speed at 57m over case period / Reference speed at 57m
1.25
1.25
1.25
1.25
1.3
Case Period:NW_17Feb020000_17Feb090000
Latitude (deg)
Longitude (deg)
41.3
41.25
41.2
41.15
41.1
41.05
-71.7
-71.65
-71.6
-71.55
-71.5
-71.45
1.3
1.25
1.2
1.15

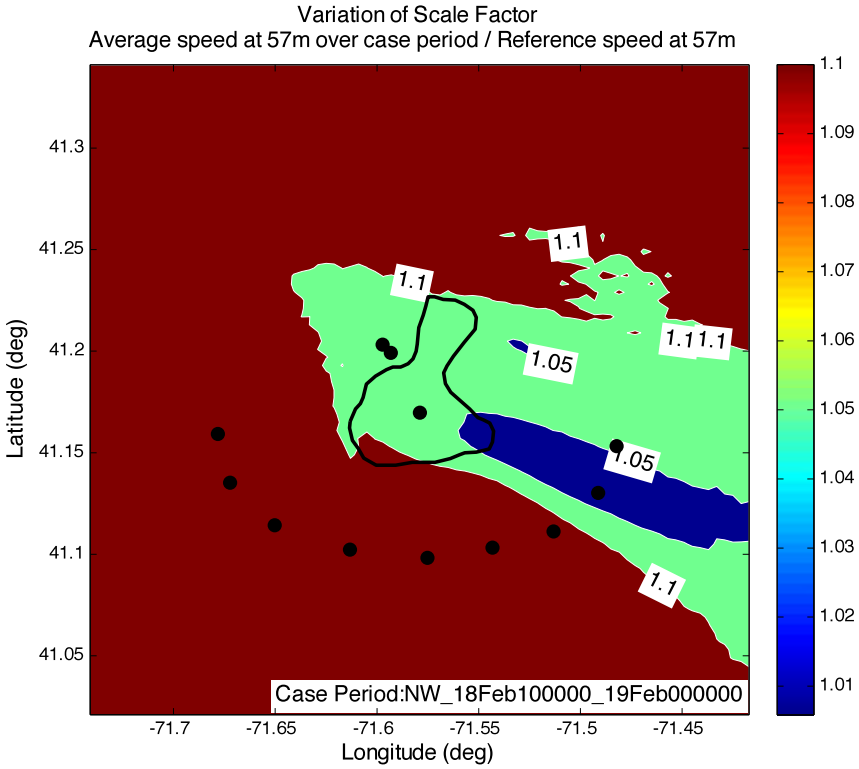
Variation of Scale Factor
Average speed at 57m over case period / Reference speed at 57m
1.1
1.1
1.1
1.1
1.05
1.05
Case Period:NW_18Feb100000_19Feb000000
Latitude (deg)
Longitude (deg)
41.3
41.25
41.2
41.15
41.1
41.05
-71.7
-71.65
-71.6
-71.55
-71.5
-71.45
1.1
1.09
1.08
1.07
1.06
1.05
1.04
1.03
1.02
1.01

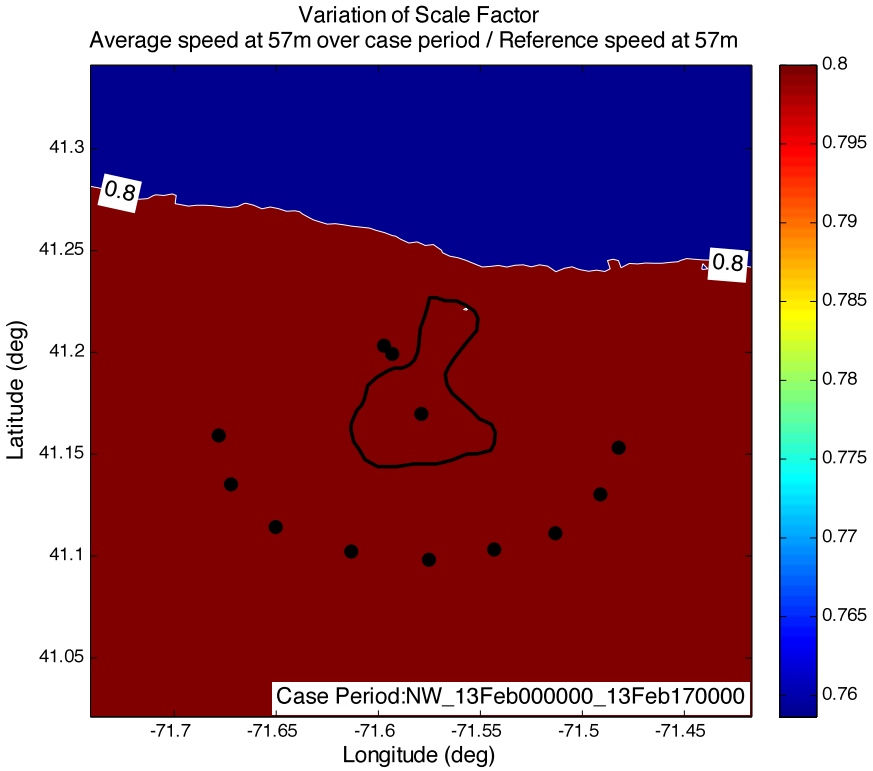
Variation of Scale Factor
Average speed at 57m over case period / Reference speed at 57m
0.8
0.8
Case Period:NW_13Feb000000_13Feb170000
Latitude (deg)
Longitude (deg)
41.3
41.25
41.2
41.15
41.1
41.05
-71.7
-71.65
-71.6
-71.55
-71.5
-71.45
0.8
0.795
0.79
0.785
0.78
0.775
0.77
0.765
0.76

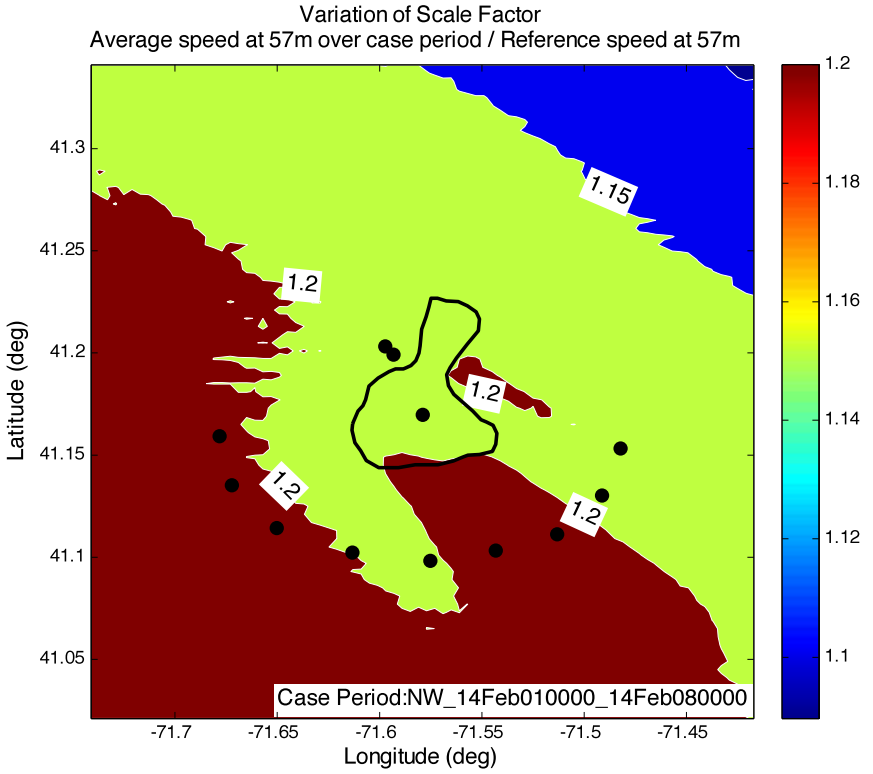
Variation of Scale Factor
Average speed at 57m over case period / Reference speed at 57m
1.15
1.2
1.2
1.2
1.2
Case Period:NW_14Feb010000_14Feb080000
Latitude (deg)
Longitude (deg)
41.3
41.25
41.2
41.15
41.1
41.05
-71.7
-71.65
-71.6
-71.55
-71.5
-71.45
1.2
1.18
1.16
1.14
1.12
1.1

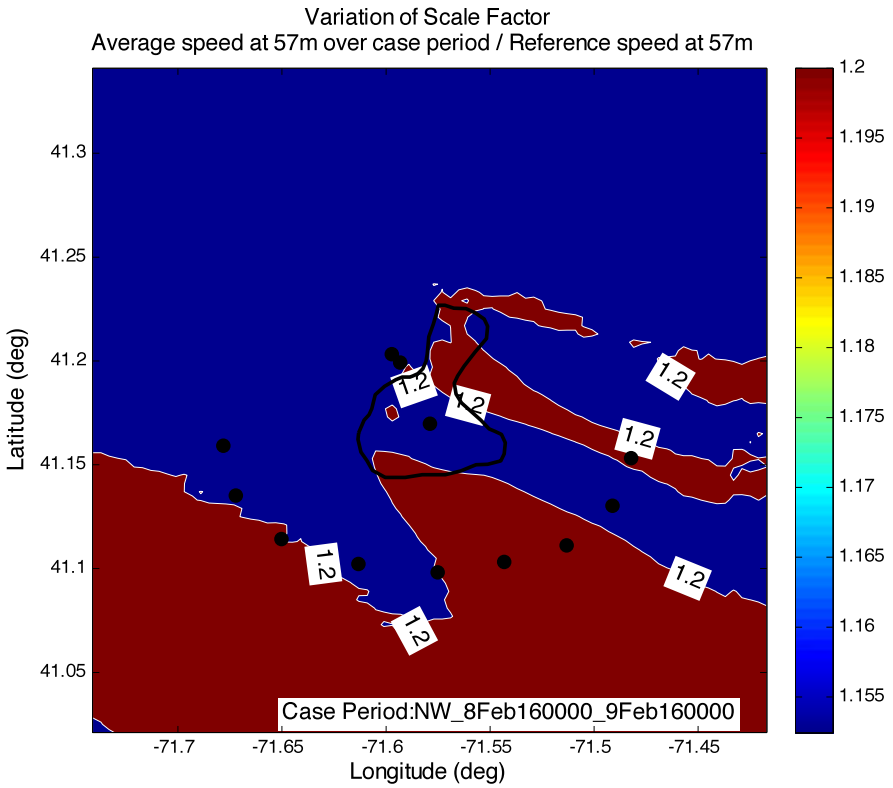
Variation of Scale Factor
Average speed at 57m over case period / Reference speed at 57m
Latitude (deg)
Longitude (deg)
Case Period:NW_8Feb160000_9Feb160000
1.2
41.3
41.25
41.2
41.15
41.1
41.05
-71.7
-71.65
-71.6
-71.55
-71.5
-71.45
1.195
1.19
1.185
1.18
1.175
1.17
1.165
1.16
1.155

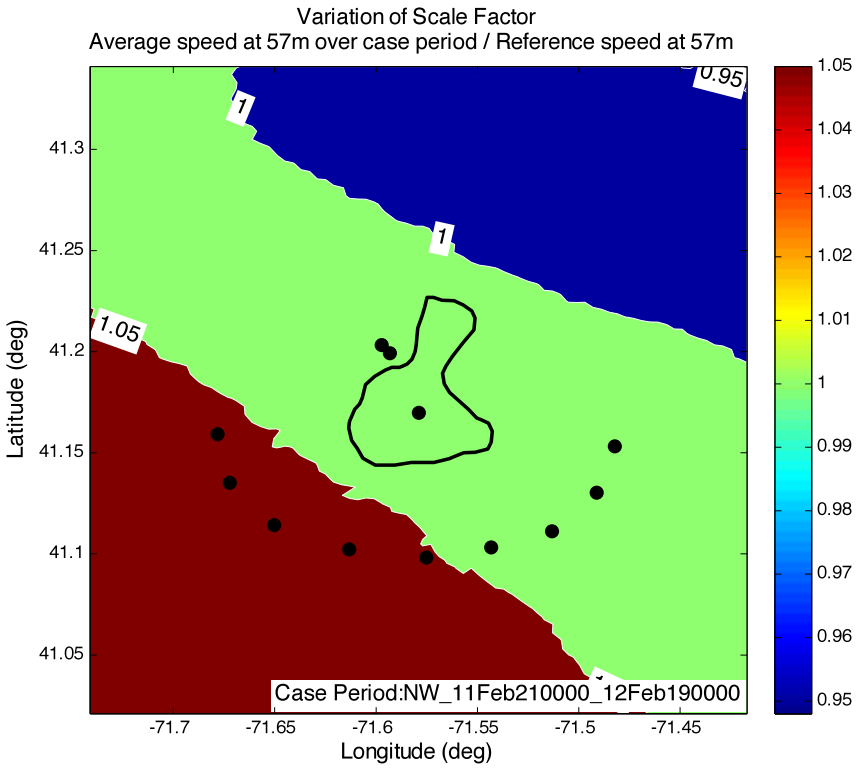
Variation of Scale Factor
Average speed at 57m over case period / Reference speed at 57m
Latitude (deg)
Longitude (deg)
Case Period:NW_11Feb210000_12Feb190000
0.95
1
1.05
41.3
41.25
41.2
41.15
41.1
41.05
-71.7
-71.65
-71.6
-71.55
-71.5
-71.45
1.04
1.03
1.02
1.01
0.99
0.98
0.97
0.96

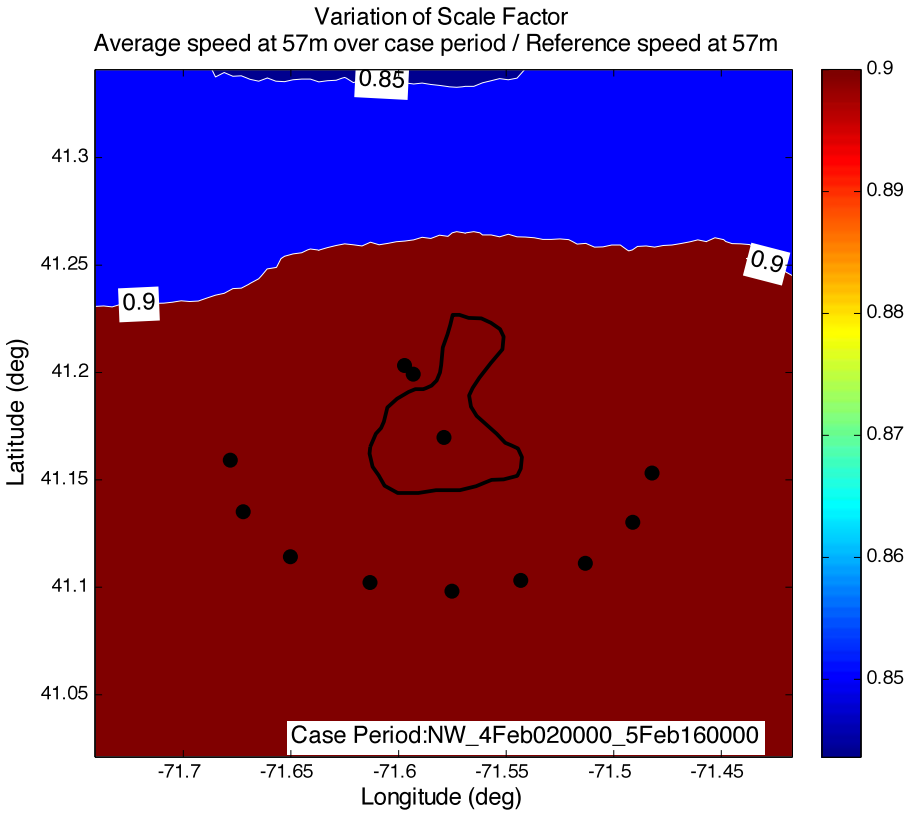
Variation of Scale Factor
Average speed at 57m over case period / Reference speed at 57m
0.85
0.9
0.9
Case Period:NW_4Feb020000_5Feb160000
Latitude (deg)
Longitude (deg)
41.3
41.25
41.2
41.15
41.1
41.05
-71.7
-71.65
-71.6
-71.55
-71.5
-71.45
0.9
0.89
0.88
0.87
0.86
0.85

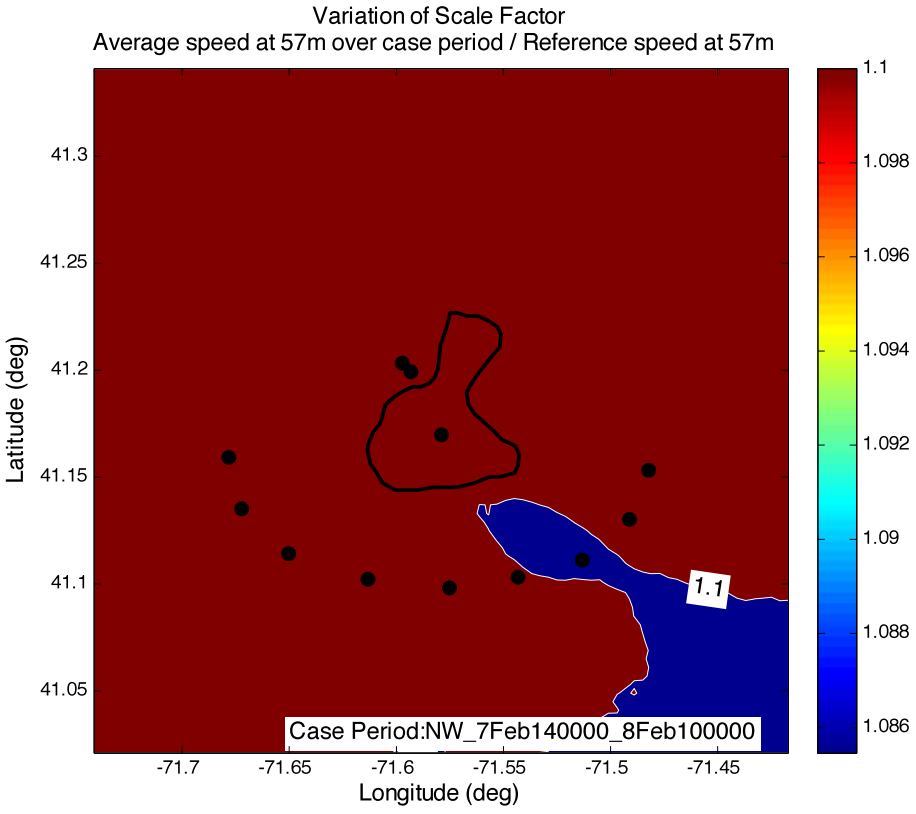
Variation of Scale Factor
Average speed at 57m over case period / Reference speed at 57m
1.1
Case Period:NW_7Feb140000_8Feb100000
Latitude (deg)
Longitude (deg)
41.3
41.25
41.2
41.15
41.1
41.05
-71.7
-71.65
-71.6
-71.55
-71.5
-71.45
1.1
1.098
1.096
1.094
1.092
1.09
1.088
1.086

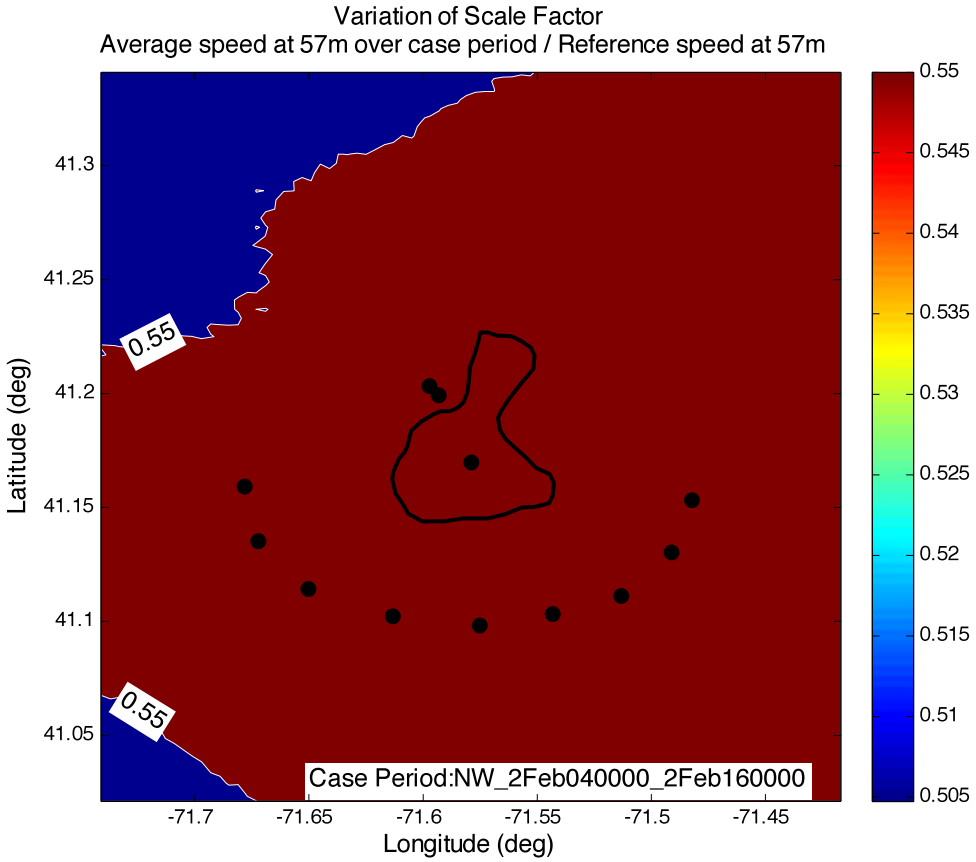
Variation of Scale Factor
Average speed at 57m over case period / Reference speed at 57m
0.55
0.55
Case Period:NW_2Feb040000_2Feb160000
Latitude (deg)
Longitude (deg)
41.3
41.25
41.2
41.15
41.1
41.05
-71.7
-71.65
-71.6
-71.55
-71.5
-71.45
0.55
0.545
0.54
0.535
0.53
0.525
0.52
0.515
0.51
0.505

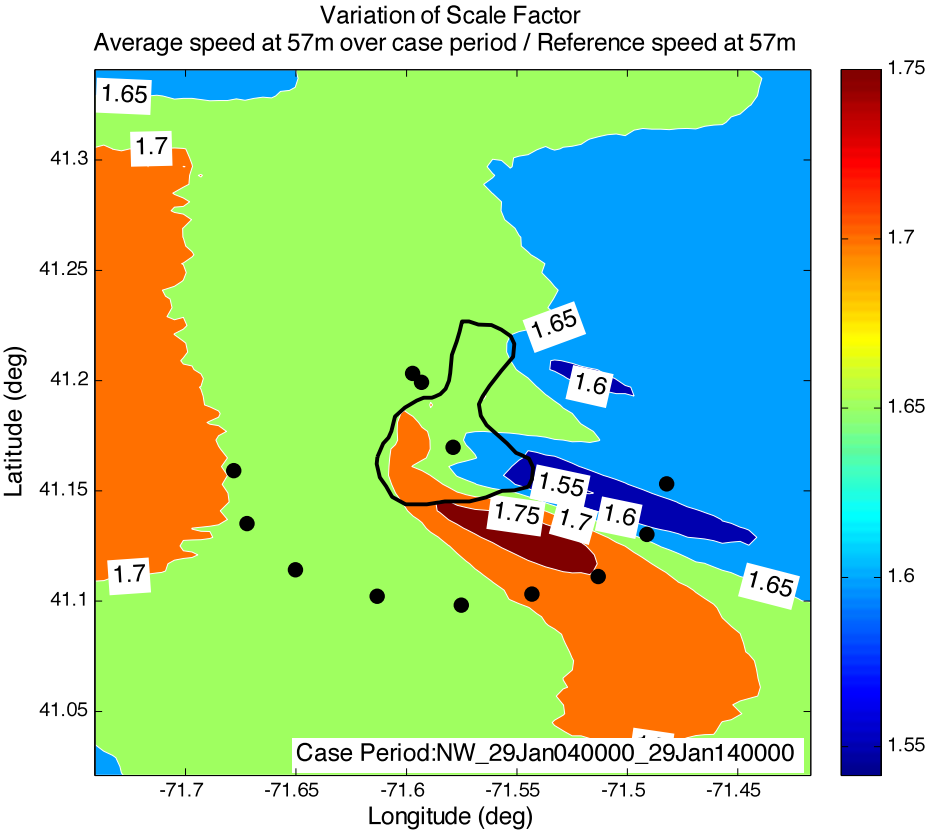
Variation of Scale Factor
Average speed at 57m over case period / Reference speed at 57m
1.65
1.7
1.65
1.6
1.55
1.75
1.7
1.6
1.7
1.65
Case Period:NW_29Jan040000_29Jan140000
Latitude (deg)
Longitude (deg)
41.3
41.25
41.2
41.15
41.1
41.05
-71.7
-71.65
-71.6
-71.55
-71.5
-71.45
1.75
1.7
1.65
1.6
1.55

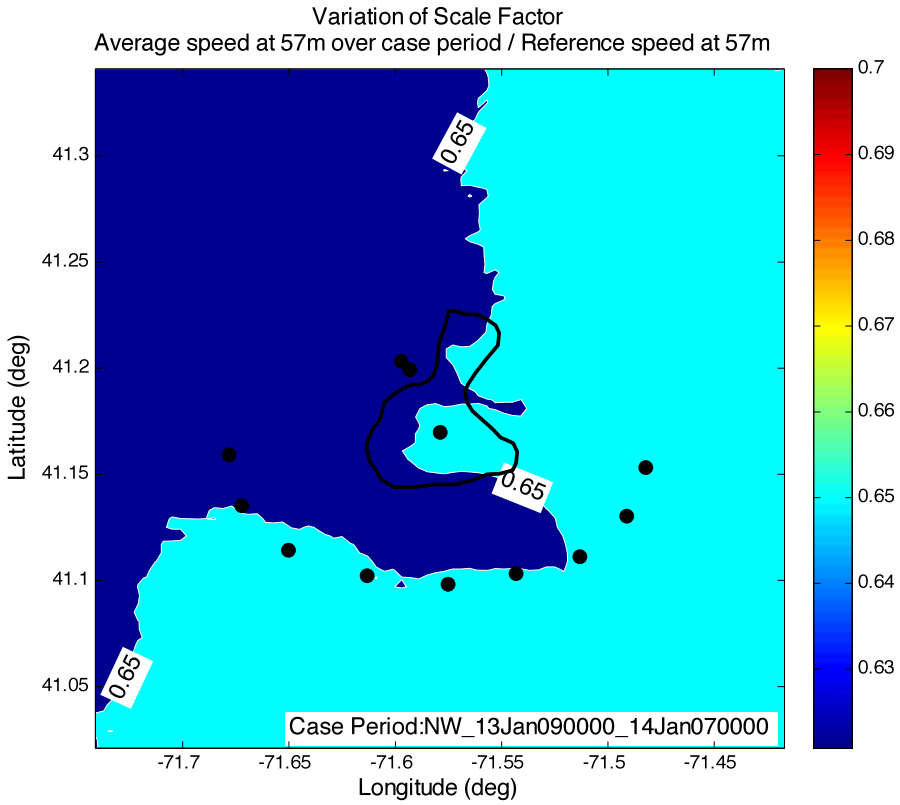
Variation of Scale Factor
Average speed at 57m over case period / Reference speed at 57m
0.65
0.65
0.65
Case Period:NW_13Jan090000_14Jan070000
Latitude (deg)
Longitude (deg)
41.3
41.25
41.2
41.15
41.1
41.05
-71.7
-71.65
-71.6
-71.55
-71.5
-71.45
0.7
0.69
0.68
0.67
0.66
0.65
0.64
0.63

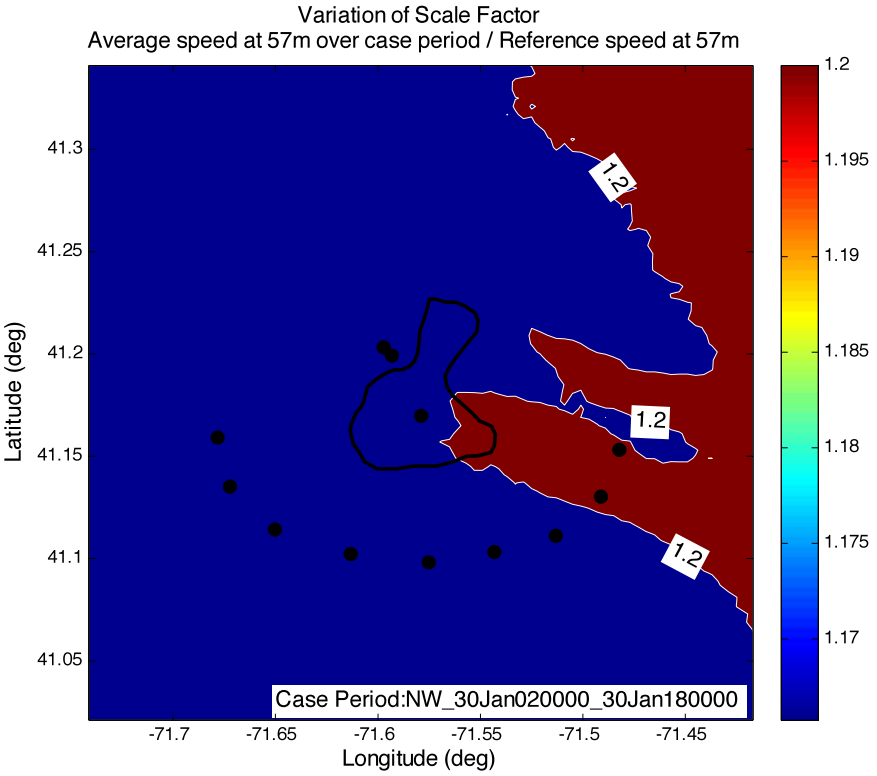
Variation of Scale Factor
Average speed at 57m over case period / Reference speed at 57m
1.2
1.2
1.2
Case Period:NW_30Jan020000_30Jan180000
Latitude (deg)
Longitude (deg)
41.3
41.25
41.2
41.15
41.1
41.05
-71.7
-71.65
-71.6
-71.55
-71.5
-71.45
1.2
1.195
1.19
1.185
1.18
1.175
1.17

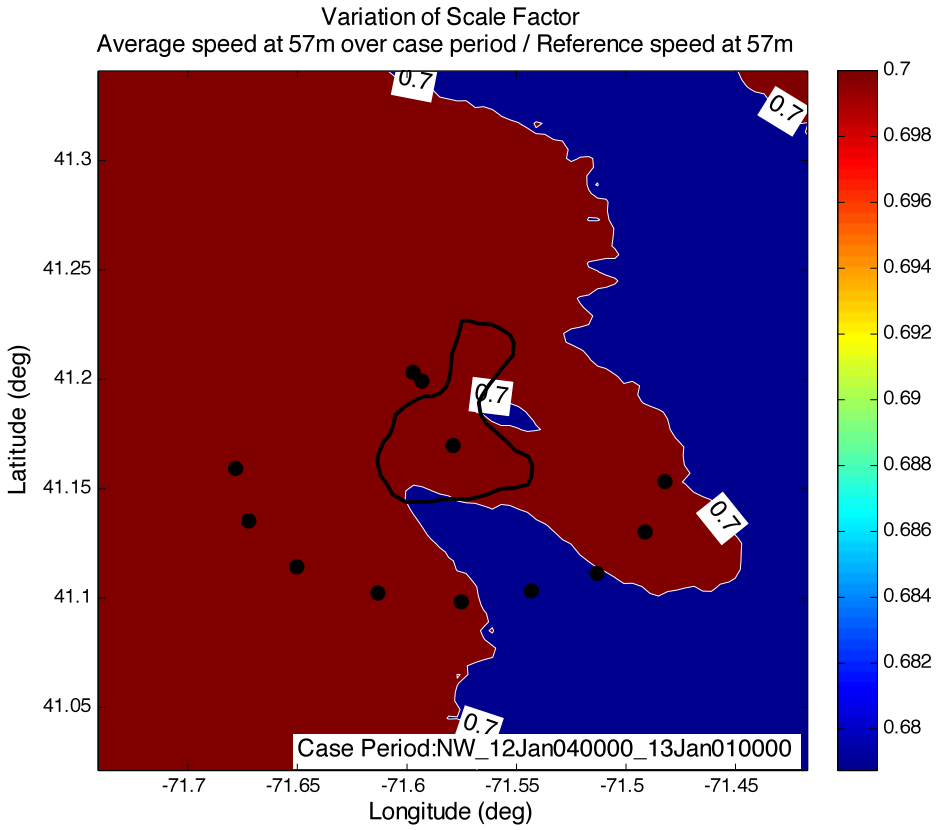
Variation of Scale Factor
Average speed at 57m over case period / Reference speed at 57m
0.7
0.7
0.7
0.7
0.7
Case Period:NW_12Jan040000_13Jan010000
41.3
41.25
41.2
41.15
41.1
41.05
Latitude (deg)
-71.7
-71.65
-71.6
-71.55
-71.5
-71.45
Longitude (deg)
0.7
0.698
0.696
0.694
0.692
0.69
0.688
0.686
0.684
0.682
0.68

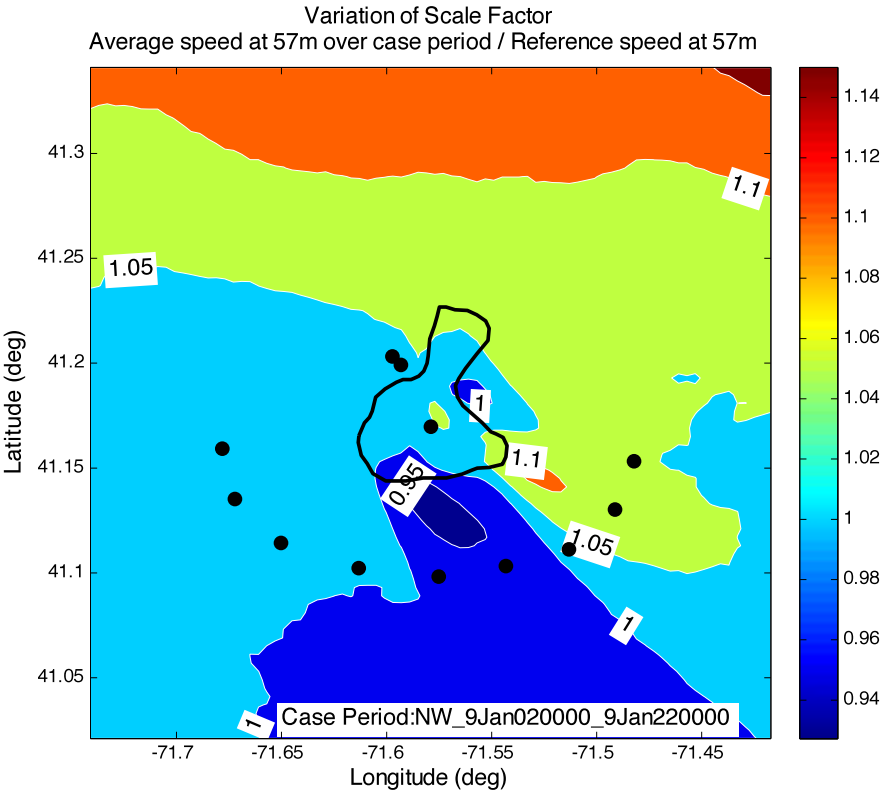
Variation of Scale Factor
Average speed at 57m over case period / Reference speed at 57m
1.1
1.05
1
1.1
0.95
1.05
1
1
Case Period:NW_9Jan020000_9Jan220000
41.3
41.25
41.2
41.15
41.1
41.05
Latitude (deg)
-71.7
-71.65
-71.6
-71.55
-71.5
-71.45
Longitude (deg)
1.14
1.12
1.1
1.08
1.06
1.04
1.02
1
0.98
0.96
0.94

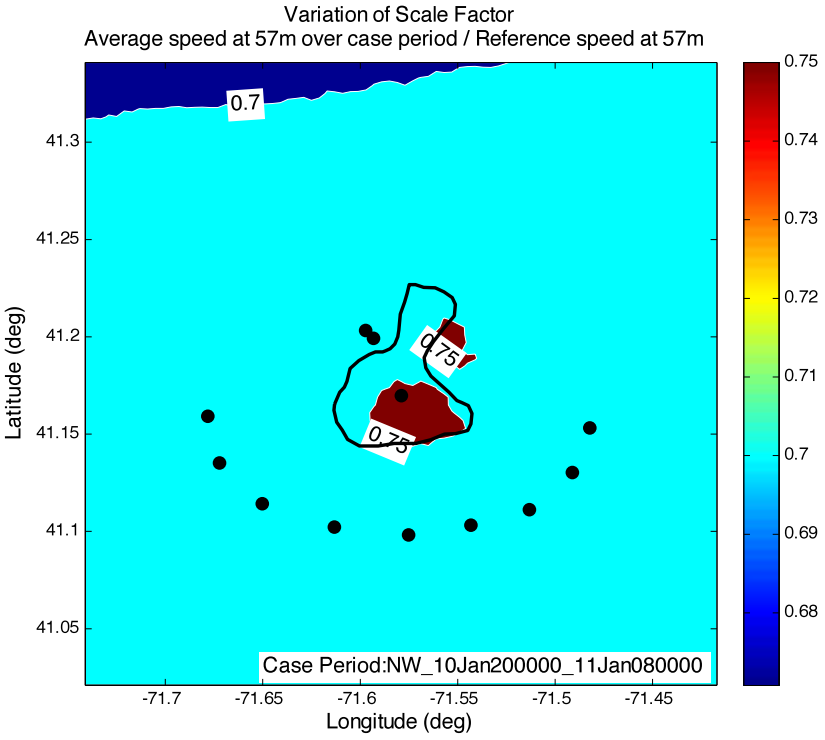
Variation of Scale Factor
Average speed at 57m over case period / Reference speed at 57m
0.7
0.75
0.75
Case Period:NW_10Jan200000_11Jan080000
Latitude (deg)
Longitude (deg)
41.3
41.25
41.2
41.15
41.1
41.05
-71.7
-71.65
-71.6
-71.55
-71.5
-71.45
0.75
0.74
0.73
0.72
0.71
0.7
0.69
0.68

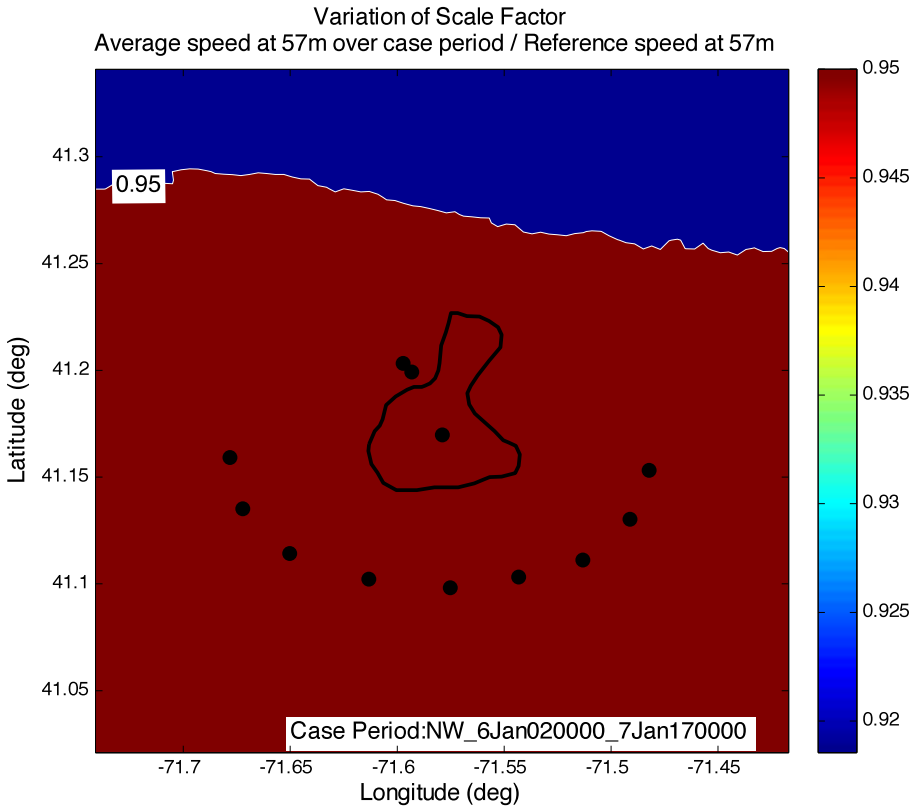
Variation of Scale Factor
Average speed at 57m over case period / Reference speed at 57m
0.95
Case Period:NW_6Jan020000_7Jan170000
Latitude (deg)
Longitude (deg)
41.3
41.25
41.2
41.15
41.1
41.05
-71.7
-71.65
-71.6
-71.55
-71.5
-71.45
0.95
0.945
0.94
0.935
0.93
0.925
0.92

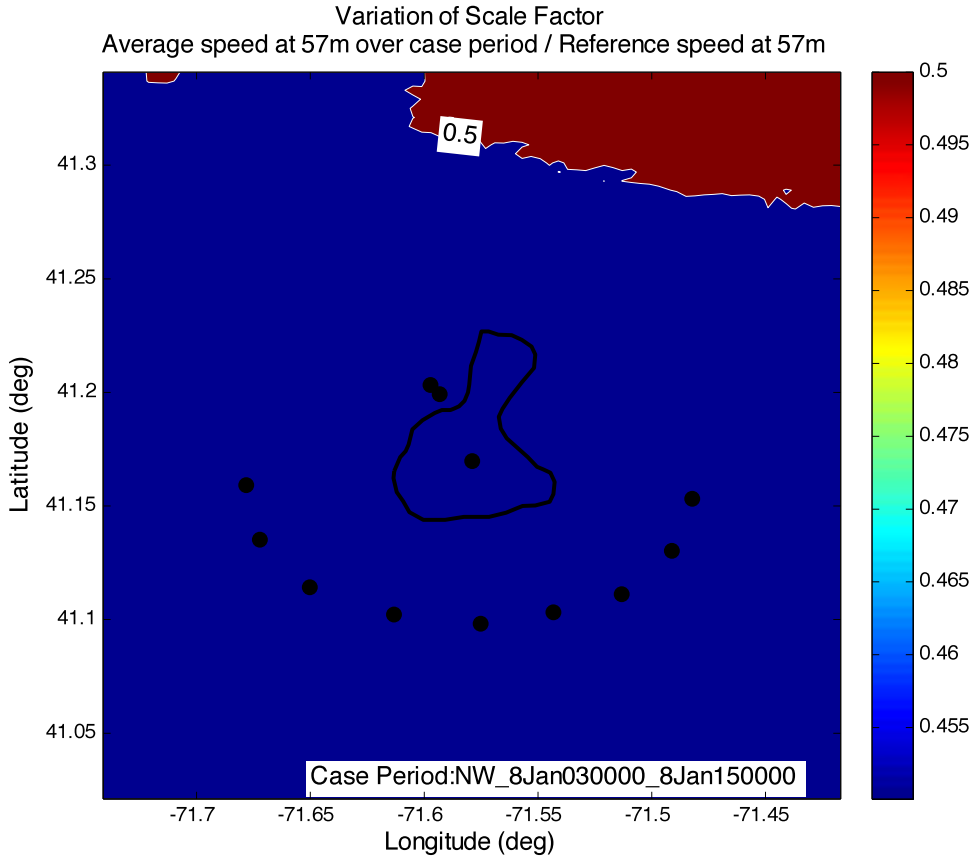
Variation of Scale Factor
Average speed at 57m over case period / Reference speed at 57m
0.5
Case Period:NW_8Jan030000_8Jan150000
Latitude (deg)
Longitude (deg)
41.3
41.25
41.2
41.15
41.1
41.05
-71.7
-71.65
-71.6
-71.55
-71.5
-71.45
0.5
0.495
0.49
0.485
0.48
0.475
0.47
0.465
0.46
0.455

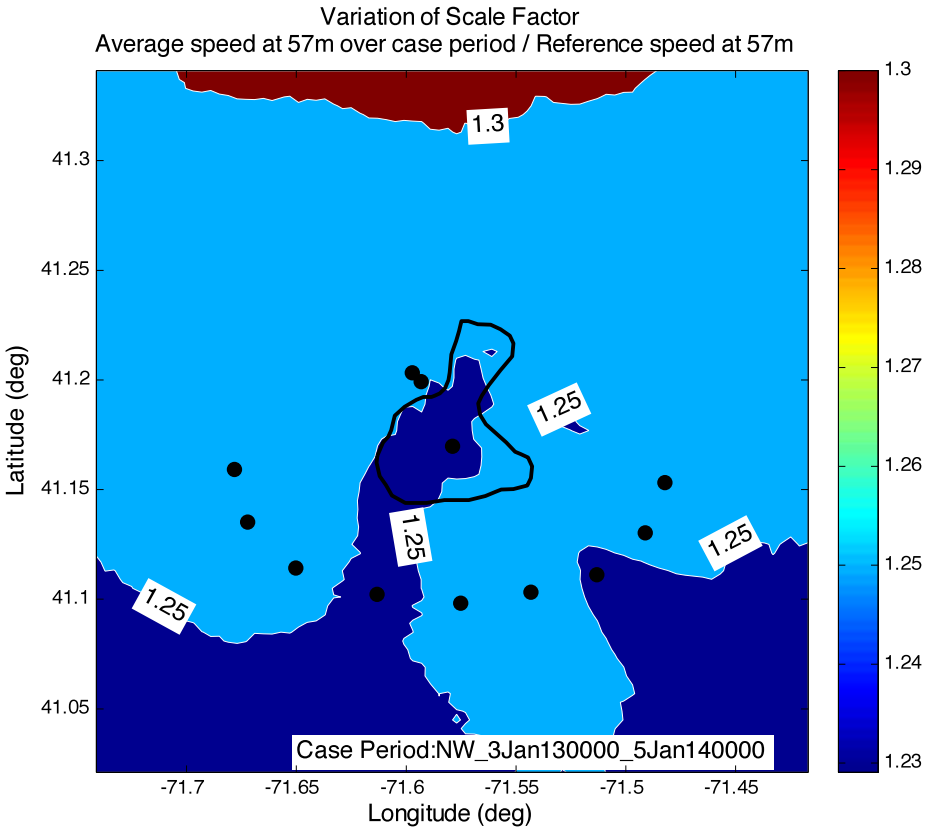
Variation of Scale Factor
Average speed at 57m over case period / Reference speed at 57m
1.3
1.25
1.25
1.25
Case Period:NW_3Jan130000_5Jan140000
Latitude (deg)
Longitude (deg)
41.3
41.25
41.2
41.15
41.1
41.05
-71.7
-71.65
-71.6
-71.55
-71.5
-71.45
1.3
1.29
1.28
1.27
1.26
1.25
1.24
1.23

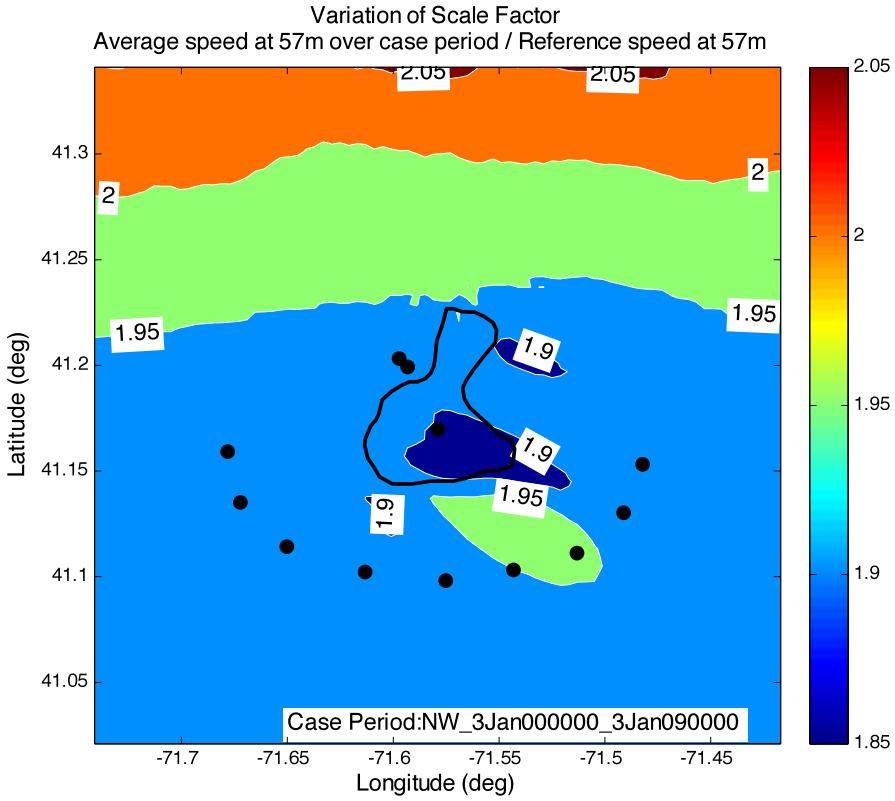
Variation of Scale Factor
Average speed at 57m over case period / Reference speed at 57m
2.05
2
1.95
1.9
1.85
Latitude (deg)
41.3
41.25
41.2
41.15
41.1
41.05
Case Period:NW_3Jan000000_3Jan090000
-71.7
-71.65
-71.6
-71.55
-71.5
-71.45
Longitude (deg)

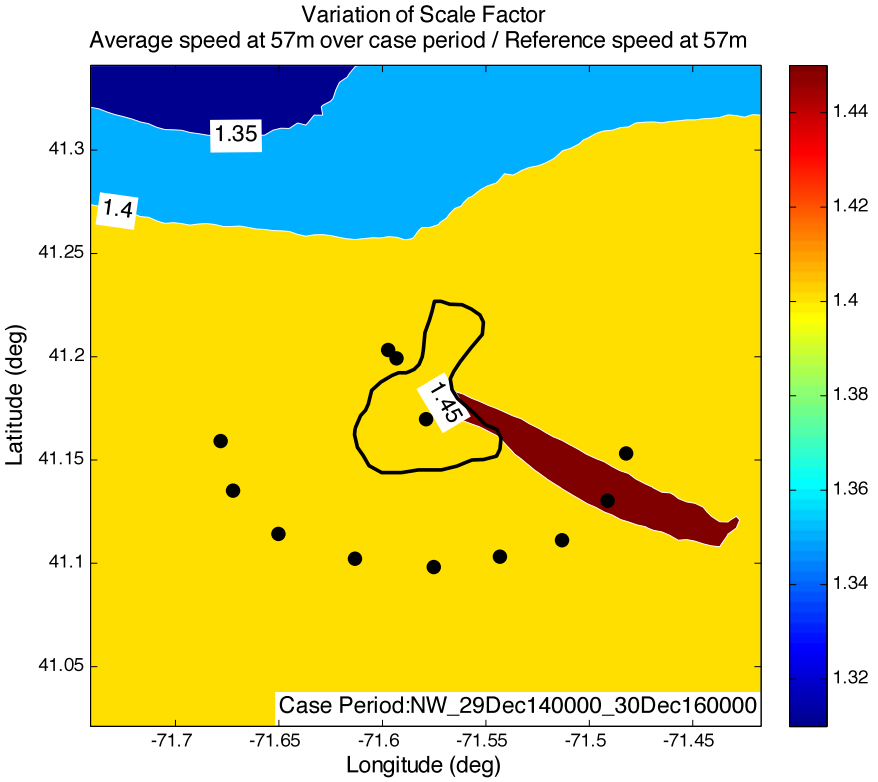
Variation of Scale Factor
Average speed at 57m over case period / Reference speed at 57m
1.35
1.4
1.45
1.44
1.42
1.38
1.36
1.34
1.32
Latitude (deg)
41.3
41.25
41.2
41.15
41.1
41.05
Case Period:NW_29Dec140000_30Dec160000
-71.7
-71.65
-71.6
-71.55
-71.5
-71.45
Longitude (deg)

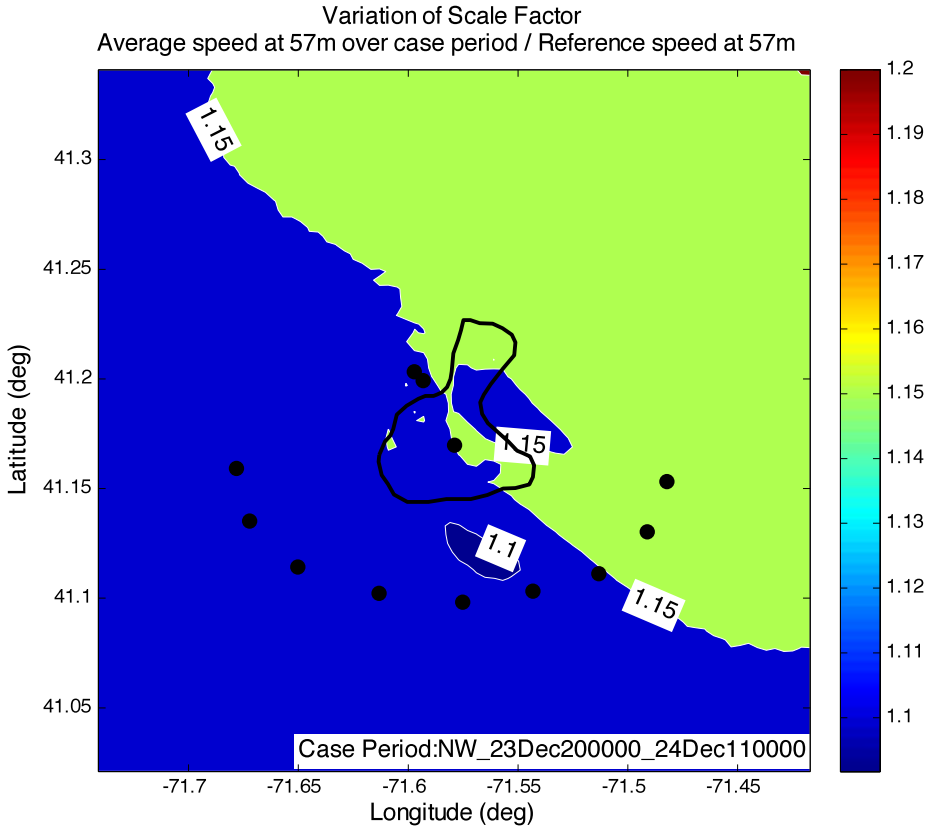
Variation of Scale Factor
Average speed at 57m over case period / Reference speed at 57m
1.15
1.15
1.1
1.15
Case Period:NW_23Dec200000_24Dec110000
Latitude (deg)
Longitude (deg)
41.3
41.25
41.2
41.15
41.1
41.05
-71.7
-71.65
-71.6
-71.55
-71.5
-71.45
1.2
1.19
1.18
1.17
1.16
1.15
1.14
1.13
1.12
1.11
1.1

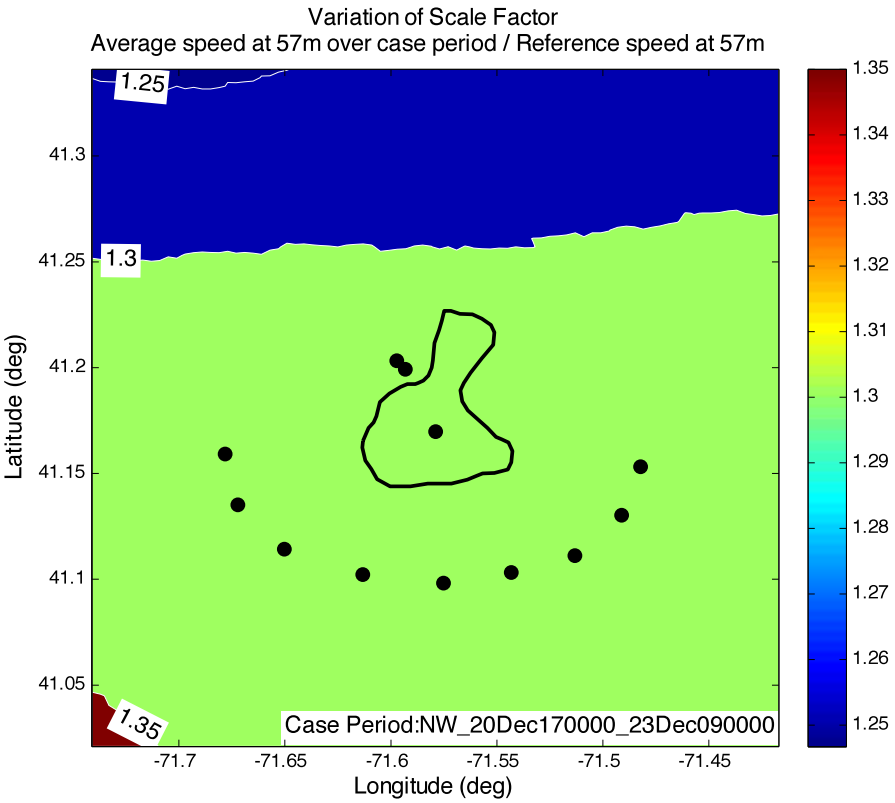
Variation of Scale Factor
Average speed at 57m over case period / Reference speed at 57m
1.25
1.3
1.35
Case Period:NW_20Dec170000_23Dec090000
Latitude (deg)
Longitude (deg)
41.3
41.25
41.2
41.15
41.1
41.05
-71.7
-71.65
-71.6
-71.55
-71.5
-71.45
1.35
1.34
1.33
1.32
1.31
1.3
1.29
1.28
1.27
1.26
1.25

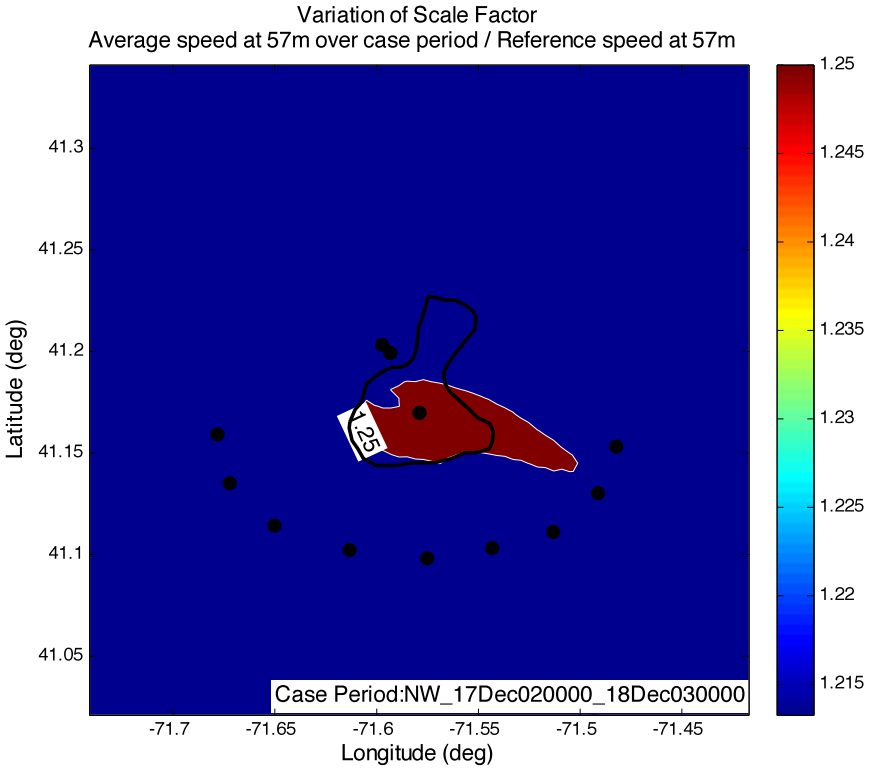
Variation of Scale Factor
Average speed at 57m over case period / Reference speed at 57m
1.25
1.25
Case Period:NW_17Dec020000_18Dec030000
Latitude (deg)
Longitude (deg)
41.3
41.25
41.2
41.15
41.1
41.05
-71.7
-71.65
-71.6
-71.55
-71.5
-71.45
1.25
1.245
1.24
1.235
1.23
1.225
1.22
1.215

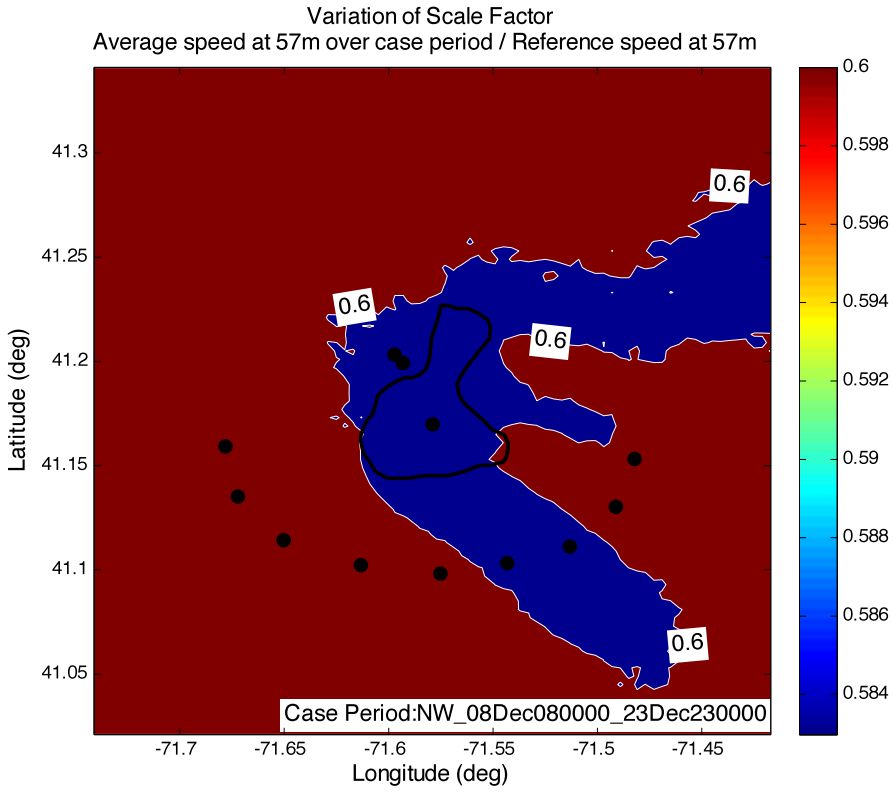
Variation of Scale Factor
Average speed at 57m over case period / Reference speed at 57m
0.6
0.6
0.6
0.6
Case Period:NW_08Dec080000_23Dec230000
Latitude (deg)
Longitude (deg)
41.3
41.25
41.2
41.15
41.1
41.05
-71.7
-71.65
-71.6
-71.55
-71.5
-71.45
0.6
0.598
0.596
0.594
0.592
0.59
0.588
0.586
0.584

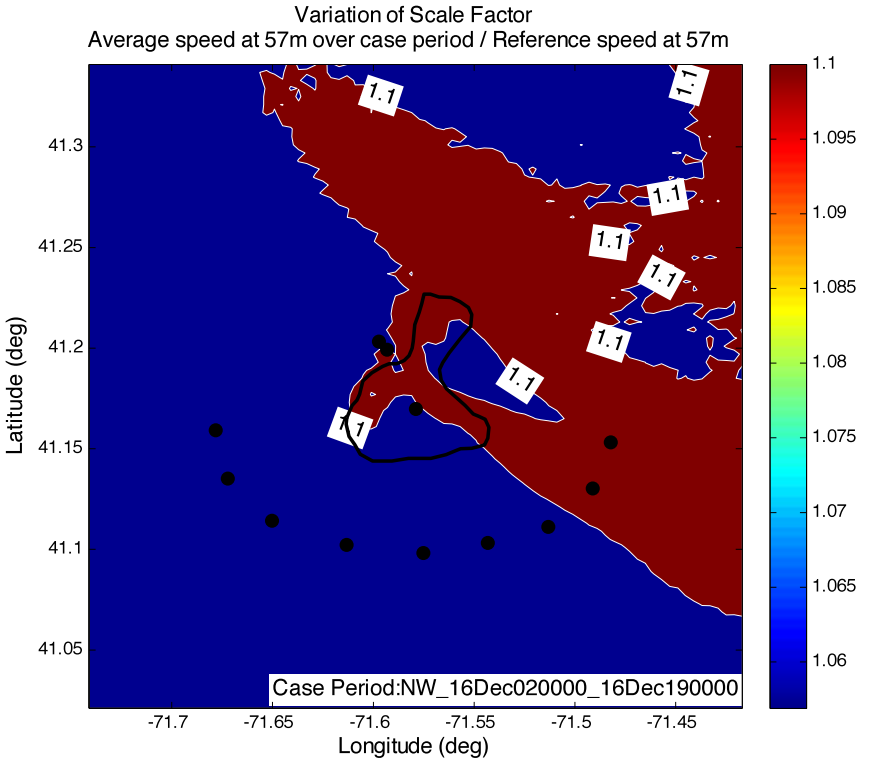
Variation of Scale Factor
Average speed at 57m over case period / Reference speed at 57m
1.1
1.095
1.09
1.085
1.08
1.075
1.07
1.065
1.06
41.3
41.25
41.2
41.15
41.1
41.05
Latitude (deg)
Case Period:NW_16Dec020000_16Dec190000
-71.7
-71.65
-71.6
-71.55
-71.5
-71.45
Longitude (deg)

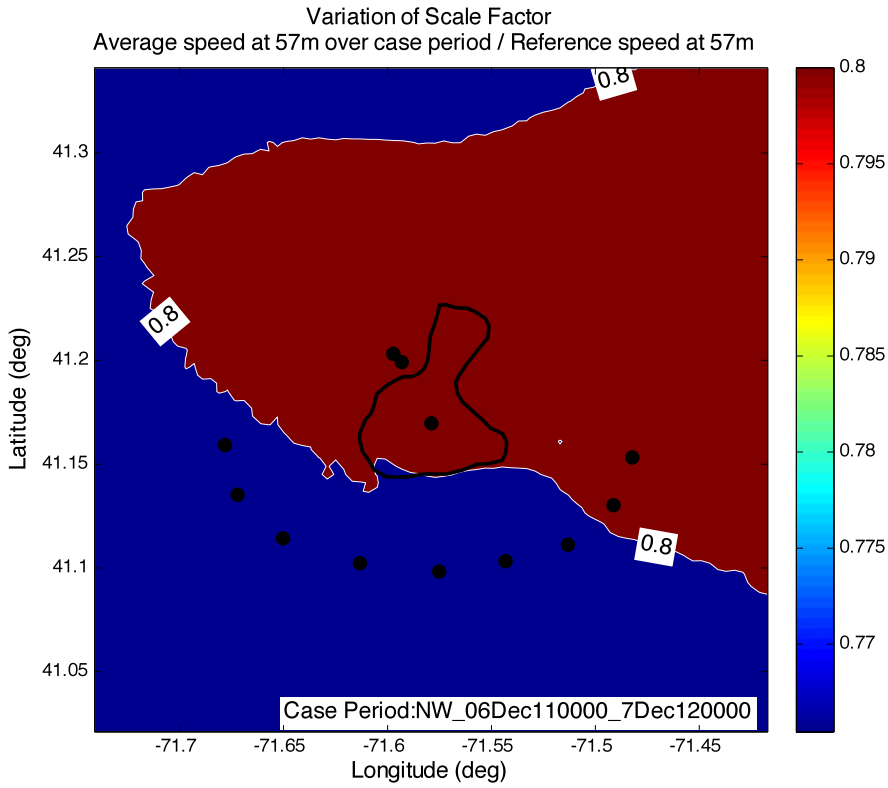
Variation of Scale Factor
Average speed at 57m over case period / Reference speed at 57m
0.8
0.795
0.79
0.785
0.78
0.775
0.77
41.3
41.25
41.2
41.15
41.1
41.05
Latitude (deg)
Case Period:NW_06Dec110000_7Dec120000
-71.7
-71.65
-71.6
-71.55
-71.5
-71.45
Longitude (deg)

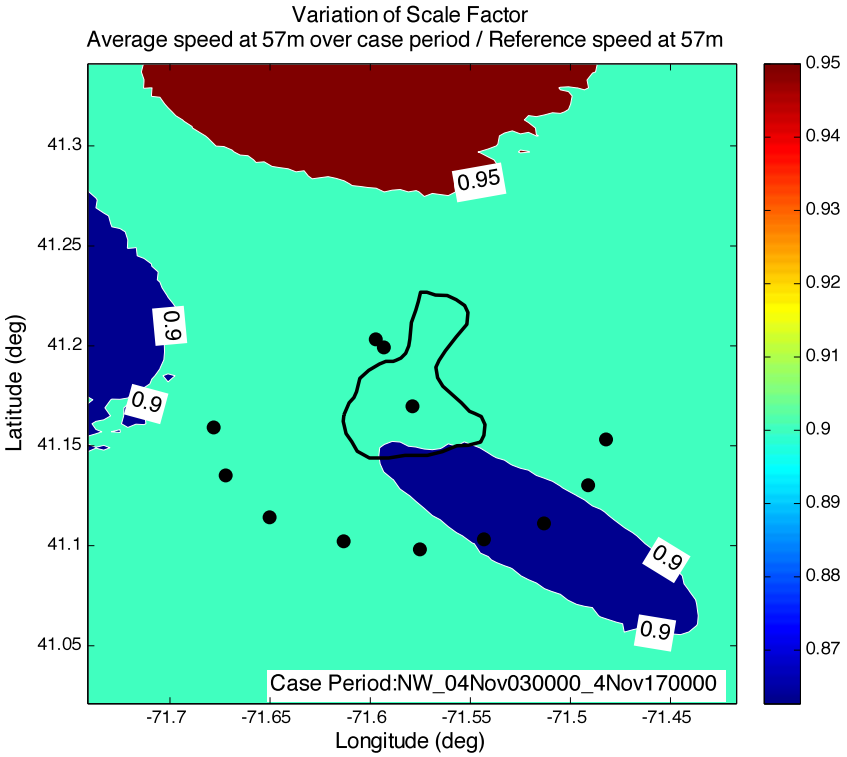
Variation of Scale Factor
Average speed at 57m over case period / Reference speed at 57m
0.95
0.9
0.9
0.9
Case Period:NW_04Nov030000_4Nov170000
Latitude (deg)
Longitude (deg)
41.3
41.25
41.2
41.15
41.1
41.05
-71.7
-71.65
-71.6
-71.55
-71.5
-71.45
0.95
0.94
0.93
0.92
0.91
0.9
0.89
0.88
0.87

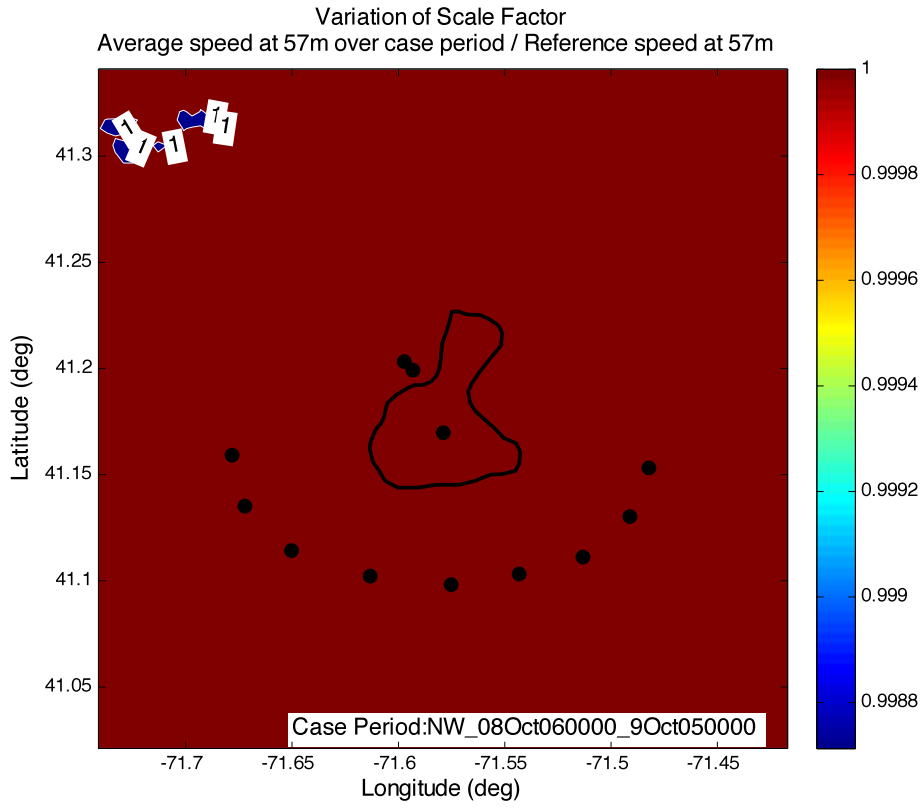
Variation of Scale Factor
Average speed at 57m over case period / Reference speed at 57m
1
1
1
1
Case Period:NW_08Oct060000_9Oct050000
Latitude (deg)
Longitude (deg)
41.3
41.25
41.2
41.15
41.1
41.05
-71.7
-71.65
-71.6
-71.55
-71.5
-71.45
1
0.9998
0.9996
0.9994
0.9992
0.999
0.9988

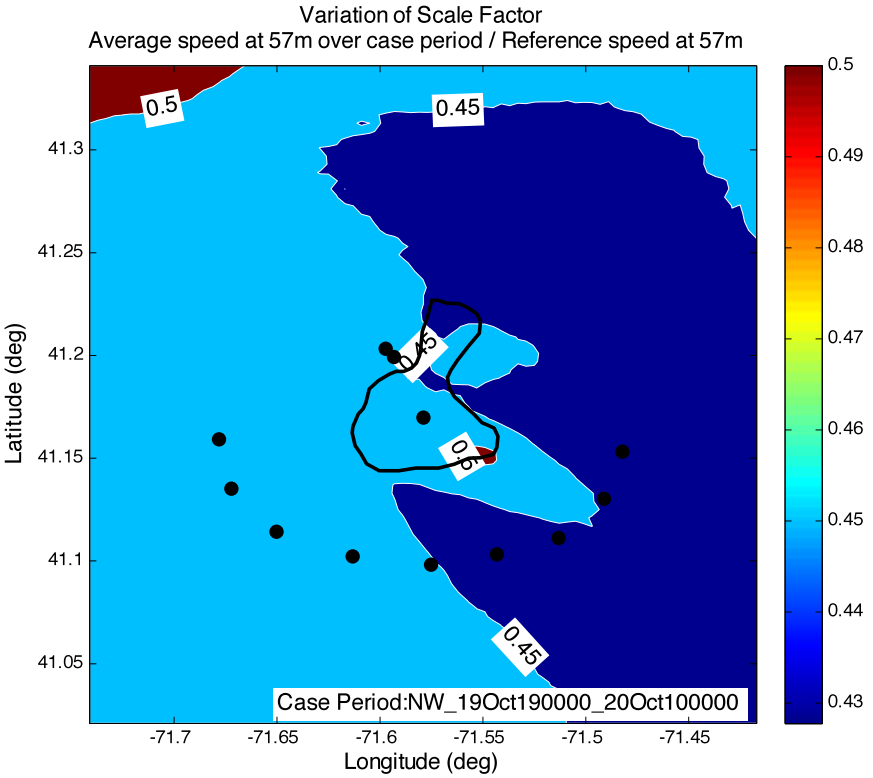
Variation of Scale Factor
Average speed at 57m over case period / Reference speed at 57m
0.5
0.45
0.45
0.45
0.45
Case Period:NW_19Oct190000_20Oct100000
41.3
41.25
41.2
41.15
41.1
41.05
-71.7
-71.65
-71.6
-71.55
-71.5
-71.45
Latitude (deg)
Longitude (deg)
0.5
0.49
0.48
0.47
0.46
0.45
0.44
0.43

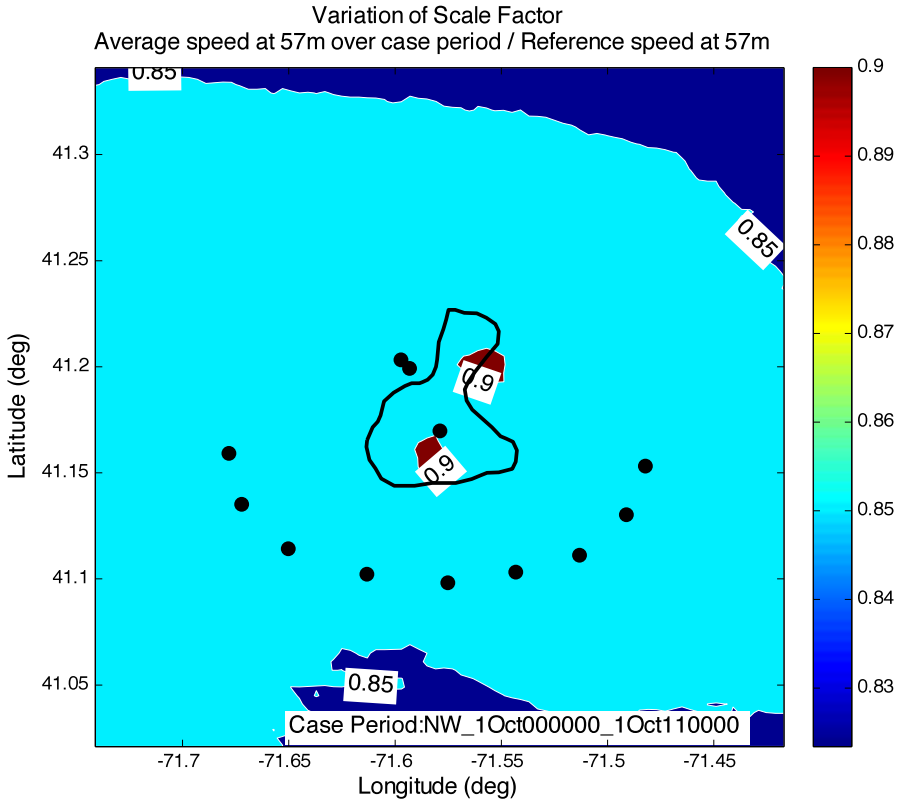
Variation of Scale Factor
Average speed at 57m over case period / Reference speed at 57m
0.85
0.85
0.9
0.9
0.85
Case Period:NW_1Oct000000_1Oct110000
41.3
41.25
41.2
41.15
41.1
41.05
-71.7
-71.65
-71.6
-71.55
-71.5
-71.45
Latitude (deg)
Longitude (deg)
0.9
0.89
0.88
0.87
0.86
0.85
0.84
0.83